

NASA Contractor Report 195010

1N-71

35342

P-194



Acoustic Properties and Durability of Liner Materials at Non-Standard Atmospheric Conditions

K. K. Ahuja, R. J. Gaeta, Jr., and J. S. Hsu
Georgia Institute of Technology
GTRI/AERO
Acoustics, Aerodynamics, and Advanced Vehicles Division
Atlanta, Georgia 30332-0800

(NASA-CR-195010) ACOUSTIC
PROPERTIES AND DURABILITY OF LINER
MATERIALS AT NON-STANDARD
ATMOSPHERIC CONDITIONS (Georgia
Inst. of Tech.) 194 p

N95-18930

Unclass

63/71 0035342

Contract NAS1-19061
(Task Assignment 15)

November 1994

National Aeronautics and
Space Administration
Langley Research Center
Hampton, Virginia 23681-0001

Foreword/Acknowledgments

This report was prepared by the Acoustics, Aerodynamics and Advanced Vehicles Division of the Aerospace Laboratory of Georgia Tech Research Institute (GTRI) for NASA Langley Research Center, Hampton, Virginia, under Task Assignment 15 of Contract NAS1-19061.

Mr. Earl Booth, Jr. was the Project Manager for NASA Langley Research Center. GTRI's Project Director was Dr. K.K. Ahuja.

Special thanks are due to Mr. Tony Parrott of NASA Langley Research Center who provided data for a ceramic honeycomb liner as well as valuable advice on methods of analyzing the data.

The authors would also like to acknowledge the assistance of Vince Ross and William Law of GTRI who developed the sub-atmospheric facility, and finally of Ian Eyre and Erik Dryer of GTRI who assisted in the data acquisition.

CONTENTS

List of Figures	v
Summary	1
1.0 INTRODUCTION.....	3
1.1 Background.....	3
1.2 Program Objective	4
1.3 Experimental Approach.....	4
2.0 TEST FACILITIES AND EXPERIMENTAL SET-UP	7
2.1 Sub-Atmospheric Facility	7
2.1.1 General Description.....	7
2.1.2 Vacuum Performance.....	10
2.2 Impedance Tube.....	10
2.2.1 General Description.....	10
2.2.2 Impedance Tube Specifications.....	12
2.2.3 Data Acquisition and Processing	15
2.3 Low Temperature/High Pressure Facility	18
2.3.1 Cryogenic Cooling Chamber	18
2.3.2 Data Acquisition and Control	25
3.0 TEST SAMPLE FABRICATION AND TEST PLAN.....	29
3.1 Liner Materials Used for Testing.....	29
3.2 Sample Cutting Process and Impedance Tube Mounting.....	29
3.3 Test Plan	31
3.3.1 Sub-Atmospheric Acoustic Test.....	31
3.3.2 Low Temperature/High Pressure Cycle Test	34
3.3.3 Mechanical Resiliency Test	34
4.0 RESULTS OF NON-STANDARD ATMOSPHERIC TESTS	37
4.1 Summary of Findings	37
4.2 Impedance Tube Results - A Confidence Check	38
4.3 A Word About Impedance Tube Data Overlap.....	41
4.4 Sub-Atmospheric Pressure Effects.....	43
4.5 Cryogenic Cycling Test - Results and Discussion	61

4.6 Cycling Effects on Acoustic Properties - Results and Discussion.....	68
5.0 RESULTS OF MECHANICAL RESILIENCY TESTS.....	75
5.1 Summary of Results	75
6.0 CONCLUDING REMARKS	77
6.1 Summary of Work Done	77
6.2 Recommendations and Future Work.....	78
7.0 REFERENCES	79
APPENDIX A	81
APPENDIX B	89

List of Figures

	Page
2.1 Schematic of Sub-Atmospheric Facility.....	8
2.2 Photograph of actual Sub-Atmospheric Facility.....	9
2.3 Evacuation rate of GTRI's vacuum chamber facility.	11
2.4 B&K 4206 impedance tube installed inside vacuum facility.....	13
2.5 Three basic set-up types for the B&K 4206 impedance tube: a) Small tube-standard; b) Large tube-standard; c) Wide spacing large tube.....	14
2.6 Schematic of the data acquisition system for the B&K 4206 impedance tube.	16
2.7 Cross section of vacuum facility with impedance tube mounted inside.	17
2.8 Cryogenic cooling test chamber.....	19
2.9 Dimensions of the cryogenic cooling material sample holder.....	20
2.10 Sample holder for the cryogenic cooling chamber with thermocouple placements....	21
2.11 Cryogenic Cooling Facility.	23
2.12 Air flowpath through the cryogenic cooling chamber.	24
2.13 Schematic of data acquisition system for the Cryogenic Cooling Facility.....	26
2.14 Generic temperature and pressure cycle profile for the Cryogenic Cooling Facility. .	27
3.1 Liner materials tested in present study.....	30
3.2 Test sample fabrication tools.	32
3.3 Hydraulic tensile/compression rig used for mechanical resiliency tests.	35
4.1 Two Thickness Method comparison with NASA CT73 ceramic honeycomb characteristic acoustic data.	39
4.2 Comparison of present data with GE data for Kevlar, L=19.05 mm (0.75 in.).....	40
4.3 Example of "data overlap" from impedance tube results of Fiberglass.....	42
4.4 Effect of pressure on absorption coefficient of Pyrell foam.	44
4.5 Effect of pressure on absorption coefficient of Fiberglass.....	45
4.6 Effect of pressure on absorption coefficient of Kevlar.	46
4.7 Effect of pressure on characteristic impedance of Fiberglass.....	47
4.8 Effect of pressure on the attenuation rate of Fiberglass.	49
4.9 Effect of test sample length on absorption coefficient of Fiberglass.....	50
4.10 Effect of test sample length on absorption coefficient of Kevlar.	51
4.11 Diminishing effectiveness of test sample length on the absorption of Kevlar.	52

	<u>Page</u>
4.12 Comparison of the Two Thickness approach to characteristic impedance calculations and the "infinite" length assumption of characteristic impedance.....	54
4.13 Comparison of present characteristic impedance data for Kevlar with NASA data (Smith & Parrott, 1983).....	56
4.14 Effect of test sample length on the absorption coefficient of Pyrell foam.....	57
4.15 Effect of pressure on characteristic impedance of Pyrell foam.....	58
4.16 Effect of pressure on the attenuation rate of Pyrell foam.....	59
4.17 Effect of test sample length on input impedance of Pyrell foam.....	60
4.18 Snapshot time history of temperature during the cryogenic cooling phase of Pyrell foam.....	62
4.19 Snapshot time history of temperature during the cryogenic cooling phase of Fiberglass.....	63
4.20 Snapshot time history of temperature during the cryogenic cooling phase of Kevlar.....	64
4.21 Snapshot time history of chamber pressure during the cryogenic cooling phase of Pyrell foam.....	65
4.22 Snapshot time history of chamber pressure during the cryogenic cooling phase of Fiberglass.....	66
4.23 Snapshot time history of chamber pressure during the cryogenic cooling phase of Kevlar.....	67
4.24 Effect of periodic cold soak on absorption coefficient of Pyrell foam.....	69
4.25 Effect of periodic cold soak on absorption coefficient of Fiberglass.....	70
4.26 Effect of periodic cold soak on absorption coefficient of Kevlar.....	71
4.27 Thawing process of Pyrell foam after being saturated with liquid nitrogen.....	72
4.28 Effect of repeated liquid nitrogen saturation of Pyrell foam on absorption coefficient.....	73
5.1 Mechanical resiliency test for Pyrell foam and Fiberglass.....	76

APPENDIX B Figures

	<u>Page</u>
B1 Absorption coefficient of Pyrell foam, P=P _{atm} , L = 50.8 mm, D = 29.0 mm.....	B.1
B2 Absorption coefficient of Pyrell foam, P=75%P _{atm} , L = 50.8 mm, D = 29.0 mm.....	B.2
B3 Absorption coefficient of Pyrell foam, P=50%P _{atm} , L = 50.8 mm, D = 29.0 mm.....	B.3
B4 Absorption coefficient of Pyrell foam, P=25%P _{atm} , L = 50.8 mm, D = 29.0 mm.....	B.4
B5 Absorption coefficient of Pyrell foam, P=P _{atm} , L = 101.6 mm, D = 29.0 mm.....	B.5
B6 Absorption coefficient of Pyrell foam, P=75%P _{atm} , L = 101.6 mm, D = 29.0 mm.....	B.6
B7 Absorption coefficient of Pyrell foam, P=50%P _{atm} , L = 101.6 mm, D = 29.0 mm.....	B.7
B8 Absorption coefficient of Pyrell foam, P=25%P _{atm} , L = 101.6 mm, D = 29.0 mm.....	B.8
B9 Absorption coefficient of Pyrell foam, P=P _{atm} , L = 50.8 mm, D = 100.0 mm.....	B.9
B10 Absorption coefficient of Pyrell foam, P=75%P _{atm} , L = 50.8 mm, D = 100.0 mm.....	B.10
B11 Absorption coefficient of Pyrell foam, P=50%P _{atm} , L = 50.8 mm, D = 100.0 mm.....	B.11
B12 Absorption coefficient of Pyrell foam, P=25%P _{atm} , L = 50.8 mm, D = 100.0 mm.....	B.12
B13 Absorption coefficient of Pyrell foam, P=P _{atm} , L = 101.6 mm, D = 100.0 mm.....	B.13
B14 Absorption coefficient of Pyrell foam, P=75%P _{atm} , L = 101.6 mm, D = 100.0 mm.....	B.14

	<u>Page</u>
B15 Absorption coefficient of Pyrell foam, P=50%P _{atm} , L = 101.6 mm, D = 100.0 mm.....	B.15
B16 Absorption coefficient of Pyrell foam, P=25%P _{atm} , L = 101.6 mm, D = 100.0 mm.....	B.16
B17 Absorption coefficient of Fiberglass foam, P=P _{atm} , L = 50.8 mm, D = 29.0 mm.....	B.17
B18 Absorption coefficient of Fiberglass foam, P=75%P _{atm} , L = 50.8 mm, D = 29.0 mm.....	B.18
B19 Absorption coefficient of Fiberglass foam, P=50%P _{atm} , L = 50.8 mm, D = 29.0 mm.....	B.19
B20 Absorption coefficient of Fiberglass foam, P=25%P _{atm} , L = 50.8 mm, D = 29.0 mm.....	B.20
B21 Absorption coefficient of Fiberglass foam, P=P _{atm} , L = 101.6 mm, D = 29.0 mm.....	B.21
B22 Absorption coefficient of Fiberglass foam, P=75%P _{atm} , L = 101.6 mm, D = 29.0 mm.....	B.22
B23 Absorption coefficient of Fiberglass foam, P=50%P _{atm} , L = 101.6 mm, D = 29.0 mm.....	B.23
B24 Absorption coefficient of Fiberglass foam, P=25%P _{atm} , L = 101.6 mm, D = 29.0 mm.....	B.24
B25 Absorption coefficient of Fiberglass foam, P=P _{atm} , L = 50.8 mm, D = 100.0 mm.....	B.25
B26 Absorption coefficient of Fiberglass foam, P=75%P _{atm} , L = 50.8 mm, D = 100.0 mm.....	B.26
B27 Absorption coefficient of Fiberglass foam, P=50%P _{atm} , L = 50.8 mm, D = 100.0 mm.....	B.27
B28 Absorption coefficient of Fiberglass foam, P=25%P _{atm} , L = 50.8 mm, D = 100.0 mm.....	B.28
B29 Absorption coefficient of Fiberglass foam, P=P _{atm} , L = 101.6 mm, D = 100.0 mm.....	B.29
B30 Absorption coefficient of Fiberglass foam, P=75%P _{atm} , L = 101.6 mm, D = 100.0 mm.....	B.30

	<u>Page</u>
B31 Absorption coefficient of Fiberglass foam, P=50%P _{atm} , L = 101.6 mm, D = 100.0 mm.....	B.31
B32 Absorption coefficient of Fiberglass foam, P=25%P _{atm} , L = 101.6 mm, D = 100.0 mm.....	B.32
B33 Absorption coefficient of Kevlar foam, P=P _{atm} , L = 28.56 mm, D = 29.0 mm.....	B.33
B34 Absorption coefficient of Kevlar foam, P=75%P _{atm} , L 28.56 = mm, D = 29.0 mm.	B.34
B35 Absorption coefficient of Kevlar foam, P=50%P _{atm} , L = 28.56 mm, D = 29.0 mm.	B.35
B36 Absorption coefficient of Kevlar foam, P=25%P _{atm} , L = 28.56 mm, D = 29.0 mm.	B.36
B37 Absorption coefficient of Kevlar foam, P=P _{atm} , L = 57.15 mm, D = 29.0 mm.....	B.37
B38 Absorption coefficient of Kevlar foam, P=75%P _{atm} , L = 57.15 mm, D = 29.0 mm.	B.38
B39 Absorption coefficient of Kevlar foam, P=50%P _{atm} , L = 57.15 mm, D = 29.0 mm.	B.39
B40 Absorption coefficient of Kevlar foam, P=25%P _{atm} , L = 57.15 mm, D = 29.0 mm.	B.40
B41 Absorption coefficient of Kevlar foam, P=P _{atm} , L = 28.56 mm, D = 100.0 mm.	B.41
B42 Absorption coefficient of Kevlar foam, P=75%P _{atm} , L = 28.56 mm, D = 100.0 mm.....	B.42
B43 Absorption coefficient of Kevlar foam, P=50%P _{atm} , L = 28.56 mm, D = 100.0 mm.....	B.43
B44 Absorption coefficient of Kevlar foam, P=25%P _{atm} , L = 28.56 mm, D = 100.0 mm.....	B.44
B45 Absorption coefficient of Kevlar foam, P=P _{atm} , L = 57.15 mm, D = 100.0 mm.	B.45
B46 Absorption coefficient of Kevlar foam, P=75%P _{atm} , L = 57.15 mm, D = 100.0 mm.....	B.46

	Page
B47 Absorption coefficient of Kevlar foam, P=50%P _{atm} , L = 57.15 mm, D = 100.0 mm.....	B.47
B48 Absorption coefficient of Kevlar foam, P=25%P _{atm} , L = 57.15 mm, D = 100.0 mm.....	B.48
B49 Characteristic Impedance of Pyrell foam, P=P _{atm} , D = 29.0 mm.....	B.49
B50 Characteristic Impedance of Pyrell foam, P=75%P _{atm} , D = 29.0 mm.....	B.50
B51 Characteristic Impedance of Pyrell foam, P=50%P _{atm} , D = 29.0 mm.....	B.51
B52 Characteristic Impedance of Pyrell foam, P=25%P _{atm} , D = 29.0 mm.....	B.52
B53 Characteristic Impedance of Pyrell foam, P=P _{atm} , D = 100.0 mm.....	B.53
B54 Characteristic Impedance of Pyrell foam, P=75%P _{atm} , D = 100.0 mm.....	B.54
B55 Characteristic Impedance of Pyrell foam, P=50%P _{atm} , D = 100.0 mm.....	B.55
B56 Characteristic Impedance of Pyrell foam, P=25%P _{atm} , D = 100.0 mm.....	B.56
B57 Characteristic Impedance of Fiberglass, P=P _{atm} , D = 29.0 mm.....	B.57
B58 Characteristic Impedance of Fiberglass, P=75%P _{atm} , D = 29.0 mm.....	B.58
B59 Characteristic Impedance of Fiberglass, P=50%P _{atm} , D = 29.0 mm.....	B.59
B60 Characteristic Impedance of Fiberglass, P=25%P _{atm} , D = 29.0 mm.....	B.60
B61 Characteristic Impedance of Fiberglass, P=P _{atm} , D = 100.0 mm.....	B.61
B62 Characteristic Impedance of Fiberglass, P=75%P _{atm} , D = 100.0 mm.....	B.62

	<u>Page</u>
B63 Characteristic Impedance of Fiberglass, P=50% P _{atm} , D = 100.0 mm.....	B.63
B64 Characteristic Impedance of Fiberglass, P=25% P _{atm} , D = 100.0 mm.....	B.64
B65 Characteristic Impedance of Kevlar, P=P _{atm} , D = 29.0 mm.....	B.65
B66 Characteristic Impedance of Kevlar, P=75%P _{atm} , D = 29.0 mm.	B.66
B67 Characteristic Impedance of Kevlar, P=50%P _{atm} , D = 29.0 mm.	B.67
B68 Characteristic Impedance of Kevlar, P=25%P _{atm} , D = 29.0 mm.	B.68
B69 Characteristic Impedance of Kevlar, P=P _{atm} , D = 100.0 mm.	B.69
B70 Characteristic Impedance of Kevlar, P=75% P _{atm} , D = 100.0 mm.....	B.70
B71 Characteristic Impedance of Kevlar, P=50% P _{atm} , D = 100.0 mm.....	B.71
B72 Characteristic Impedance of Kevlar, P=25% P _{atm} , D = 100.0 mm.....	B.72
B73 Attenuation rate of Pyrell foam, P=P _{atm} , D = 29.0 mm.....	B.73
B74 Attenuation rate of Pyrell foam, P=75%P _{atm} , D = 29.0 mm.	B.74
B75 Attenuation rate of Pyrell foam, P=50%P _{atm} , D = 29.0 mm.	B.75
B76 Attenuation rate of Pyrell foam, P=25%P _{atm} , D = 29.0 mm.	B.76
B77 Attenuation rate of Pyrell foam, P=P _{atm} , D = 100.0 mm.	B.77
B78 Attenuation rate of Pyrell foam, P=75% P _{atm} , D = 100.0 mm.....	B.78

	Page
B79 Attenuation rate of Pyrell foam, P=50% P _{atm} , D = 100.0 mm.....	B.79
B80 Attenuation rate of Pyrell foam, P=25% P _{atm} , D = 100.0 mm.....	B.80
B81 Attenuation rate of Fiberglass, P=P _{atm} , D = 29.0 mm.....	B.81
B82 Attenuation rate of Fiberglass, P=75%P _{atm} , D = 29.0 mm.	B.82
B83 Attenuation rate of Fiberglass, P=50%P _{atm} , D = 29.0 mm.	B.83
B84 Attenuation rate of Fiberglass, P=25%P _{atm} , D = 29.0 mm.	B.84
B85 Attenuation rate of Fiberglass, P=P _{atm} , D = 100.0 mm.	B.85
B86 Attenuation rate of Fiberglass, P=75% P _{atm} , D = 100.0 mm.....	B.86
B87 Attenuation rate of Fiberglass, P=50% P _{atm} , D = 100.0 mm.....	B.87
B88 Attenuation rate of Fiberglass, P=25% P _{atm} , D = 100.0 mm.....	B.88
B89 Attenuation rate of Kevlar, P=P _{atm} , D = 29.0 mm.....	B.89
B90 Attenuation rate of Kevlar, P=P _{atm} , D = 29.0 mm.....	B.90
B91 Phase Constant of Pyrell foam, P=P _{atm} , D = 29.0 mm.....	B.91
B92 Phase Constant of Pyrell foam, P=75%P _{atm} , D = 29.0 mm.	B.92
B93 Phase Constant of Pyrell foam, P=50%P _{atm} , D = 29.0 mm.	B.93
B94 Phase Constant of Pyrell foam, P=25%P _{atm} , D = 29.0 mm.	B.94

	<u>Page</u>
B95 Phase Constant of Fiberglass, P=P _{atm} , D = 29.0 mm.....	B.95
B96 Phase Constant of Fiberglass, P=75%P _{atm} , D = 29.0 mm.....	B.96
B97 Phase Constant of Fiberglass, P=50%P _{atm} , D = 29.0 mm.....	B.97
B98 Phase Constant of Fiberglass, P=25%P _{atm} , D = 29.0 mm.....	B.98

Summary

This report documents the results of an experimental study on how acoustic properties of certain absorbing liner materials are affected by non-standard atmospheric conditions. This study was motivated by the need to assess risks associated with incorporating acoustic testing capability in wind tunnels with semi-cryogenic high Reynolds number aerodynamic and/or low pressure capabilities. The study consisted of three phases: 1) Measurement of acoustic properties of selected liner materials at sub-atmospheric pressure conditions, 2) Periodic cold soak and high pressure exposure of liner materials for 250 cycles, and 3) Determination of the effect of periodic cold soak on the acoustic properties of the liner materials at sub-atmospheric conditions and the effect on mechanical resiliency.

The selected liner materials were Pyrell foam, Fiberglass, and Kevlar. A vacuum facility was used to create the sub-atmospheric environment in which an impedance tube was placed to measure acoustic properties of the test materials. Results of the Phase I tests revealed that lower ambient pressure reduced the absorption effectiveness of the liner materials to varying degrees.

An automated cryogenic cooling system was used to perform the Phase II tests. Super-cooled air was passed through the liner material placed inside a specially-designed chamber to reduce the material temperature. A computer was used to automate and control the data acquisition and cycling of each material test. A cycle consisted of reducing the material temperature to -150 °F, then pressurizing to 5 atmospheres, and then returning the material back to ambient temperature and pressure. Each liner material was subjected to a total of 250 cycles.

Finally, Phase I tests were repeated to determine the effect of periodic cold soak and high pressure cycling on the acoustic properties of the liner materials. Results indicate that no significant change in the acoustic properties occurred after the periodic cold soak. Furthermore, mechanical resiliency tests were carried out which indicated that no change in the liner material resiliency had occurred.

1.0 INTRODUCTION

1.1 Background

The need for new acoustic testing facilities has been chronicled in several recent reports that have examined the national wind tunnel testing capabilities^{1,2}. However, in this current environment of fiscal restraint, it is likely that any new facility built in the foreseeable future will have to accommodate several purposes. Acoustic testing capability is completely compatible with low speed wind tunnel design, if considered in the beginning of the design cycle. One of the most urgent requirements for low speed research is in the area of high lift aerodynamics, which will require a high Reynolds number testing capability at low speed^{3,4}. One possible method of reaching the high Reynolds number flow required is to use cryogenic or semi-cryogenic temperatures which would increase the Reynolds number similar to National Transonic Facility (NTF) and the newly commissioned European Transonic Wind tunnel (ETW). If a decision was made to incorporate acoustic testing capability at ambient temperatures into a wind tunnel with semi-cryogenic high Reynolds number aerodynamic testing capabilities, a number of design risks would have to be addressed.

Although the NTF incorporates some acoustic treatment on the fan nacelle⁵, use of conventional sound absorbing materials in a wind tunnel that is exposed to extremely low temperatures may pose a threat to acoustic liner durability. In particular, two aspects, should be addressed: (1) will the acoustic liner material's absorption characteristics change and (2) will the acoustic material mechanical properties change if the liner material is exposed to extremely cold temperature on a routine basis. If the acoustic absorption characteristics of the material change, then the prospect of combining acoustic testing in this facility diminishes. Similarly, if the material mechanically breaks down, then the possibility of loose acoustic material could interfere with the operation as an aerodynamic testing facility. Much of the advantage of combining acoustic testing in such a facility would be lost if the acoustic material had to be periodically replaced, or worse yet, required a frequent cleaning of the anti-turbulence screens.

Additionally, acoustic testing requirements may call for testing in a higher velocity range than that available in a facility optimized for high Reynolds number at low speeds. In such a case, it may be possible to reach higher velocities in the test section at lower tunnel internal pressure. What are the effects of pressure on the absorption characteristics of acoustic liner material?

1.2 Program Objective

The overall program objective was to study the effect of periodic cold soak and elevated and reduced ambient pressure on the acoustic and mechanical properties of selected sound absorption materials.

1.3 Experimental Approach

In order to study the effects of periodic cold soak and reduced ambient pressure on acoustic performance of typical liner materials, a three phase test program was initiated at the Georgia Tech Research Institute (GTRI).

- Phase I. Acoustic properties were determined for candidate liner material at sub-atmospheric pressure conditions via an impedance tube.
- Phase II. Periodic cold soak and high pressure exposure of liner material was accomplished via a cryogenic test chamber with controlled environment.
- Phase III. Re-evaluation of acoustic properties were determined for the liner material at sub-atmospheric pressure conditions as in phase I in order to establish effects of periodic cold soak. Mechanical resiliency was also examined by compression tests of the liner material before and after periodic cold soak.

Three commonly used liner materials were chosen for testing: Pyrell foam, Fiberglass, and Kevlar. Acoustic properties were determined using a two-microphone impedance tube⁶. The two-microphone method provides acoustic properties for a range of broadband frequencies

simultaneously. Characteristic acoustic properties were computed using the Two Thickness Method, which has been documented by Smith and Parrott⁷. This method has the advantage of being relatively simple to apply.

Phase I tests were conducted in GTRI's sub-atmospheric facility which consists of a large vacuum chamber 154 inches long with a 60 inch inner diameter. Four atmospheric pressure levels were examined: Standard atmospheric, 75%, 50% and 25% of standard.

Phase II tests were conducted in a low temperature/high pressure facility which consists of a cryogenic chamber capable of housing multiple test samples. The chamber environment was controlled automatically by computer which allowed air to alternately cool or heat as well as pressurize and de-pressurize the test samples.

Phase III acoustic tests were conducted in an identical fashion to those conducted in Phase I. The resiliency tests of Phase III were performed on a hydraulic tensile/compression testing machine.

2.0 TEST FACILITIES AND EXPERIMENTAL SET-UP

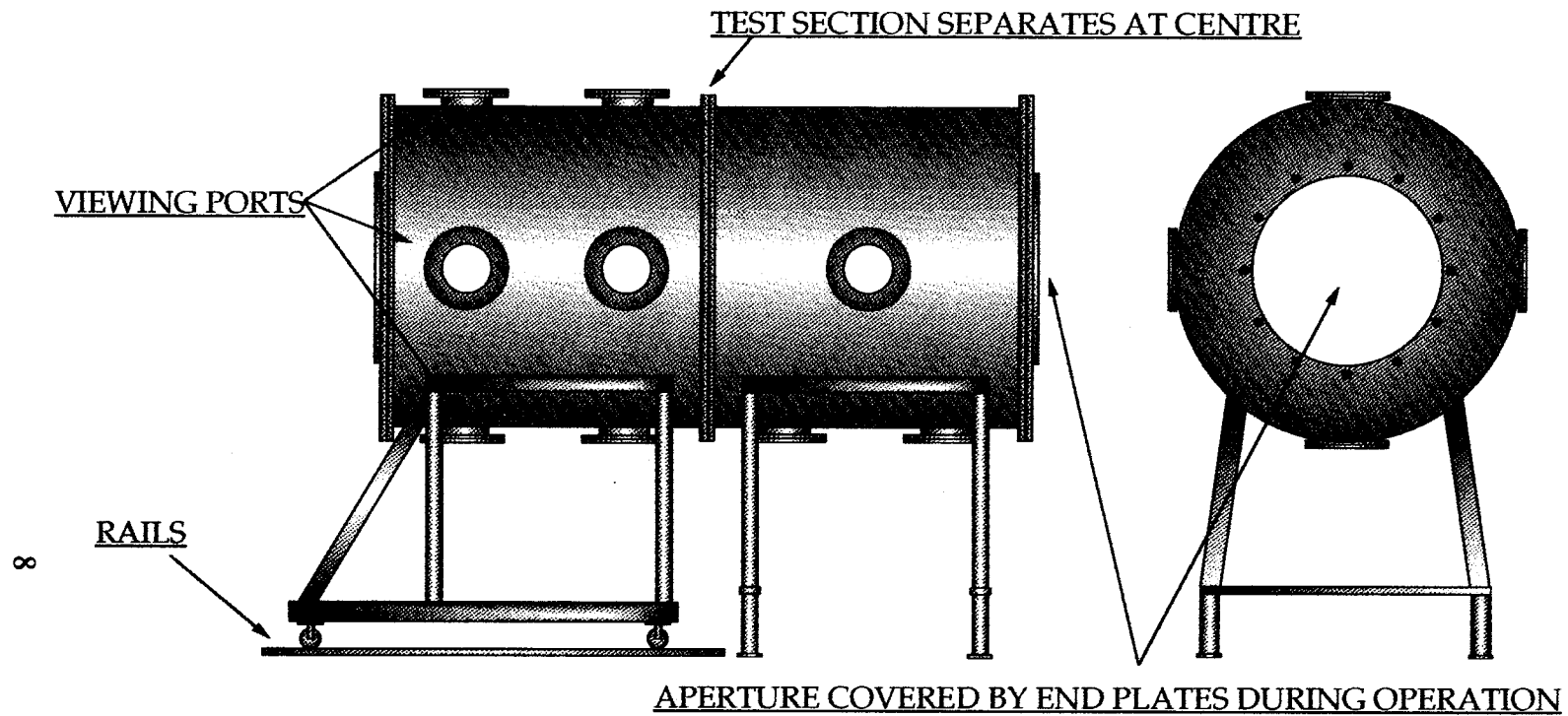
Two main test facilities were used to accomplish the objectives of this program: The Sub-Atmospheric Facility and the Low Temperature/High Pressure Facility. The Sub-Atmospheric facility was used to study the acoustic properties of pressures lower than ambient. The Low Temperature/High Pressure Facility was used to subject the test materials to periodic cold soak and high pressure exposure. Acoustic properties of the candidate bulk materials were evaluated using a two microphone, industrial quality, impedance tube. For the sub-atmospheric tests, the impedance tube was placed inside the vacuum chamber that formed much of the Sub-Atmospheric Facility. Mechanical resiliency tests were performed on a hydraulic tensile/compression testing machine. Descriptions of these facilities and test configurations will be discussed in this section.

2.1 Sub-Atmospheric Facility

2.1.1 General Description

To establish the desired non-standard atmospheric conditions, a suitable testing chamber was developed which could create a low (sub-atmospheric) pressure environment. An existing plenum chamber was converted into a vacuum chamber, capable of housing an impedance tube for acoustic testing. Figure 2.1 shows a schematic of the vacuum facility while figure 2.2 shows the actual facility. The chamber is constructed of 301 stainless steel, with an overall length of 153.8 inches and a test section diameter of 60.0 inches. The test section is lined with 4 inches of Pyrell acoustic foam. A vacuum attachment port is located on the top of the chamber and is connected through flexible metal tubing to a vacuum pump located in a shed outside the building housing the chamber. The port has a manually operated valve to seal the chamber when it reaches the desired test condition.

As shown in figure 2.1, the chamber has two sections: one fixed to the floor (the right hand side section) and the other movable. The movable section glides on rails allowing for easy access to the test section. The chamber is also equipped with a number of access ports which can be used as viewing windows or electronic data interface locations. At present, the chamber has one port equipped with a Plexiglas window for viewing access to the test section.



DIMENSIONS:

Overall length: 153.8"

Overall height: 111.9"

Test section diameter: 60"

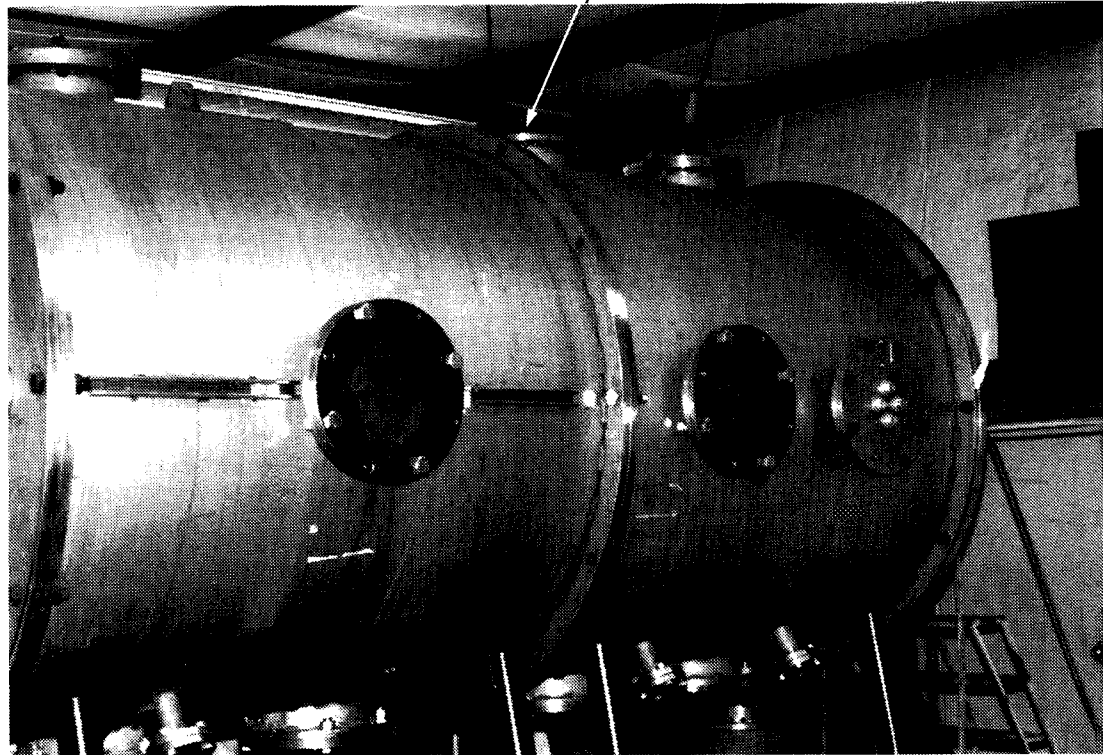
Test section length: 120"

Centre-line above floor: 80"

Viewport diameter: 10.89"

2.1 Schematic of Sub-Atmospheric Facility.

VACUUM PUMP ATTACHMENT



Vacuum Chamber used for sub-atmospheric impedance tube tests.

2.2 Photograph of actual Sub-Atmospheric Facility.

The data interface consists of a plate mounted with four separate circular connectors, three 17 pin connector and one 7 pin connector. The 7 pin connector is used for power supply, while one of the 17 pin connector is used as a data interface. The data interface allowed 8 BNC type electrical connectors to be passed from inside the vacuum chamber test section to the outside for data transfer during vacuum operation. Microphone cables are passed through a small opening on the side of the chamber and sealed separately.

2.1.2 Vacuum Performance

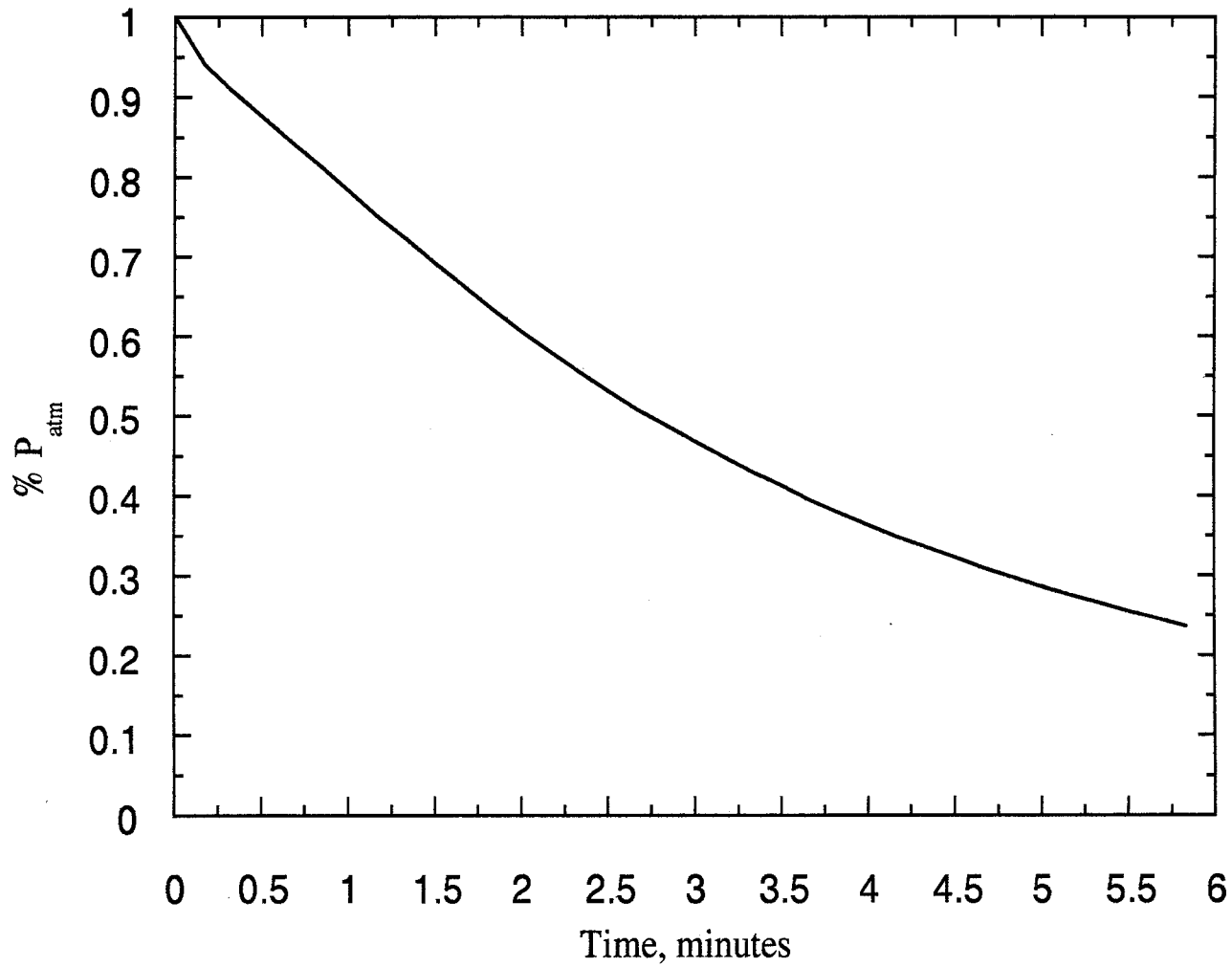
The pump used to evacuate the large vacuum chamber is a model 1395 Sargent-Welch Scientific vacuum pump with 41 Hp at 340 RPM capable of displacing 71 cubic feet per minute. The pump was connected to the vacuum chamber via a 4-inch diameter flexible metal tubing. The vacuum chamber's internal ambient pressure was monitored by a digital pressure transducer. An open port attached to the fixed end of the chamber was connected to the transducer via copper tubing. The internal temperature was monitored with a thermocouple which was placed inside the test section with the display panel fixed in the viewing port.

Once the movable portion of the vacuum chamber was bolted to the fixed portion of the chamber, the vacuum pump was operated until the desired internal ambient pressure was reached. Initial checkout of the vacuum operation showed that an internal ambient pressure of approximately 5% of standard atmosphere could be reached in 30 minutes. Figure 2.3 shows the pressure history during vacuum operation. Note that approximately 8-10 minutes are required to reach 25% of standard atmosphere, the lowest pressure examined in this study. Return to the outside ambient pressure is achieved in approximately 15 seconds by opening one of four 2-inch diameter ports to the chamber.

2.2 Impedance Tube

2.2.1 General Description

An industrial-quality impedance tube, B&K 4206, from Bruel and Kjaer (B&K) was used for the evaluation of acoustic properties of candidate liner material. The B&K 4206 impedance tube utilizes the two microphone method⁶ of determining materials impedance. The 4206 impedance tube provides impedance data for a range of frequencies simultaneously through broadband sound radiation from the tube's acoustic driver. This feature allows relatively quick



2.3 Evacuation rate of GTRI's vacuum chamber facility.

determination of input impedance of liner materials compared to a standing wave impedance tube which acquires data at one frequency at a time. A frequency range of 50 Hz to 6400 Hz is possible by configuring the impedance tube with two measurement tube diameters.

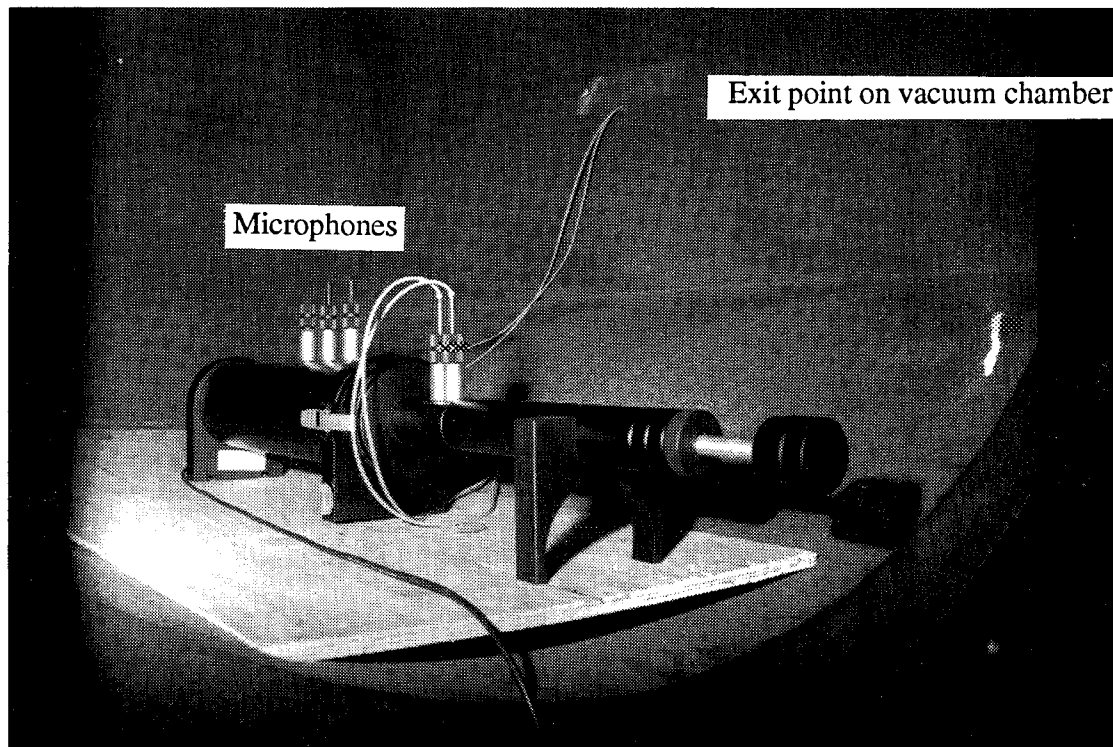
Since the impedance tube relies on plane wave impingement of sound onto the test sample, the tube diameter is critical to the frequency range of interest. The B&K 4206 impedance tube has a 100 mm diameter tube and a 29 mm diameter tube. This ensures plane wave propagation from 50 Hz to 1600 Hz (with the 100 mm diameter tube) and from 500 Hz to 6400 Hz (with the 29 mm diameter tube). The impedance tube was used to determine the acoustic absorption and reflection coefficients as well as normalized input impedance for all candidate liner materials. Material acoustic impedance values were calculated from these measurements.

2.2.2 Impedance Tube Specifications

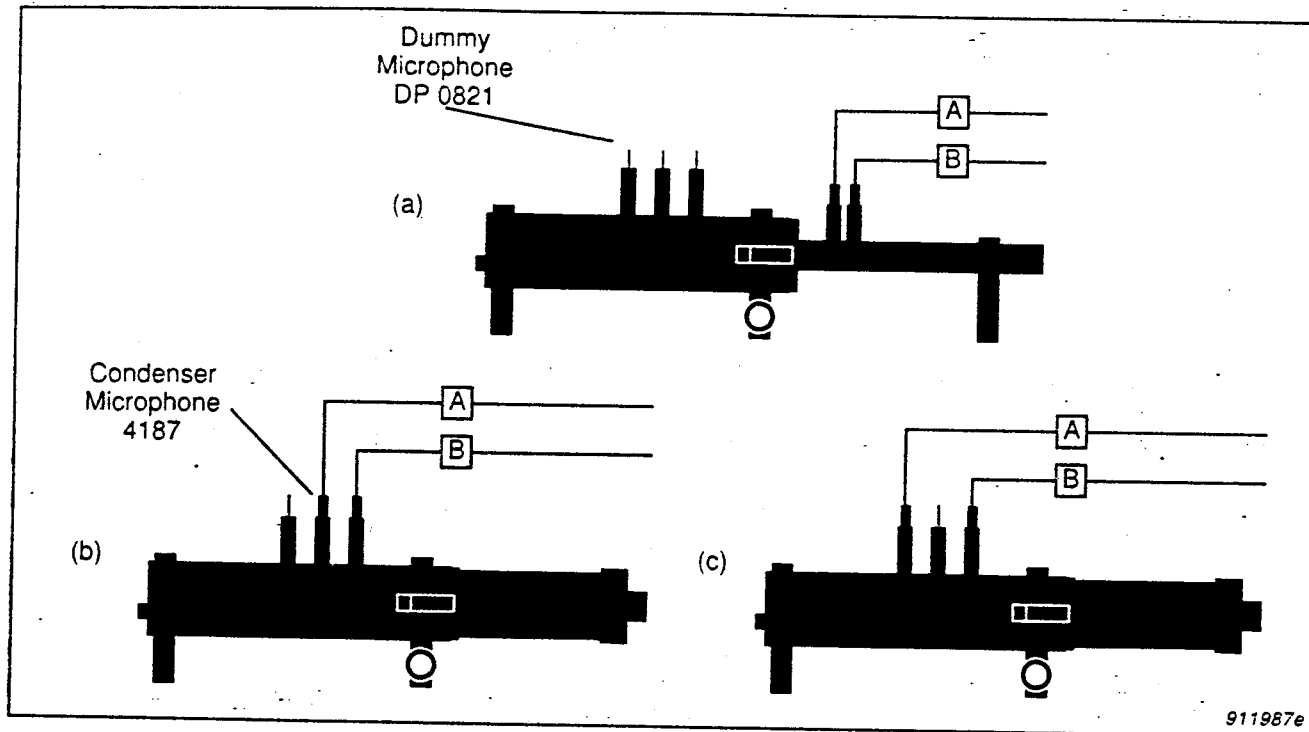
The B&K 4206 Two Microphone Impedance Measurement Tube, shown in figure 2.4, consists of a large and a small measurement tube which corresponds to a large and small sample holder, respectively. The three basic tube set-up types are shown in figure 2.5. The acoustic sound source for the 4206 impedance tube is an 80 mm (3.15 in.) diameter loudspeaker mounted at one end of the tube with a maximum power of 10 Watts. A frequency weighting unit is also provided with the speaker with user-selectable settings of low pass, linear or high pass weighting of the input signal.

The large measurement tube (100 mm diameter) has three flush-mounted microphone ports which allow for two different microphone spacing configurations. Wide microphone spacing (100 mm) gives better measurement coherence at frequencies below 100 Hz. The normal large tube set-up spaces the microphones 50 mm apart for a nominal frequency range of 100 Hz to 1600 Hz and a bandwidth of 2 Hz.

The small measurement tube (29 mm diameter) is mounted directly into the large measurement tube (see figure 2.4) and has two flush mounted microphone ports similar to the large tube microphone ports. The microphone ports are spaced 20 mm apart. The small tube set-up has a nominal frequency range of 500 Hz to 6400 Hz with a bandwidth of 8 Hz.



2.4 B&K 4206 impedance tube installed inside vacuum facility.



2.5 Three basic set-up types for the B&K 4206 impedance tube: a) Small tube-standard; b) Large tube-standard; c) Wide spacing large tube.

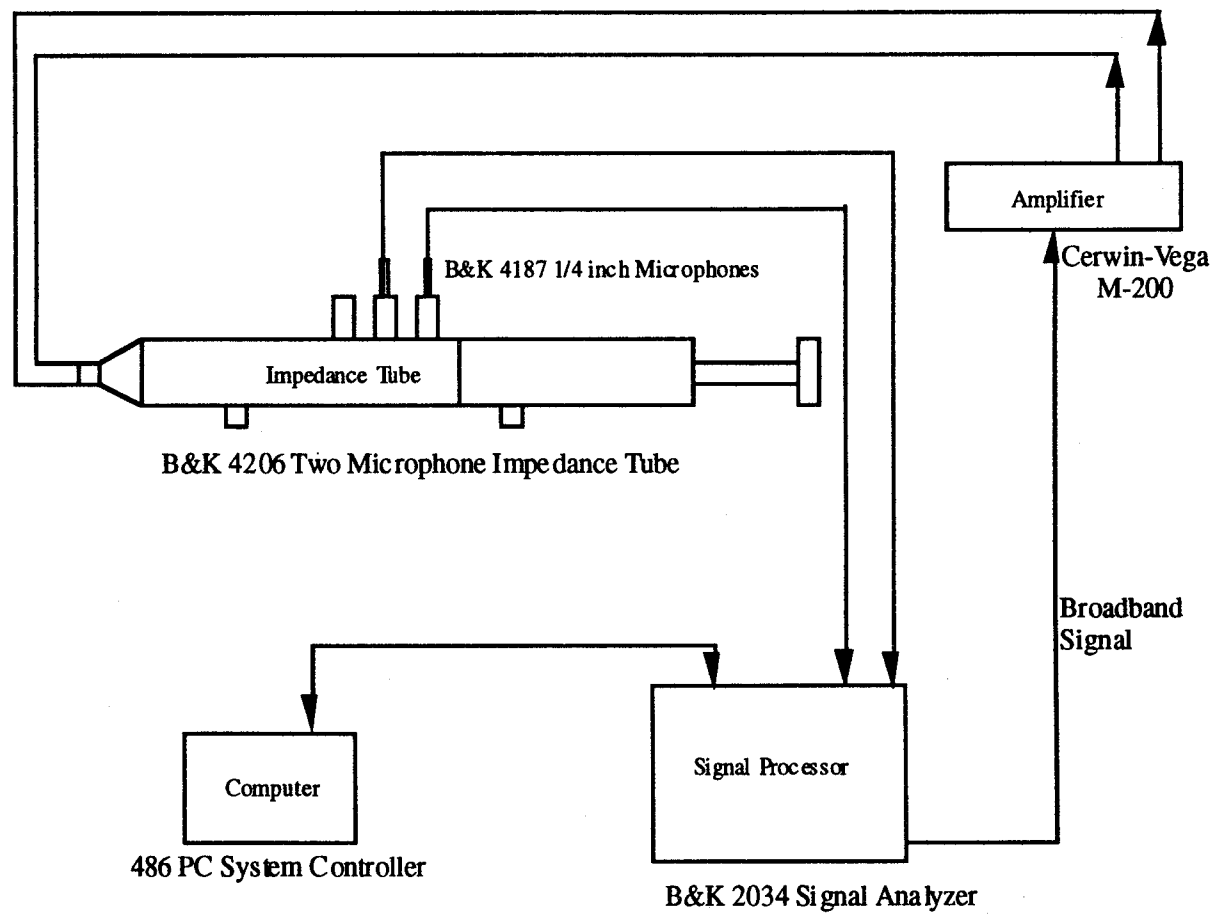
The 4206 impedance tube is supplied with two one-quarter inch B&K Condenser Microphones Type 4187. These microphones are designed to reduce air leakage from the inside of the impedance tube, thus the microphones are well defined with respect to phase. Dummy microphones are also supplied to seal up unused microphone ports in the tube during operation.

2.2.3 Data Acquisition and Processing

The B&K 4206 impedance tube is supplied with application software which works in concert with a two-channel signal analyzer and a 486-based computer to automate the data acquisition process. A B&K 2034 Dual Channel Signal Analyzer was used for the signal processing and a WIN 486 PC was used to control data acquisition. The B&K 2034 analyzer provided a broadband signal which was passed through a Cerwin-Vega amplifier before being sent to the speaker in the impedance tube. The microphone signals were input into pre-amp ports on the dual channel analyzer. Figure 2.6 shows a schematic of the data acquisition system.

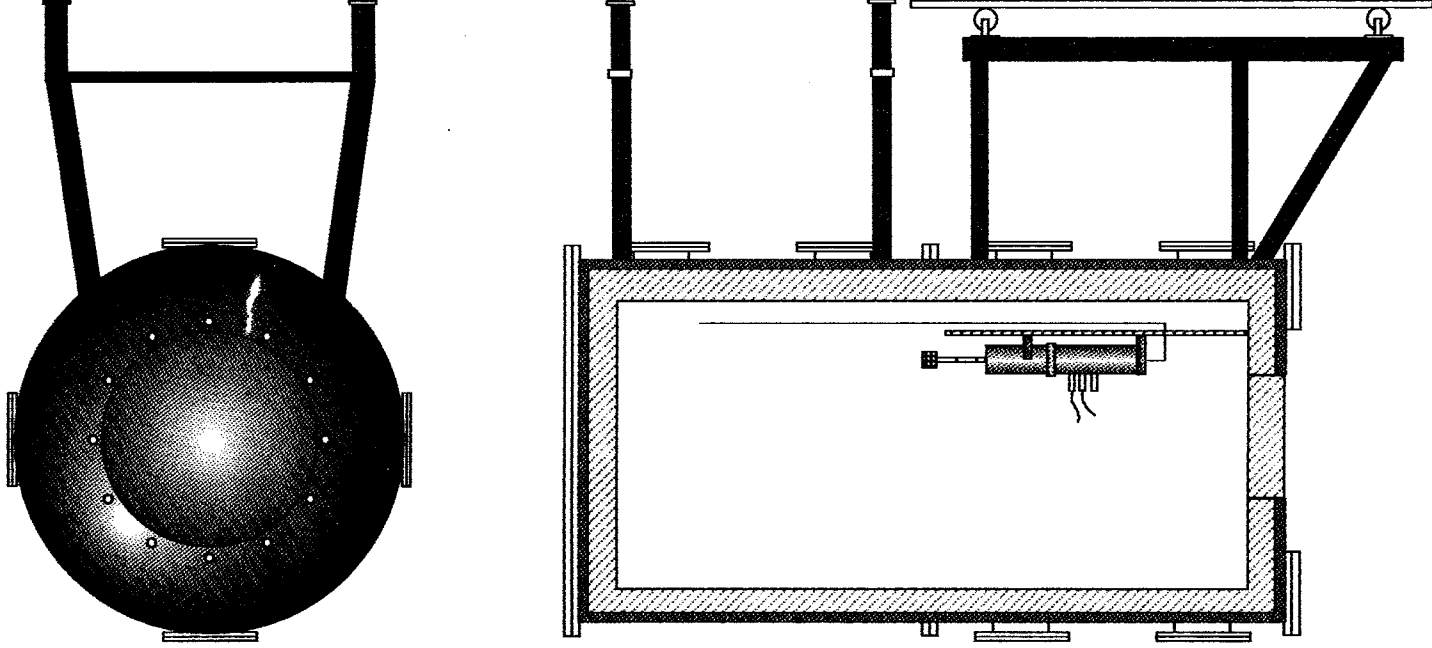
Besides driving the signal analyzer and the B&K 4206 impedance tube, the application software processes the acquired microphone data and calculates reflection and absorption coefficients as well as normalize impedance of the test sample. The software also automated the impedance tube calibration which was performed for each change of tube set-up and atmospheric condition. Acquired spectra for absorption, reflection, and normalized impedance was stored automatically on the computer's hard disk where further processing can be performed.

Sub-atmospheric operation of the impedance tube was performed by placing the tube inside the Sub-Atmospheric Facility as shown in figure 2.7. A very small hole on the underside of the 4206 impedance tube ensures that the inside of the tube reaches the same ambient pressure as the outer environment (in this case, the inside of the vacuum chamber). The equalization of pressure between the inside and outside of the impedance tube was checked qualitatively. A balloon was fastened around an open microphone port on the impedance tube and the vacuum chamber was allowed to reach approximately 25% of atmospheric pressure. As expected, the



2.6 Schematic of the data acquisition system for the B&K 4206 impedance tube.

2.7 Cross section of vacuum facility with impedance tube mounted inside.



balloon expanded as the external pressure decreased faster than the internal pressure of the impedance tube. Within a few seconds, however, the balloon collapsed indicating an equalization of internal and external pressure.

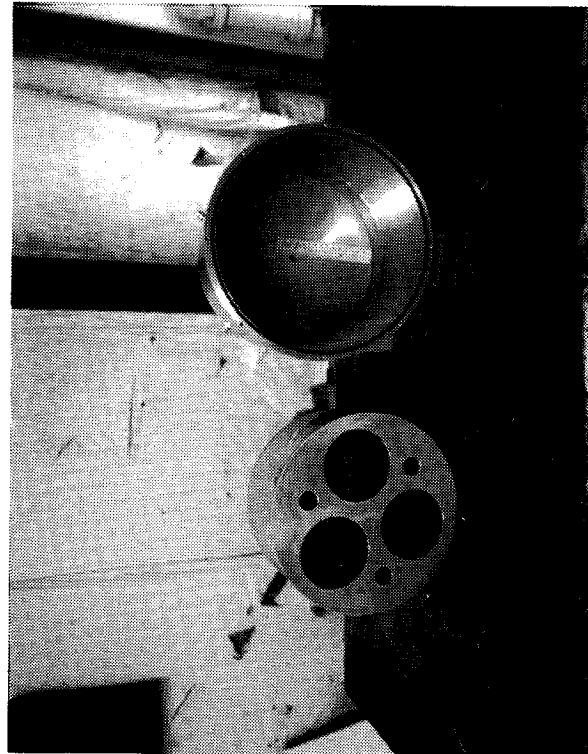
2.3 Low Temperature/High Pressure Facility

A separate facility was developed to simulate a low temperature and high pressure environment for the candidate test materials. The purpose of this facility is to provide a non-standard environment in a cyclic manner. In this way, wind tunnel testing over a long period of time can be simulated in a shorter time frame. Materials exposed to these cycles can then be tested in the impedance tube to determine what, if any, changes have occurred in their acoustic properties. The facility used refrigerants flowing through a test chamber to reduce the temperature of the material to cryogenic temperatures on the order of -150 °F. The details of this system are given below.

2.3.1 Cryogenic Cooling Chamber

Two refrigerants were evaluated for their performance in the system: cooled compressed helium and cooled compressed air. In addition, the chamber design was a blow down system and did not recirculate the refrigerant. This meant that the large number of cycles planned for the present study would consume a considerable amount of refrigerant. Cooled helium was the preferable refrigerant but it was quite costly. Tests with air produced a number of serious problems primarily associated with freezing of air moisture and liquid oxygen which clogged air paths. However as shown below, we were able to circumvent most such problems. Air was thus chosen as the material refrigerant. The chamber which houses the liner material is shown in figure 2.8. The chamber can hold up to three samples of 100 mm diameter and three samples of 29 mm diameter which match the B&K 4206 impedance tube dimensions. The material sample holder which is placed inside the test chamber is shown in figure 2.9.

The temperature of the liner material was monitored with Omega "T" type hypodermic thermocouples. The metal sheath of the thermocouples provides for the use of compression fittings to allow the thermocouples to be connected to the chamber. Three hypodermic thermocouples were inserted into the material sample. To ensure relatively consistent material temperature readings, two thermocouples were placed in one sample: one in the center and one near the outer edge of the 100 mm diameter sample (see figure 2.10 for thermocouple

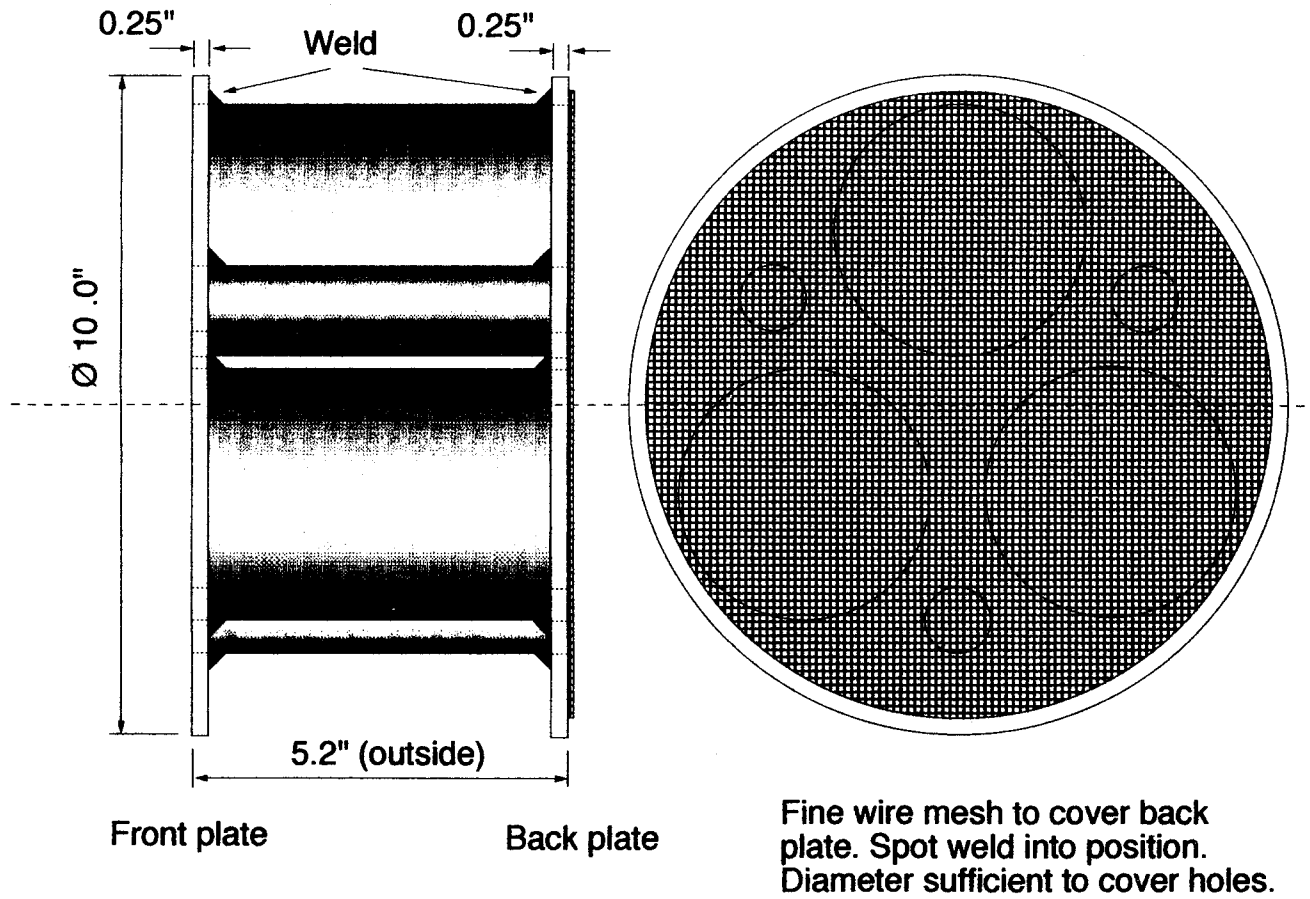


Thermocouple Installation

Sample Holder

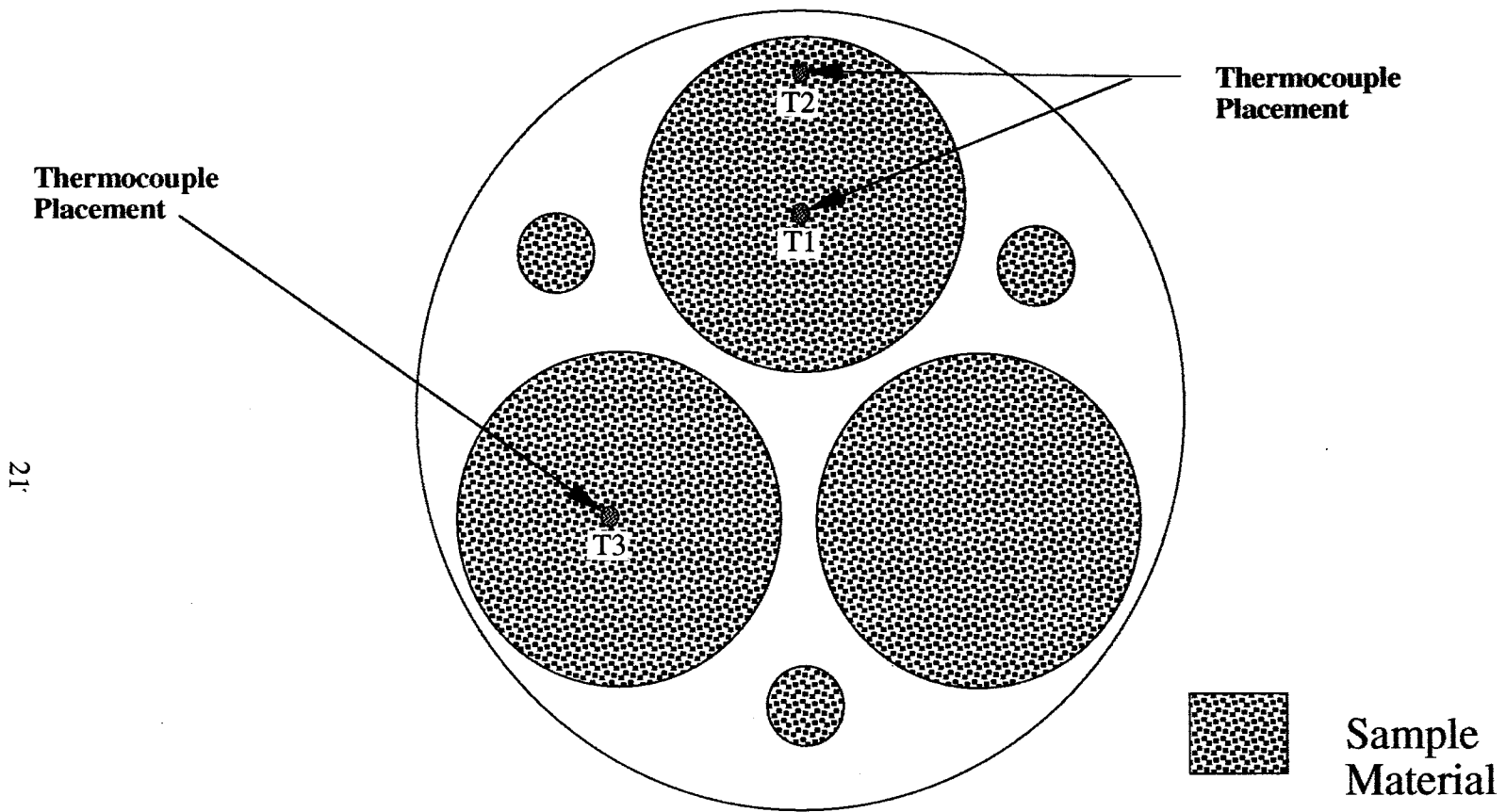
2.8 Cryogenic cooling test chamber.

Cylinder I.D. = 3.8 & 1.0 inches (wall thickness to fit)



20

2.9 Dimensions of the cryogenic cooling material sample holder.



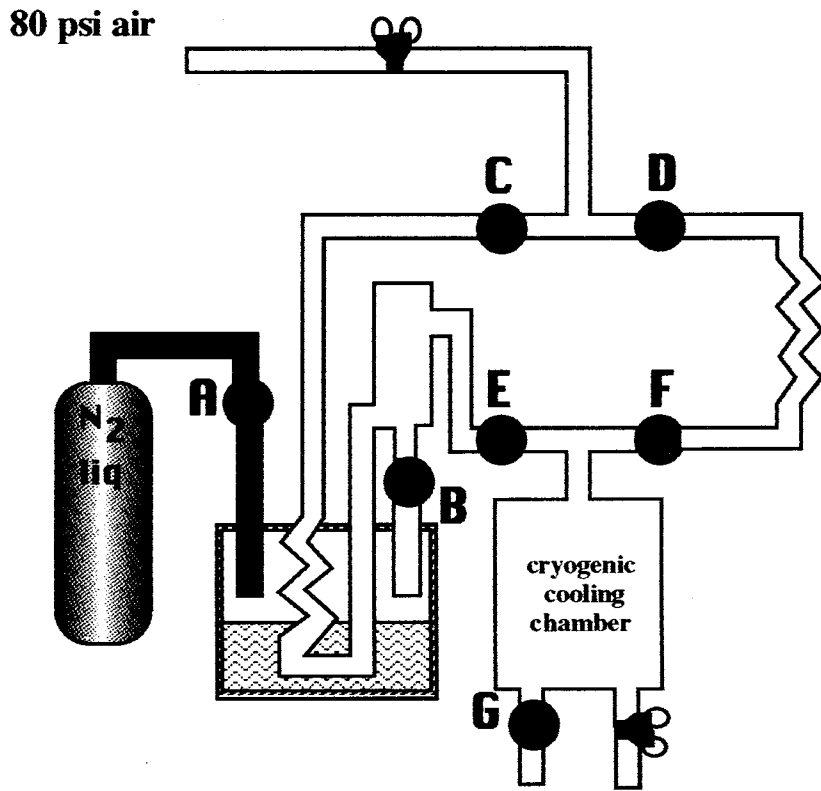
2.10 Sample holder for the cryogenic cooling chamber with thermocouple placements.

locations). The third thermocouple was placed in the center of another 100 mm diameter sample. The larger diameter samples were chosen for thermocouple insertion as any material damage or loss due to the piercing by the sensor would be a small percentage of the overall material volume. Internal chamber pressure was monitored via a digital pressure transducer which was connected directly to the chamber wall with a compression fitting.

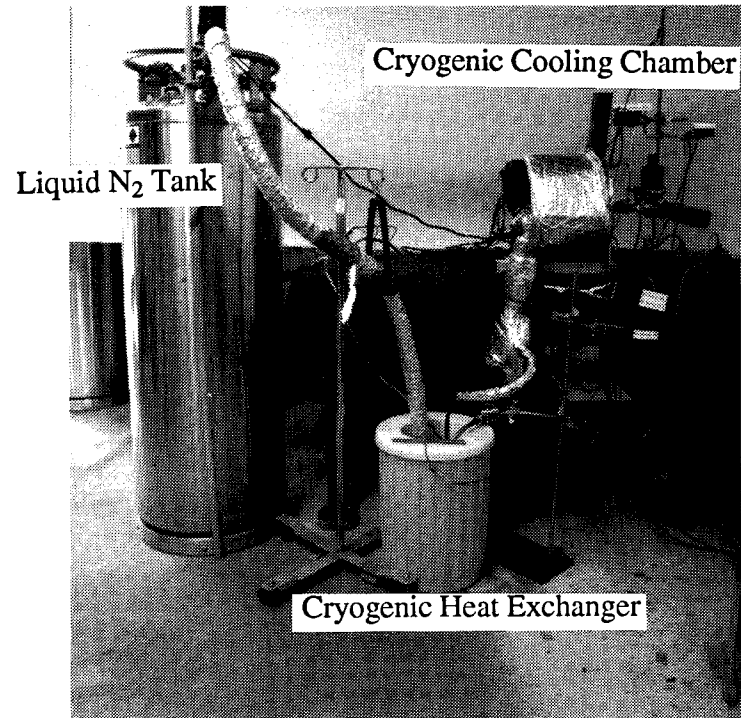
The liner samples were subjected to three phases of cycling: (1) cooling phase, (2) pressurizing phase, and (3) warming phase. A short description of each phase is now provided. A schematic of the entire cryogenic cooling system as well as a photograph of the actual facility is shown in figure 2.11. The air flow through the facility was controlled with solenoid valves which are labeled A through G in figure 2.11. Valves A, B, E, F, and G are special cryogenic solenoid valves, able to withstand temperatures as low as -400°F .

Cooling Phase

In order to cool the liner material samples in the test chamber, super cooled air must be produced. Compressed air (approximately 80 psi) is first passed through a heat exchanger which consists of coiled copper tubing submerged in liquid nitrogen. It was imperative that the air be as dry as possible before entering the heat exchanger because any moisture would freeze quickly and potentially clog the flowpath. Initially, this problem was encountered but it was abated by using an industrial air dryer upstream of the facility. The air dryer along with low humidity atmospheric conditions sufficiently alleviated the clogging problem. A precaution was taken to ensure that liquid oxygen was prevented from being blown into the test chamber. The cryogenic cooling of the air via liquid nitrogen reduced the air temperature close to or below the boiling temperature of molecular oxygen (-280°F). Accordingly, an oxygen "trap" was inserted after the heat exchanger but before the test chamber, which used gravity to separate the liquid oxygen formed from the air (valve B in figure 2.11). Once during every cycle, the liquid oxygen is dumped into the liquid nitrogen container. Once cooled, the air enters the test chamber and flows through the liner material samples placed in the six cylindrical sample-holding slots. Figure 2.12 shows how the air flow passed through the material samples in the cryogenic cooling chamber. When the hypodermic thermocouples read an average desired temperature, the next phase began.



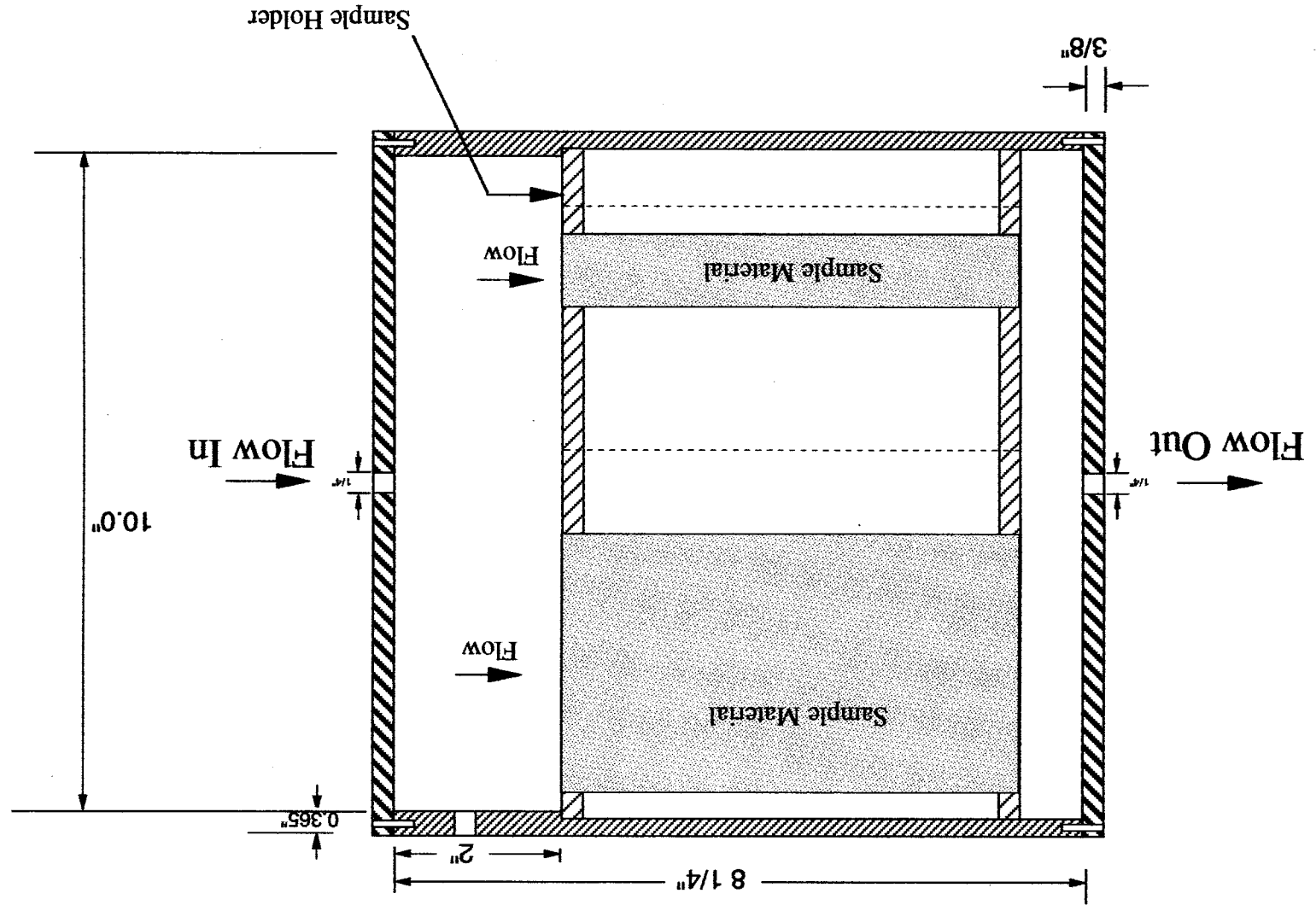
Schematic of Cooling/Heating System



Actual System

2.11 Cryogenic Cooling Facility.

2.12 Air flowpath through the cryogenic cooling chamber.



Pressurizing Phase

At the desired reduced liner material temperature, the exhaust valve on the back of the test chamber (valve G in figure 2.11) is closed and the pressure is allowed to build to a specified value. Once this pressure is reached, it is held for a pre-determined length of time. Then the chamber is vented back to ambient pressure.

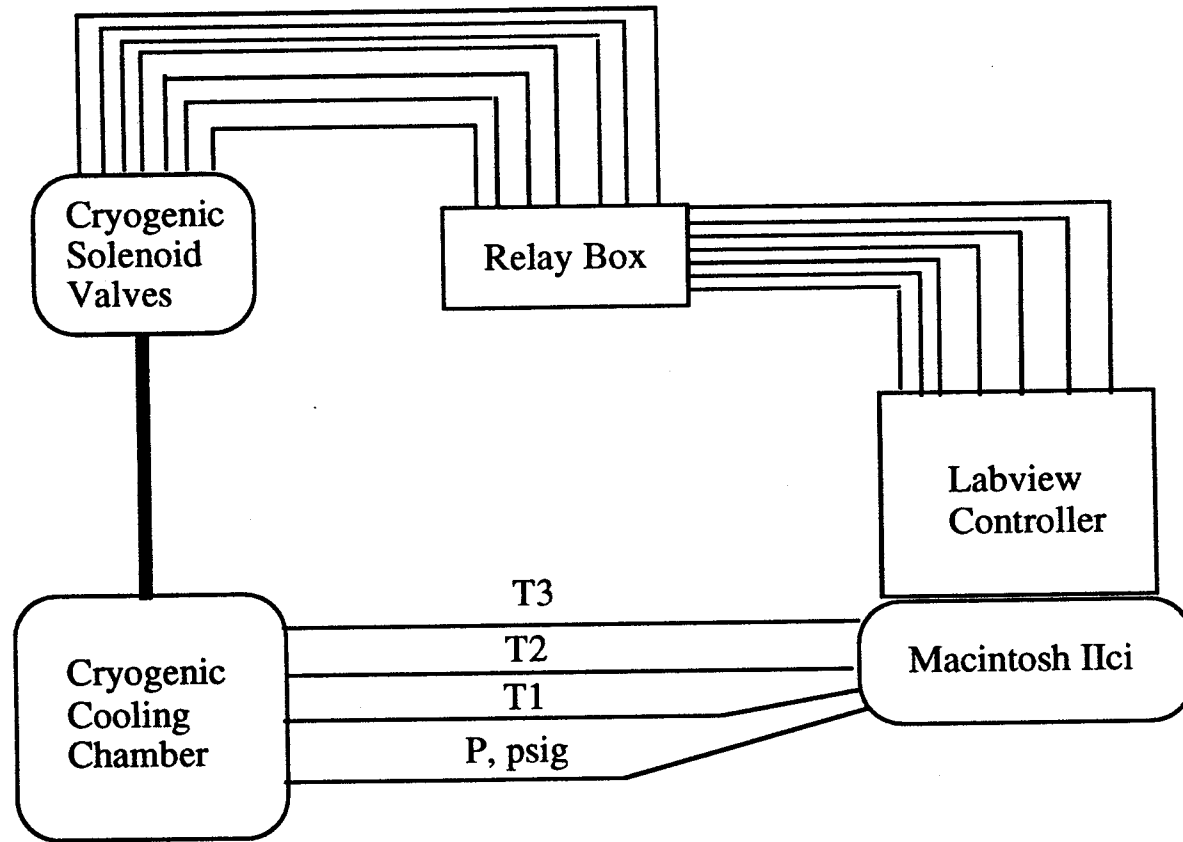
Warming Phase

To complete the cycle, the liner material needs to be brought back to its ambient temperature condition. This is done by passing the compressed air through another heat exchanger which has coiled copper tubing immersed in a bath of hot water. The water is heated with an industrial quality immersion heater. Once the average liner material reaches ambient condition, the cycle begins again with the cooling phase.

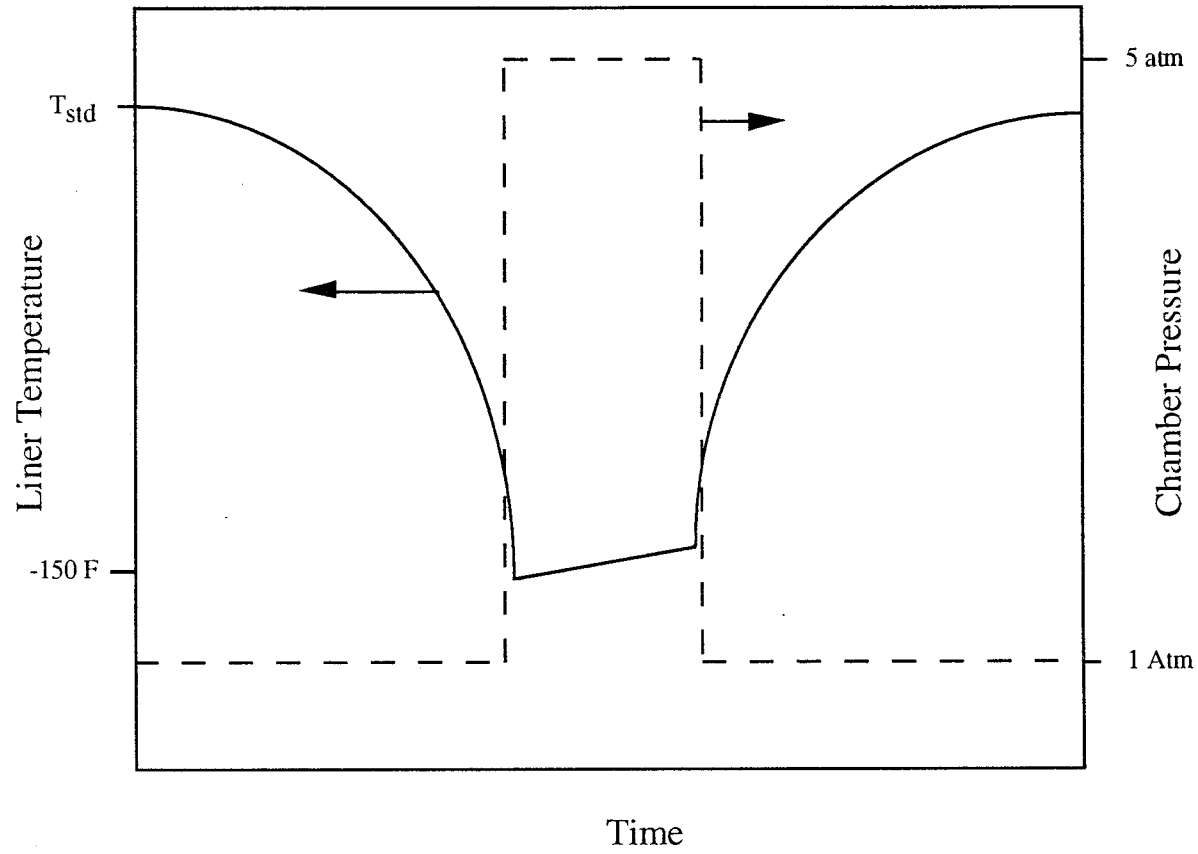
2.3.2 Data Acquisition and Control

The cycle process previously outlined was executed 250 times for each liner material tested. Therefore, the facility was designed to operate automatically under computer control. The solenoid valves, which are marked A-G in figure 2.11, were used to control the air flow and the liquid nitrogen and were programmed to operate at prescribed times. A graphical language program called LabView (National Instruments) was used to implement the cycle process on a Macintosh IIfx platform. Using feedback from the hypodermic thermocouples as well as the test chamber pressure and liquid nitrogen temperature, LabView alternately opened and closed the correct valves. This allowed for "hands off" operation of the facility and provided consistency in testing for the numerous cycles that were performed. The only manual part of the operation was the changing of the liquid nitrogen tanks. A schematic of the computer-facility data acquisition and control system is shown in figure 2.13.

The LabView program sampled the hypodermic thermocouple as well as the chamber pressure transducer every 20 seconds. The data were stored real time on the computer's hard disk. A cycle profile, with target temperatures and pressures for valve switching, was input in the computer program. Figure 2.14 shows a temperature and pressure profile for a generic cycle process.



2.13 Schematic of data acquisition system for the Cryogenic Cooling Facility.



2.14 Generic temperature and pressure cycle profile for the Cryogenic Cooling Facility.

3.0 TEST SAMPLE FABRICATION AND TEST PLAN

3.1 Liner Materials Used for Testing

Three liner material samples were chosen for testing. There were: typical open-celled foam called Pyrell, a form of Fiberglass, and layered Kevlar fabric. These materials represent a wide range of bulk densities and porosities. Table 3.1 lists the porosity and density of each test sample.

	Porosity (% open space)	Density (g/cm ³)	Remarks
<i>Pyrell Foam</i>	91	0.03328	Open-Celled Foam
<i>Fiberglass</i>	95	0.05437	Layered Fibers
<i>Kevlar</i>	87	0.09454	Compressed Fiber Cloth

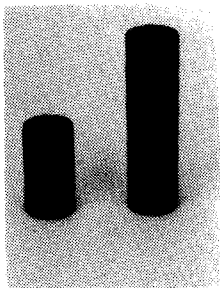
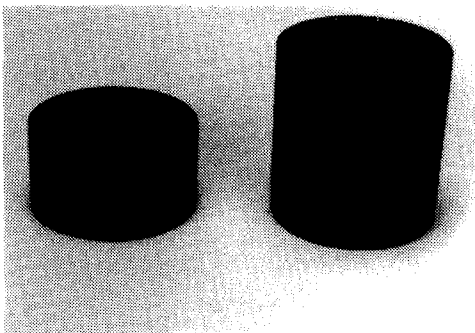
Table 3.1 Physical properties of liner material chosen for present study.

Figure 3.1 shows photographically the three liner materials tested. Each test material was obtained from a different source and was not available in the same thickness. The Pyrell foam existed in 4-inch thick sheets. The Fiberglass came in 2-inch thick sheets while the Kevlar fabric was available in the form of 0.375-inch sheets.

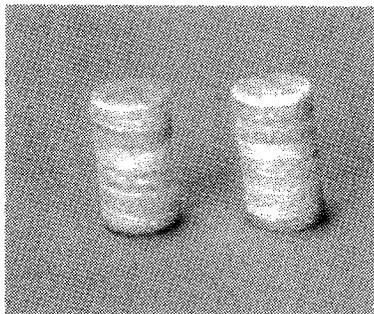
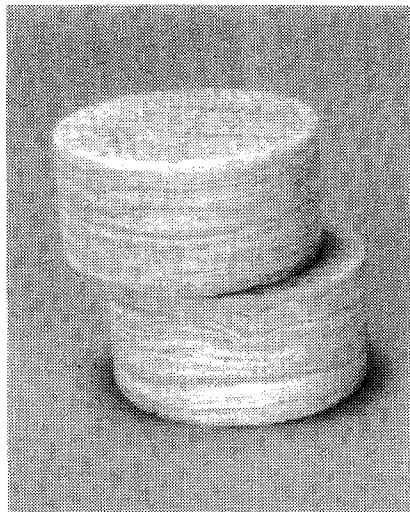
Characteristic acoustic properties were calculated using the Two Thickness Method, relying on impedance testing of two different thicknesses of each material, specifically, one sample being twice as thick as the other sample. Details of this approach and measurement technique are presented in appendix A.

3.2 Sample Cutting Process and Impedance Tube Mounting

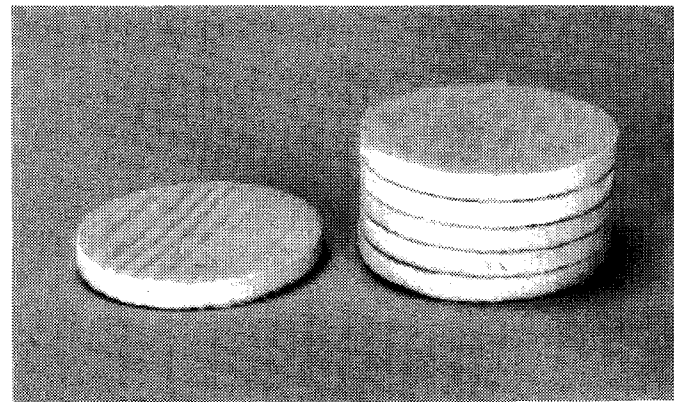
Two different thicknesses of each material were cut using a circular cutting tool. Two different diameter cutting tools were fabricated which correspond to the diameters of the B&K



Pyrell Foam



Fiberglass



Kevlar

3.1 Liner materials tested in present study.

4206 impedance tube. The cutting tool was used in conjunction with a sample holding jig which holds a square material sample. By placing the cutting tool and holding jig on a lathe, a circular sample can be cut as the holding jig is forced into the spinning cutting tool. Figure 3.2 shows one of the sample cutting tools and its corresponding sample holding jig. Various lathe rpm's were tried before quality cylindrical samples could be cut.

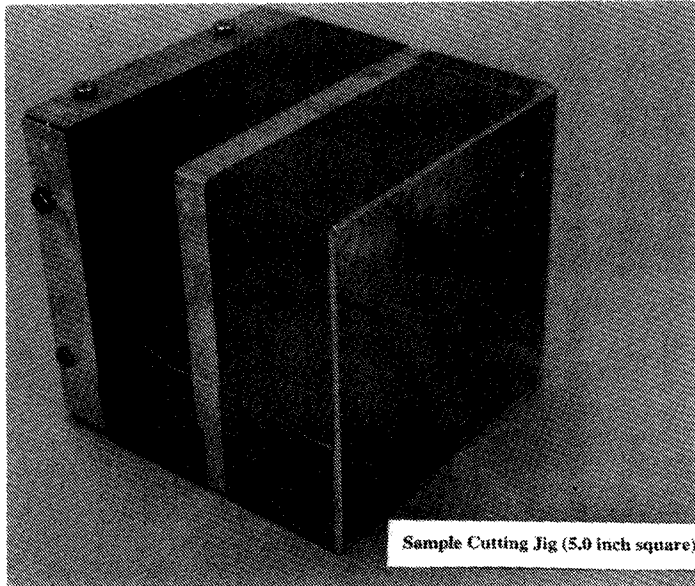
Once cut into cylindrical pieces, the samples can be placed either in the B&K 4206 impedance tube or the cryogenic cooling chamber. No special mounting techniques were employed for impedance tube mounting (i.e., no epoxy or tape was used). Mounting test samples is an important factor in impedance tube testing. If the boundary conditions are not completely satisfied, the measurement technique loses accuracy. The boundary conditions required to be met in an impedance tube are that the test sample is in contact with an acoustically hard or rigid surface everywhere except that portion which faces the sound source. Thus, if any air gaps (or conversely, compression of material, i.e., too tight a fit) exist around the sample, the measurement of acoustic properties would not be completely accurate. With this in mind, care was taken in the cutting of the liner samples to fit in the impedance tube. In general, good quality "fits" were produced using the method described above.

The samples fit into the sample tube of the B&K 4206, which was mounted horizontally in the sub-atmospheric facility (see figure 2.7). Because of the fixed thicknesses which the material was originally available in, stacked mounting was used to achieve desired thicknesses of Fiberglass and Kevlar. The interface surfaces were not continuous and thus do not reflect exactly a sample of continuous bulk density. How this mounting technique affects the calculation of the acoustic properties will be discussed later.

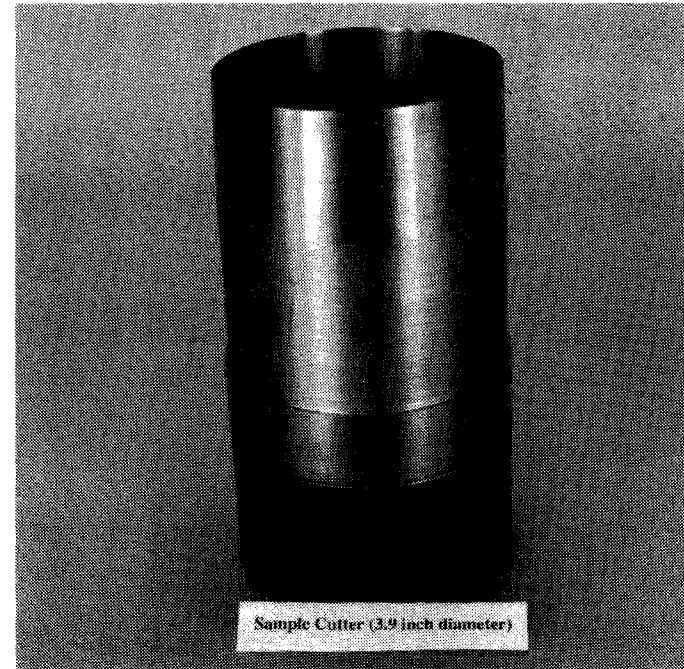
3.3 Test Plan

3.3.1 Sub-Atmospheric Acoustic Test

Tests performed in the B&K 4206 impedance tube were carried out before and after the Low Temperature/High Pressure cycle test. Each material was tested for two different thicknesses, two different diameters and at four different atmospheric pressure conditions. Table 3.2 shows the test matrix followed for this study.



Sample Holding Jig



Cutting Tool

3.2 Test sample fabrication tools.

Material	Diameter	Pressure	Length
Pyrell	29.0 mm	100%,75%,50%,and 25% of ambient	50.8 mm
"	"	"	"
"	"	"	101.6 mm
"	"	"	"
"	100.0 mm	"	50.8 mm
"	"	"	"
"	"	"	101.6 mm
"	"	"	"
Fiberglass	29.0 mm	100%,75%,50%,and 25% of ambient	50.8 mm
"	"	"	"
"	"	"	101.6 mm
"	"	"	"
"	100.0 mm	"	50.8 mm
"	"	"	"
"	"	"	101.6 mm
"	"	"	"
Kevlar	29.0 mm	100%,75%,50%,and 25% of ambient	28.6 mm
"	"	"	"
"	"	"	57.2 mm
"	"	"	"
"	100.0 mm	"	28.6 mm
"	"	"	"
"	"	"	57.2 mm
"	"	"	"

Table 3.2 Test matrix for sub-atmospheric study of liner material acoustic properties.

3.3.2 Low Temperature/High Pressure Cycle Test

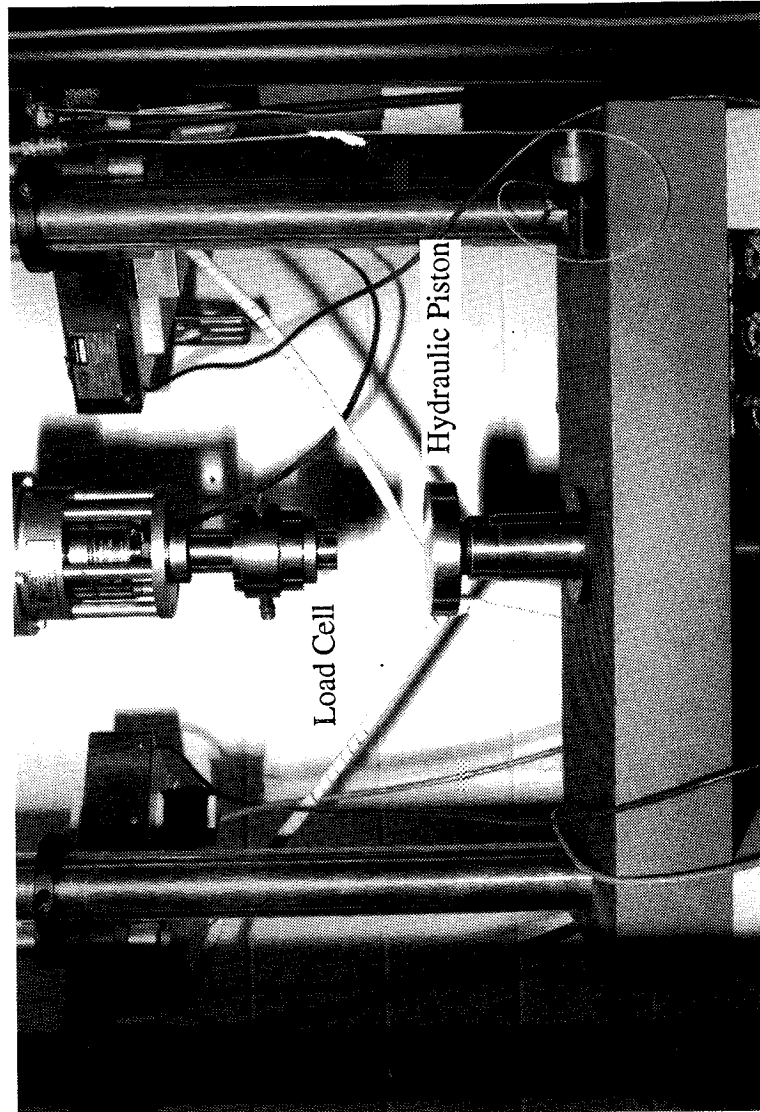
The low temperature/high pressure cycle test for each material was carried out after the initial acoustic property tests were completed. Each material was subjected to 250 cycles in the cryogenic cooling test chamber. Only one material was tested in the chamber at a time, so a total of three, 250 cycle, tests were conducted. For each test, the material sample was cooled to -150 °F nominally. At this low temperature, the test chamber was pressurized to 500% atmospheric pressure nominally. This condition was held for 1 minute until the chamber was returned to atmospheric pressure. The samples were then warmed back to nominal temperature of 70 °F, thus completing the cycle.

3.3.3 Mechanical Resiliency Test

As a way of determining the mechanical effects of continuous cycling on acoustic liners, a test was set up which measured the material's resiliency before and after continuous cycling. Only Pyrell and Fiberglass materials were used for this test. The nature of the Kevlar fabric along with its available thickness precluded any useful results in this test. A hydraulic tensile/compression machine was used to compress the liner samples (see figure 3.3). The hydraulic drive compressed the samples to a specified thickness (one-half, one-quarter the total thickness). The sample was then unloaded and allowed to return to its original shape. Any differences from the original thickness was recorded. Results from the before and after cycled material were then compared to ascertain any evidence of reduced resiliency.

Each test sample was also examined visually for any obvious changes in structure, color, and hardness.

ORIGINAL PAGE
BLACK AND WHITE PHOTOGRAPH



3.3 Hydraulic tensile/compression rig used for mechanical resiliency tests.

4.0 RESULTS OF NON-STANDARD ATMOSPHERIC TESTS

4.1 Summary of Findings

The results of sub-atmospheric acoustic tests, before and after cycling through a very low temperature and high pressure environment, are summarized in the following statements:

- 1). Sub-Atmospheric pressure reduces the absorption performance of the bulk materials tested. However, this trend is not linear.
- 2). Repeated cryogenic cooling and pressurization of tested materials seem to have no effect on acoustic properties.
- 3). Repeated cryogenic cooling and pressurization have no effect on mechanical resiliency (only Pyrell and Fiberglass).

These are the basic conclusions of the present work and they directly address the questions posed in Section 1. The results indicate that prolonged exposure of acoustic liners to non-standard atmospheric conditions, have no detrimental effects on the acoustic properties of this material. This has positive implications for wind tunnel designs that may have acoustic as well as aerodynamic testing capability.

In addition to the central conclusions stated above, insight was obtained on the acoustic absorption characteristics of the different materials tested. For example, it was found that Kevlar reached its peak absorption performance after approximately one inch of thickness is achieved. Also, some limitations were observed in the application of the Two Thickness Method to determine the characteristic properties. Detailed results of the impedance tube, cryogenic cooling and mechanical resiliency tests will follow. Note that only select data will be presented in the forthcoming discussion. The data in its entirety will appear in Appendix B. Finally, unless otherwise stated, all acoustic impedances quoted in this report are normalized i.e., the measured acoustic impedance is normalized with respect to the ambient impedance of air.

4.2 Impedance Tube Results - A Confidence Check

To obtain confidence in the accuracy of results obtained from the B&K 4206 impedance tube system described in Section 2 of this report and also in the "Two Thickness Method" of determining characteristic acoustic properties, comparison with other available data was made. This was done by using data acquired under another task funded by NASA under the technical monitorship of Mr. Tony Parrott⁸. A ceramic honeycomb material (CT73) obtained from NASA Langley Research Center was cut into two samples with diameter of 29 mm and thickness of 43.94 mm (1.73 inches) and 87.88 mm (3.46 inches), respectively. The samples were mounted in the impedance tube with no special sample mounting attachment, (i.e., no epoxy or tape). Figure 4.1 shows a comparison of characteristic acoustic property data acquired at GTRI and data acquired at NASA and provided by Mr. Tony Parrott. The NASA data were acquired with a non-circular impedance tube (thus a non-circular test sample) with a material surface area somewhat larger than that used in the GTRI data. Also the NASA test sample was mounted in the impedance tube with epoxy. Even with these noted differences, figure 4.1 shows very good agreement between GTRI data and NASA data. The GTRI results were obtained using the Two Thickness Method outlined in appendix A.

To obtain further confidence in our results, absorption coefficient and input impedance data were also compared with data from GE⁹. Figure 4.2 shows comparison of GTRI acquired impedance data with those of GE for Kevlar fabric. There is very good agreement with between the GTRI data and the GE data. The Kevlar samples were provided to GTRI by NASA in 9.525 mm (0.375 inch) thick sheets. To produce a 19.05 mm (0.75 inch) thick sample for comparison with GE data, two samples were placed on top of each other in the B&K 4206 impedance tube. The type of impedance tube and mounting conditions were not specified in the reference where the GE data was found. However, the apparent discrepancy with the GTRI data at about 2250 Hz in figure 4.2 can be explained by the non-continuous Kevlar sample. By placing sheets of sample on top of each other to obtain a pseudo-continuous thickness, the possibility of impedance mis-matching between surfaces is almost certain.

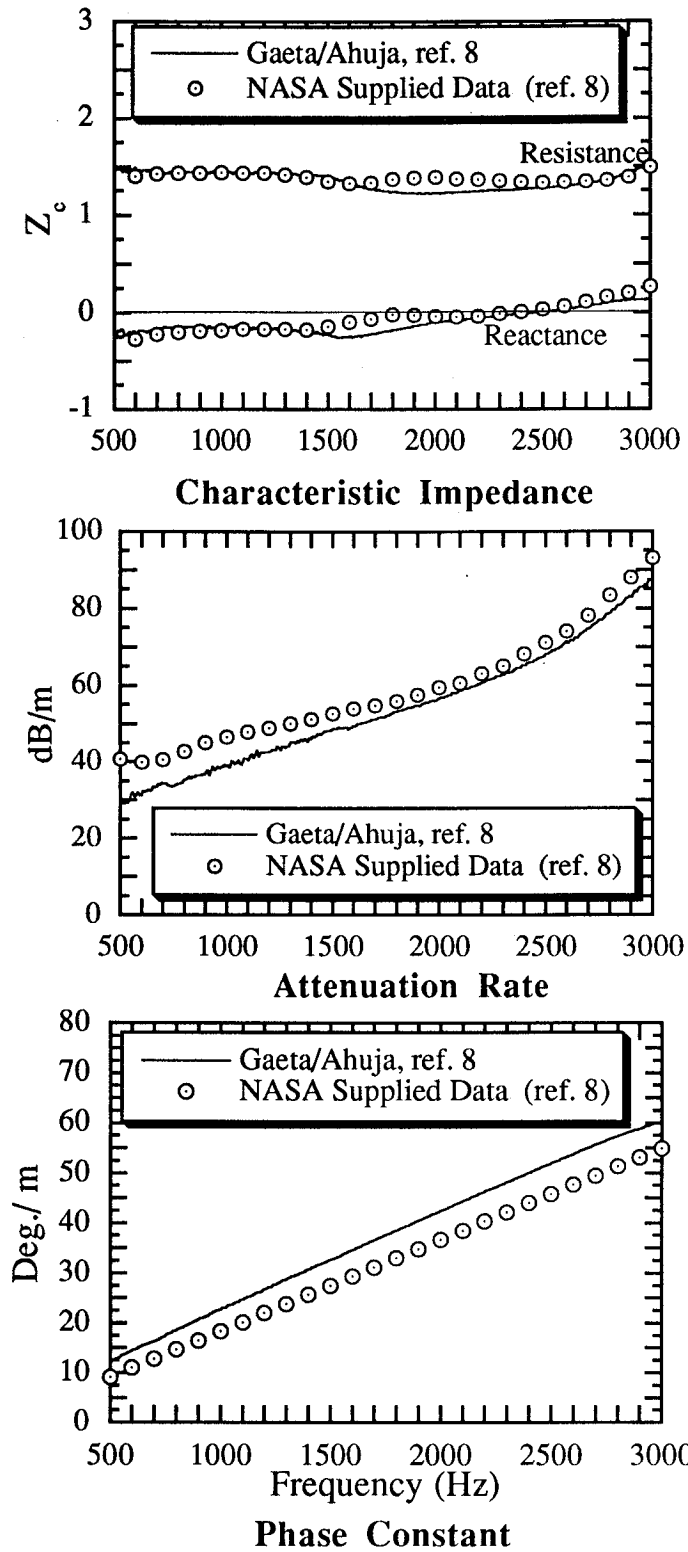
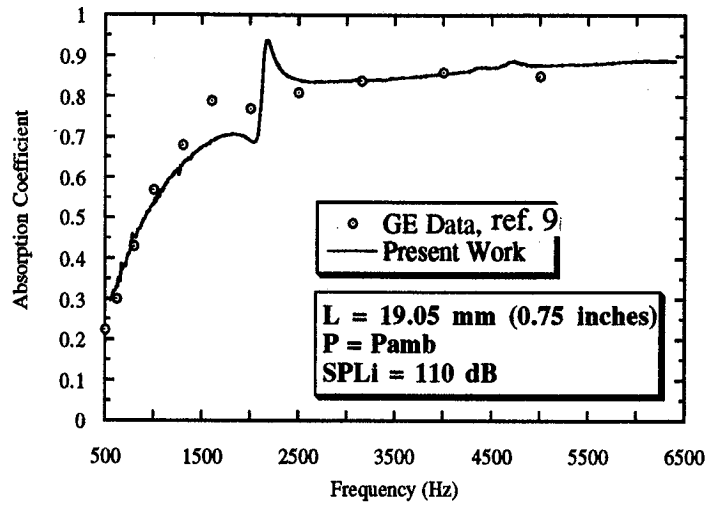
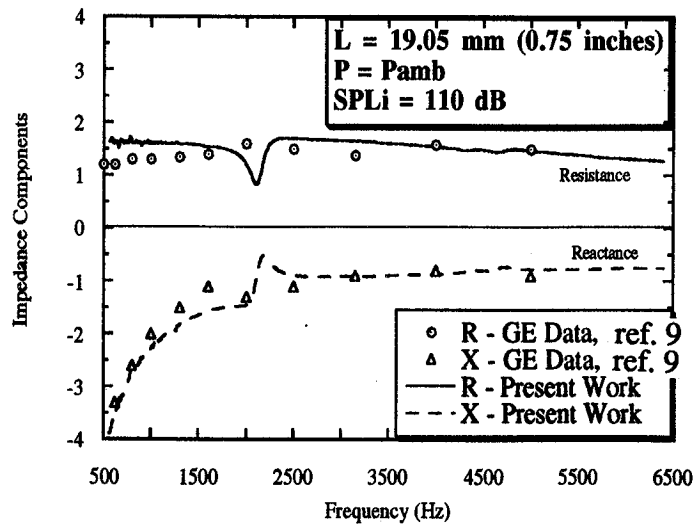


Figure 4.1 Two Thickness Method comparison with NASA CT73 ceramic honeycomb characteristic acoustic data.



Absorption Coefficient



Specific Input Impedance

Figure 4.2 Comparison of present data with GE data for Kevlar, L=19.05 mm (0.75 in.)

4.3 A Word About Impedance Tube Data Overlap

The operating principles of an impedance tube require that a planar sound wave travel from one end of the tube and strike a sample at the other end of the tube. For this to occur, higher order duct modes must be not be excited. For a given tube cross sectional area (in the present case, diameter), a plane wave can be sustained with no higher order modes up to a certain frequency known as the "cut on" frequency. The "cut on" frequency is that which excites the next higher order duct mode.

The B&K 4206 impedance tube is equipped with two sample holding diameter sections (see Section 2). This is to provide a wider range of frequencies which will produce plane wave propagation inside the tube. The 100-mm diameter tube has a plane wave frequency range of 16 Hz to 1600 Hz. The 29-mm diameter tube has a frequency range of 500 Hz to 6400 Hz. Note that there is a range, 500 Hz to 1600 Hz, where the data from both tube sizes overlap. One should expect that the data in this range should be identical for each tube size. This is rarely the case in practice. There are two main reasons for this. First, there is no adequate way of ensuring the same mounting conditions for the samples used in the small tube and the large tube without introducing epoxies and other foreign material. Since the mounting conditions are not identical, the measured input impedance is not identical. Secondly, any surface non-uniformities in the material may be small as a percentage of surface area for the large-tube sample but relatively large for the small-tube sample. This may result in different measured impedances.

Nevertheless, even though a perfect data match will not occur in the overlap region, one should expect to see similar trends. As an example of this reality, figure 4.3 shows absorption coefficient results for Fiberglass with the two impedance tube diameters. Note that the trends are similar even though the actual data are not identical in the overlap range. Since the small-diameter tube covers a larger frequency range, all data shown in this section of the report uses data from the 29- mm diameter impedance tube. More comprehensive data including the larger impedance tube diameter are presented in Appendix B.

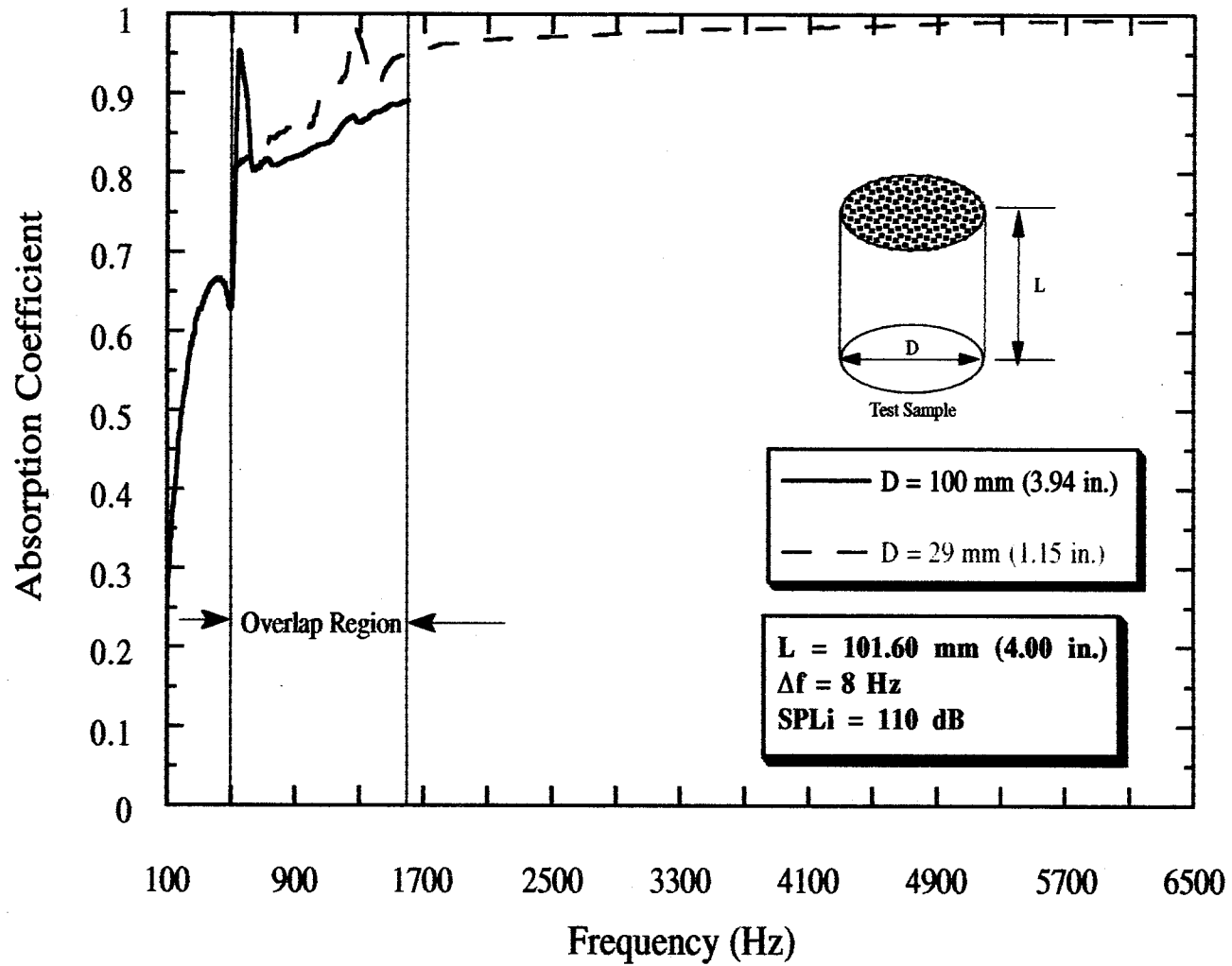


Figure 4.3 Example of "data overlap" from impedance tube results of Fiberglass.

4.4 Sub-Atmospheric Pressure Effects

Following the test matrix shown in table 3.2, reduced-pressure effects on the acoustic properties of the liner materials were carried out in the vacuum chamber facility. The effect of reduced pressure on the bulk materials tested was a diminished degree of sound absorption. This effect was more pronounced in Kevlar and less pronounced in Fiberglass and Pyrell. Figures 4.4, 4.5, and 4.6 show the absorption coefficient spectra for Pyrell, Fiberglass, and Kevlar, respectively. The data shown in these figures were obtained from the 29-mm diameter samples of specified lengths, thus the frequency range was 500 Hz to 6400 Hz with a band width of 8 Hz. Similar trends were found with the larger diameter samples with a frequency range of 100 Hz to 1600 Hz and band width of 2 Hz. There is an apparent discontinuity in the Fiberglass and Kevlar data in figures 4.5 and 4.6, respectively. For Fiberglass, this occurs around 1250 Hz and for Kevlar around 1750 Hz. As alluded to earlier in this section, it is believed that this phenomenon is the result of surface discontinuities inherent in the test samples arising from the multiply-stacked layers of material needed to achieve the desired length. The discontinuity is more prevalent in the Kevlar where six layers were stacked together to achieve a thickness of 57.5 mm (2.25 inches). Only two layers of Fiberglass material were used to obtain a 101.6 mm (4.0 inch) test sample.

Fiberglass Results

Characteristic acoustic properties were computed and were consistent with the absorption coefficient data presented above. For Fiberglass, the lengths tested were 50.8 mm (2.0 inches) and 101.6 mm (4.0 inches). From the input impedance of these two tests the characteristic impedance was calculated (see Appendix A for calculation details) and is presented in figure 4.6. Figure 4.7 shows only the two extreme ambient pressures tested, namely, atmospheric and 25% of atmospheric. The trends show that the reactance for the 25% case is more negative than the atmospheric case. Also the resistance for the 25% case is more positive than the atmospheric case. It is this trend that is reflected in the reduced absorption coefficient for 25% atmospheric pressure. This is consistent with the theory of sound absorbing bulk materials¹⁰ which states that perfect absorption occurs when the normalized resistance is unity and the reactance is zero.

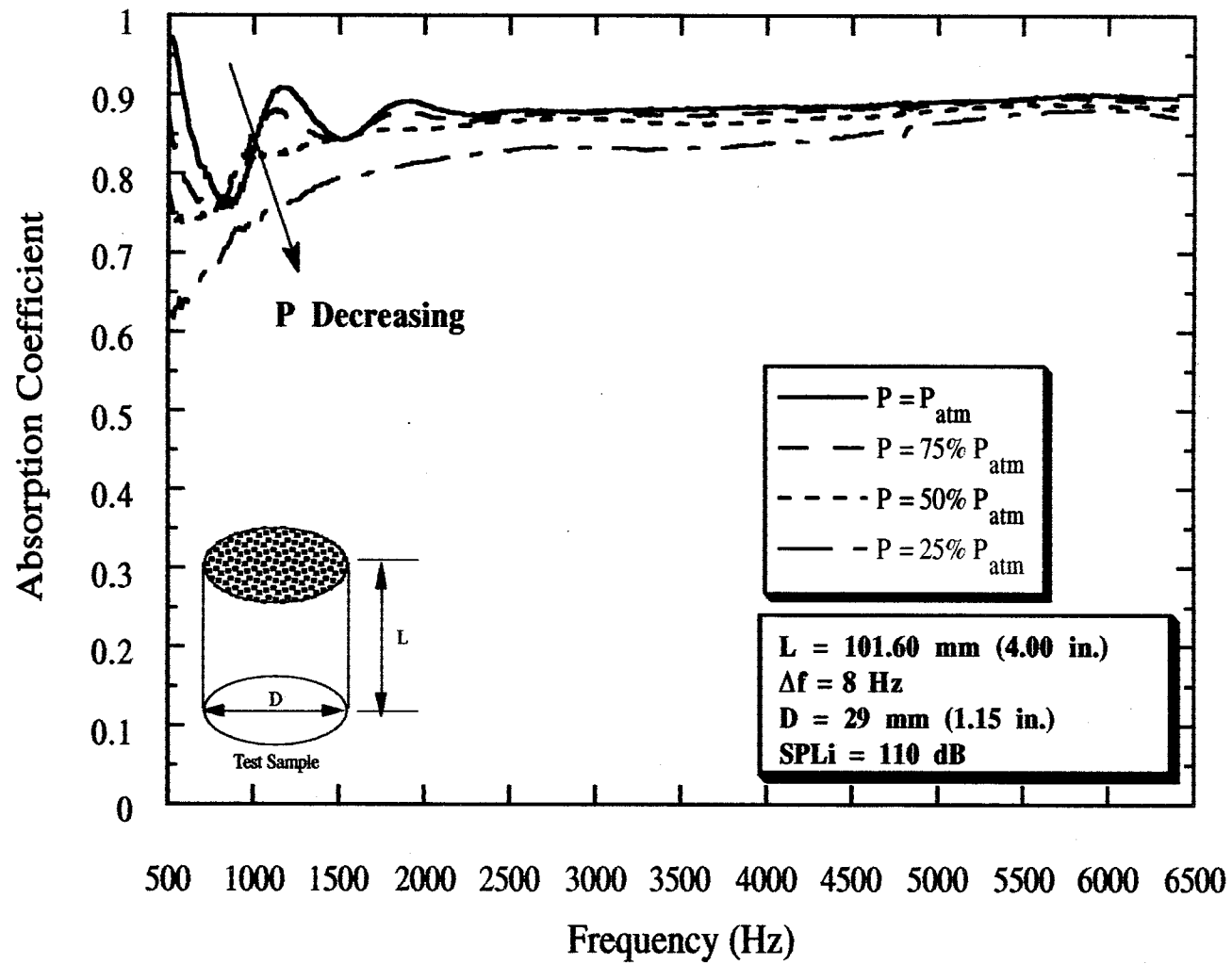


Figure 4.4 Effect of pressure on absorption coefficient of Pyrell foam.

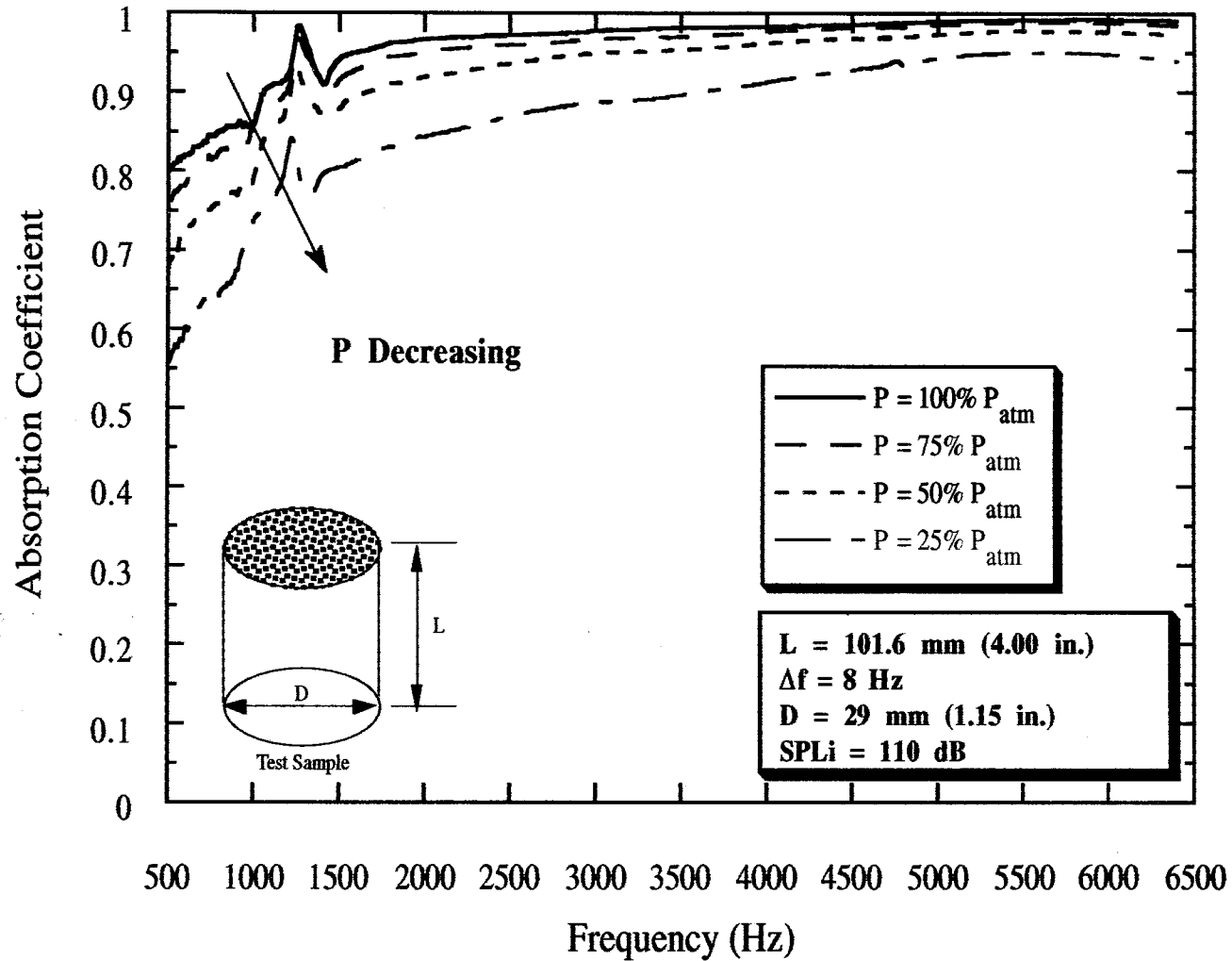


Figure 4.5 Effect of pressure on absorption coefficient of Fiberglass.

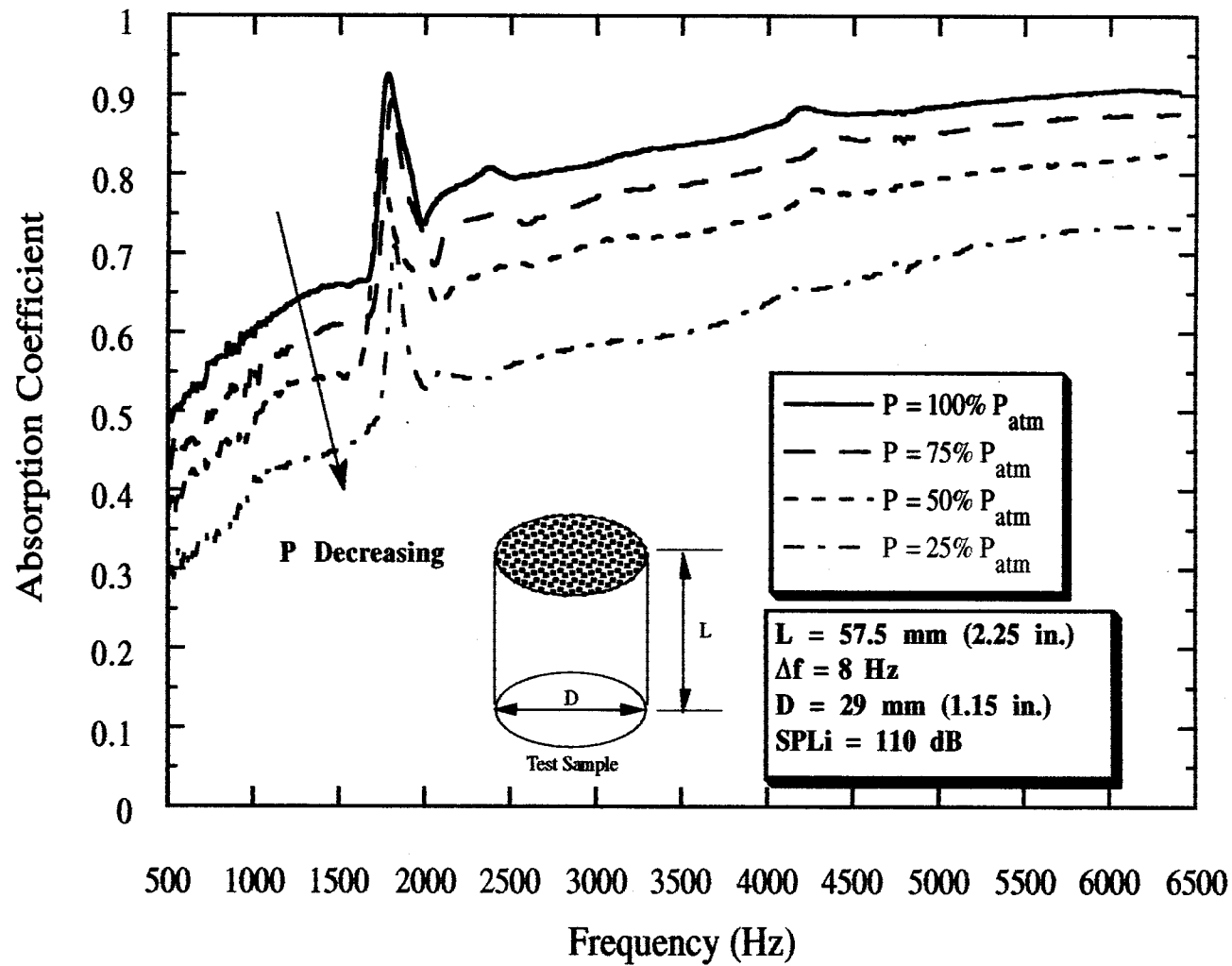


Figure 4.6 Effect of pressure on absorption coefficient of Kevlar.

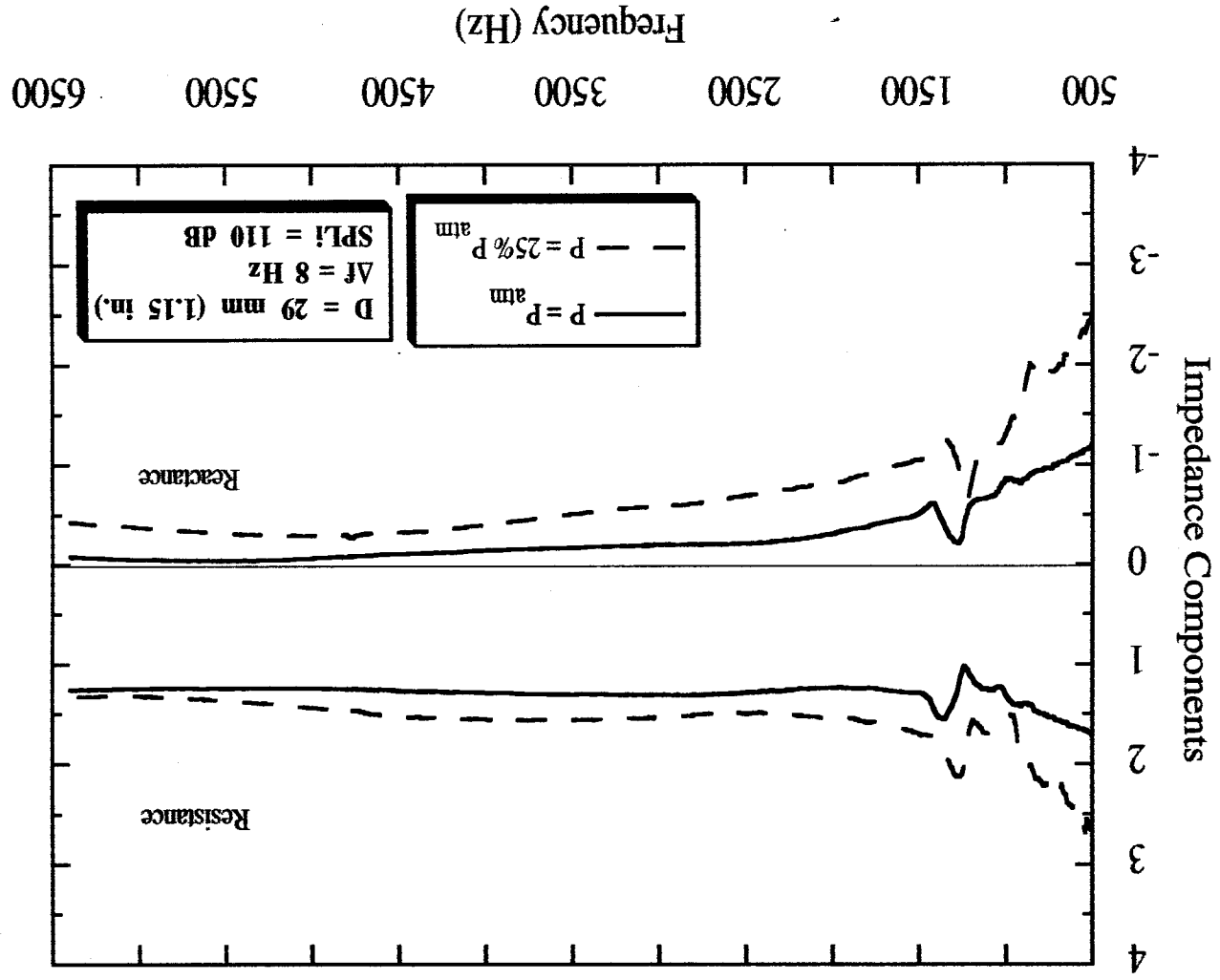


Figure 4.7 Effect of pressure on the characteristic impedance of Fiberglass.

The attenuation rate is the real component of the propagation constant and is a characteristic measure of the sound dissipation of a bulk material. The attenuation rate of Fiberglass is shown in figure 4.8. Again, only the two extreme ambient pressures are shown. The dissipation rate seems to be constant for the frequency range tested with discontinuities in the same frequency range as in figure 4.5. Also, the lower pressure case has lower attenuation than the higher pressure case, which is consistent with figure 4.5

The effect of length and pressure on the absorption coefficient of Fiberglass is shown in figure 4.9. The results confirm intuition in that the thicker test sample absorbs more sound, although at atmospheric pressure the difference is not so pronounced.

Kevlar Results

Results from the impedance testing of Kevlar proved to be very interesting. The two thicknesses used for the characteristic computations were chosen rather arbitrarily at 28.575 mm (1.125 inches) and 57.15 mm (2.25 inches). Since the Kevlar samples came only in 9.525 mm (0.375 inch) thick sheets, three layers were stacked for the 28.575 mm (1.125 inch) thick sample and six layers were stacked for the 57.15 mm (2.25 inches) thick sample. The absorption coefficient spectra for these two thicknesses were nearly identical as shown in figure 4.10, where 29 mm diameter data at P_{atm} data are presented. This behavior was also observed with 100 mm diameter data. Note that the discontinuous "spike" in absorption coefficient in figure 4.10 is similar to that seen in figure 4.6. As discussed earlier, it is believed that this is due to the interface mismatching between layers of the individual Kevlar sheets. If the two samples of different thicknesses have the same input impedance, the Two Thickness Method (TTM) for determining characteristic acoustic properties fails. This is described in detail in appendix A. Thus, for the two thicknesses of Kevlar tested, characteristic properties could not be computed, at least with the method described in appendix A.

After cryogenic testing on Kevlar was completed, input impedance of Kevlar as a function of number of sample layers was measured in the impedance tube for both diameter test sample sizes. A diminishing effect of thickness of Kevlar was observed. Figure 4.11 shows absorption coefficient of Kevlar as a function of thickness for selected frequencies. Note that

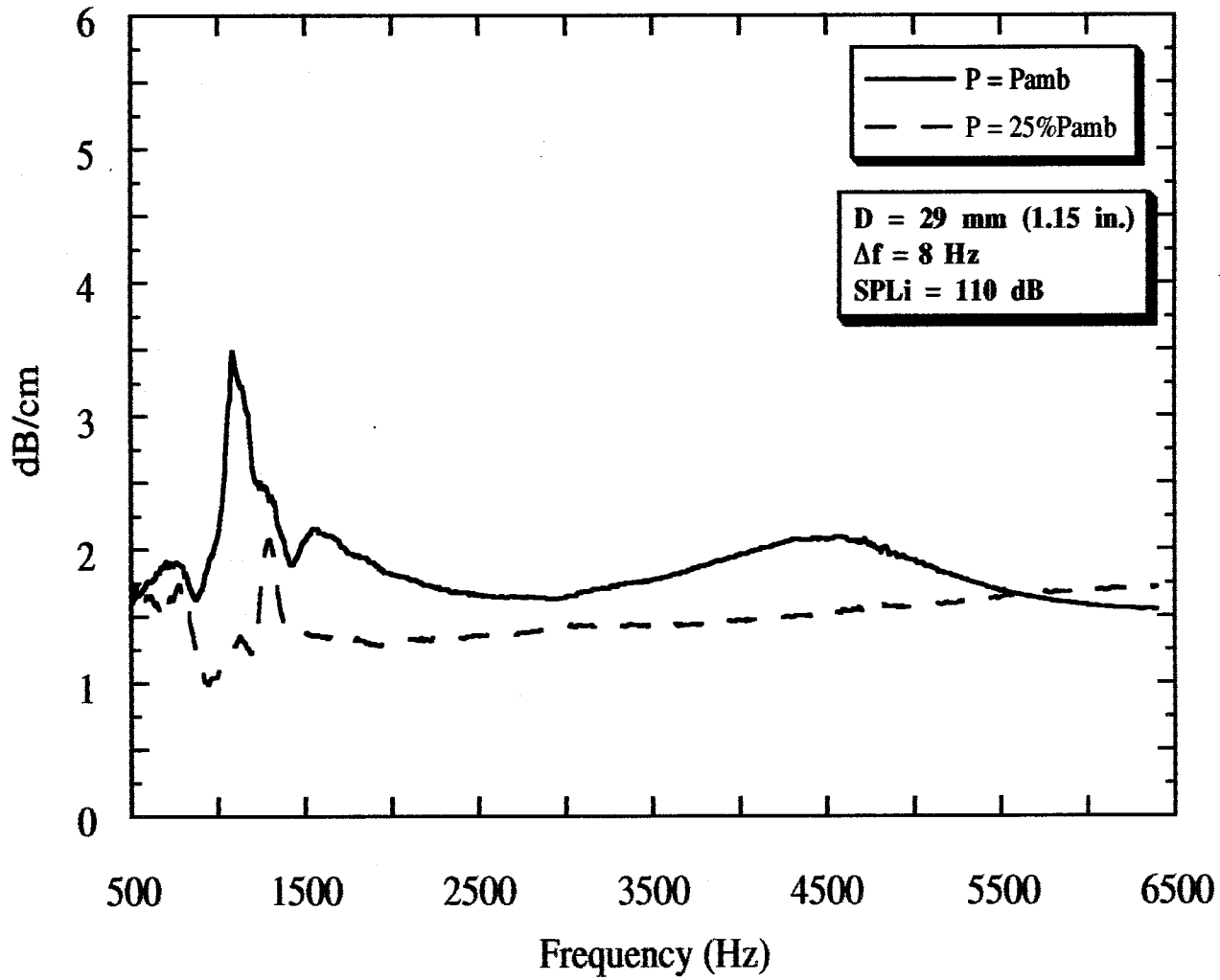
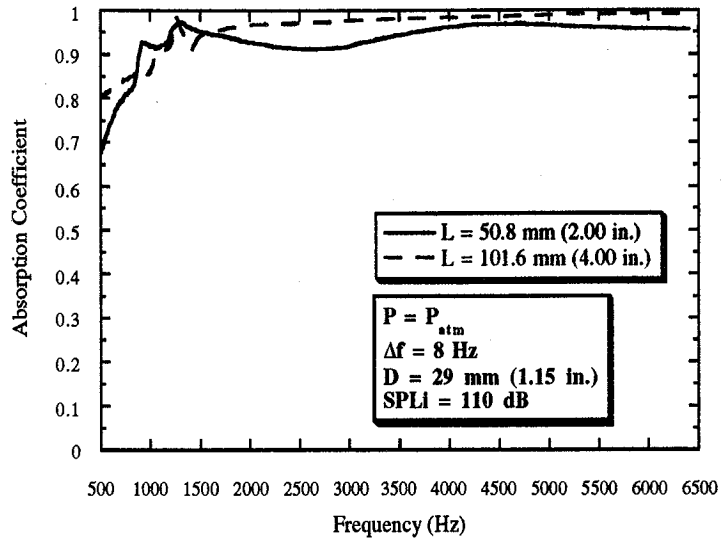
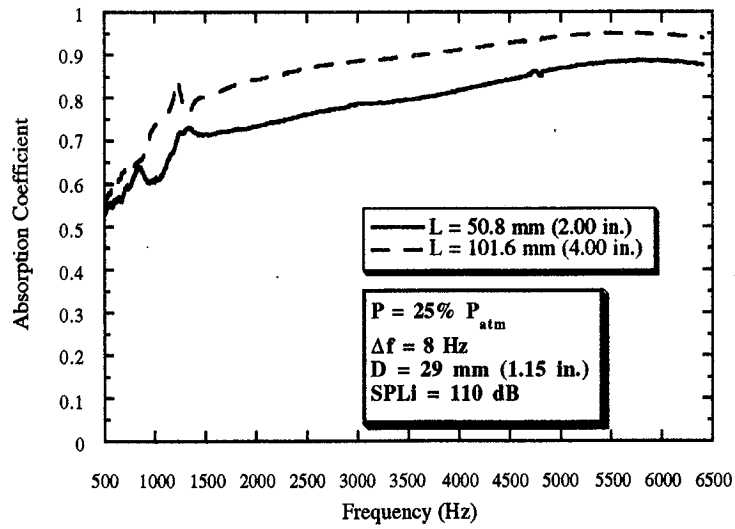


Figure 4.8 Effect of pressure on attenuation rate of Fiberglass.



$P = P_{atm}$



$P = 25\% P_{atm}$

Figure 4.9 Effect of test sample length on absorption coefficient of Fiberglass

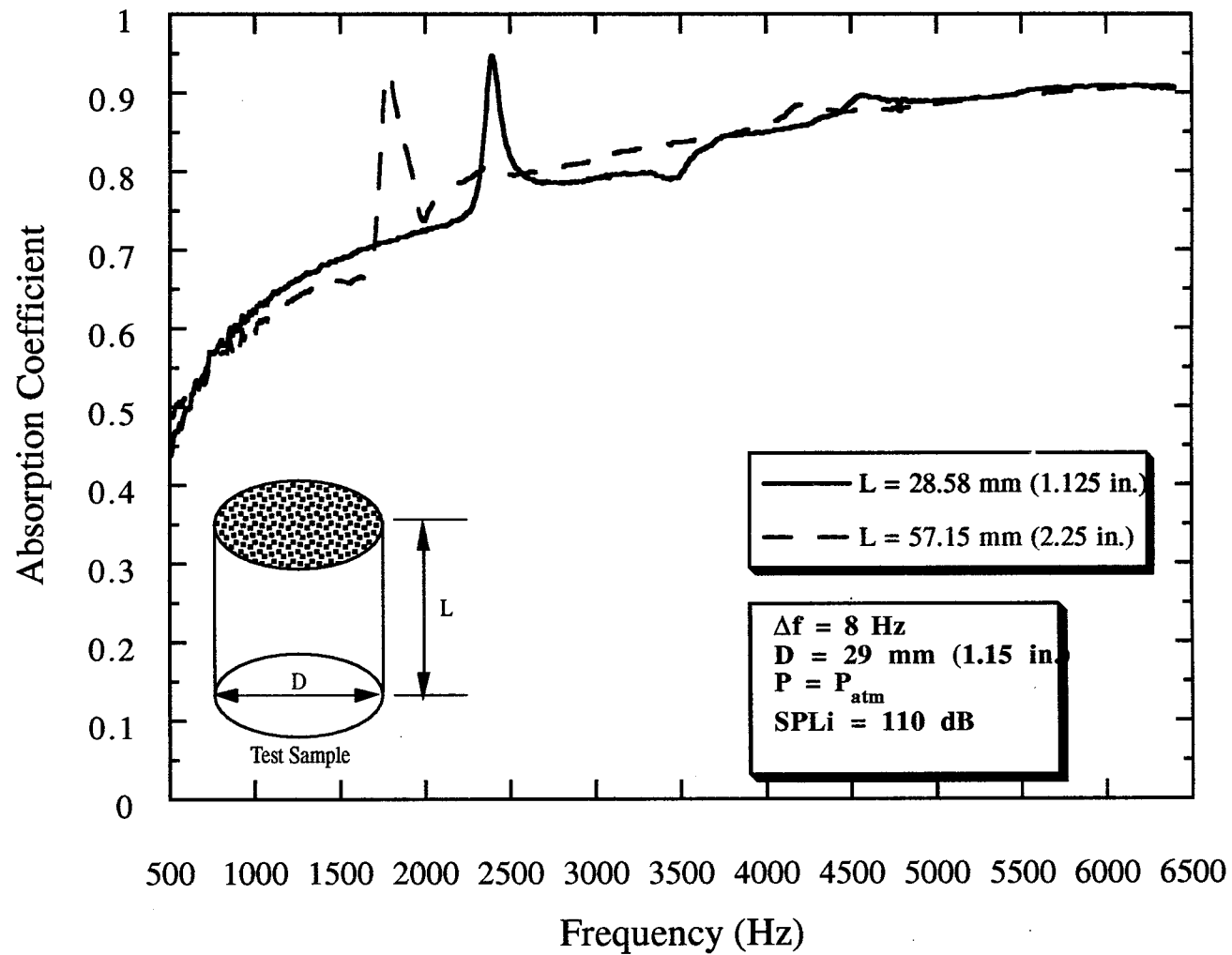
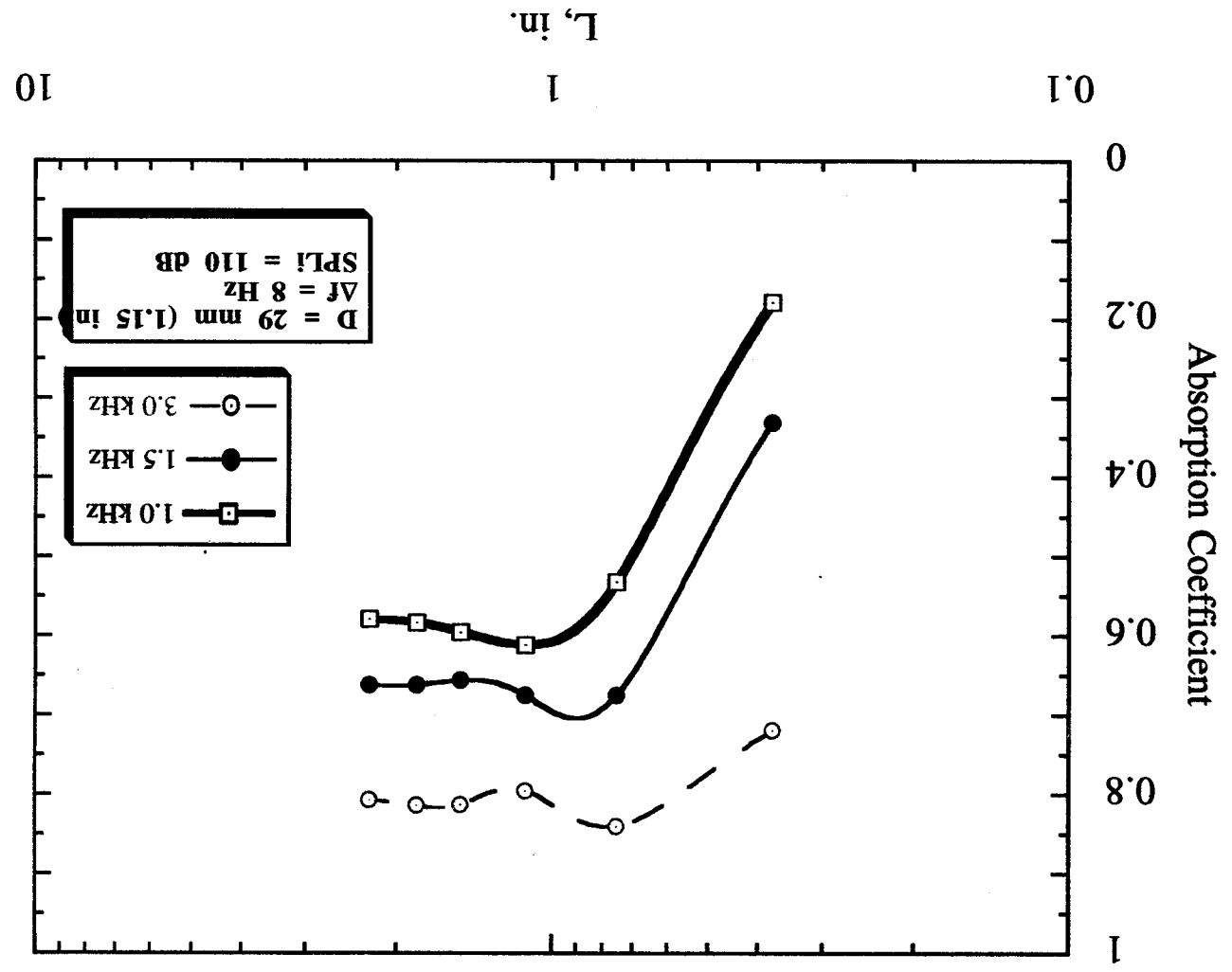


Figure 4.10 Effect of sample length on absorption coefficient of Kevlar.

Figure 4.11 Diminishing effectiveness of test sample length on the absorption of Kevlar.



after exceeding a thickness of approximately 1 inch, the absorption coefficient approaches a constant value. These results are consistent with figure 4.10 and with data of Hersh and Walker¹¹.

By increasing the thickness of Kevlar, it appears that a limit of absorption has been reached. This is precisely what one would expect if one were to use an infinitely thick absorption material. This is equivalent to stating that input impedance is equal to characteristic impedance. This is further elaborated below. It can be postulated that after 1 inch of thickness, Kevlar behaves as if it is "infinitely" thick.

The input impedance of a material can be expressed by the equation:

$$z_i = z_c \coth(\gamma l)$$

where z_i and z_c are the input and characteristic impedances, respectively. This is based on the boundary conditions imposed by the impedance tube on the material sample. (See Appendix A for details.). If the sample length, l , were considered to be infinite, then the hyperbolic cotangent of γl becomes unity. Thus the input impedance becomes equal to the characteristic impedance.

In the present case, for Kevlar, there is no increase in absorption after a thickness of 1 inch is reached. This behaviour is similar to that of an infinitely thick material. Thus in view of the above argument, the implication of this result is that the input impedance data of 57.15 mm (2.25 inches)-thick Kevlar is also the characteristic impedance.

To further confirm this hypothesis, the characteristic impedance of Kevlar was obtained in two ways. First, the Two Thickness Method was applied to the data for 0.375-inch and 0.75-inch thick Kevlar. Note that from figure 4.11, the absorption coefficient is significantly different between these two cases. Second, the input impedance from a 2.25-inch thick Kevlar sample was taken as the characteristic impedance. Figure 4.12 shows the characteristic impedance of Kevlar, comparing the Two Thickness Method with the "infinite" thickness length assumption. There is very good agreement and therefore all of the 2.25 inch thick data of Kevlar can be assumed to be the characteristic acoustic data. As a final confirmation of the

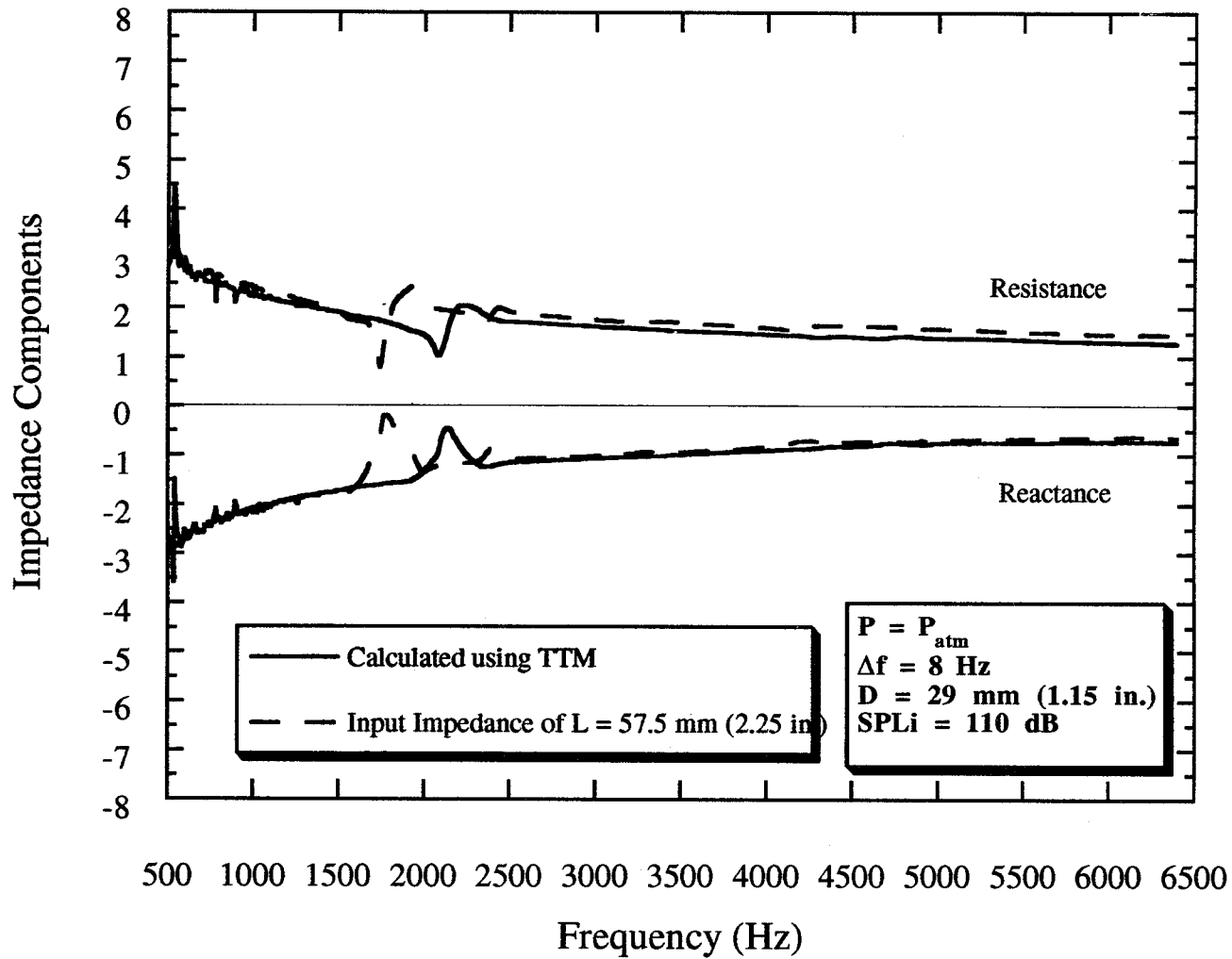


Figure 4.12 Comparison of Two Thickness approach to characteristic impedance calculations and the "infinite" length assumption of characteristic impedance.

validity of this assumption, characteristic impedance data of Kevlar obtained by Smith and Parrott at NASA LaRC⁷ were compared with present results and are presented in figure 4.13. The data agreed favorably over a range of frequencies.

Pyrell Results

The initial sub-atmospheric acoustic impedance tests of the Pyrell foam produced unexpected results. For both frequency range (and thus sample diameter size) data, at 25% of atmospheric pressure, the absorption coefficient for the 2-inch thick foam was found to be *higher* than that for 4-inch thick foam. At atmospheric pressure, this trend is not as evident. Figure 4.14 shows the absorption coefficient of 2 and 4.0 inch Pyrell foam at atmospheric and 25% atmospheric pressure. At 25% P_{atm} , the absorption coefficient is higher for the 2.0 inch case across the whole frequency range. At atmospheric pressure, this trend is somewhat mitigated by the oscillatory nature of the 2.0 inch data. Using these data, the characteristic impedance was calculated and is presented in figure 4.15. The absorption coefficient trend with decreasing pressure is reflected in figure 4.15.

Another unexpected result is the attenuation rate of Pyrell. Figure 4.16 shows the attenuation rate of Pyrell for the two extreme pressure cases. Note, at about 4250 Hz for the atmospheric pressure case, a large spike in attenuation rate is observed. This can be explained by the existence of a singularity in the method of calculation (see appendix A). If the two input impedances which contribute to the propagation constant are nearly identical at a given frequency, the resulting attenuation rate is theoretically infinite at that frequency. Figure 4.17 shows the two components of input impedance for Pyrell foam. Note that there is a small frequency range where both components of the impedance show that the two input impedances are identical. This range corresponds to the spike in the attenuation rate in figure 4.16. Also, at frequencies below 4000 Hz, figure 4.16 shows that the attenuation constant for the 25% P_{atm} case is larger than that for the atmospheric case. This is counter to the absorption data presented earlier in figure 4.4. In summary, out of the three materials tested, Fiberglass and Kevlar appear to indicate a decrease in the value of the attenuation constant with decreasing pressure. For Pyrell, the attenuation constant increases in value at lower pressures. No explanation is available at this stage to explain this difference.

Impedance Components

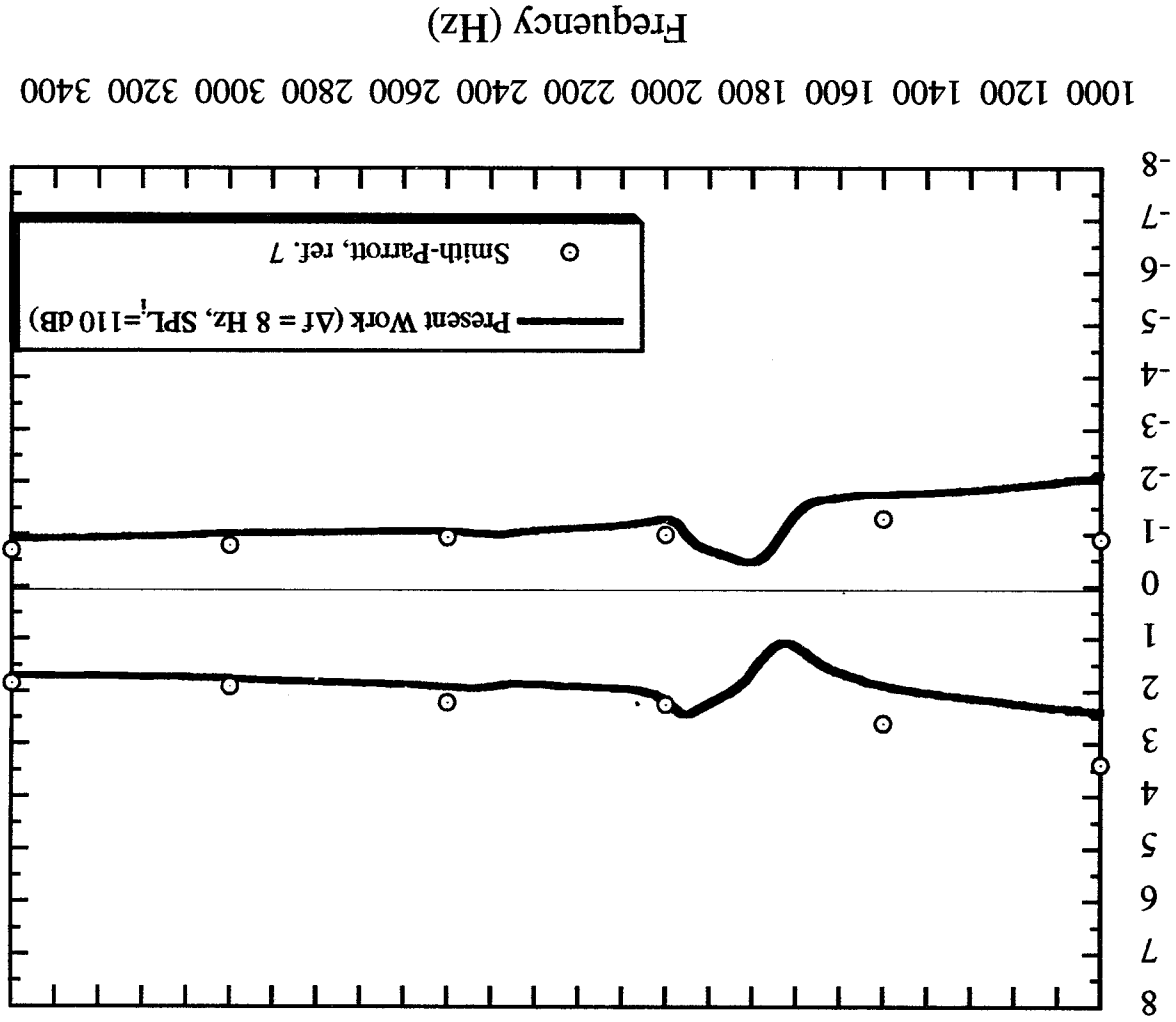
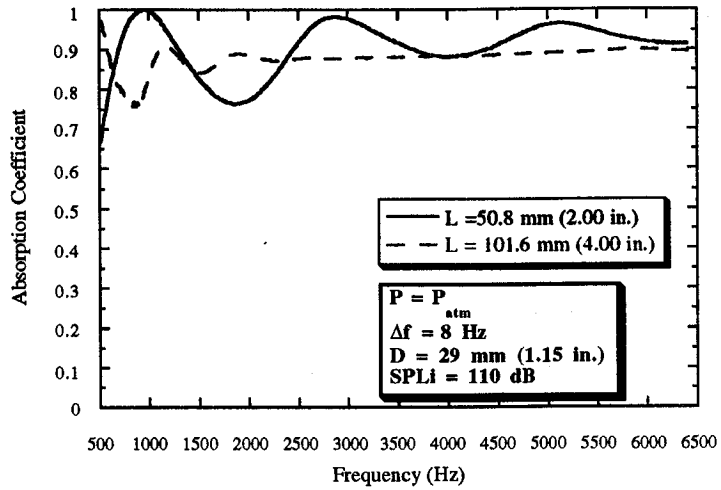
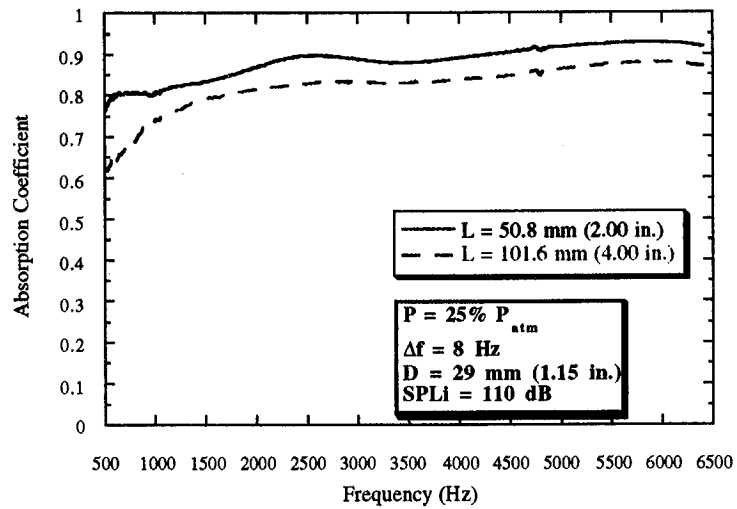


Figure 4.13 Comparison of present characteristic impedance data of Kevlar with NASA data (Smith & Parrott,



P = P_{atm}



P = 25% P_{atm}

Figure 4.14 Effect of test sample length on the absorption coefficient of Pyrell foam.

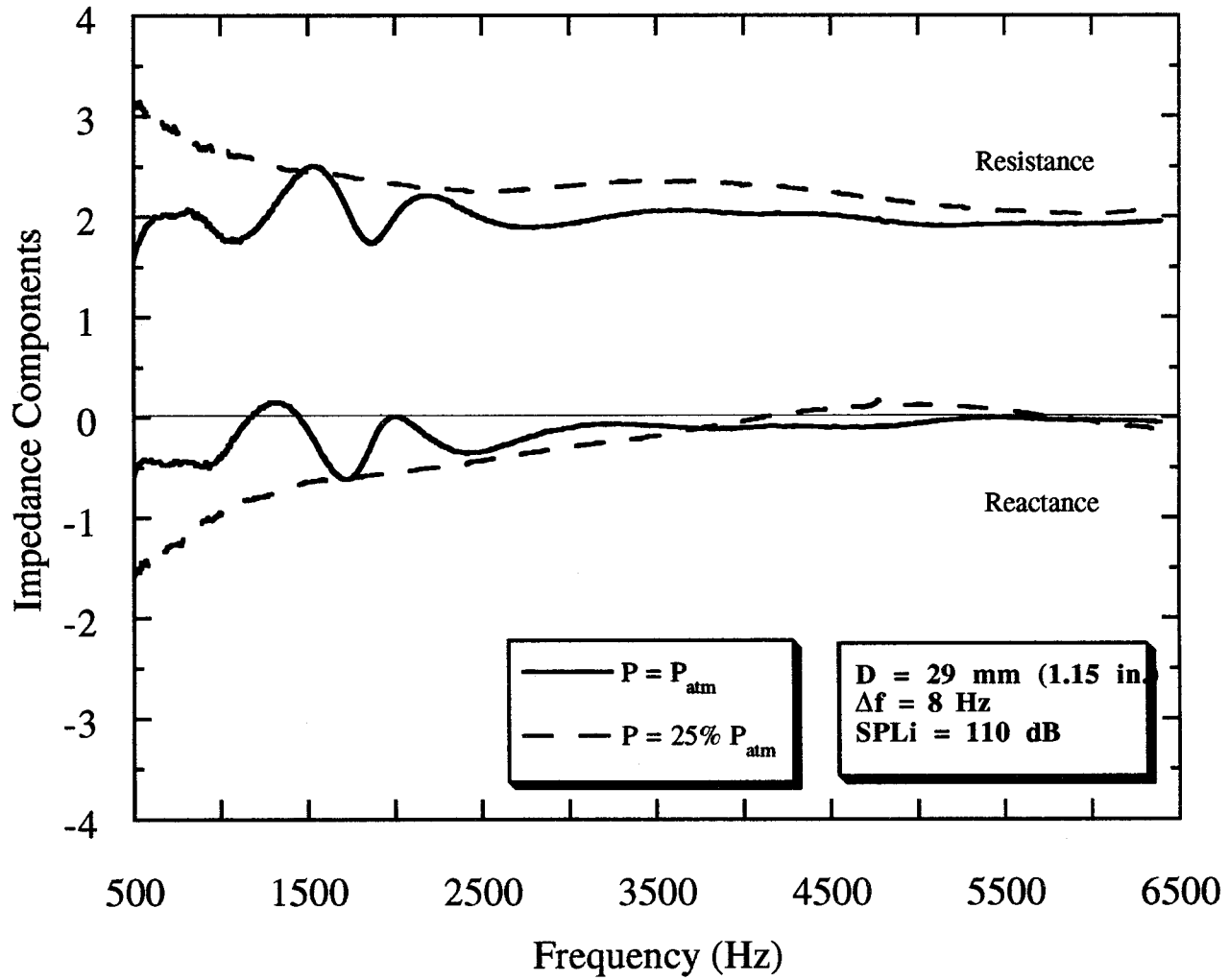


Figure 4.15 Effect of pressure characteristic impedance of Pyrell Foam.

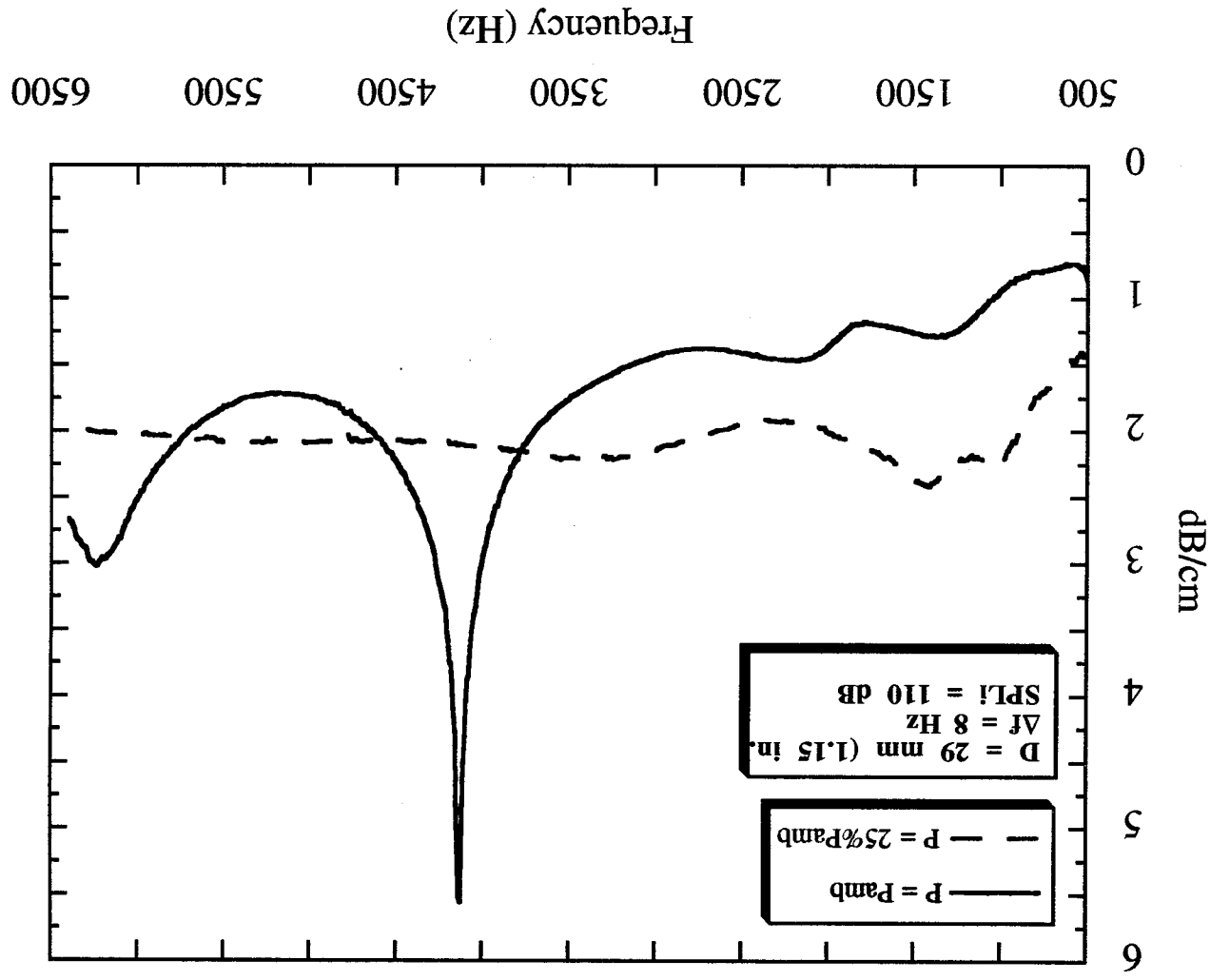


Figure 4.16 Effect of pressure on attenuation rate of Pyrell foam.

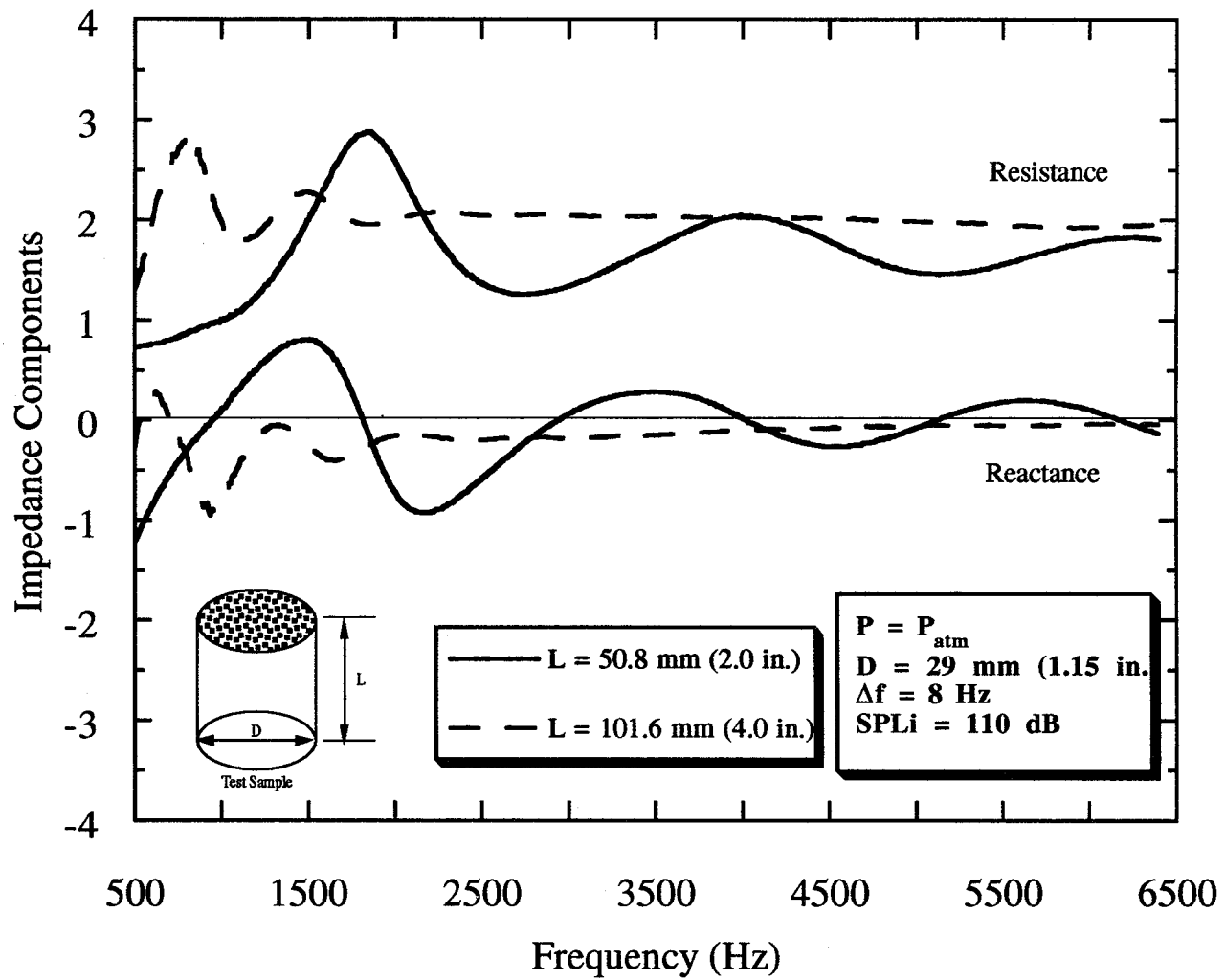


Figure 4.17 Effect of test sample length on input impedance of Pyrell foam.

Due to the small diameter to length ratio of the samples fabricated for the small diameter impedance tube, the quality of the cut was not as reliable. This was particularly evident in the fabrication of the Pyrell foam sample with diameter and length dimensions of 29.0 mm (1.15 in.) and 101.6 mm (4.0 inches) respectively. All samples fit in the tube with a good snug fit, with the exception of the 101.6 mm-inch Pyrell sample mentioned above. In this case the fit was not as snug as the other samples, yet it was sufficient to keep it in place in the impedance tube against the force of gravity. All measurements taken have an error arising from the quality of the impedance tube/test sample boundary conditions. For this study, various cuts of the same dimensions were not used to determine the extent of this error or to obtain an "average" measurement.

4.5 Cryogenic Cycling Test - Results and Discussion

After testing the material samples in the sub-atmospheric facility, they were placed in the cryogenic cooling facility for repeated low temperature/high pressure exposure. Each test sample was tested separately. The general operation of the facility is described in section 2. The cycle times averaged approximately 8 minutes. The tests were performed for a total of 250 cycles which took an average of 33 hours. Testing was not continuous. The liquid nitrogen tank generally lasted 3-4 hours and the facility had to be stopped to replace the empty tank. Most of the testing occurred in 5-8 hour segments separated by as much as 15 hours.

The hypodermic thermocouples were calibrated before each new material was placed in the cooling chamber and at the half way point of the 250 cycles. Calibration consisted of placing the thermocouples alternately in a glass of ice water and a pot of boiling water. The computer controlled facility was set to cool the samples to an average temperature of -150 °F and warm to an average temperature of 70 °F. The test was also monitored with a video camera which allowed the facility to be left unmanned at times.

Figures 4.18 through 4.20 show the temperature histories of the three tested materials during cryogenic cooling for only a "snapshot" hour. Figures 4.21 through 4.23 show the pressure histories for selected time segments of the tests. These figures show that a fairly consistent cycling of the environment was achieved. This was a direct result of the computer controlled test operation. Also, note that for Kevlar, there are only two temperature curves.

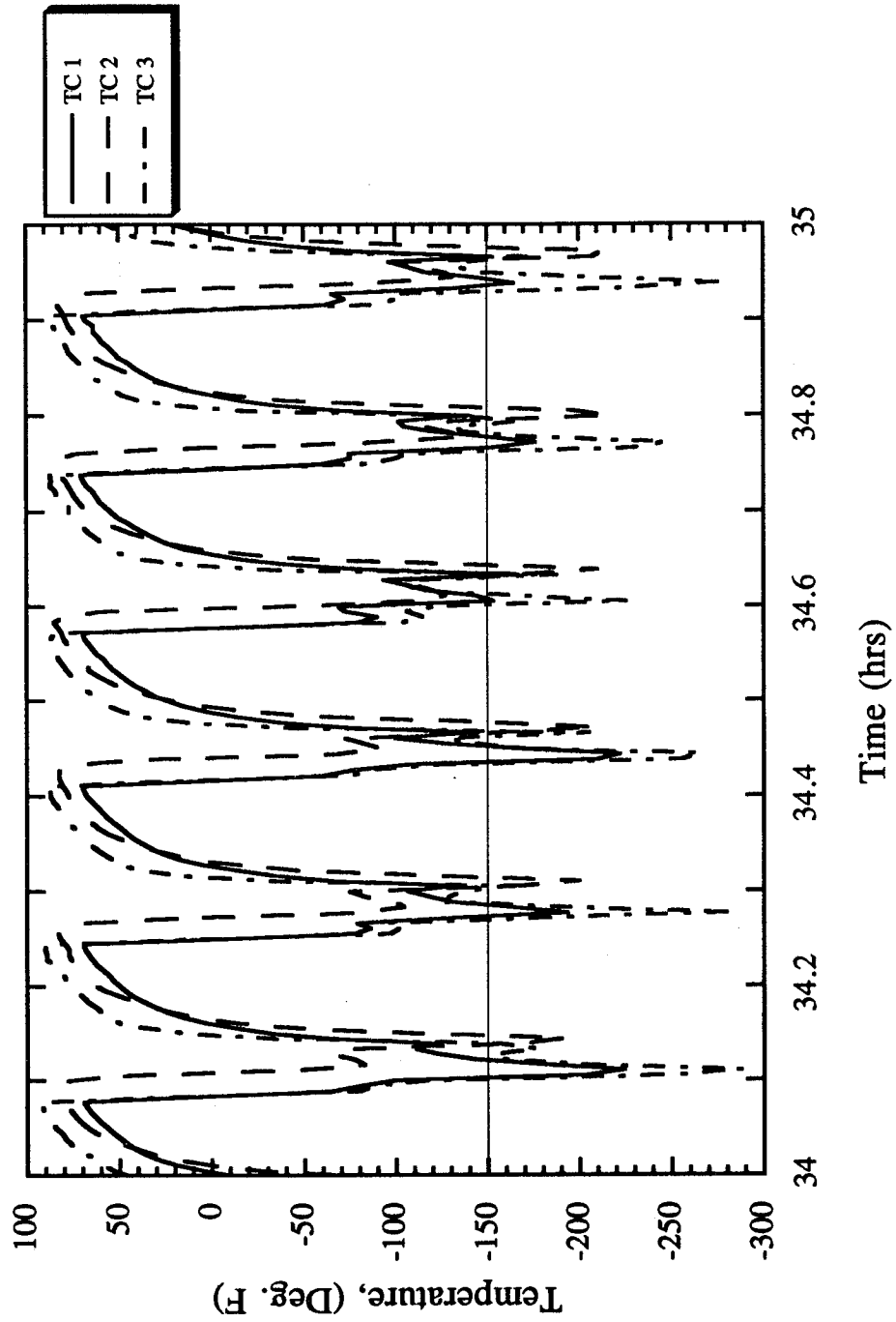


Figure 4.18 Snapshot time history of temperature during the cryogenic cooling phase of Pyrell foam.

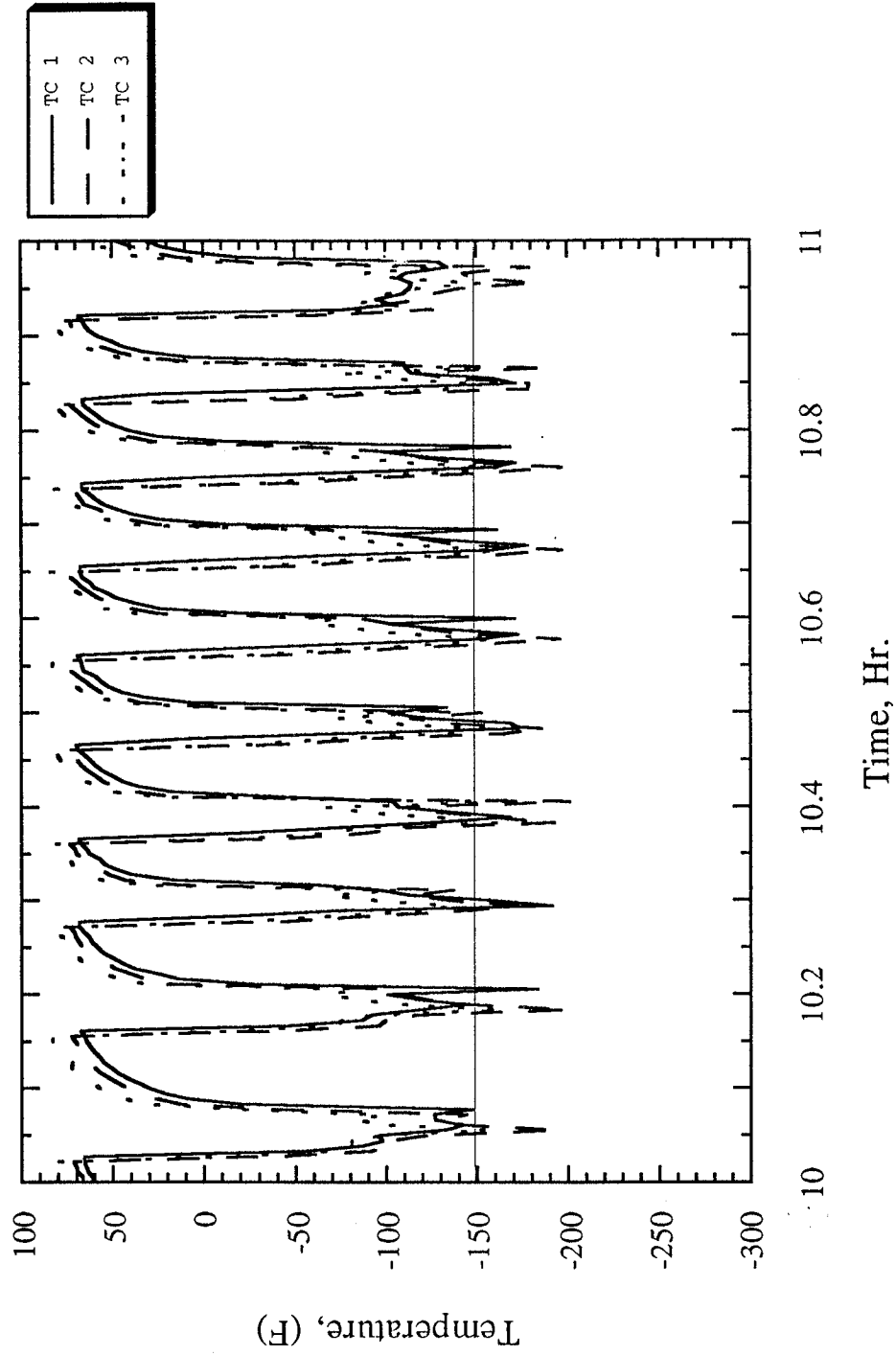


Figure 4.19 Snapshot time history of temperature during cryogenic cooling phase of Fiberglass.

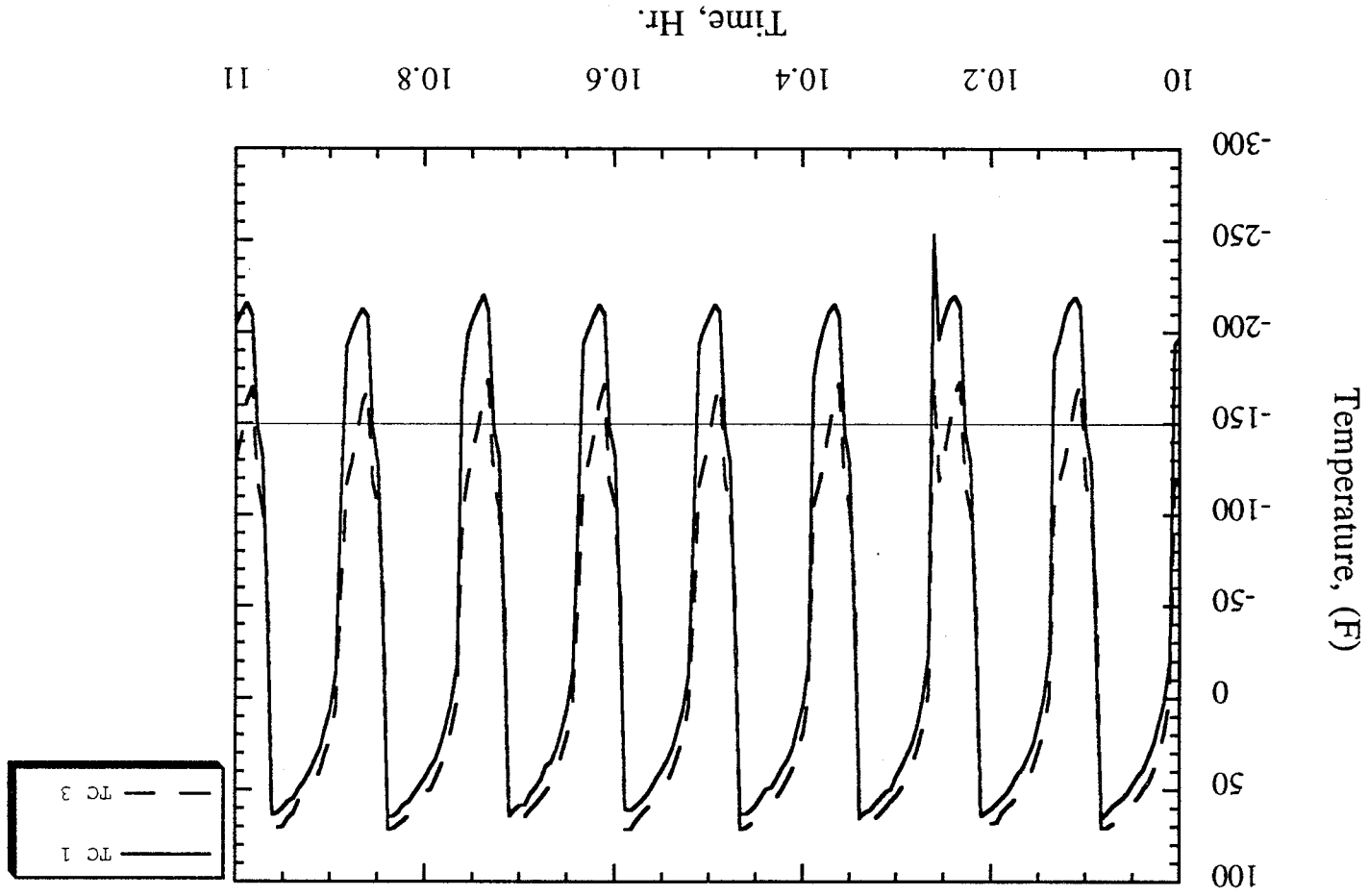


Figure 4.20 Snapshot time history of temperature during cryogenic cooling phase of Kevlar.

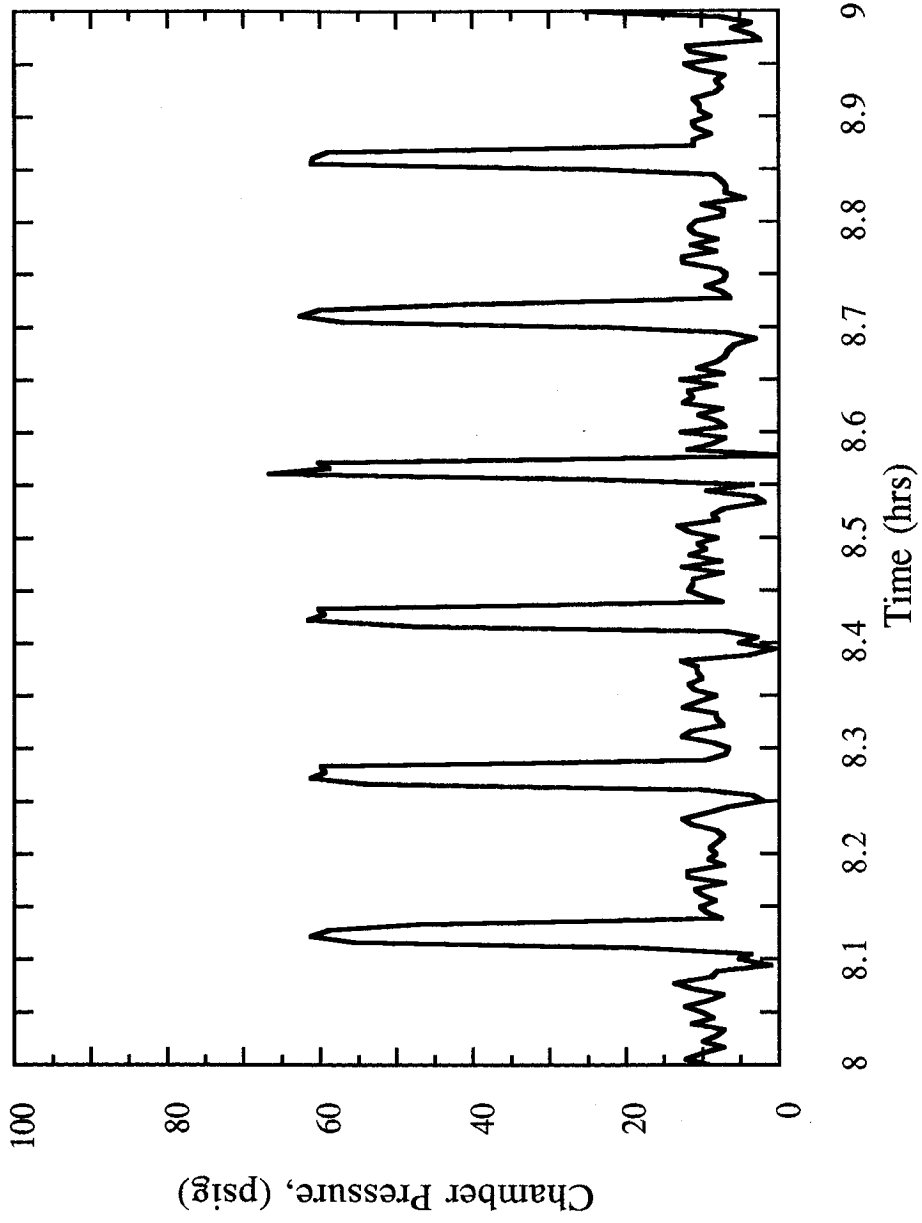


Figure 4.21 Snapshot time history of chamber pressure during cryogenic cooling phase of Pryell.

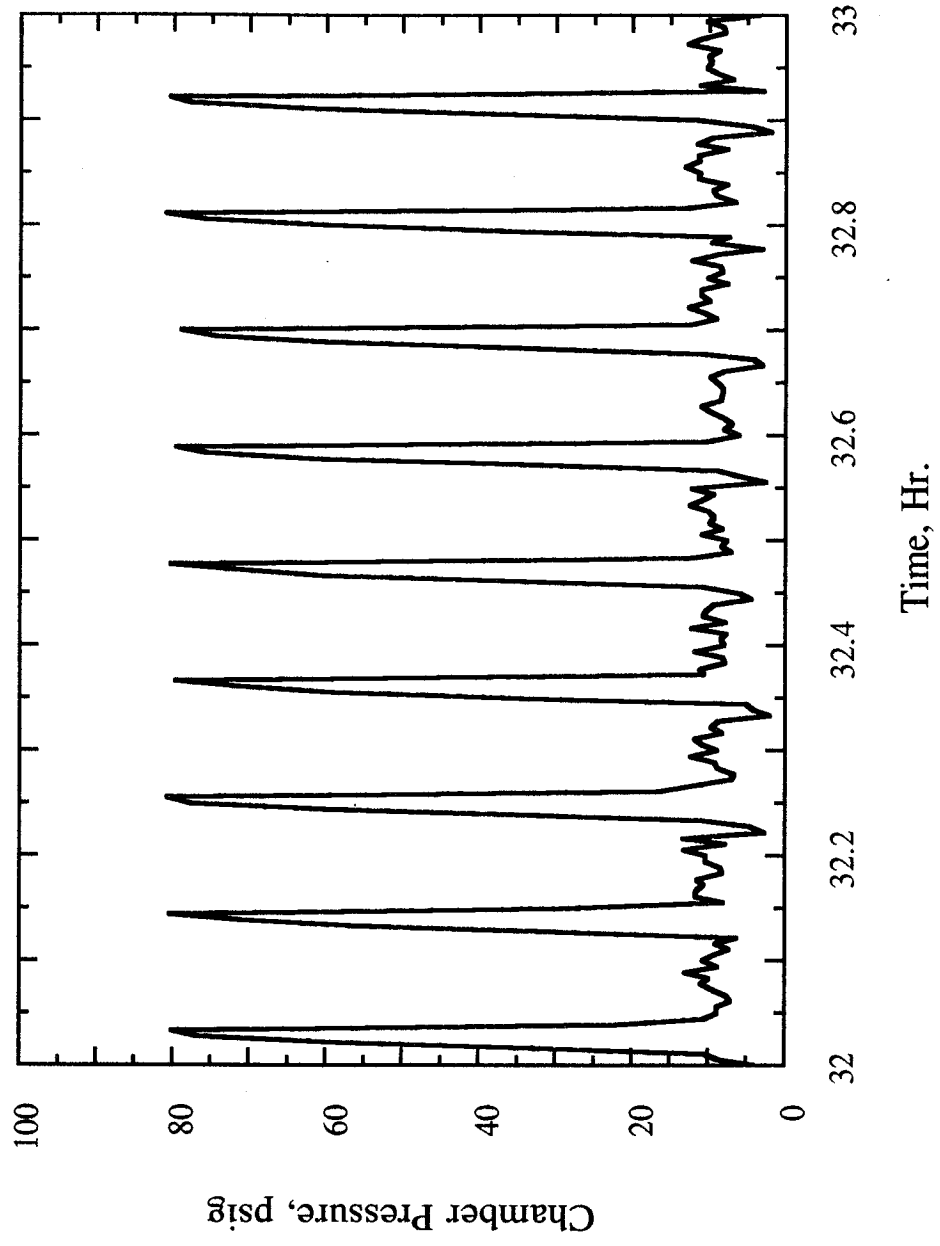


Figure 4.22 Snapshot time history of chamber pressure during cryogenic cooling phase of Fiberglass.

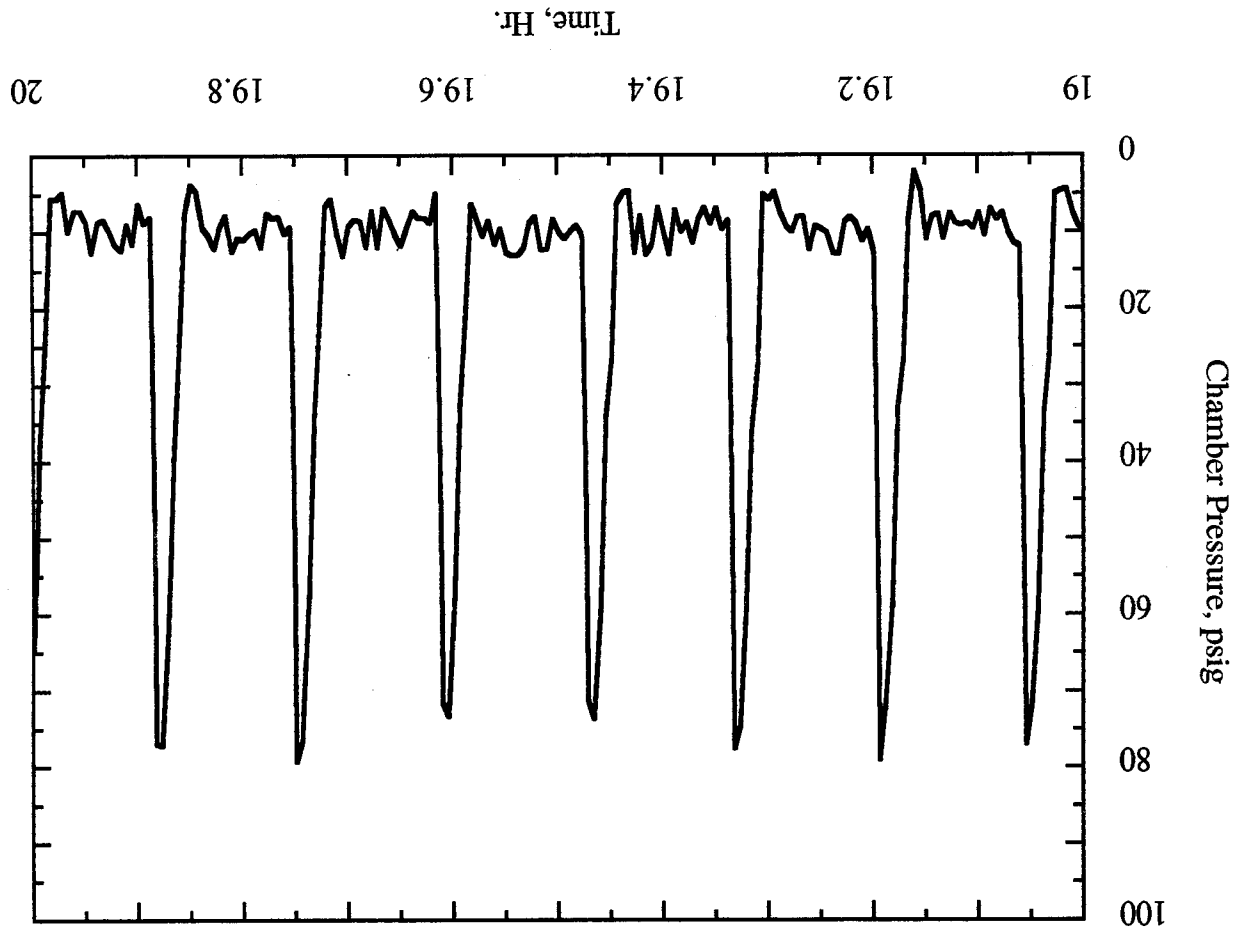


Figure 4.23 Snapshot time history of chamber pressure during cryogenic cooling phase of Kevlar.

This is a result of an erroneous reading of one of the hypodermic thermocouples which was spotted earlier on in the Kevlar cycling, thus, only the remaining two thermocouples were used to form an average material temperature.

4.6 Cycling Effects on Acoustic Properties - Results and Discussion

After 250 cycles of low temperature and high pressure exposure, the liner material samples were re-tested in the sub-atmospheric facility to identify changes, if any, to the acoustic properties. The liner samples were inspected visually for any physical damage that may have occurred. The samples seemed to be in the same physical condition (macroscopically) as they were before the 250 cycle test. The test matrix shown in table 3.2 was followed again. Figures 4.24 through 4.26 show absorption coefficient spectra of the three tested materials for the 29 mm diameter sample size. The cooling and pressurizing cycles appear to have no characteristic effect on the absorbing performance of each of the liner materials. This implies that all of the acoustic properties (e.g., impedance, propagation constant, etc.) are unaffected by the cycling. This is one of the main results of this study. As will be shown in the next section, the cycling did not affect the resiliency of the materials either.

The results of the periodic cold soak for Pyrell foam were further substantiated by a harsher test¹³. Separate Pyrell foam test samples for the 29-mm diameter impedance tube were cut in 2 and 4-inch thicknesses. To simulate periodic cold soak, the test samples were immersed completely in a vat of liquid nitrogen. The samples were taken out of the vat after they were saturated. The test samples were allowed to thaw to ambient conditions and then they were immersed in the liquid nitrogen again. This cycle was repeated ten times¹². Figure 4.27 shows a photograph of the Pyrell foam samples as they are thawing to ambient conditions. Before the first immersion into liquid nitrogen and after the final thawing, the test samples were placed in the B&K 4206 impedance tube and acoustic properties were obtained. Figure 4.28 shows the absorption coefficients for the 2-inch thick test sample. The results show that exposure to a very severe cold environment does not affect the acoustic properties of Pyrell foam.

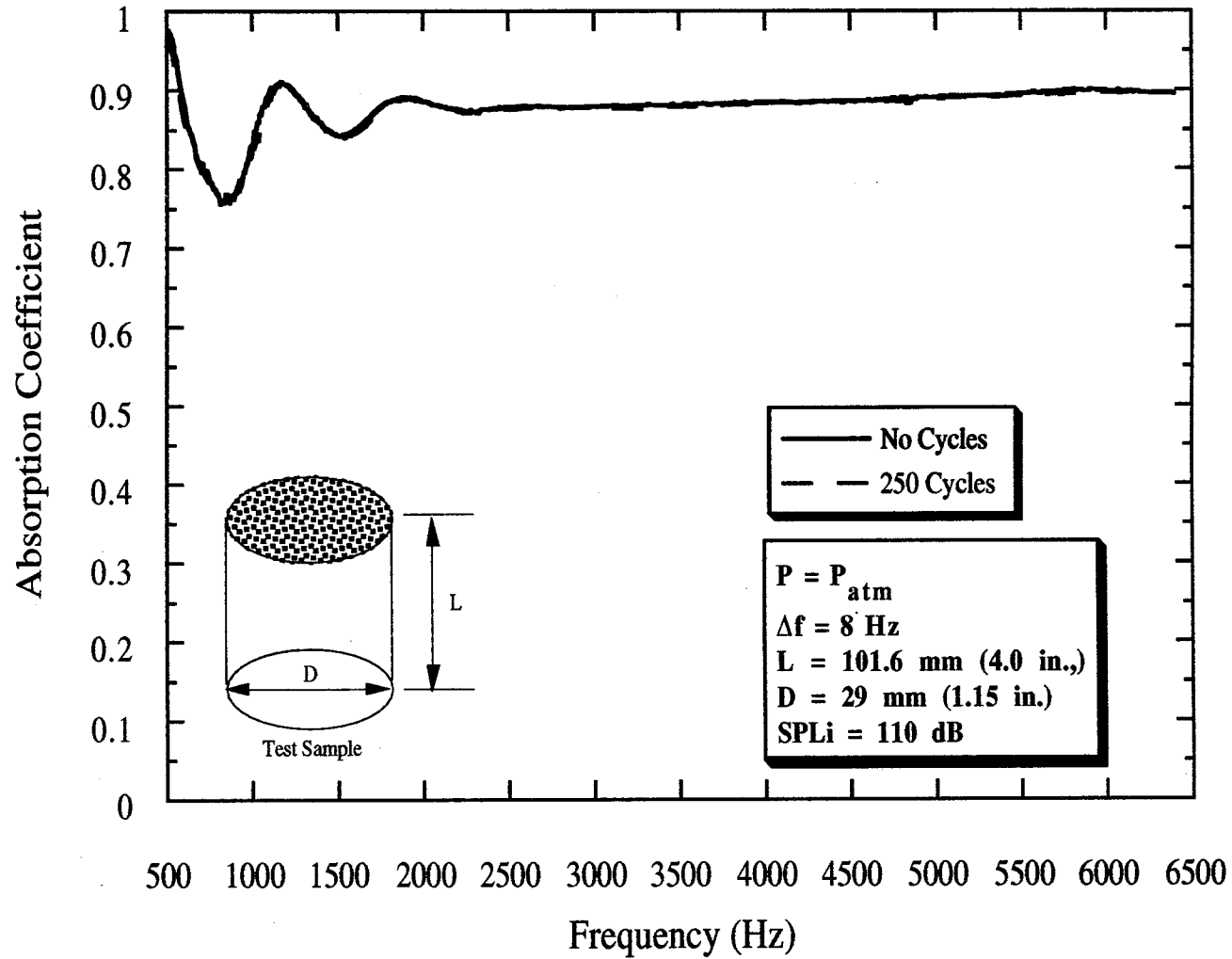


Figure 4.24 Effect of periodic cold soak on absorption coefficient of Pyrell Foam.

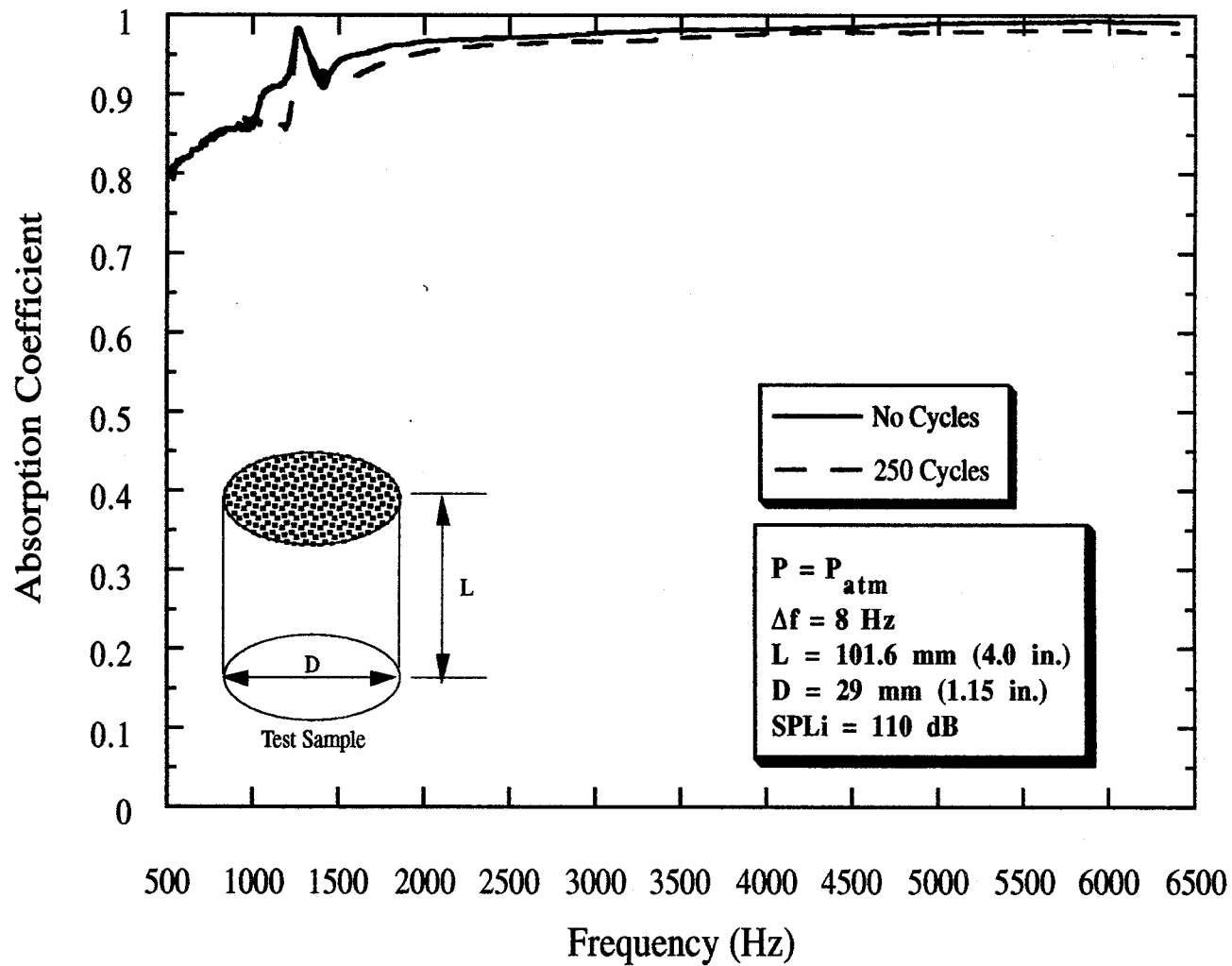


Figure 4.25 Effect of periodic cold soak on absorption coefficient of Fiberglass.

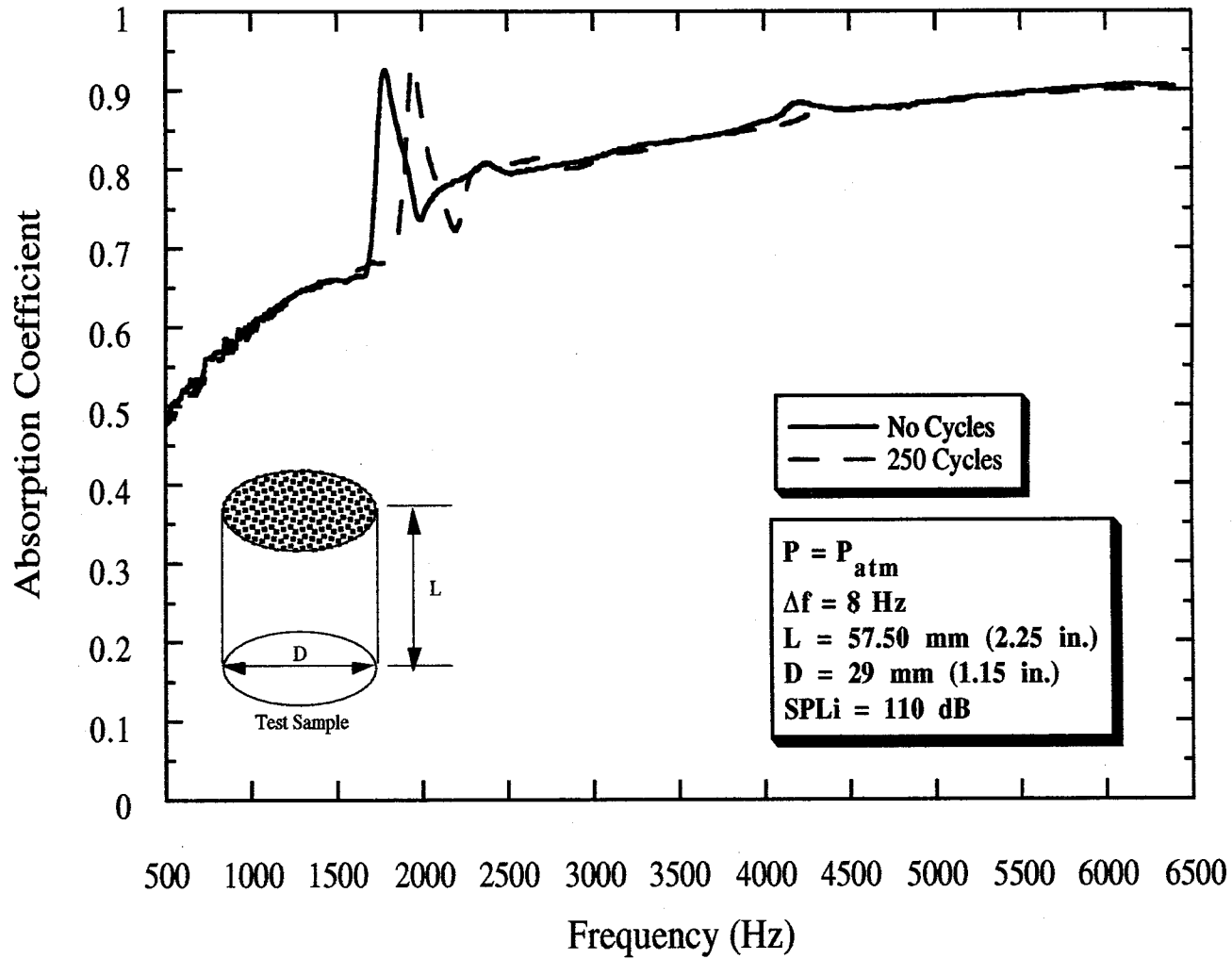
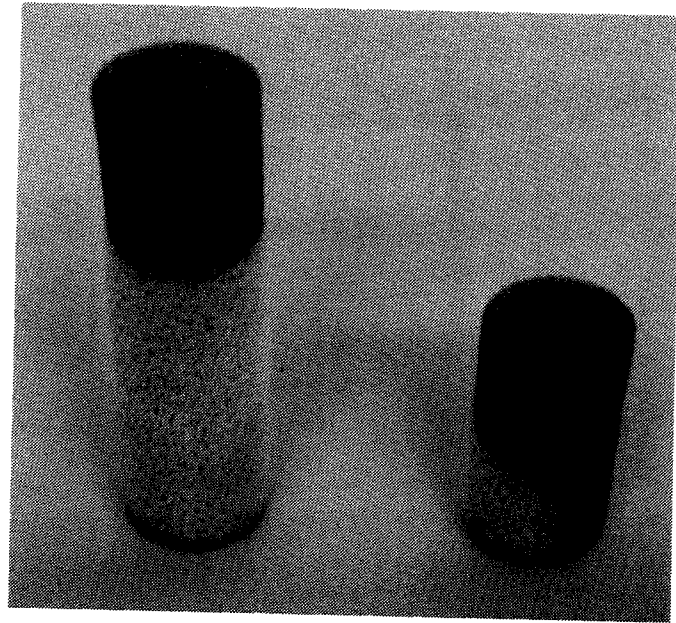
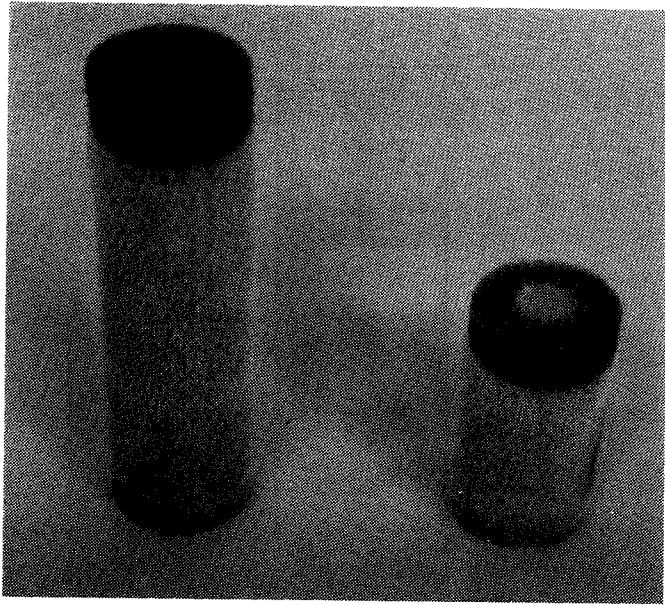


Figure 4.26 Effect of periodic cold soak on absorption coefficient of Kevlar.



4.27 Thawing process of Pyrell foam after being saturated with liquid nitrogen.

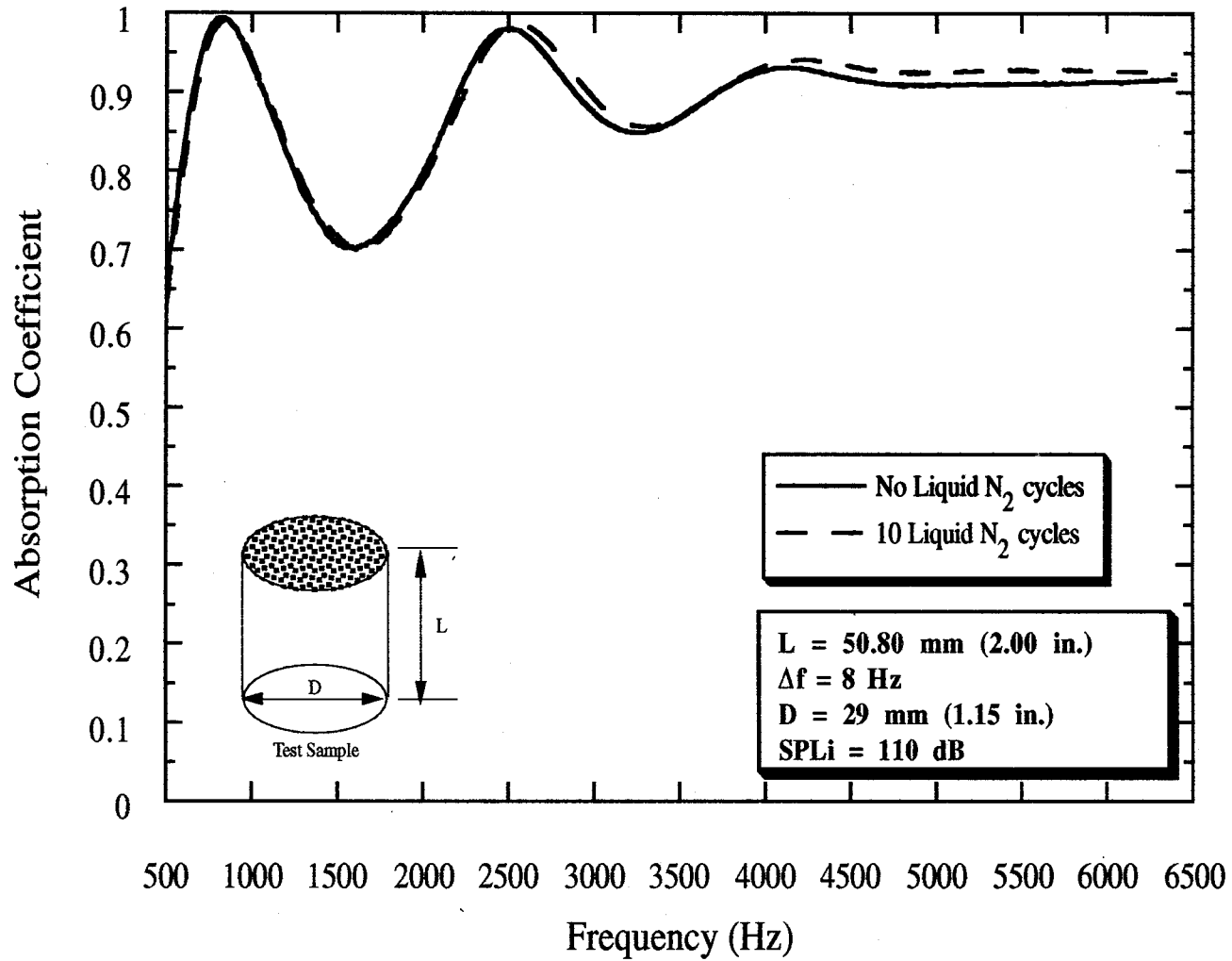


Figure 4.28 Effect of repeated liquid nitrogen saturation of Pyrell foam on absorption coefficient.

5.0 RESULTS OF MECHANICAL RESILIENCY TESTS

5.1 Summary of Results

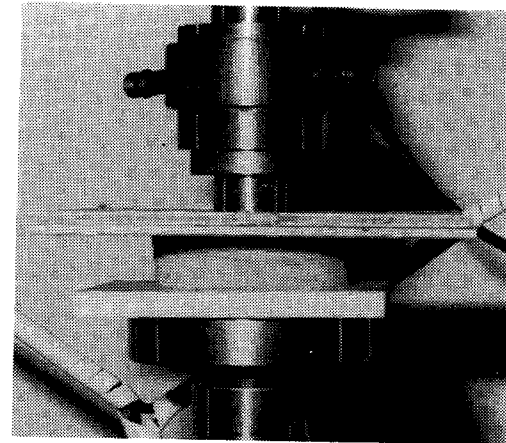
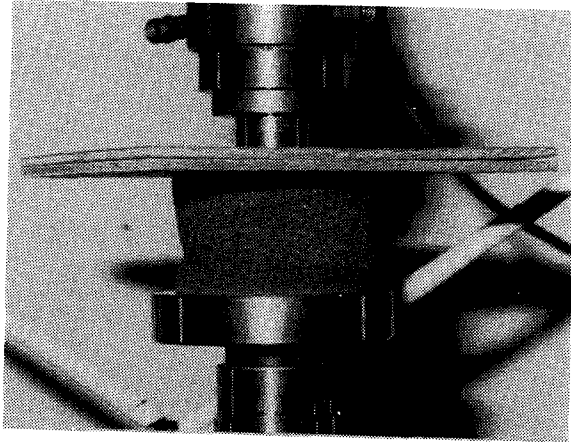
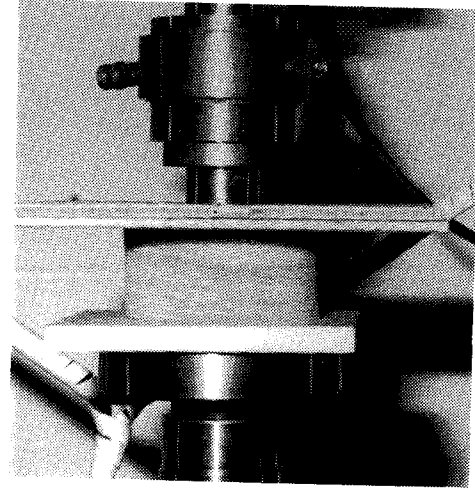
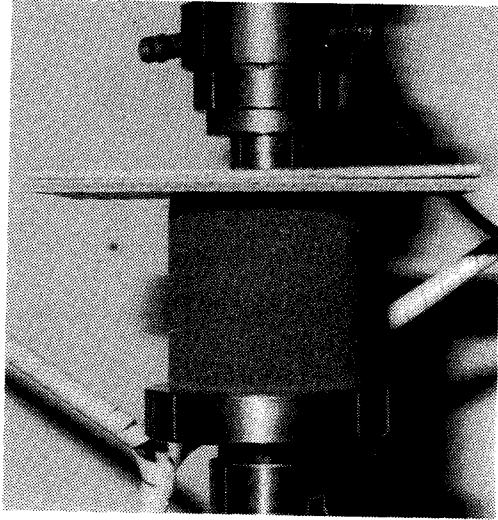
As a part of the effort to determine the effects of periodic cold soak on acoustic liner material, a measurement of the mechanical response was made. A test was performed to provide a measure of the mechanical resiliency of the liner materials. The test consisted of compressing a sample of the liner material to 25% of its length, releasing, and letting the material return to its natural state. Measurements of the sample length were made before and after the compression.

The tests were carried out on Pyrell foam and Fiberglass. Due to the nature of the Kevlar fabric, it was determined that this type of test would not be useful. The Pyrell samples were a nominal four inches in length and 100 mm in diameter. The Fiberglass samples were a nominal two inches in length and 100 mm in diameter. The tensile/compression rig used for this test was shown in figure 3.3. Figure 5.1 shows Pyrell and Fiberglass samples mounted in the test rig before and during compression. A wooden plate was used to allow a uniform force to compress the samples.

Table 5.1 shows the results of the resiliency tests. Two sets of Pyrell and Fiberglass samples were used, one set which has been periodically cold soaked in the cryogenic cooling chamber. The other set was from the unsoaked samples. It was concluded from these results that the periodic cold soak did not affect the mechanical resiliency of the Pyrell or the Fiberglass. The differences in the length between the two cases are attributable to nominal measurement

	Uncycled			Cycled		
	Initial	Final	% Δ L	Initial	Final	% Δ L
<i>Pyrell</i>	4.12	4.08	0.97	4.08	4.04	0.98
<i>Fiberglass</i>	2.00	1.97	1.50	2.00	1.97	1.50

Table 5.1 Results from mechanical resiliency tests on Pyrell and Fiberglass samples.



Pyrell Foam

Fiberglass

5.1 Mechanical resiliency test for Pyrell foam and Fiberglass.

6.0 CONCLUDING REMARKS

6.1 Summary of Work Done

This report documents the results of an experimental study on how acoustic properties of certain absorbing liner materials are affected by non-standard atmospheric conditions. This study was motivated by the need to assess risks associated with incorporating acoustic testing capability in wind tunnels with semi-cryogenic high Reynolds number aerodynamic and/or low pressure capabilities. The study consisted of three phases: 1) Measurement of acoustic properties of selected liner materials at sub-atmospheric pressure conditions, 2) Periodic cold soak and high pressure exposure of liner materials for 250 cycles, and 3) Determination of the effect of periodic cold soak on the acoustic properties of the liner materials at sub-atmospheric conditions and the effect on mechanical resiliency.

The selected liner materials were Pyrell foam, Fiberglass, and Kevlar. A vacuum facility was used to create the sub-atmospheric environment in which an impedance tube was placed to measure acoustic properties of the test materials. Results of the Phase I tests revealed that lower ambient pressure reduced the absorption effectiveness of the liner materials to varying degrees.

An automated cryogenic cooling system was used to perform the Phase II tests. Super-cooled air was passed through the liner material placed inside a specially-designed chamber to reduce the material temperature. A computer was used to automate and control the data acquisition and cycling of each material test. A cycle consisted of reducing the material temperature to -150 °F, then pressurizing to 5 atmospheres, and then returning the material back to ambient temperature and pressure. Each liner material was subjected to a total of 250 cycles.

Finally, Phase I tests were repeated to determine the effect of periodic cold soak and high pressure cycling on the acoustic properties of the liner materials. Results indicate that no significant change in the acoustic properties occurred after the periodic cold soak.

Furthermore, mechanical resiliency tests were carried out which indicated that no change in the liner material resiliency had occurred.

6.2 Recommendations and Future Work

The results of the present study raise some interesting questions:

1. Since sub-atmospheric ambient pressure conditions seem to decrease the absorption characteristics of certain bulk liner materials, what is the physical basis for this phenomena and how do other sound absorbing materials behave under similar conditions?
2. How do the acoustic properties of potential liner materials change in the presence of flow?
3. How does the acoustic performance of potential liner materials differ when oblique incident sound energy is present?
4. How do reactive liners perform at non-standard atmospheric conditions?

The answers to these questions will contribute to a more complete understanding of the main objective outlined in Section 1 of this report, namely, how can one integrate acoustic requirements into the initial phase of wind tunnel designs.

7.0 REFERENCES

1. Committee of Assessment of National Aeronautical Wind Tunnel Facilities, ASEB, "Review of Aeronautical Wind Tunnel Facilities," National Academy Press, 1988.
2. Wind Tunnel Study Task Team, National Aeronautics and Space Administration, "Assessment of NASA's Major Wind Tunnel Facilities with respect to Current and Future National Needs", 1987.
3. Kirkpatrick D. L. I., and Woodward D. S., "Priorities for High-Lift Testing in the 1990's," AIAA 16th Aerodynamic Ground Testing Conference, June 18-20, 1990. AIAA paper 90-1413.
4. Lynch, F. T., "Experimental Necessities for Subsonic Transport Configuration Development," 30th Aerospace Sciences Meeting and Exhibit, Jan 6-9, 1992. AIAA Paper 92-0158.
5. Lassiter, W. S., "Design Predictions for Noise Control in the Cryogenic National Transonic Facility," Noise Control Engineering, September-October 1981, pp. 76-84.
6. Bruel & Kjaer, "Two-microphone Impedance Measurement Tube Type 4206 - Technical Documentation," B&K, Naerum, Denmark, January, 1992.
7. Smith C. D., and Parrott T. L., "Comparison of Three Methods for Measuring Acoustic Properties of Bulk Materials," Journal of Acoustics Society America, Vol. 74, No. 5, TP. 577-1582, Nov. 1983.
8. Ahuja, K. K. (PI.), Gaeta, R. J., and Dreyer, E. Unpublished results from Task 14, NASA Langley Contract NAS1-19061, "High Temperature Liner Investigation," Final report to be issued, March, 1995.
9. Anonymous, "CF6 Bulk Absorber Inlet Acoustic Treatment Investigation," General Electric Technical Memorandum, May, 1976.
10. Zwicker, C., and Kosten, C. W., "Sound Absorbing Materials," *Elsevier Publishing Company, Inc.*, New York, 1949.
11. Hersh, Alan S., and Walker, Bruce, "Acoustic Behavior of Fibrous Bulk Materials," AIAA 80-0986, Presented at the AIAA 6th Aeroacoustic Conference, Hartford, CT, June 4-6, 1980.
12. Ross, V. N., Law, W., Ahuja, K.K., Gaeta, R.J., and Hsu, J., "A Unique Facility to Measure Acoustic Properties of Various Materials at Non-Standard Atmospheric Conditions," AIAA 93-4385, Presented at the 15th Aeroacoustics Conference, Long Beach, CA, October 25-27, 1993.

APPENDIX A

A.1 Calculation of Characteristic Acoustic Properties of Bulk Materials.

A.1.1 Theory of sound absorption by homogenous materials.

The determinations of acoustic properties for the bulk liner materials tested in this report was based on the theory of sound absorption by homogenous materials outlined by Zwicker and Kosten¹¹. If one considers a layer of bulk absorbing material of thickness l , bounded at $x_1 = 0$ by impedance z_1 and at $x_2 = l$ by impedance z_2 (see figure A1), the governing equation for the impedance at x_1 is:

$$z_1 = z_c \frac{z_2 \cosh(\gamma l) + z_c \sinh(\gamma l)}{z_2 \sinh(\gamma l) + z_c \cosh(\gamma l)}$$

where

A-1

$z_c \equiv$ Complex Characteristic Impedance

$\gamma \equiv$ Complex Propagation Constant

A special case of $z_2 = \infty$ results in the governing equation being reduced to the simplified form of:

$$z_1 = z_c \coth(\gamma l)$$

A-2

Equation A-2 is valuable for investigating bulk absorbing material with a completely hard back wall, as shown in figure A2. Equation A-2 then becomes the basic equation used for the computation of the characteristic acoustic properties of a bulk absorbing material.

A.1.2 Two Thickness Method of Analysis - Sample Calculations

It is shown above that for absorbing materials with a rigid back wall the governing equation for the input impedance is a function of the characteristic impedance, propagation constant, and the thickness of the material. The objective is to find the characteristic acoustic properties of the bulk liner materials. Following Smith and Parrott⁷, two samples of the same material (one

thickness being twice of the other) can be used to find the characteristic properties. From the previous section, the governing equations for two thicknesses of material backed by a rigid wall are:

$$\begin{aligned} z_1 &= z_c \coth(\gamma l) \\ z_2 &= z_c \coth(\gamma 2l) \end{aligned} \tag{A-3}$$

The task is now to find z_c and γ by solving equation A-1 given l and the complex input impedances z_1 and z_2 . Solving for the characteristic impedance yields:

$$z_c = \sqrt{z_1(2z_2 - z_1)} \tag{A-4}$$

Solving for the propagation constant yields:

$$\gamma = \frac{1}{2l} \ln \left[\frac{1+u}{1-u} \right] \tag{A-5}$$

where

$$u = \left[\frac{2z_2 - z_1}{z_1} \right]^{\frac{1}{2}} \tag{A-6}$$

From equations A-5 and A-6, it is evident that if the complex impedances z_1 and z_2 are equal, then the propagation constant becomes infinite. As an example on how the characteristic properties are calculated from equations A-4 through A-6, data from impedance tube tests of ceramic honeycomb material (CT73) will be used to calculate characteristic impedance and propagation constant. From impedance tube measurements, the input impedance of two thicknesses of CT73 at a frequency of 1000 Hz are:

$$\begin{aligned} z_1 &= 0.3077 - 0.9304i & \text{for } l = 1.73 \text{ inches} \\ z_2 &= 0.6913 + 0.4877i & \text{for } l = 3.46 \text{ inches} \end{aligned}$$

Substituting into equation A-3 and solving yields:

$$\begin{aligned}
z_c &= \left[(0.3077 - 0.9304i)(2(0.6913 + 0.4877i) - (0.3077 - 0.9304i)) \right]^{\frac{1}{2}} \\
&= \left[(0.3077 - 0.9304i)((1.3826 + 0.9754i) - (0.3077 - 0.9304i)) \right]^{\frac{1}{2}} \\
&= [0.3307 + 0.5864i - 1.0001i + 1.7732]^{\frac{1}{2}} \\
&= [2.1039 - 0.4137i]^{\frac{1}{2}} \\
&= [2.1442e^{i(-11.1244)}]^{\frac{1}{2}} \\
&= 1.4643e^{i(-5.5622)} \\
z_c &= \underbrace{1.4574}_{R_c} - \underbrace{0.1419i}_{X_c}
\end{aligned}$$

As noted previously, the impedances are normalized to the impedance of the ambient air. The real and imaginary components of the characteristic impedance are the characteristic resistance and reactance, respectively. Using the same input impedances, the propagation constant is now computed, starting from equation A-6:

$$\begin{aligned}
u &= \left[\frac{2(0.6913 + 0.4877i) - (0.3077 - 0.9304i)}{(0.3077 - 0.9304i)} \right]^{\frac{1}{2}} \\
&= \left[\frac{(1.0749 + 1.9058i)}{0.3077 - 0.9304i} \right]^{\frac{1}{2}} \\
&= \left[\frac{2.1880e^{i(60.5763)}}{0.9800e^{i(-71.7000)}} \right]^{\frac{1}{2}} \\
&= [2.2327e^{i(132.2763)}]^{\frac{1}{2}} \\
u &= 1.4942e^{i(66.1382)} = 0.6045 + 1.365i
\end{aligned}$$

Using $l = 1.73$ inches = 0.04394 m and substituting into equation A-5 yields:

$$\begin{aligned}
\gamma &= \frac{1}{2l} \ln \left[\frac{1 + (0.6045 + 1.3665i)}{1 - (0.6045 + 1.3665i)} \right] \\
&= \frac{1}{2(0.04394)} \ln \left[\frac{(1.6045 + 1.3665i)}{(0.3955 - 1.3665i)} \right] \\
&= \frac{1}{0.087884} \ln \left[\frac{2.1075e^{i(40.4199)}}{1.4226e^{i(-73.8582)}} \right] \\
&= 11.3786 \ln \left[1.4814e^{i(114.2781)} \right] \\
&= 11.3786 [\ln(1.4814) + 1.9945i] \\
\gamma &= \underbrace{4.4716}_{\alpha} + \underbrace{22.6946i}_{\beta}
\end{aligned}$$

The real component of γ is the attenuation rate (α) and the imaginary component is the phase constant (β). In order to express the attenuation rate in dB/m the following computations need to be made:

$$\begin{aligned}
p_1 &= e^{-\alpha l_1} \\
p_2 &= e^{-\alpha l_2} \\
\alpha_{\frac{dB}{m}} &= 20 \log \left(\frac{p_1}{p_2} \right) \\
&= 20 \log \left(\frac{e^{-\alpha l_1}}{e^{-\alpha l_2}} \right) \\
&= 20 \log \left(e^{\alpha(l_2 - l_1)} \right) \\
&= \alpha 20 \log \left(e^{(l_2 - l_1)} \right)
\end{aligned}$$

with $l_2 - l_1 = 1$

$$\alpha_{\frac{dB}{m}} = [20 \log e] \alpha$$

or

$$\alpha_{\frac{dB}{m}} = 8.6859 \alpha$$

Thus the propagation constant computed previously becomes:

$$\gamma = \underbrace{38.8399}_{\alpha} + \underbrace{22.6946i}_{\beta}$$

Where the attenuation rate, α and the phase constant, β are in dB/m and rad/m respectively.

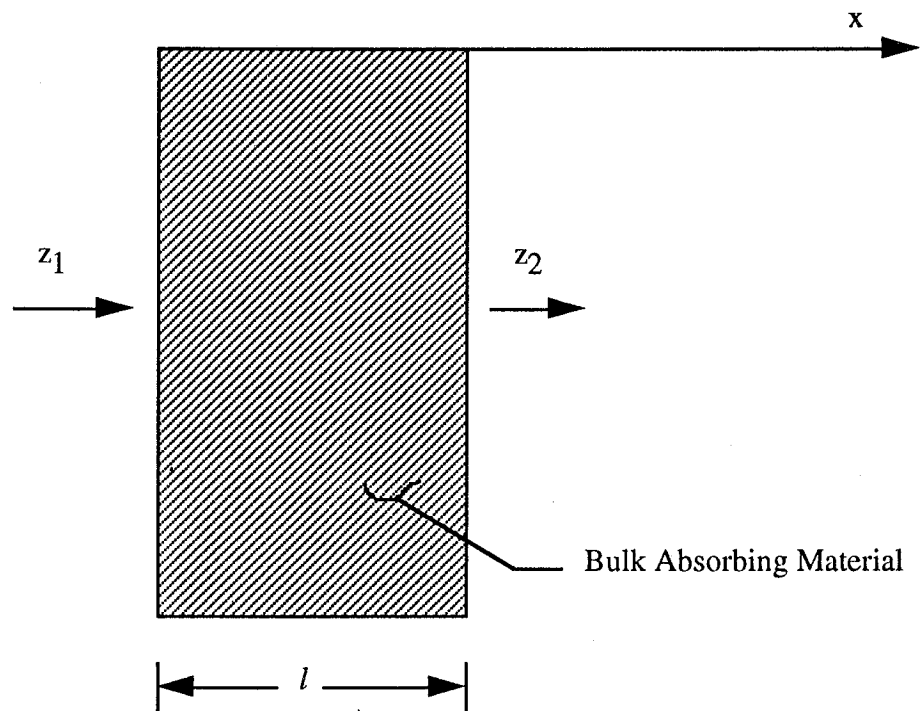


Figure A1. Model for Bulk Absorbing Material Calculations.

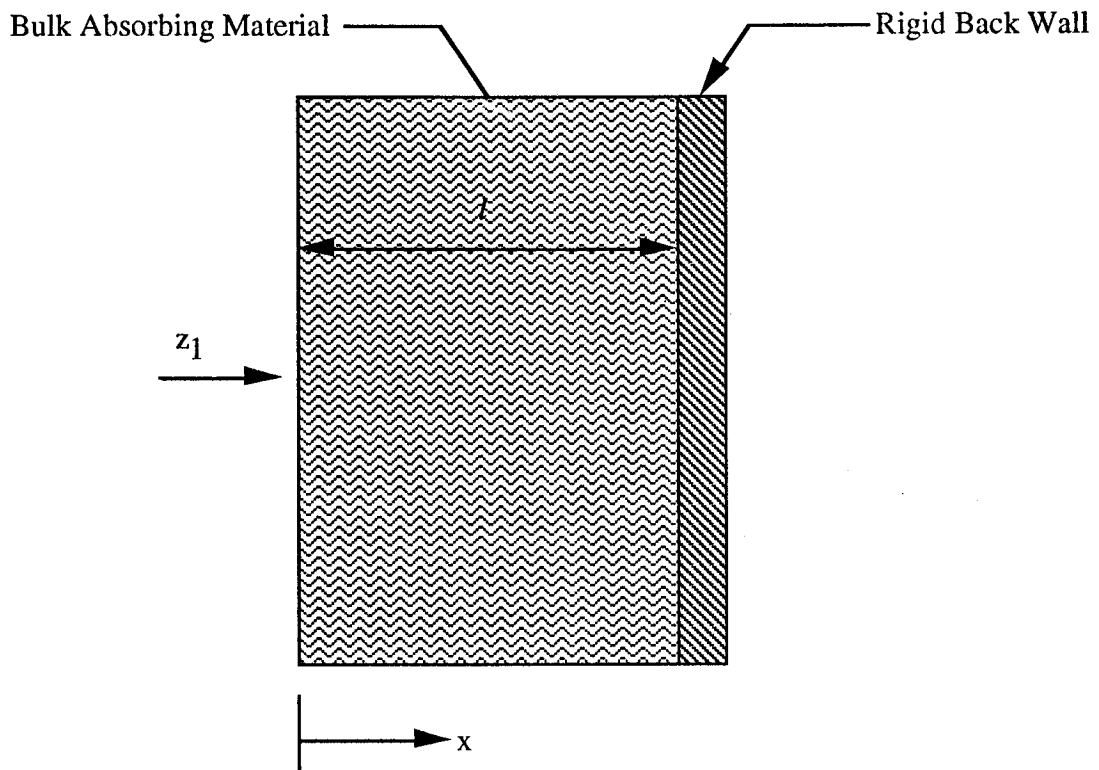


Figure A2. Rigid Back Wall Boundary Condition applied to Bulk Absorbing Layer.

APPENDIX B

This Appendix contains acoustic property data obtained from Phase I and Phase III of this program (see Section 1 of this report). This data includes absorption coefficient, normalized characteristic impedance, attenuation rate, and phase constant spectra. In general, as stated in the concluding remarks of this report, a significant change in the acoustic properties was not observed after periodic cold soak of the liner materials. However, it is believed that any significant differences that appear in the foregoing appendix are due to the inability of reproducing the exact vacuum pressure condition in both cases.

Before and after periodic cold soak results are presented in each figure with the following exceptions: figure B10, figure B42, figure B46, figure B70 and figure B78. Only data from Phase I was presented for these plots because the Phase III data was lost on a computer during a power outage.

Figure B88 does not contain Phase I data because of an inability to calculate the attenuation constant by the Two Thickness Method. The input data for figure B88 are the impedance of Fiberglass at 25% P_{amb} . A comparison of this input data reveals that z_1 and z_2 are sufficiently close in value as to prevent accurate calculation of the attenuation constant (see Appendix A for characteristic property calculation). This is a similar problem which was experienced with Kevlar and discussed in detail in the report.

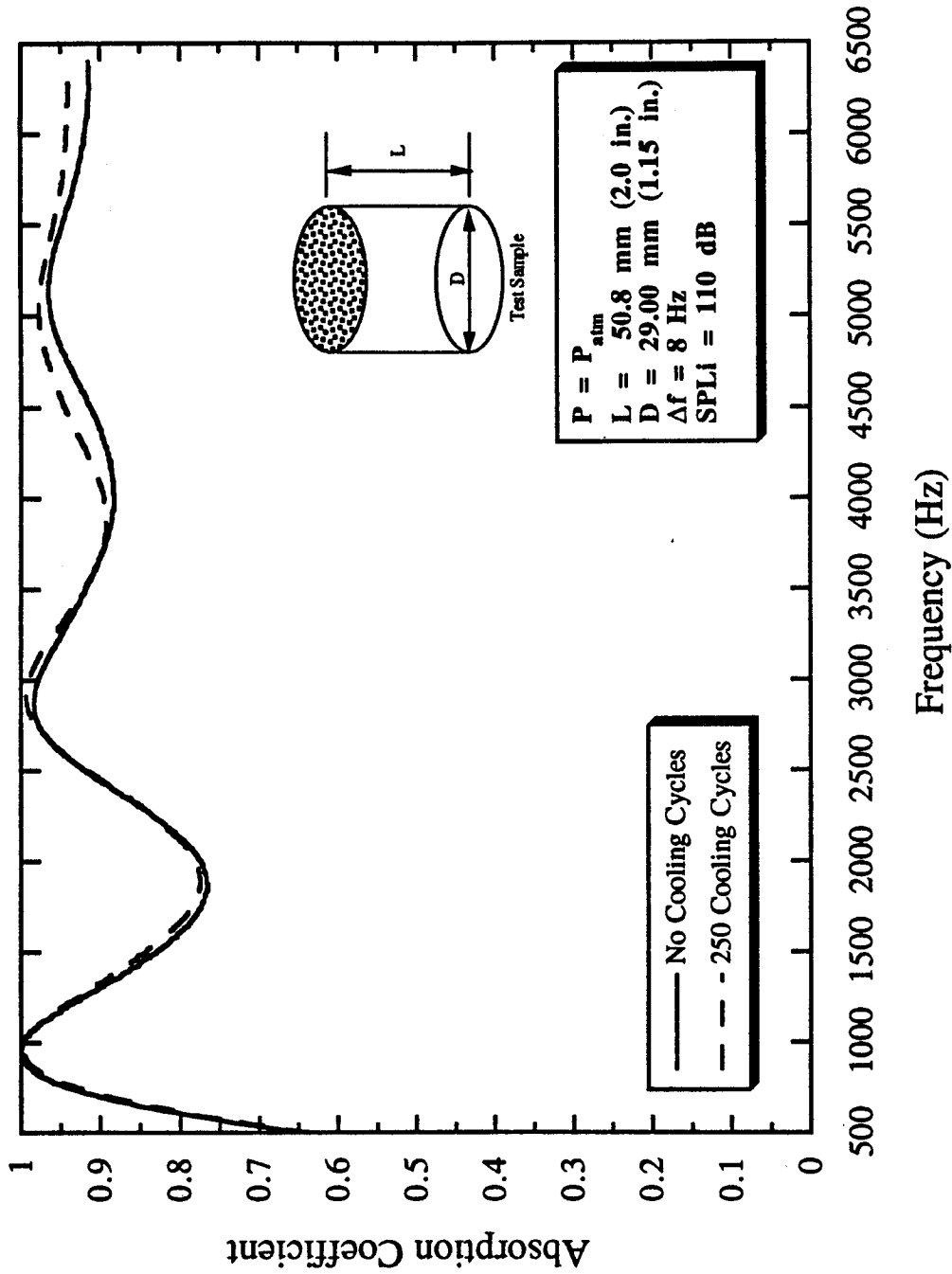


Figure B1. Absorption coefficient of Pyrell foam, $P = P_{atm}$, $L = 50.8 \text{ mm}$, $D = 29.0 \text{ mm}$.

B-2

B.2

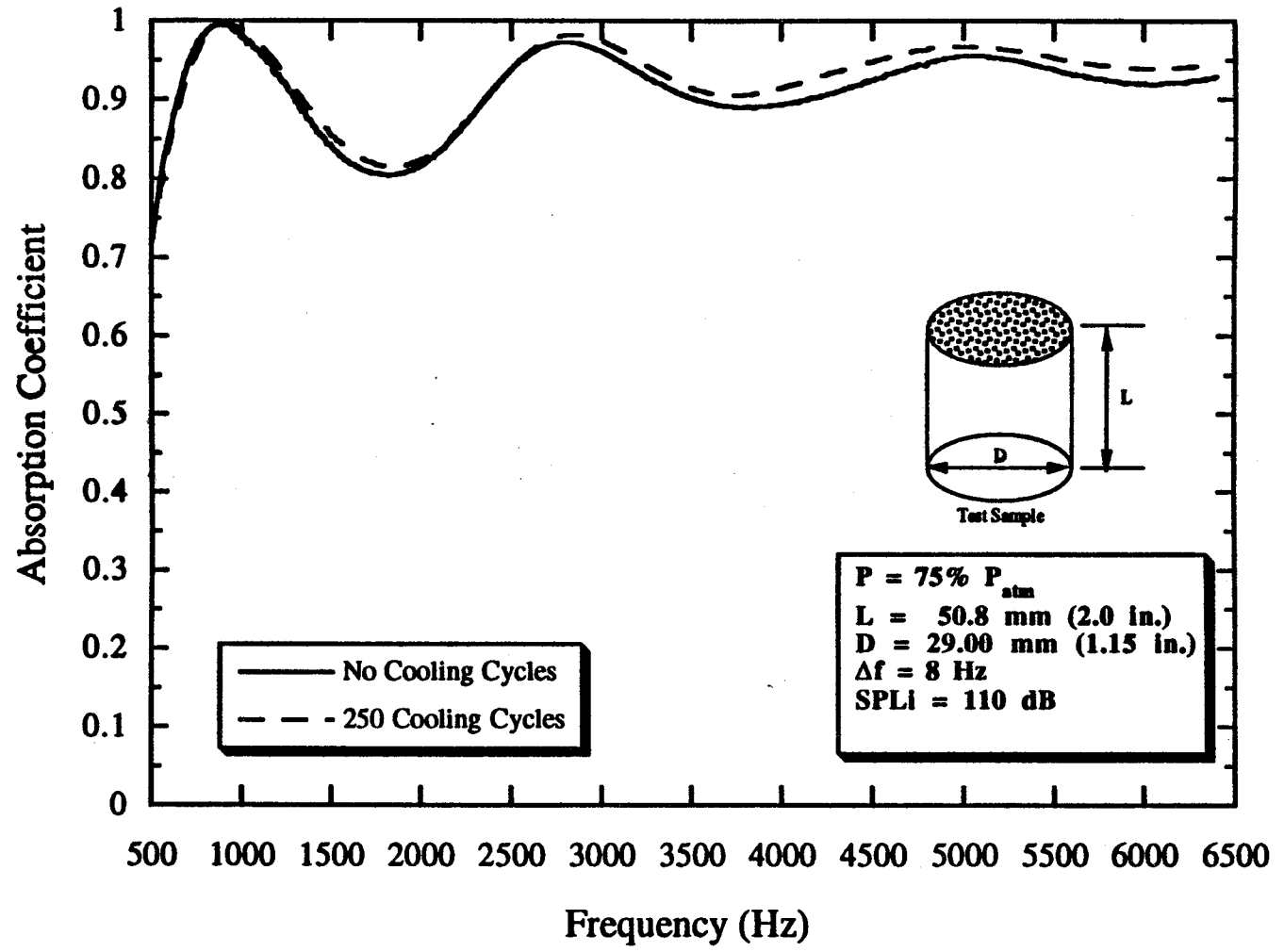


Figure B2. Absorption coefficient of Pyrell foam, $P = 75\% P_{atm}$, $L = 50.8 \text{ mm}$, $D = 29.0 \text{ mm}$.

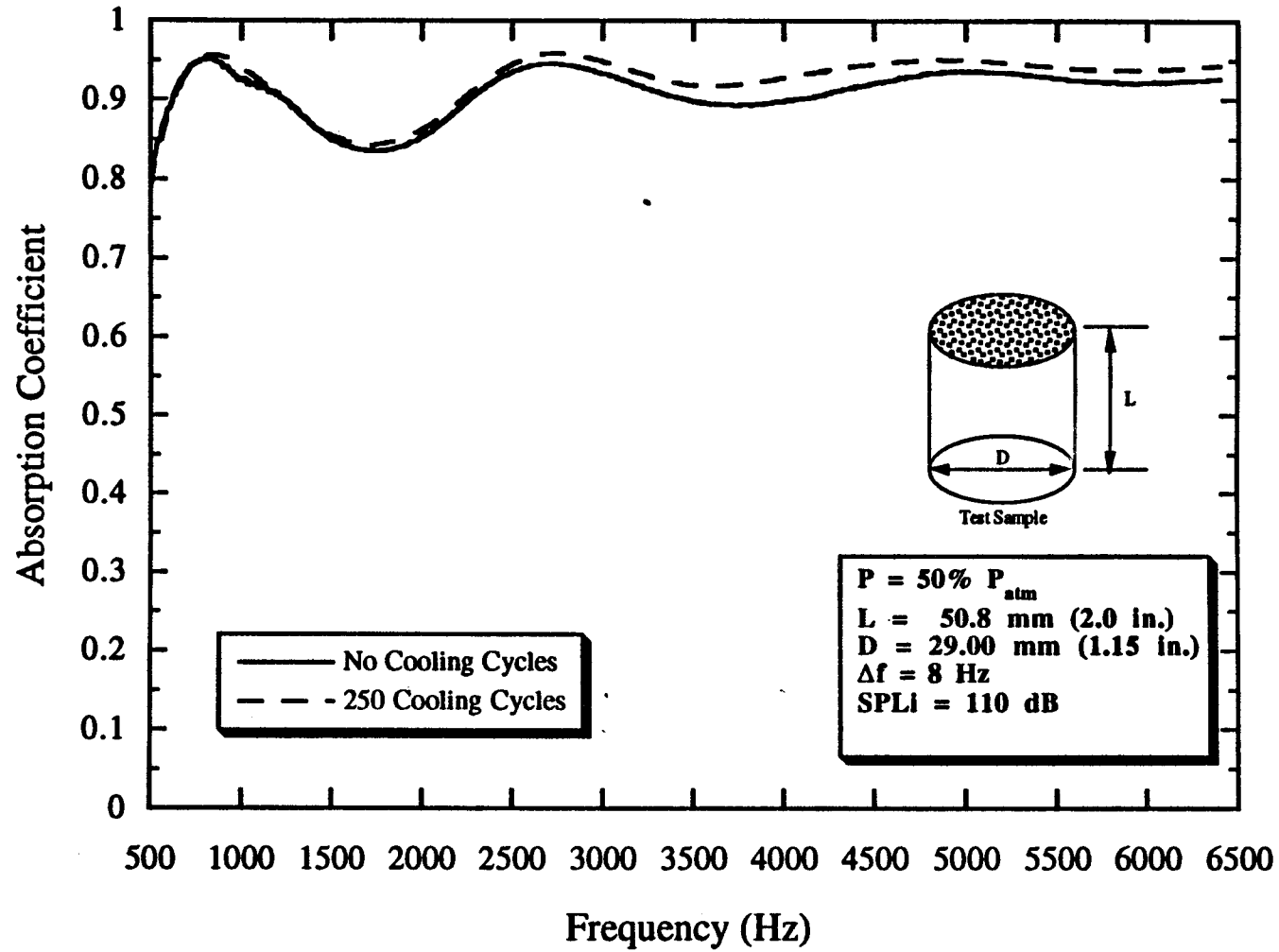


Figure B3. Absorption coefficient of Pyrell foam, $P = 50\% P_{atm}$, $L = 50.8 \text{ mm}$, $D = 29.0 \text{ mm}$.

B.4

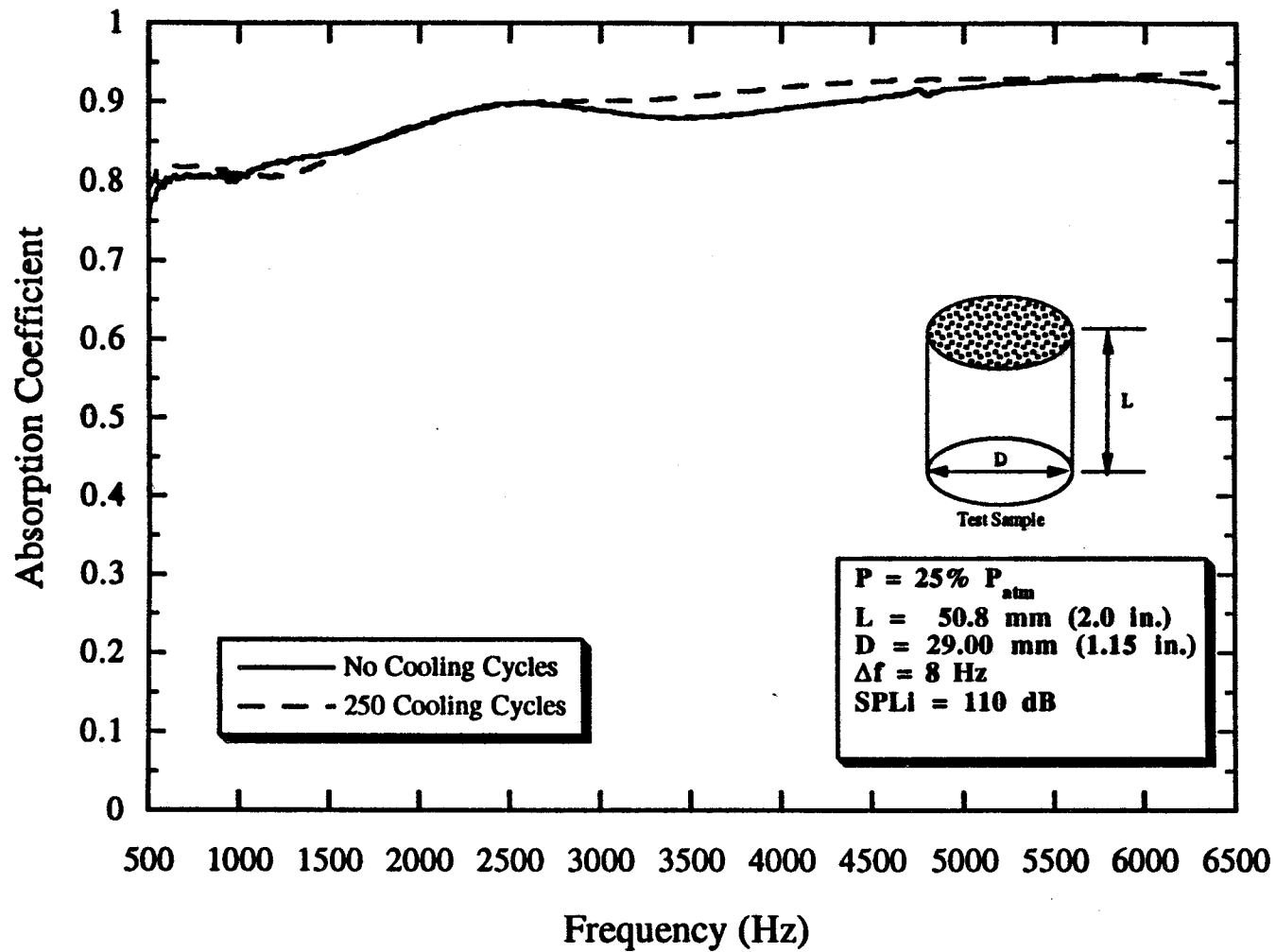


Figure B4. Absorption coefficient of Pyrell foam, $P = 25\% P_{atm}$, $L = 50.8 \text{ mm}$, $D = 29.0 \text{ mm}$.

B.5

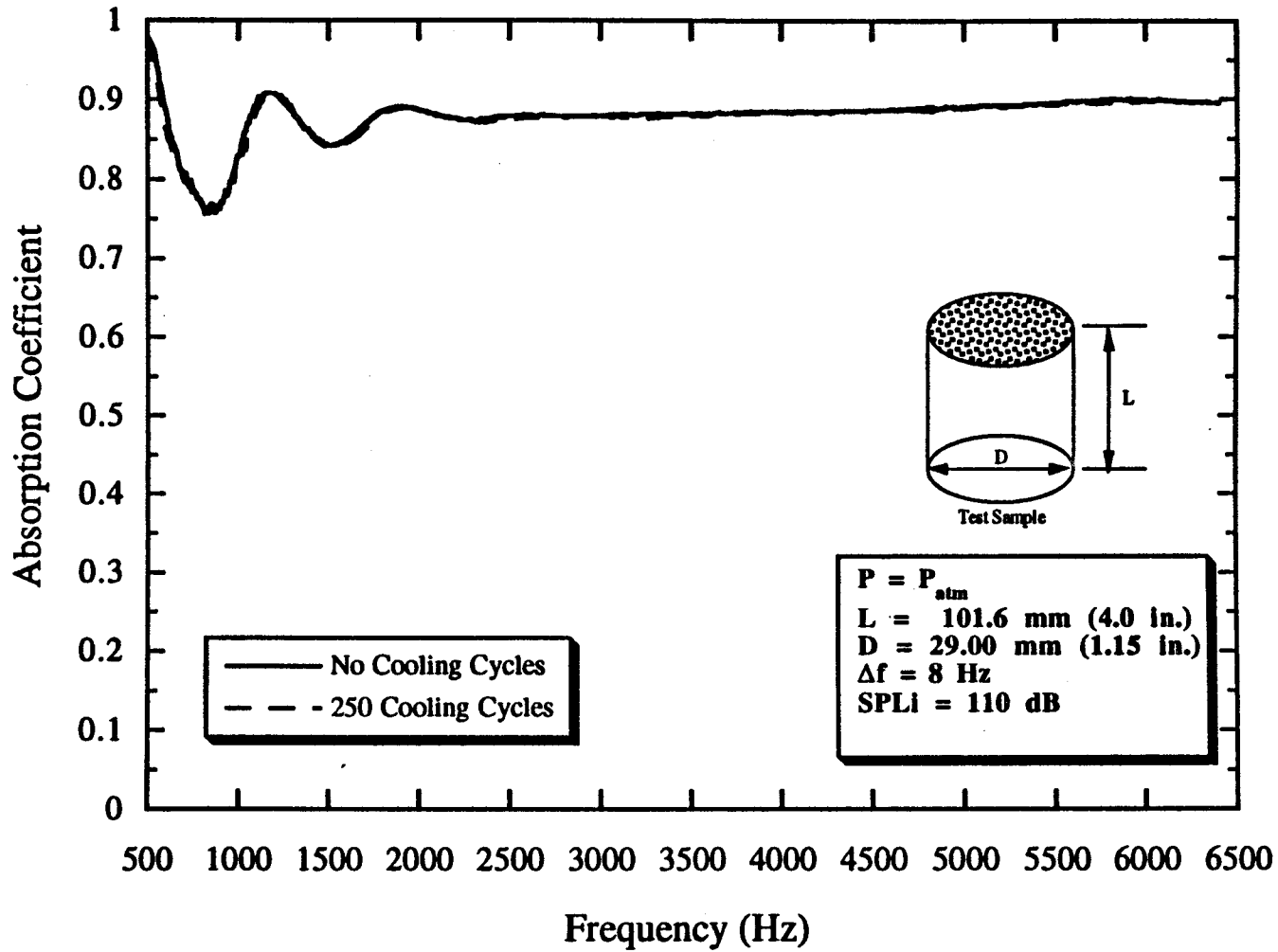


Figure B5. Absorption coefficient of Pyrell foam, $P = P_{atm}$, $L = 101.6\text{mm}$, $D = 29.0 \text{ mm}$.

B.6

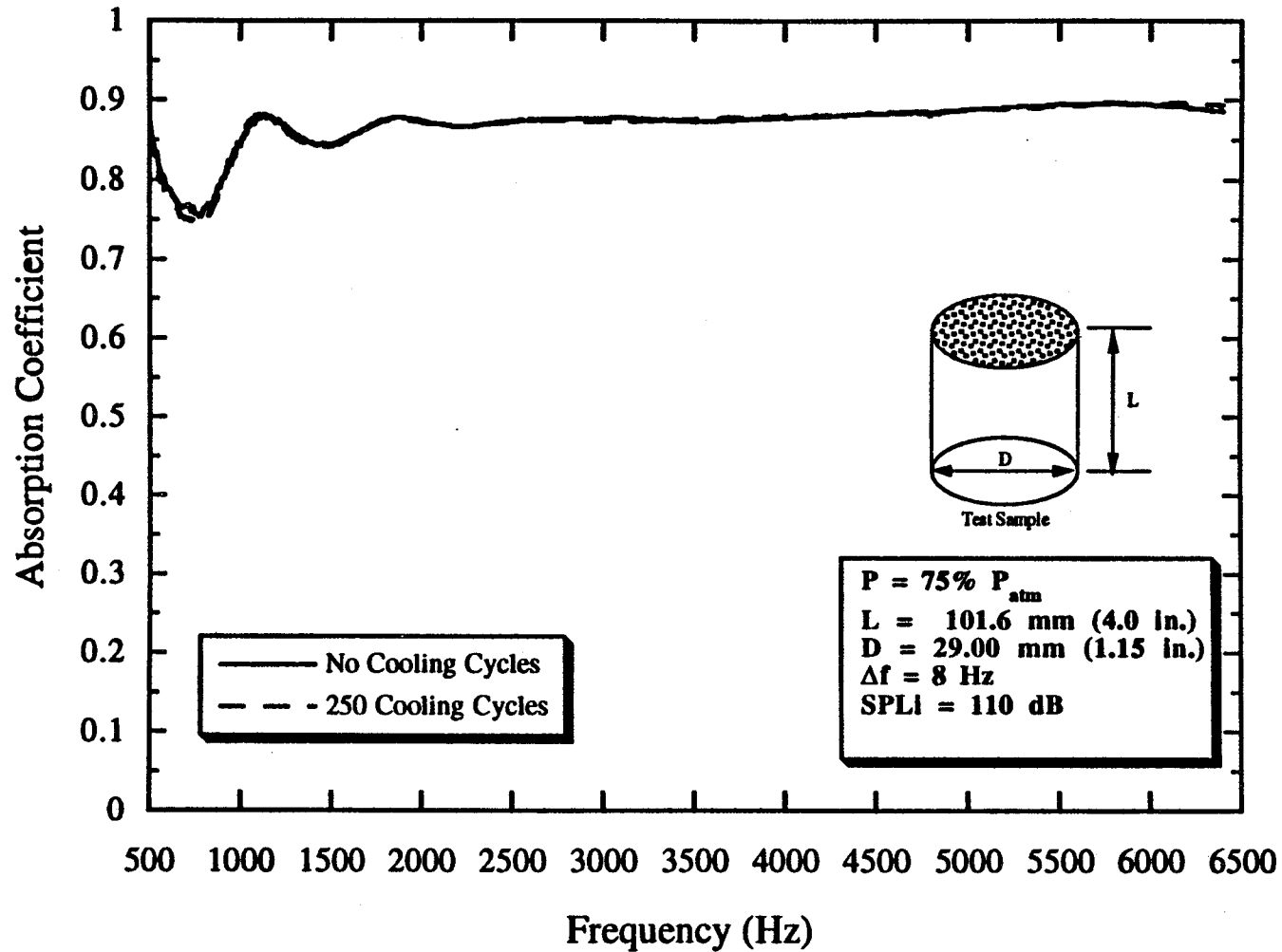


Figure B6. Absorption coefficient of Pyrell foam, $P = 75\% P_{atm}$, $L = 101.6\text{mm}$, $D = 29.0 \text{ mm}$.

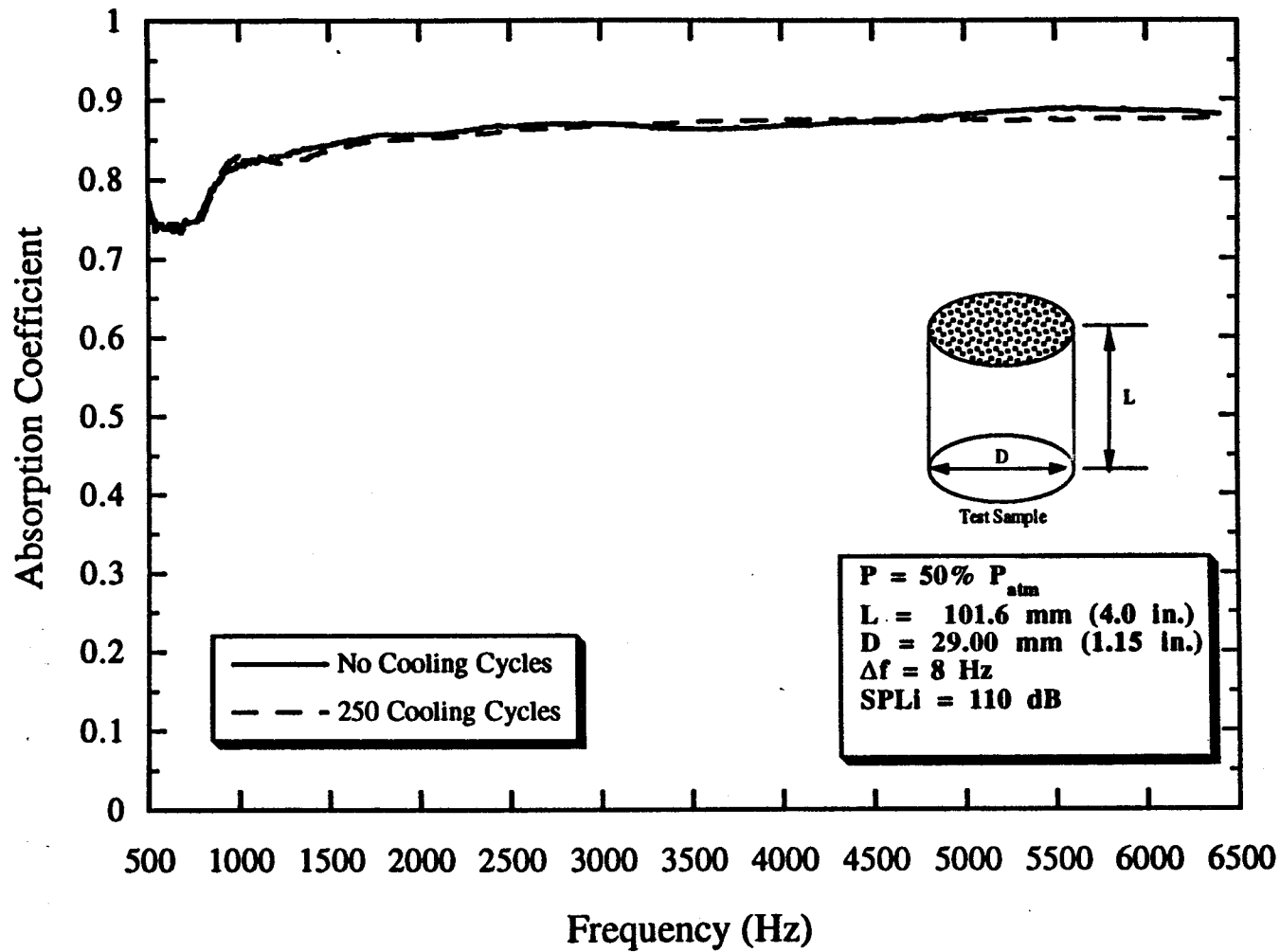


Figure B7. Absorption coefficient of Pyrell foam, $P = 50\% P_{atm}$, $L = 101.6\text{mm}$, $D = 29.0 \text{ mm}$.

B.8

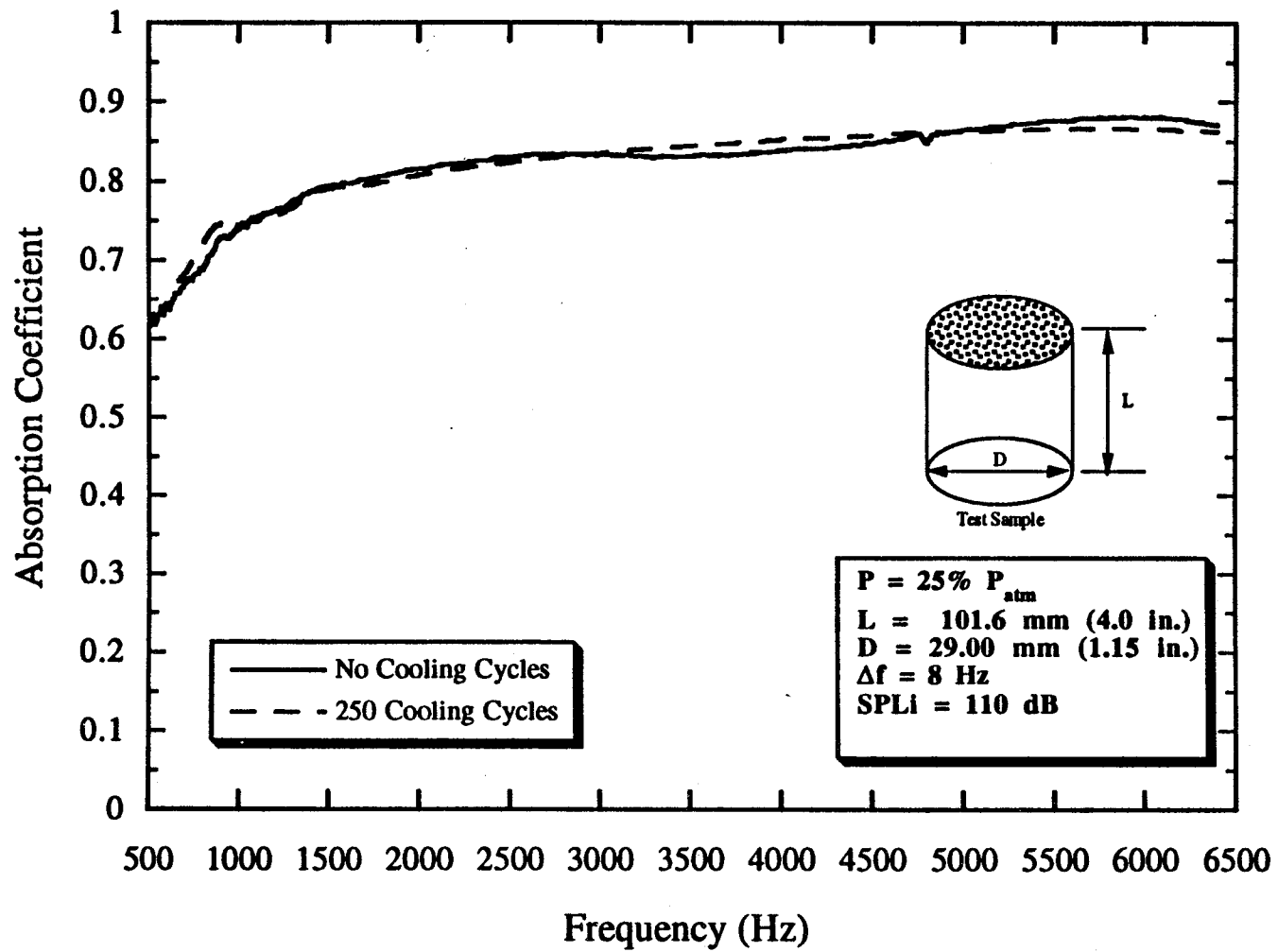


Figure B8. Absorption coefficient of Pyrell foam, $P = 25\% P_{atm}$, $L = 101.6\text{mm}$, $D = 29.0 \text{ mm}$.

B.9

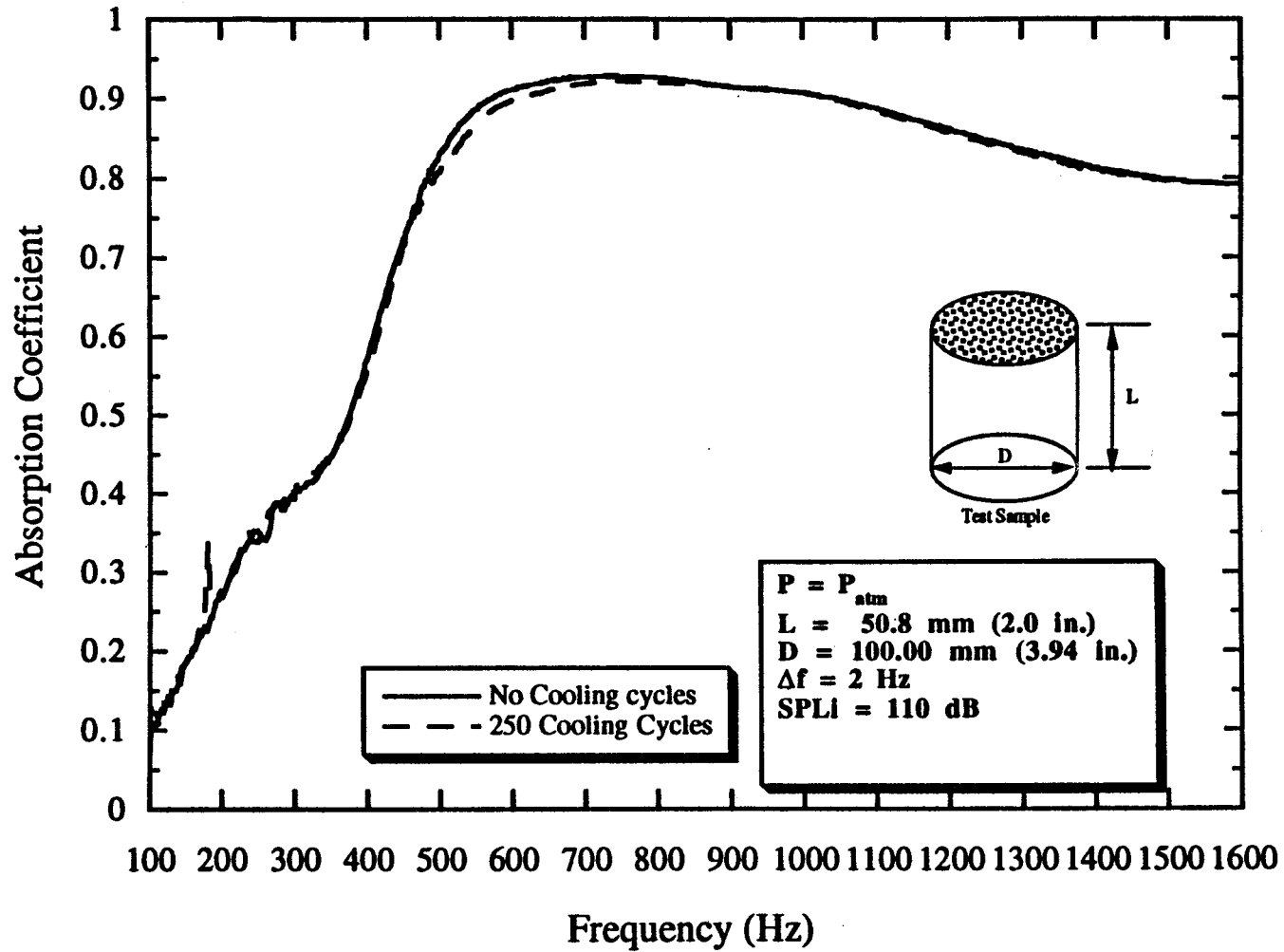


Figure B9. Absorption coefficient of Pyrell foam, $P = P_{atm}$, $L = 50.8 \text{ mm}$, $D = 100.0 \text{ mm}$.

B.10

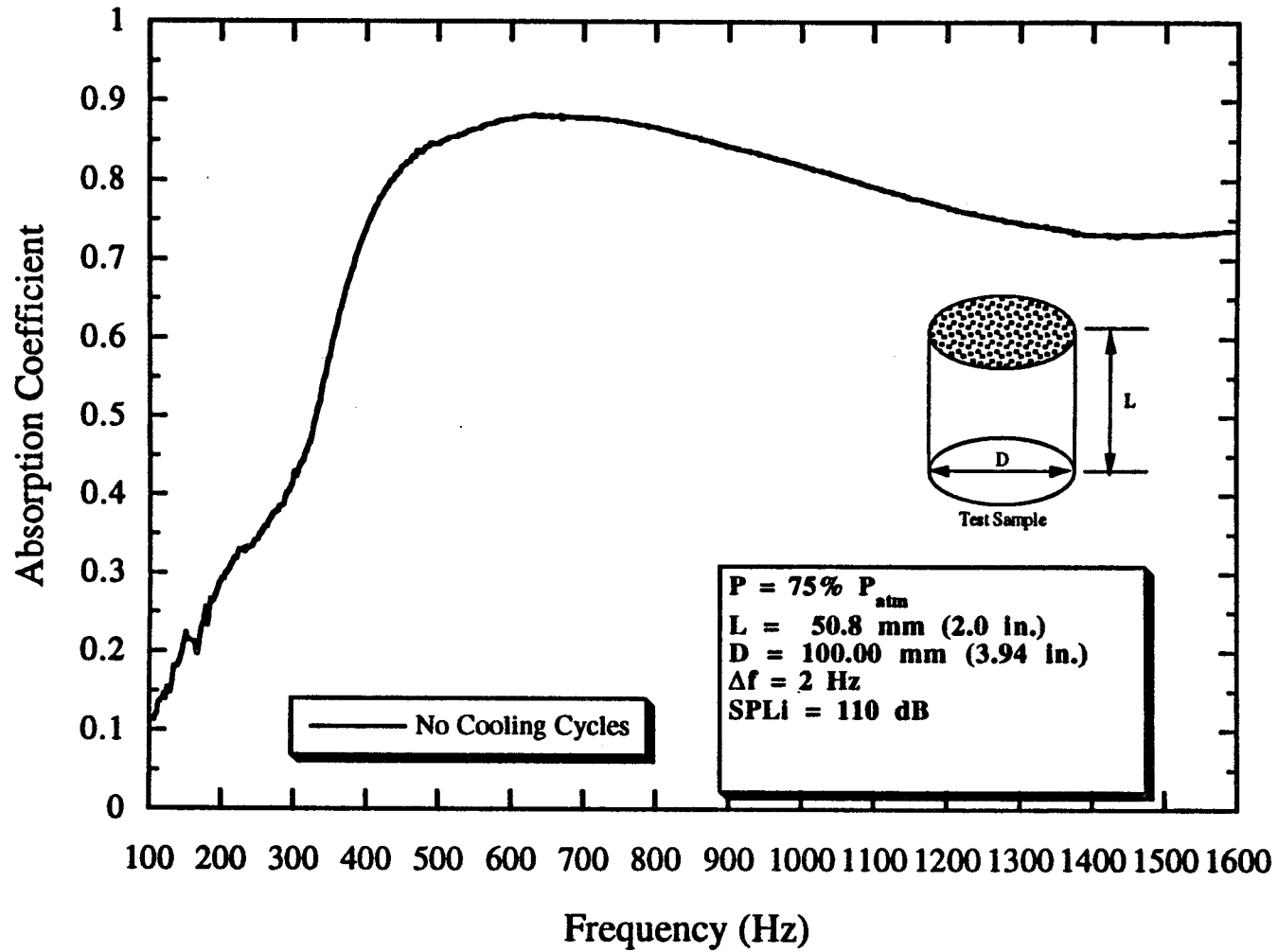


Figure B10. Absorption coefficient of Pyrell foam, $P = 75\% P_{atm}$, $L = 50.8 \text{ mm}$, $D = 100.0 \text{ mm}$.

B.11

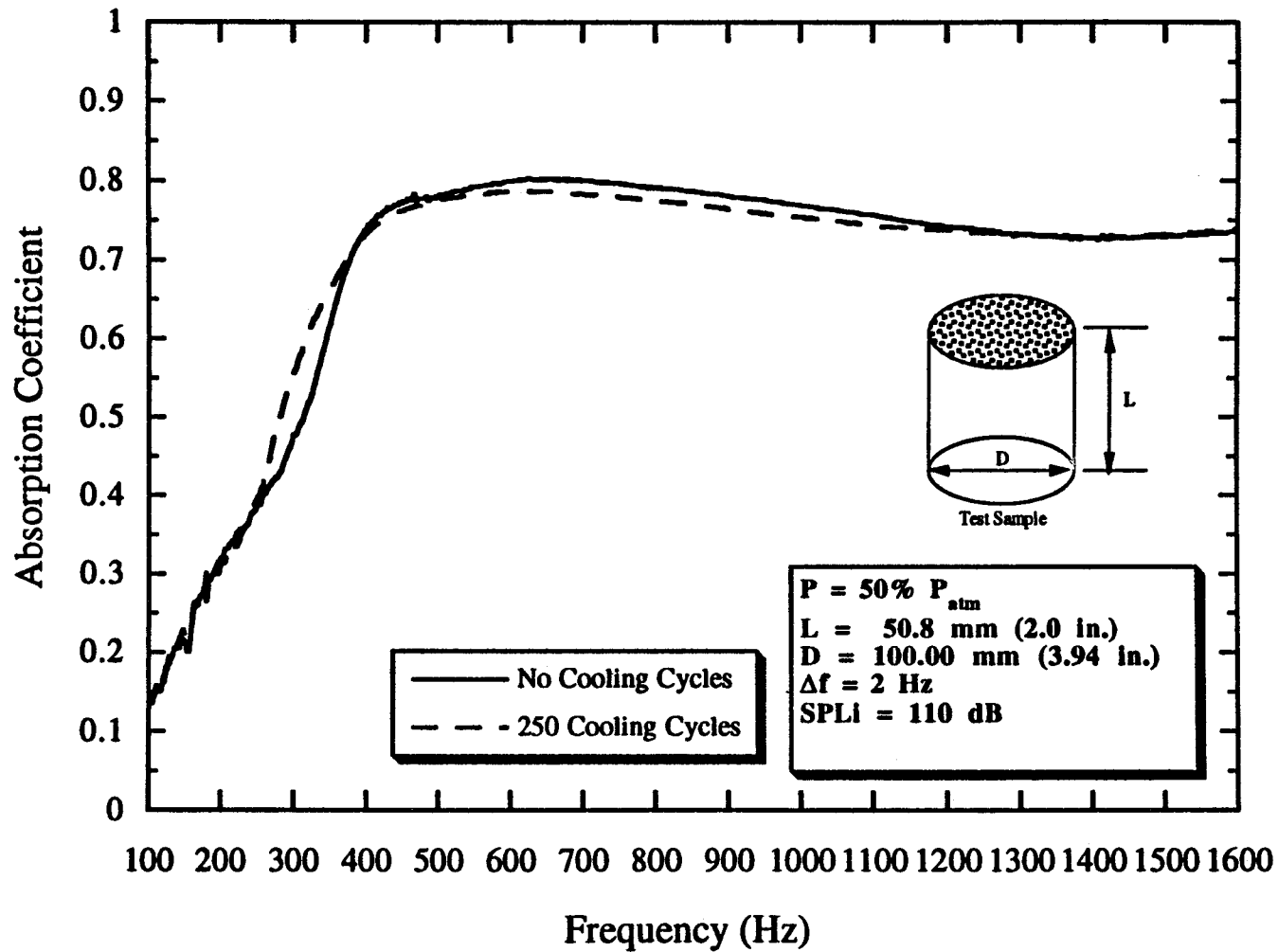


Figure B11. Absorption coefficient of Pyrell foam, $P = 50\% P_{atm}$, $L = 50.8 \text{ mm}$, $D = 100.0 \text{ mm}$.

B.12

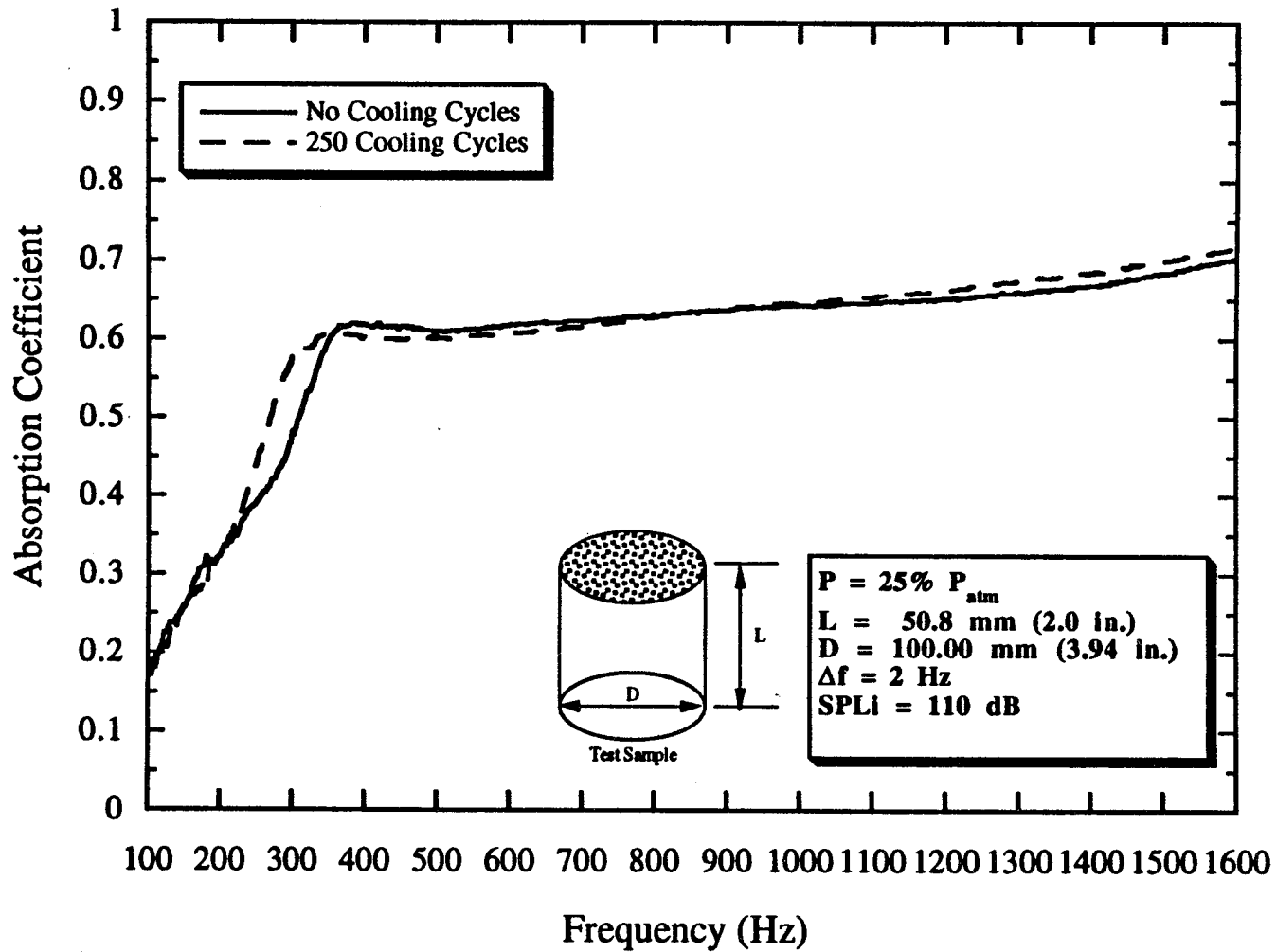


Figure B12. Absorption coefficient of Pyrell foam, $P = 25\% P_{atm}$, $L = 50.8 \text{ mm}$, $D = 100.0 \text{ mm}$.

B.13

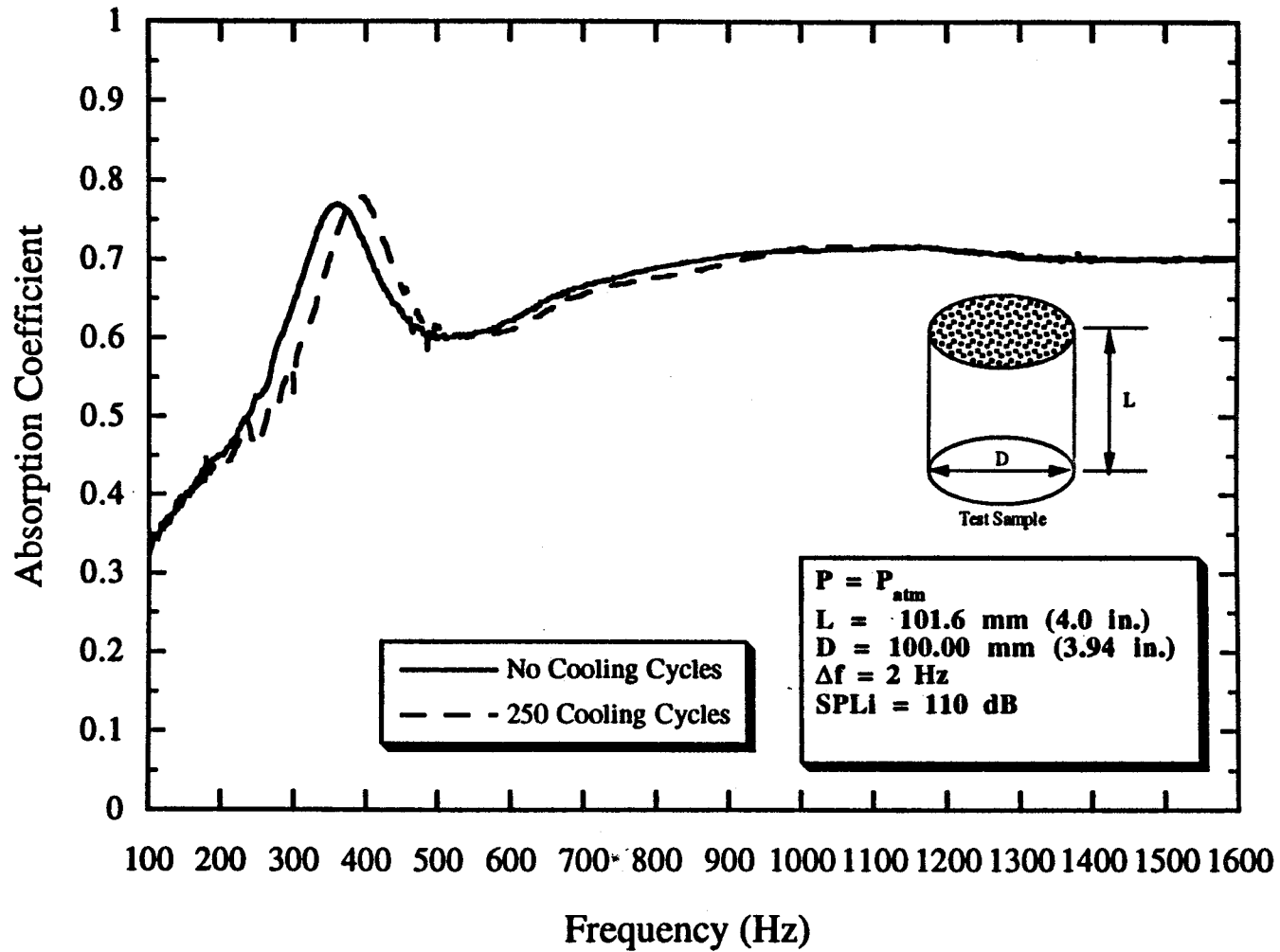


Figure B13. Absorption coefficient of Pyrell foam, $P = P_{atm}$, $L = 101.6 \text{ mm}$, $D = 100.0 \text{ mm}$.

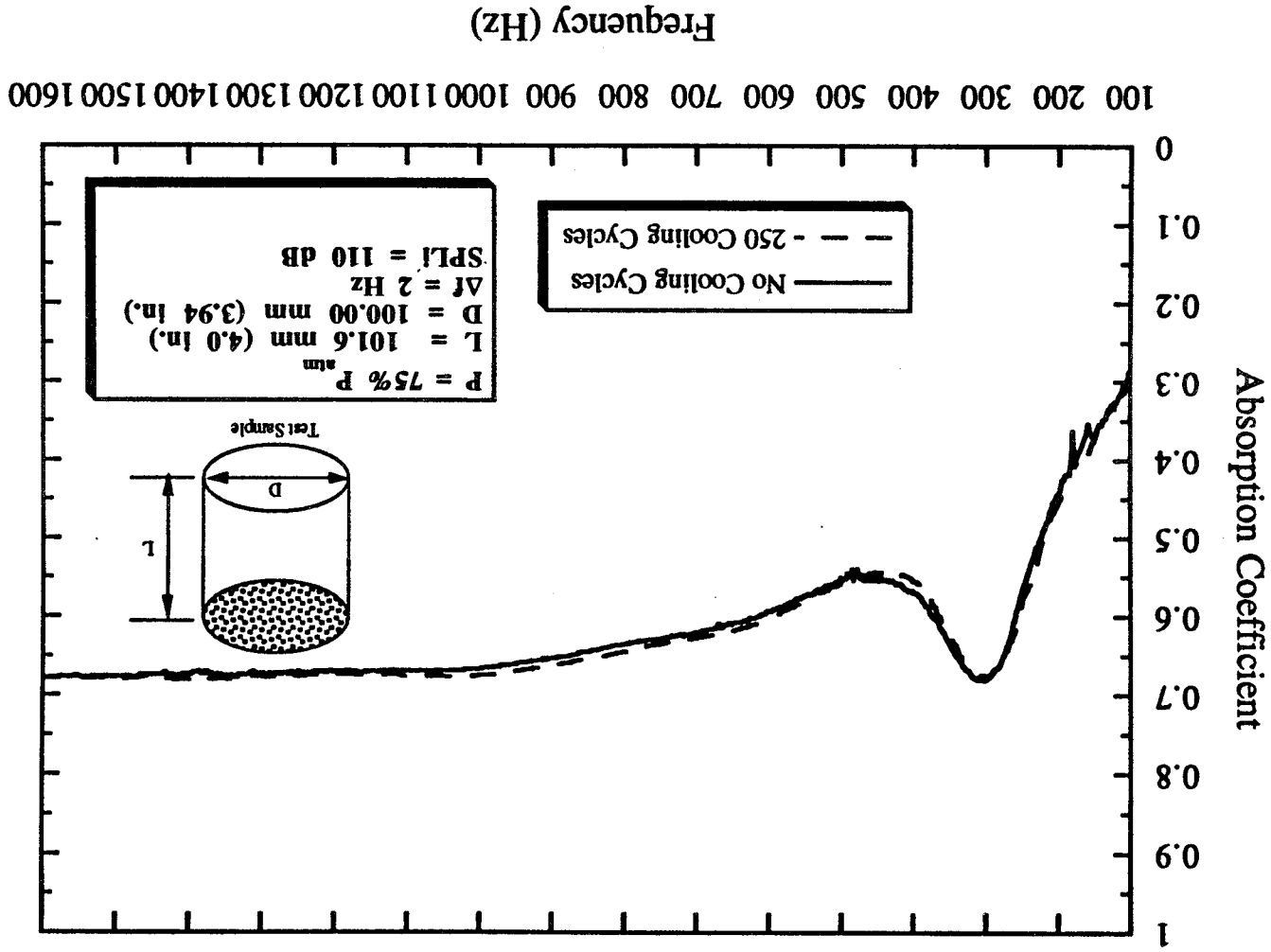


Figure B14. Absorption coefficient of Pyrell foam, $P = 75\% P_{atm}$, $L = 101.6 \text{ mm}$, $D = 100.0 \text{ mm}$.

B.15

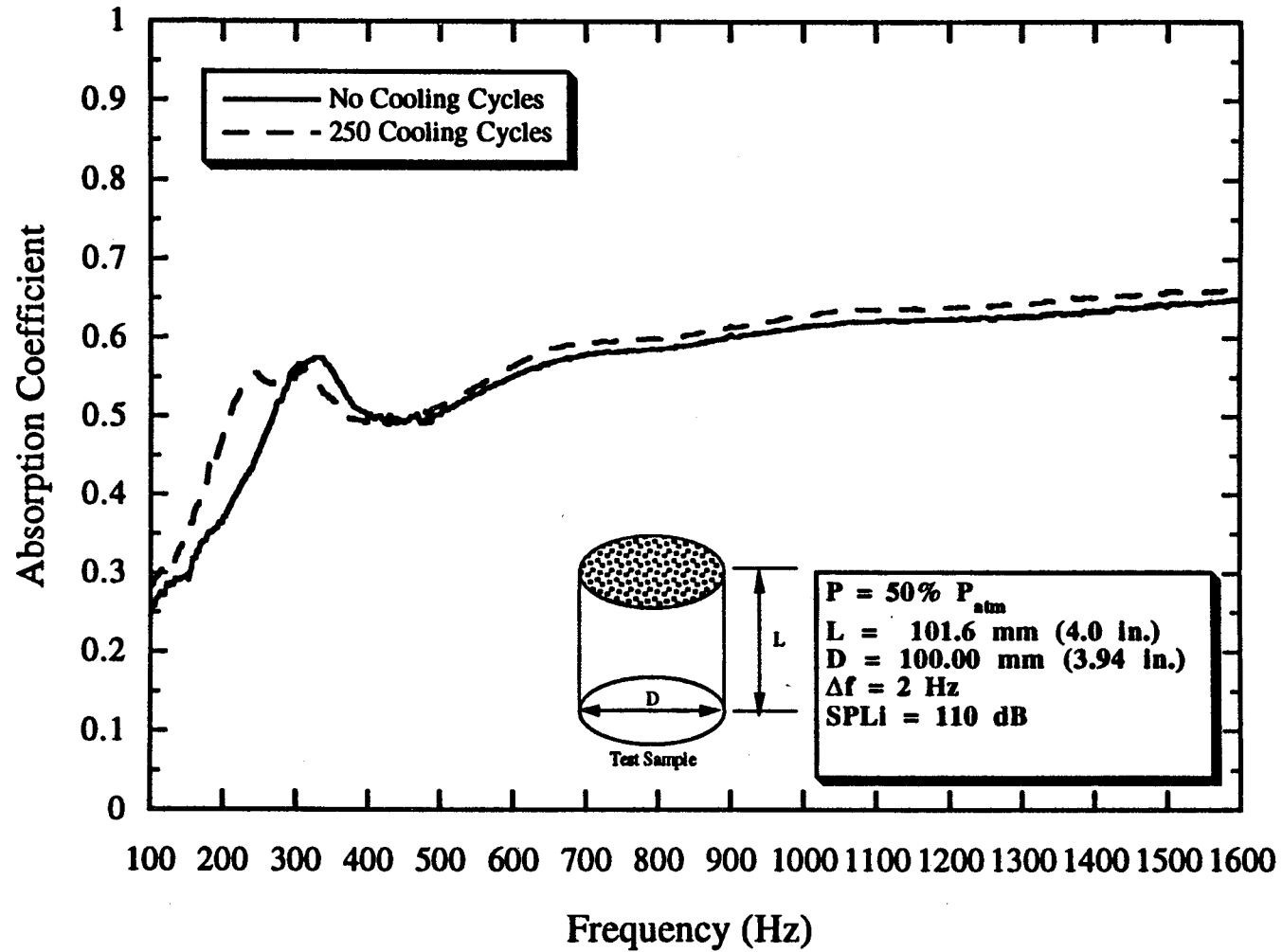


Figure B15. Absorption coefficient of Pyrell foam, $P = 50\% P_{atm}$, $L = 101.6 \text{ mm}$, $D = 100.0 \text{ mm}$.

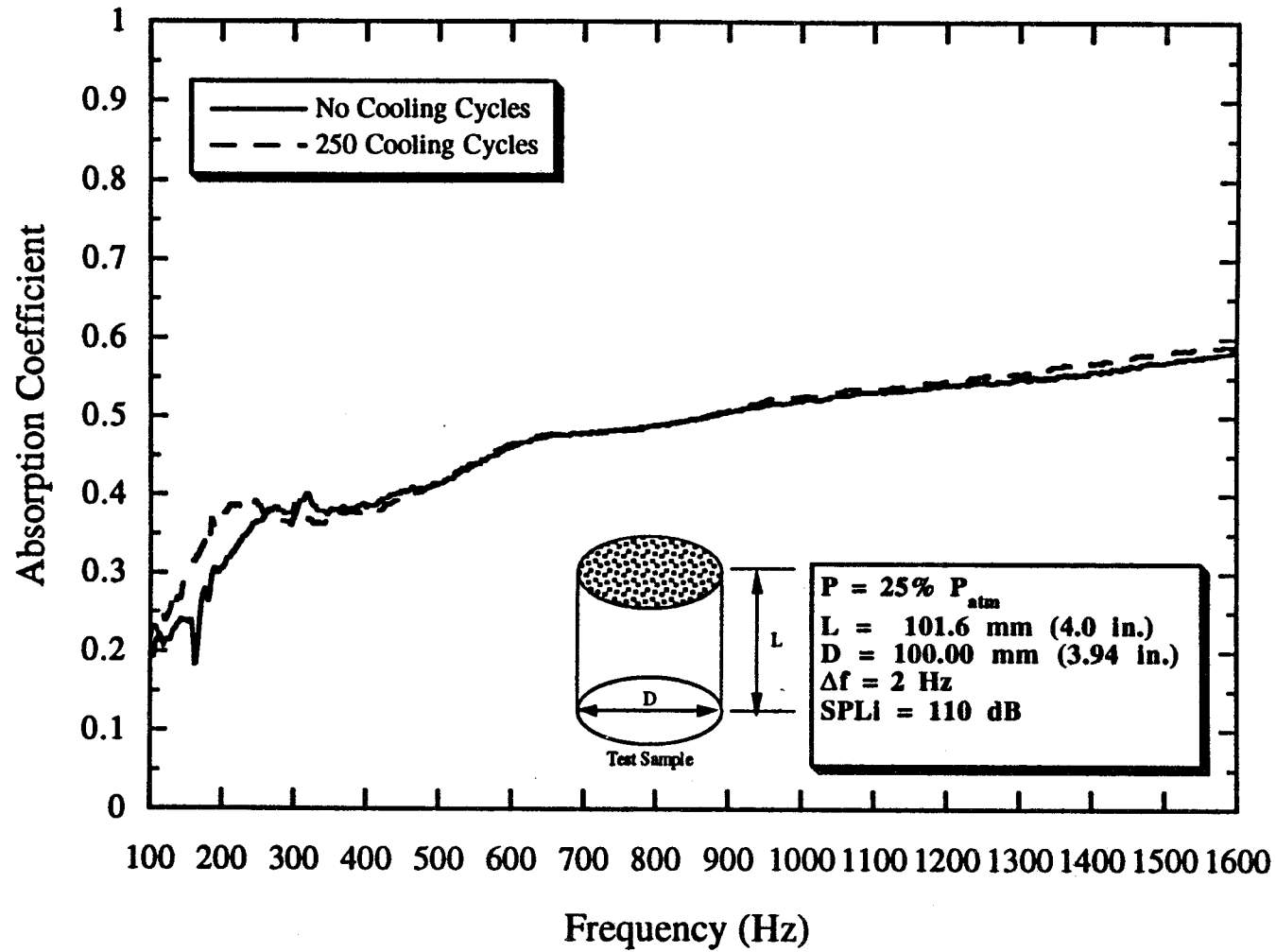


Figure B16. Absorption coefficient of Pyrell foam, $P = 25\% P_{atm}$, $L = 101.6 \text{ mm}$, $D = 100.0 \text{ mm}$.

B.17

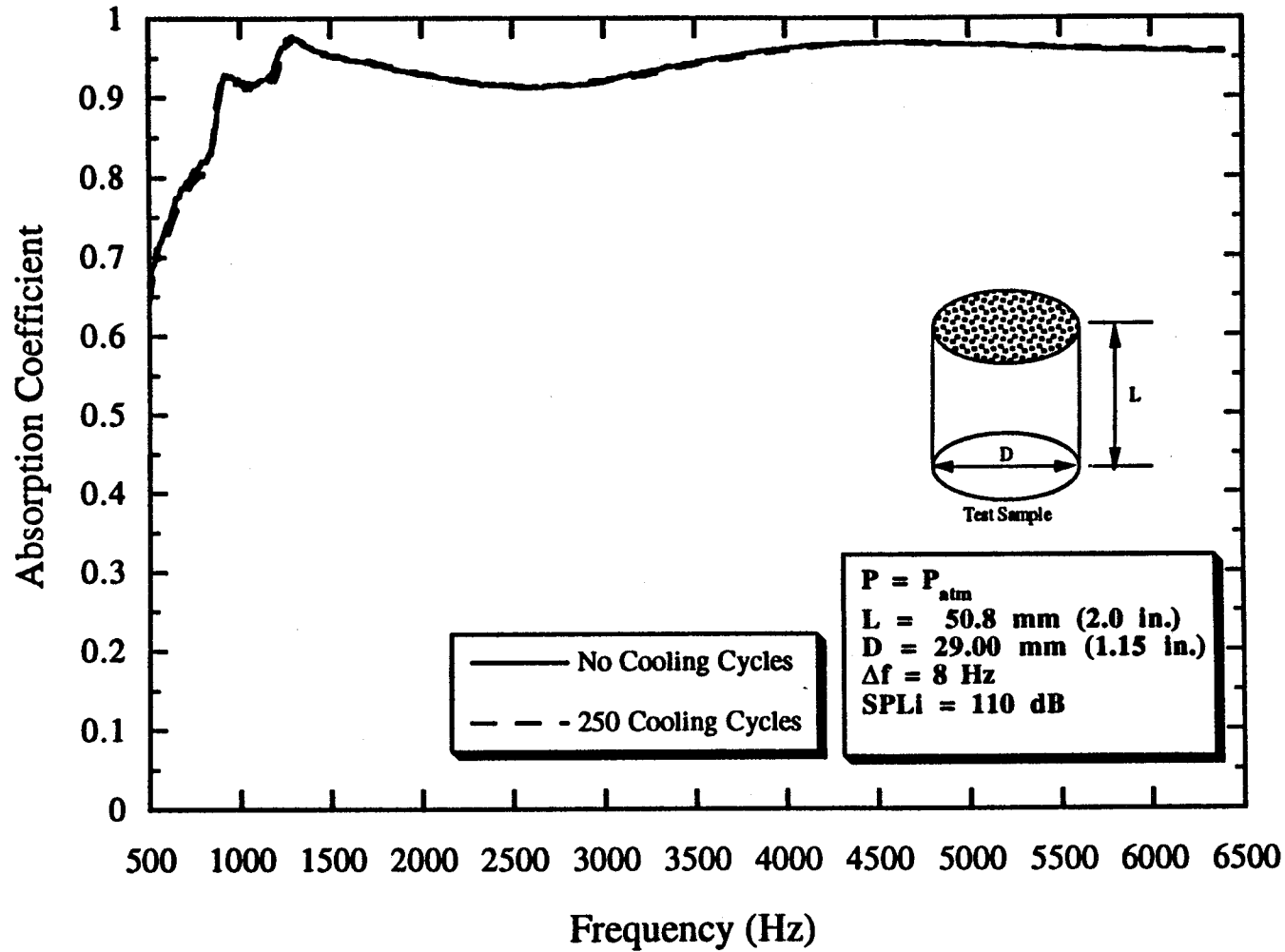


Figure B17. Absorption coefficient of Fiberglass, $P = P_{atm}$, $L = 50.8 \text{ mm}$, $D = 29.0 \text{ mm}$.

B.18

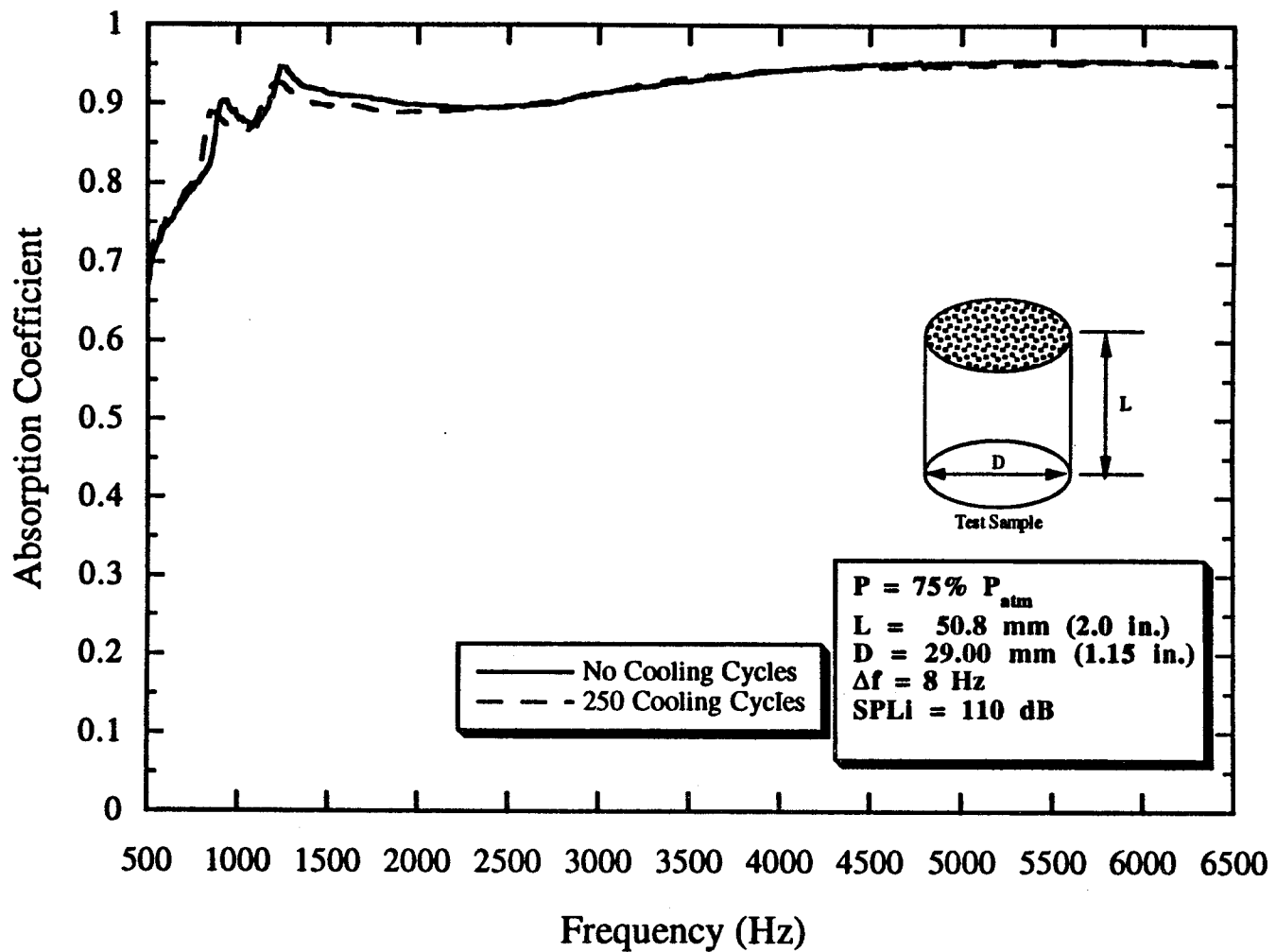


Figure B18. Absorption coefficient of Fiberglass, $P = 75\% P_{atm}$, $L = 50.8 \text{ mm}$, $D = 29.0 \text{ mm}$.

B.19

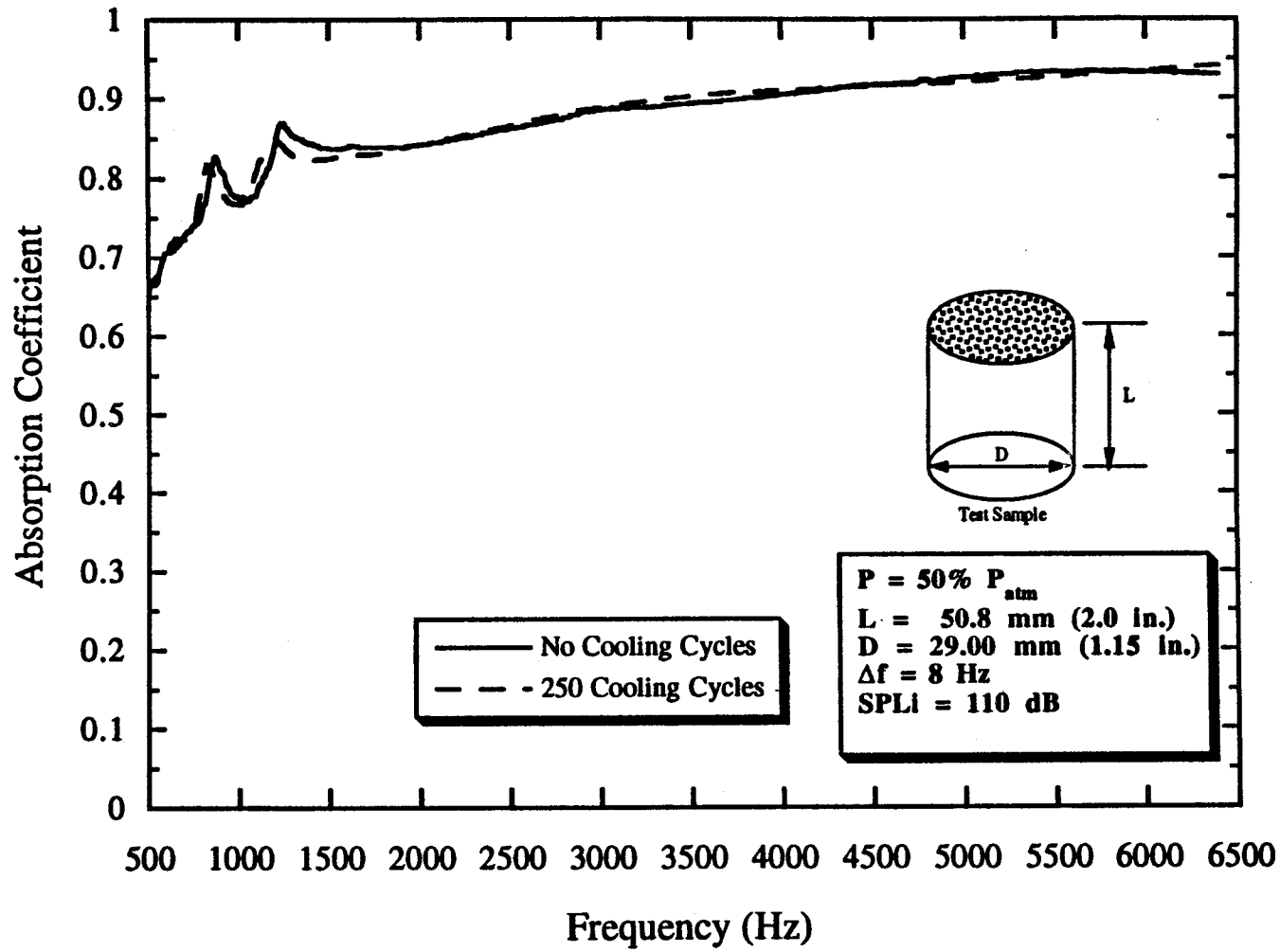


Figure B19. Absorption coefficient of Fiberglass, $P = 50\% P_{atm}$, $L = 50.8 \text{ mm}$, $D = 29.0 \text{ mm}$.

B.20

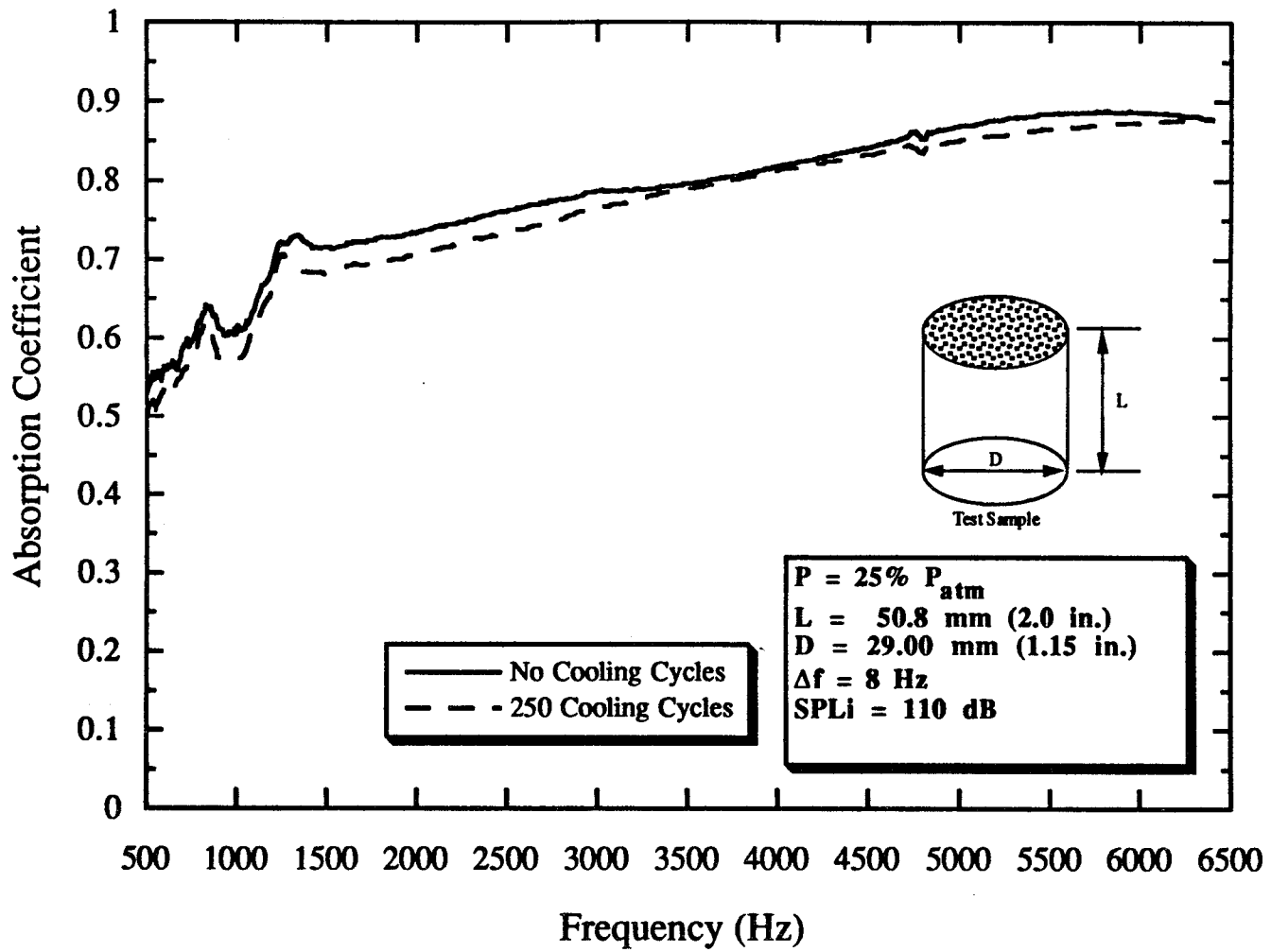


Figure B20. Absorption coefficient of Fiberglass, $P = 25\% P_{atm}$, $L = 50.8 \text{ mm}$, $D = 29.0 \text{ mm}$.

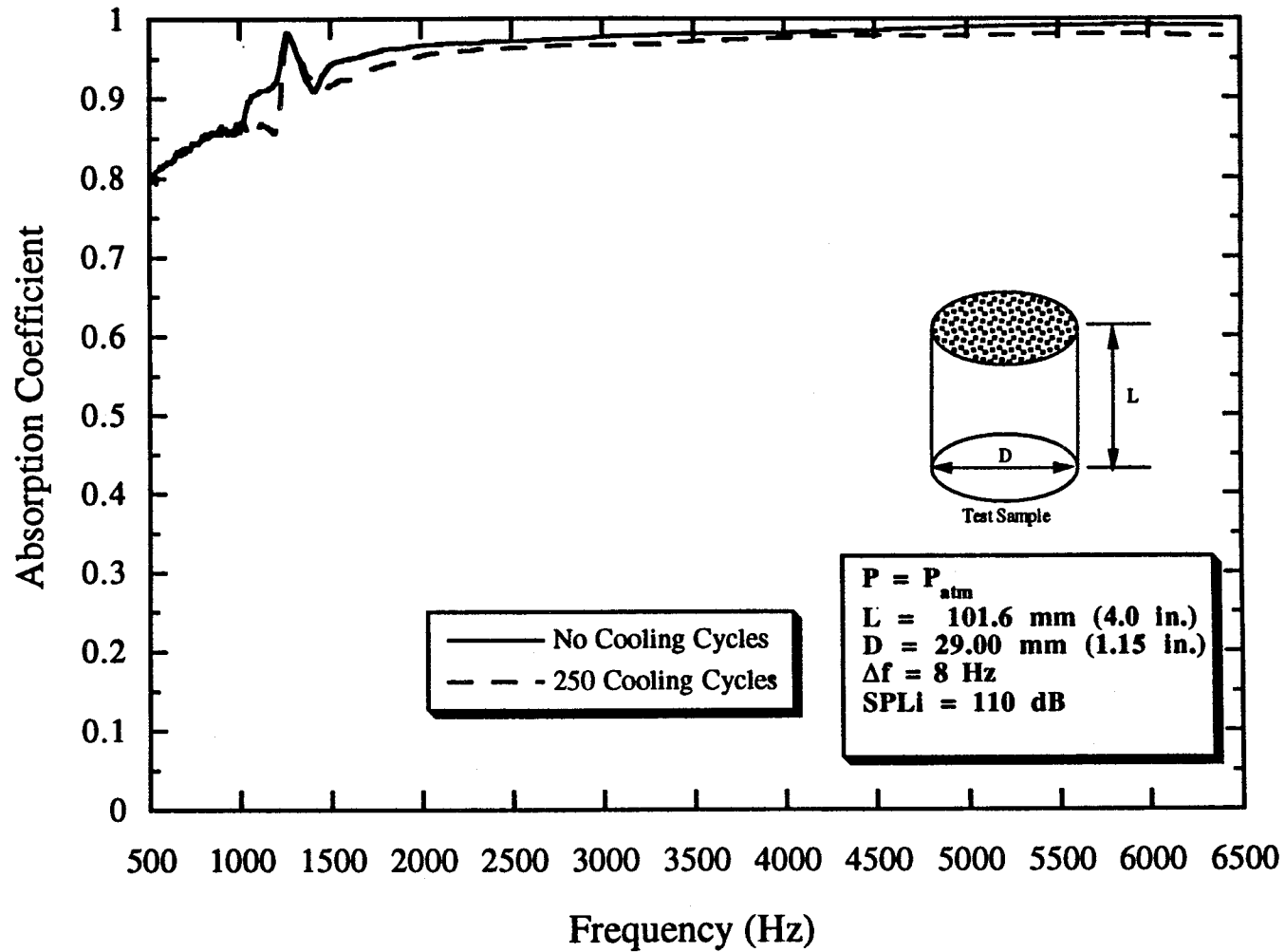


Figure B21. Absorption coefficient of Fiberglass, $P = P_{atm}$, $L = 101.6\text{mm}$, $D = 29.0 \text{ mm}$.

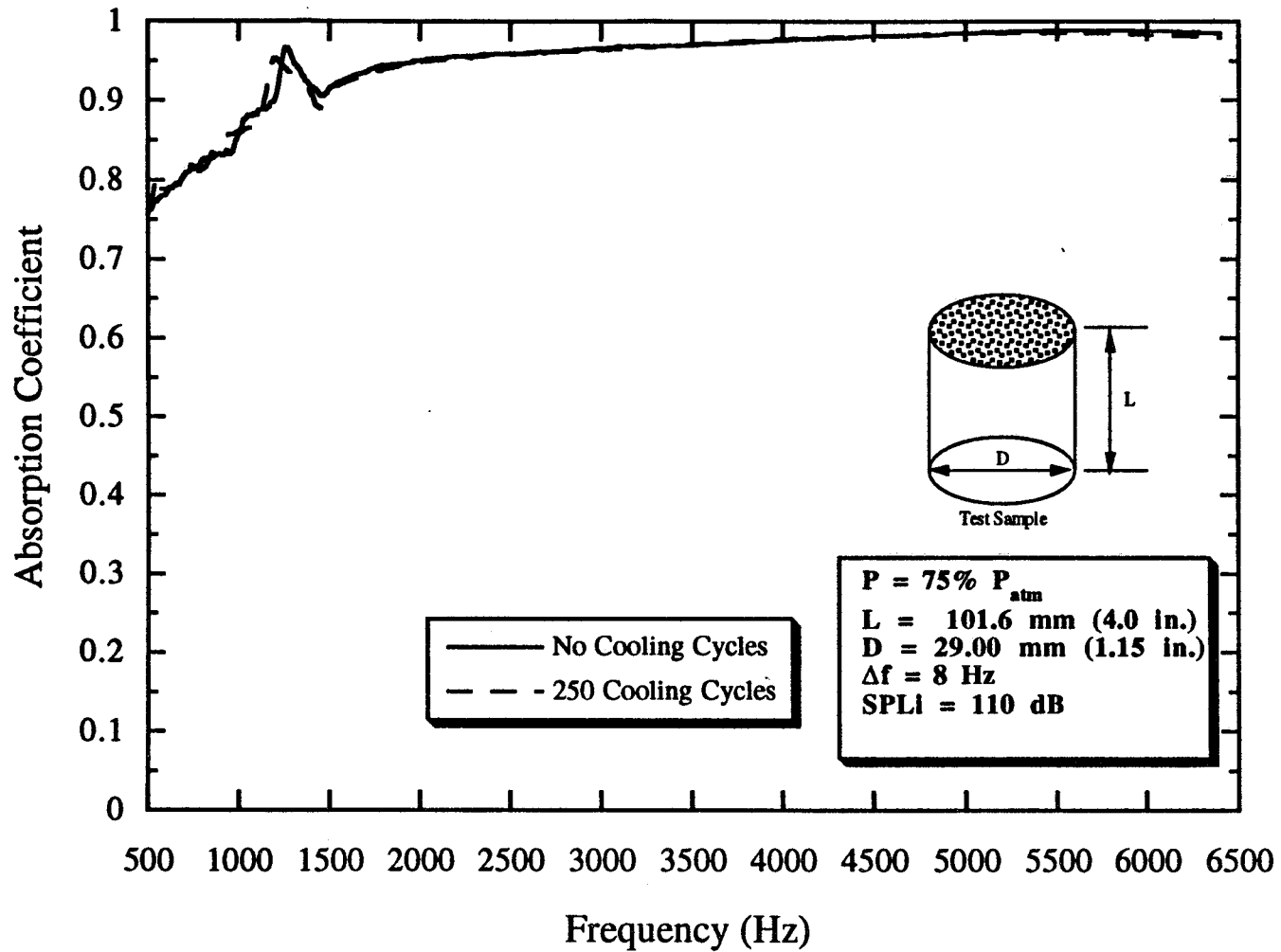


Figure B22. Absorption coefficient of Fiberglass, $P = 75\% P_{atm}$, $L = 101.6\text{mm}$, $D = 29.0 \text{ mm}$.

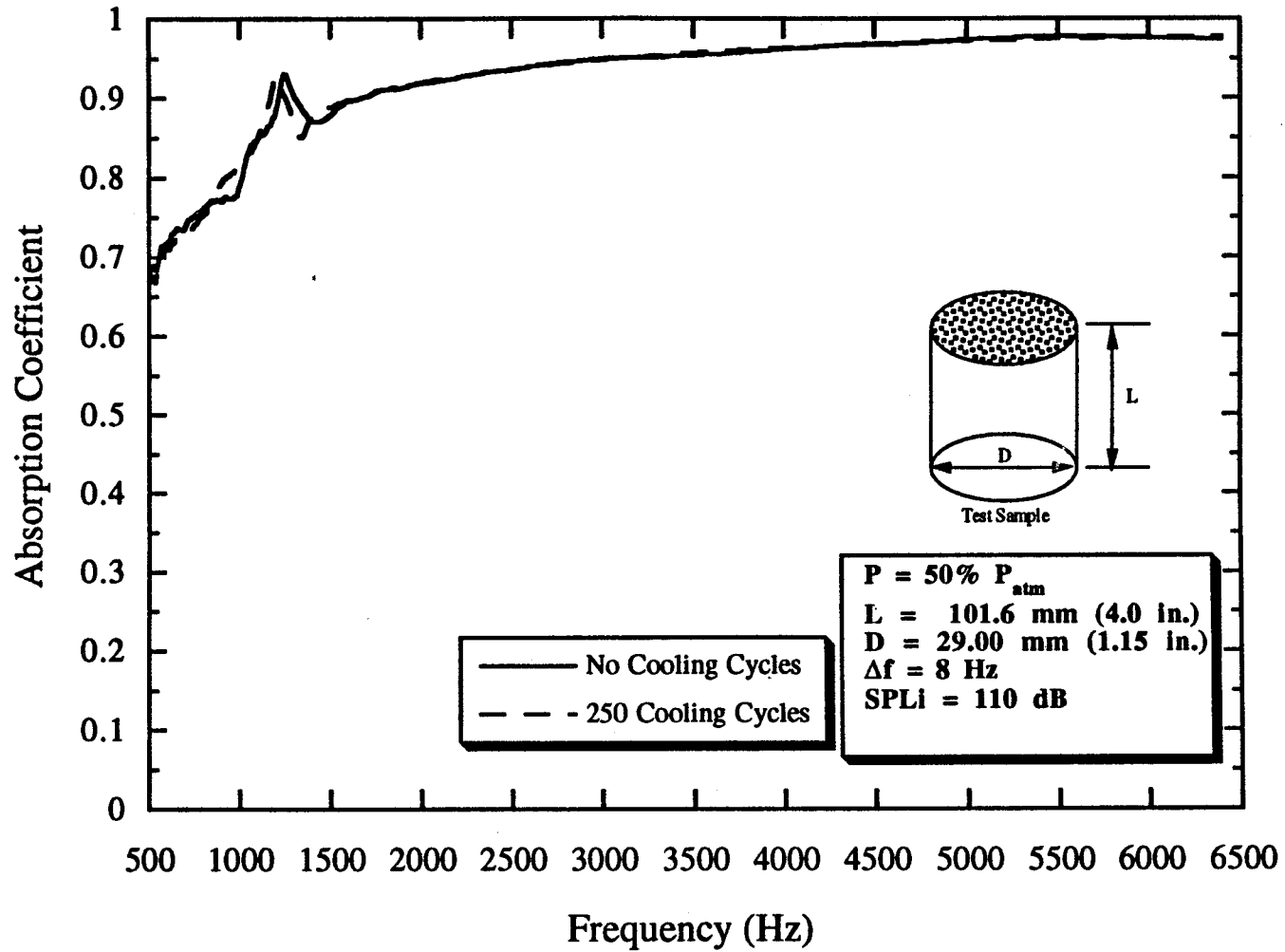


Figure B23. Absorption coefficient of Fiberglass, $P = 50\% P_{atm}$, $L = 101.6\text{mm}$, $D = 29.0 \text{ mm}$.

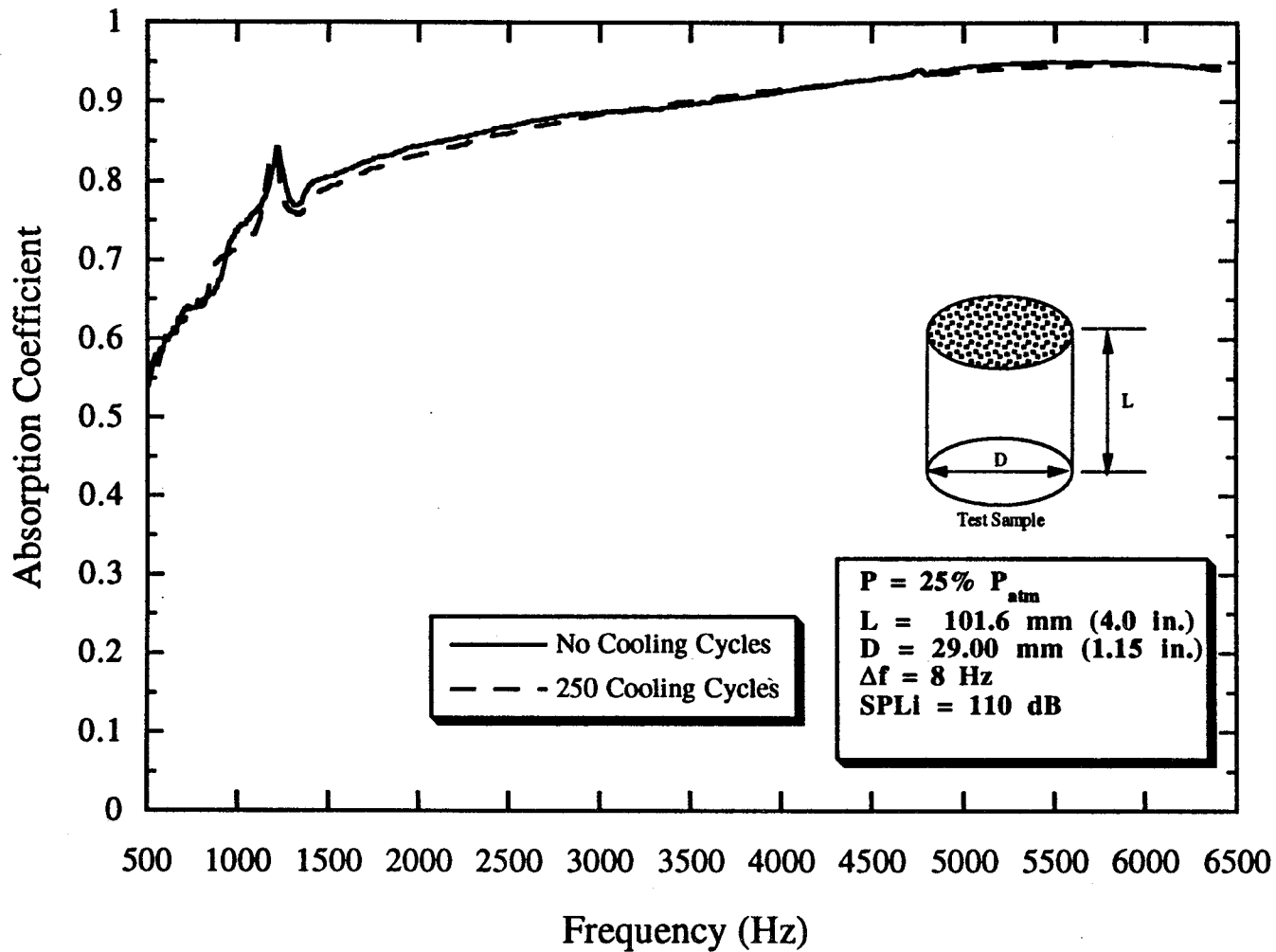


Figure B24. Absorption coefficient of Fiberglass, $P = 25\% P_{atm}$, $L = 101.6\text{mm}$, $D = 29.0 \text{ mm}$.

B.25

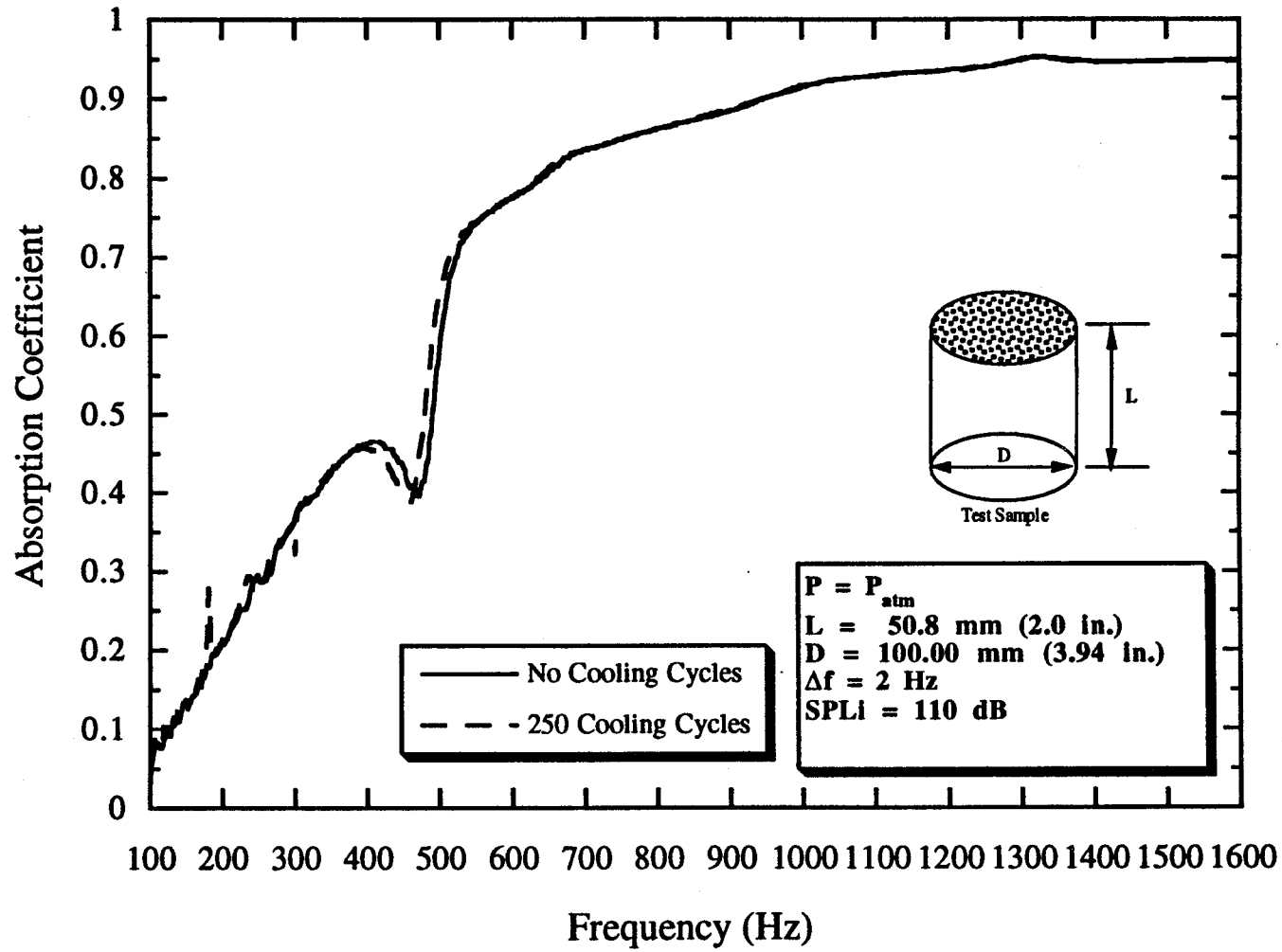


Figure B25. Absorption coefficient of Fiberglass, $P = P_{atm}$, $L = 50.8 \text{ mm}$, $D = 100.0 \text{ mm}$.

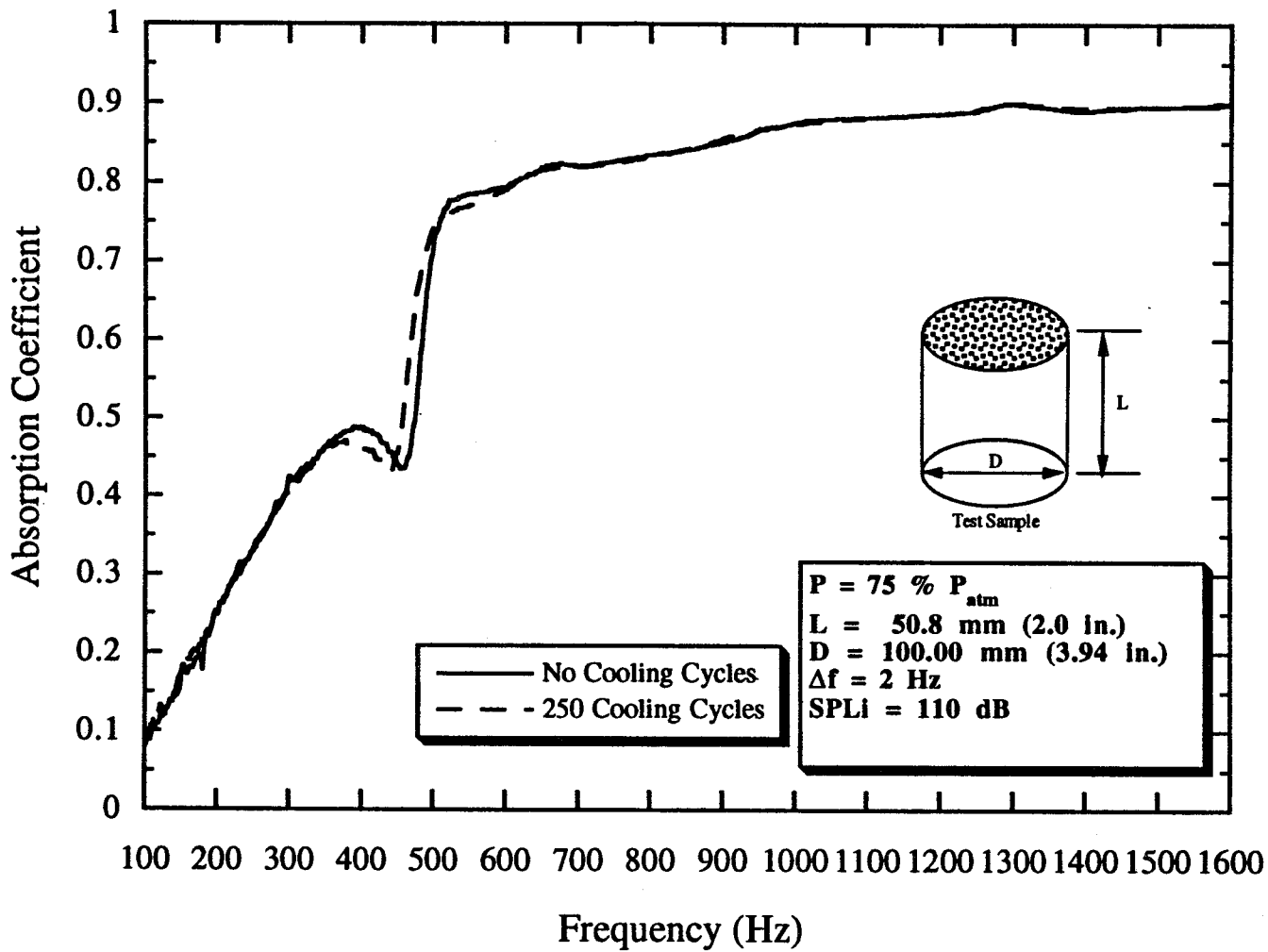


Figure B26. Absorption coefficient of Fiberglass, $P = 75\% P_{atm}$, $L = 50.8 \text{ mm}$, $D = 100.0 \text{ mm}$.

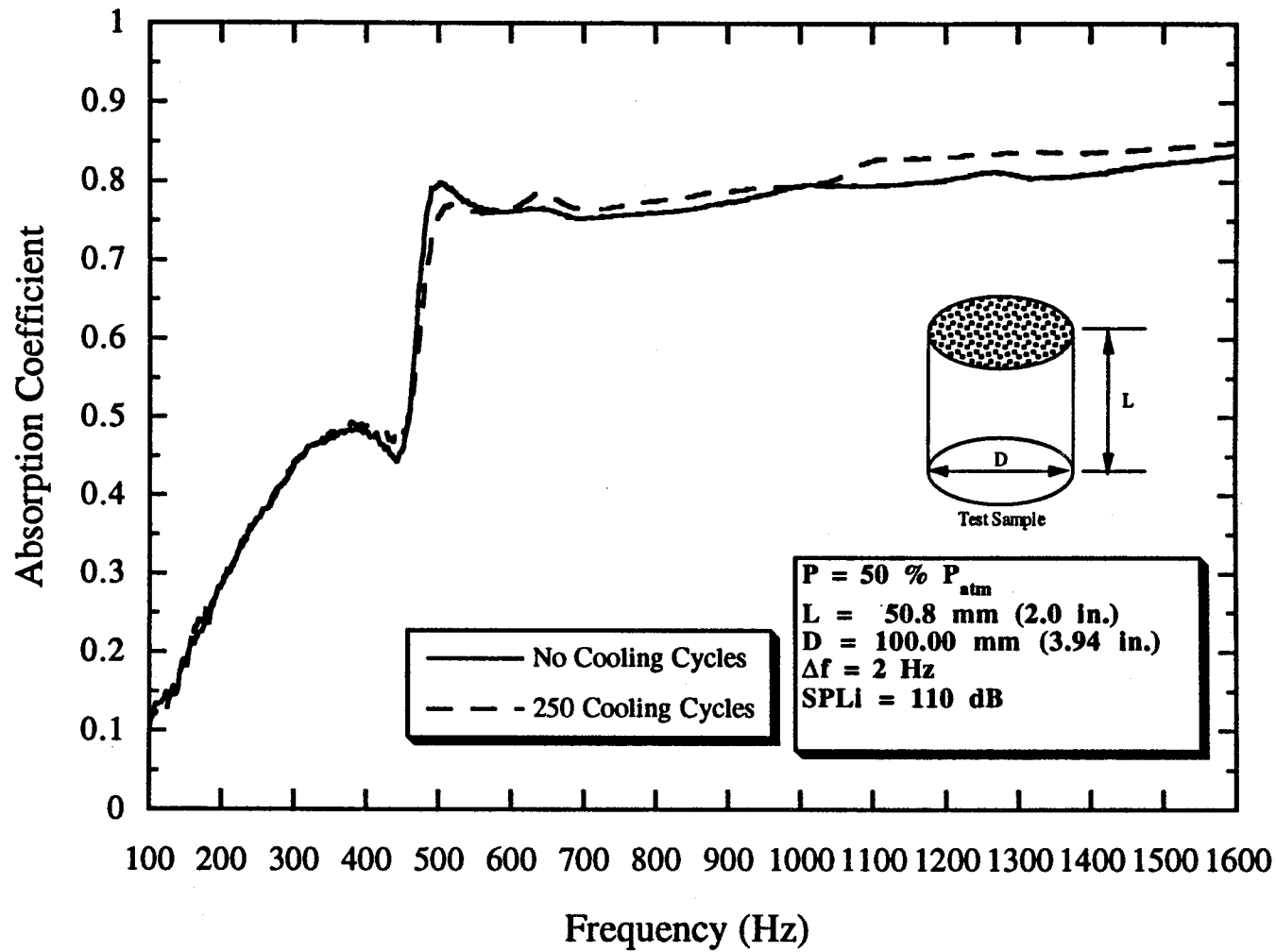


Figure B27. Absorption coefficient of Fiberglass, $P = 50\% P_{atm}$, $L = 50.8 \text{ mm}$, $D = 100.0 \text{ mm}$.

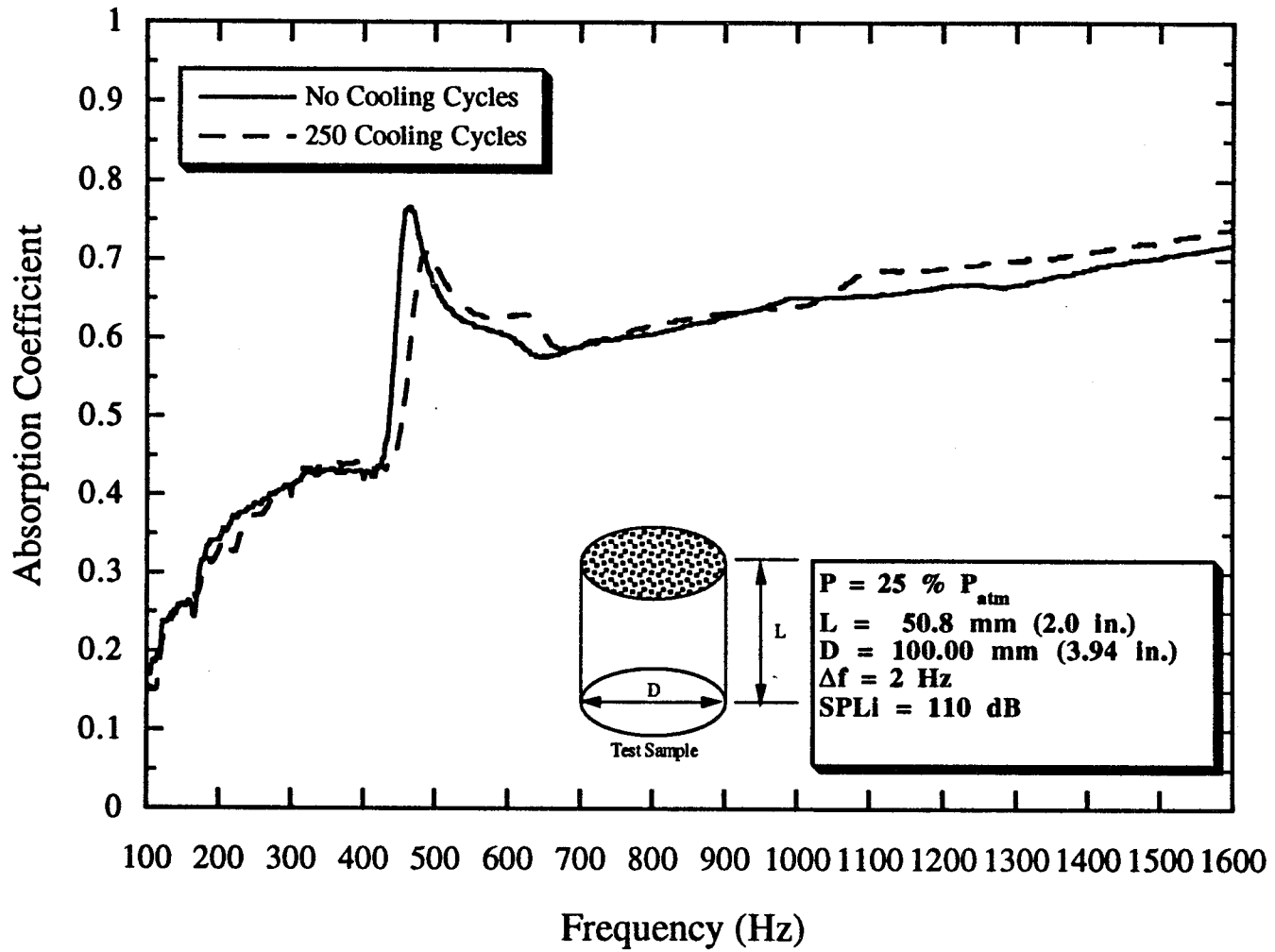


Figure B28. Absorption coefficient of Fiberglass, $P = 25\% P_{atm}$, $L = 50.8\text{ mm}$, $D = 100.0\text{ mm}$.

B.29

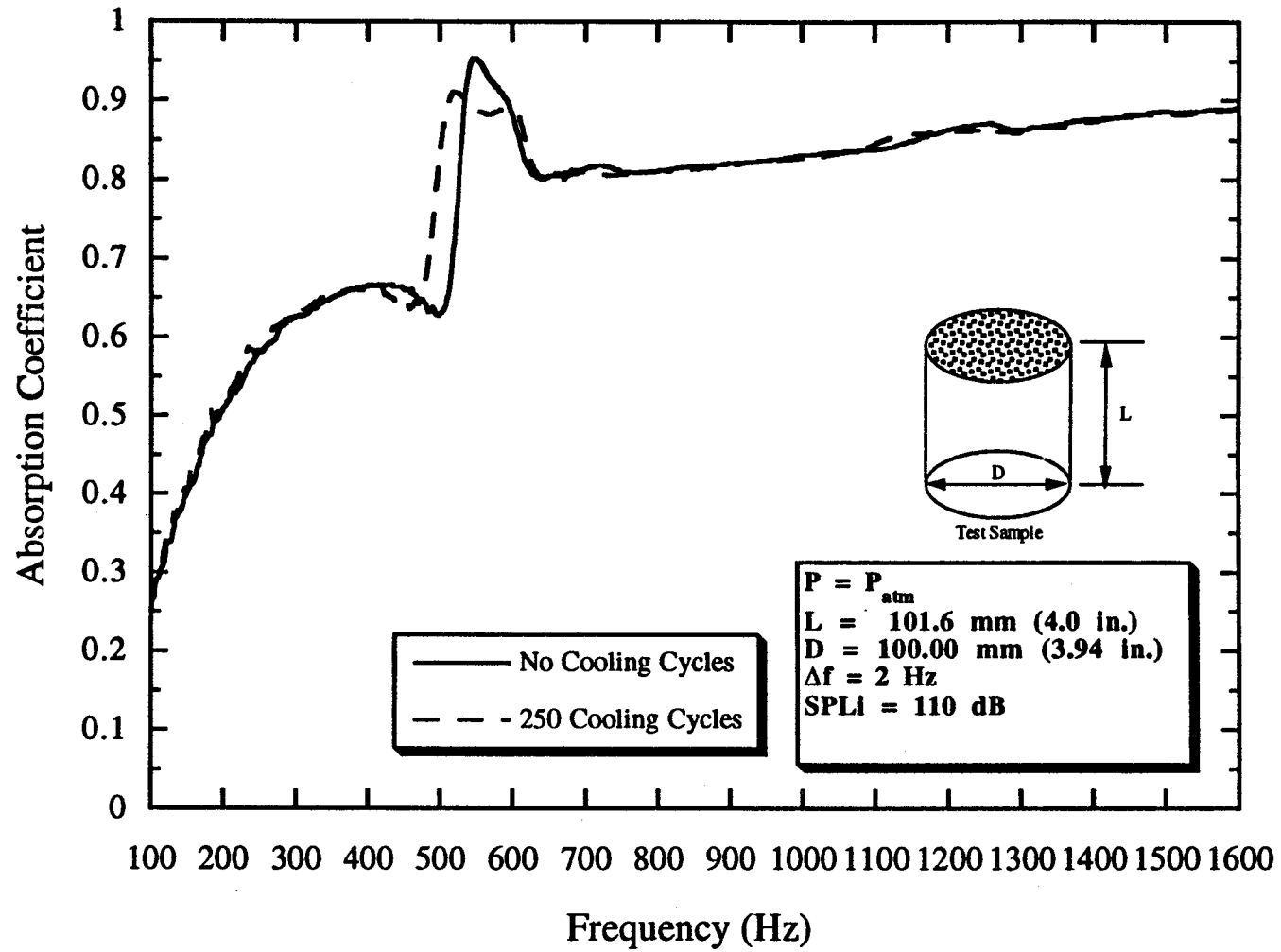


Figure B29. Absorption coefficient of Fiberglass, $P = P_{atm}$, $L = 101.6 \text{ mm}$, $D = 100.0 \text{ mm}$.

B.30

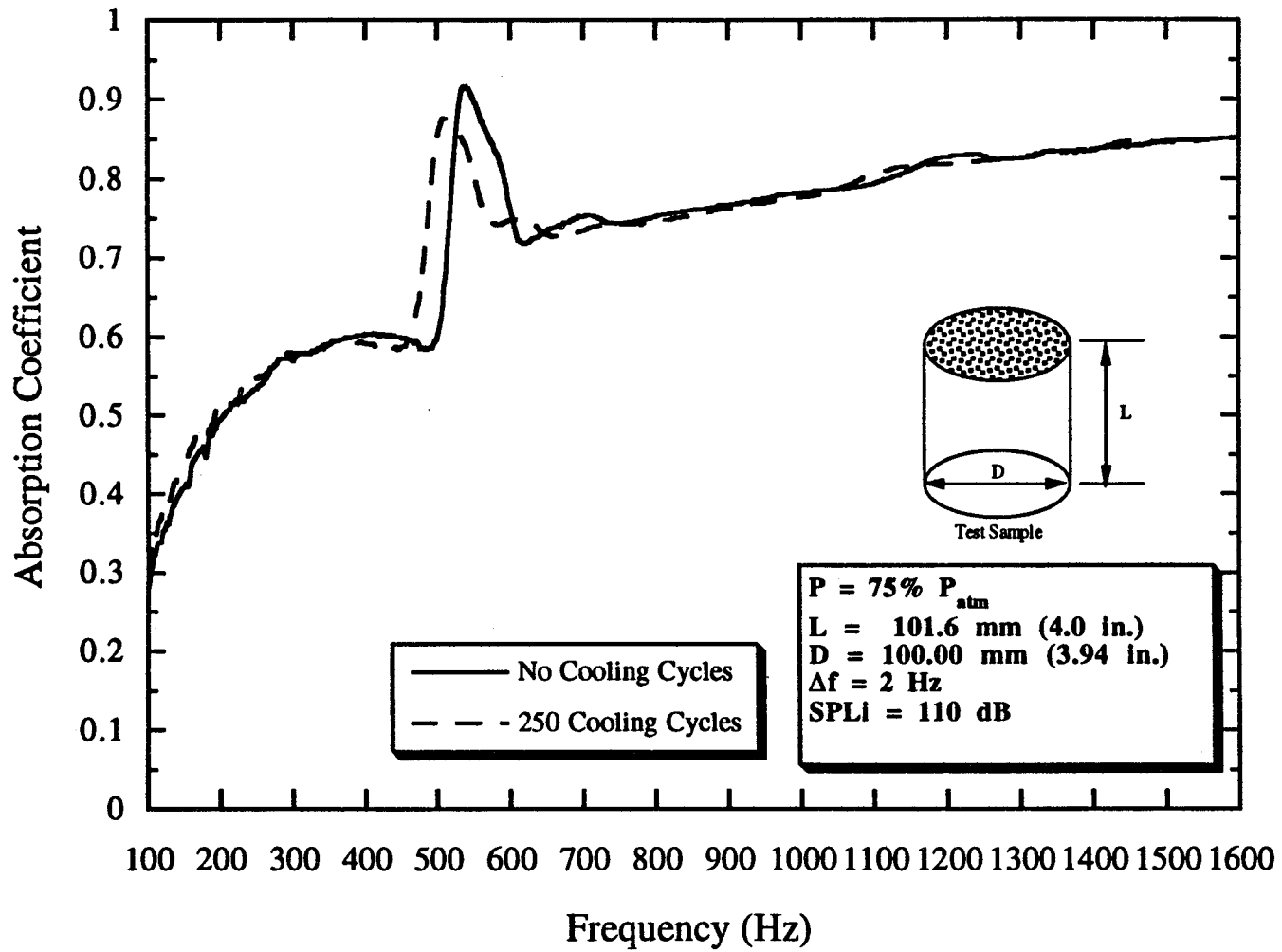


Figure B30. Absorption coefficient of Fiberglass, $P = 75\% P_{atm}$, $L = 101.6 \text{ mm}$, $D = 100.0 \text{ mm}$.

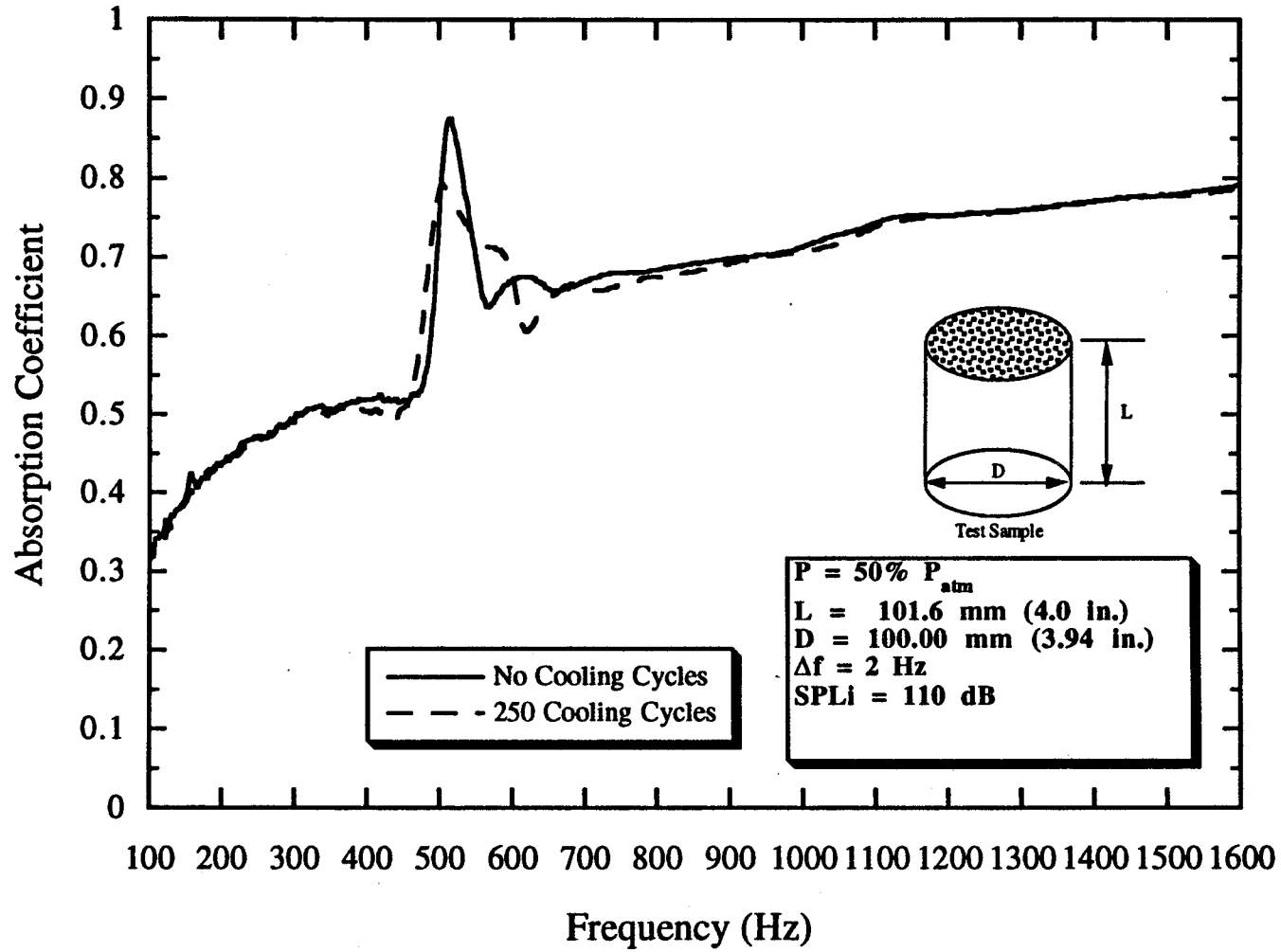


Figure B31. Absorption coefficient of Fiberglass, $P = 50\% P_{atm}$, $L = 101.6 \text{ mm}$, $D = 100.0 \text{ mm}$.

B.32

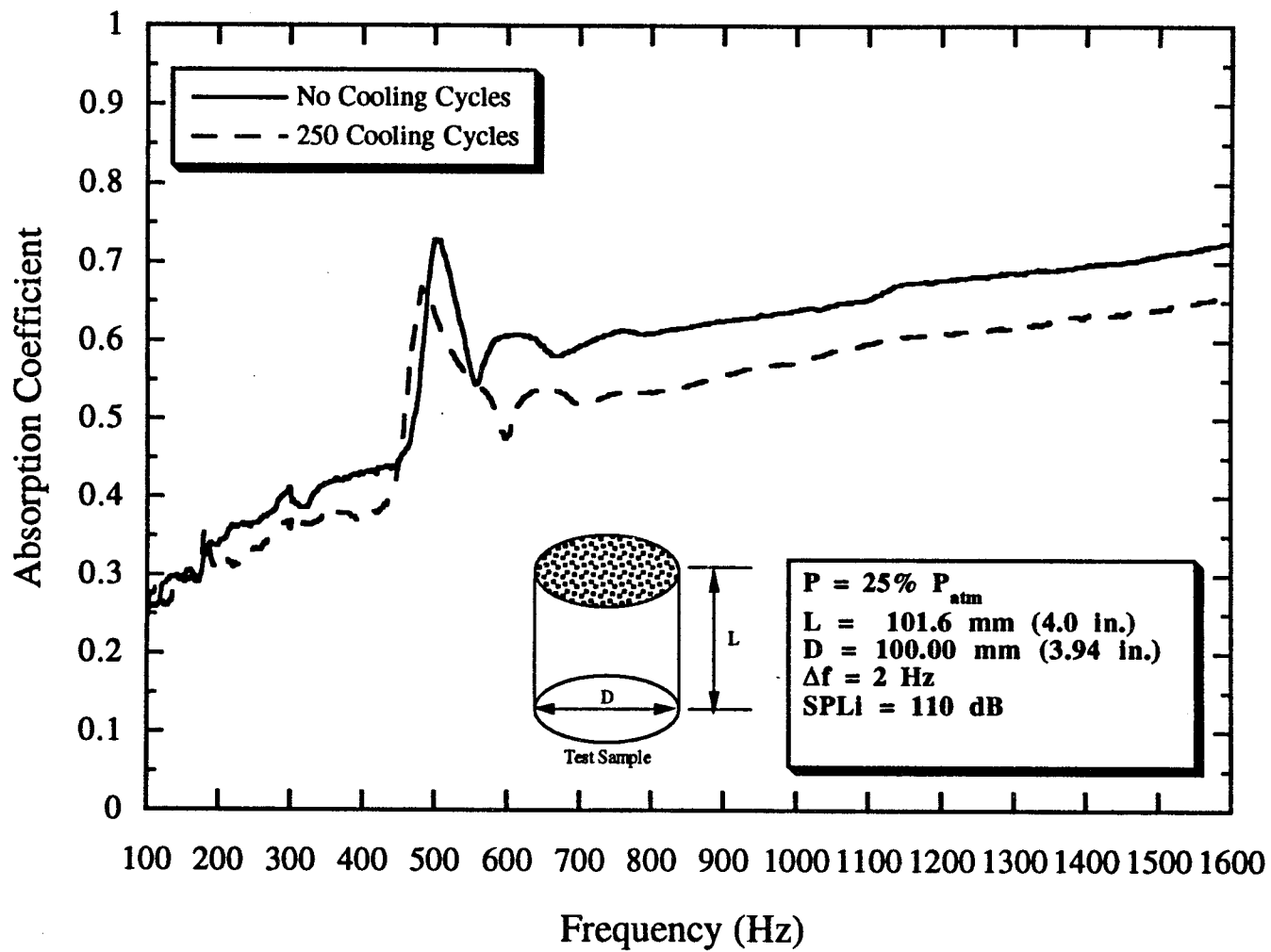


Figure B32. Absorption coefficient of Fiberglass, $P = 25\% P_{atm}$, $L = 101.6 \text{ mm}$, $D = 100.0 \text{ mm}$.

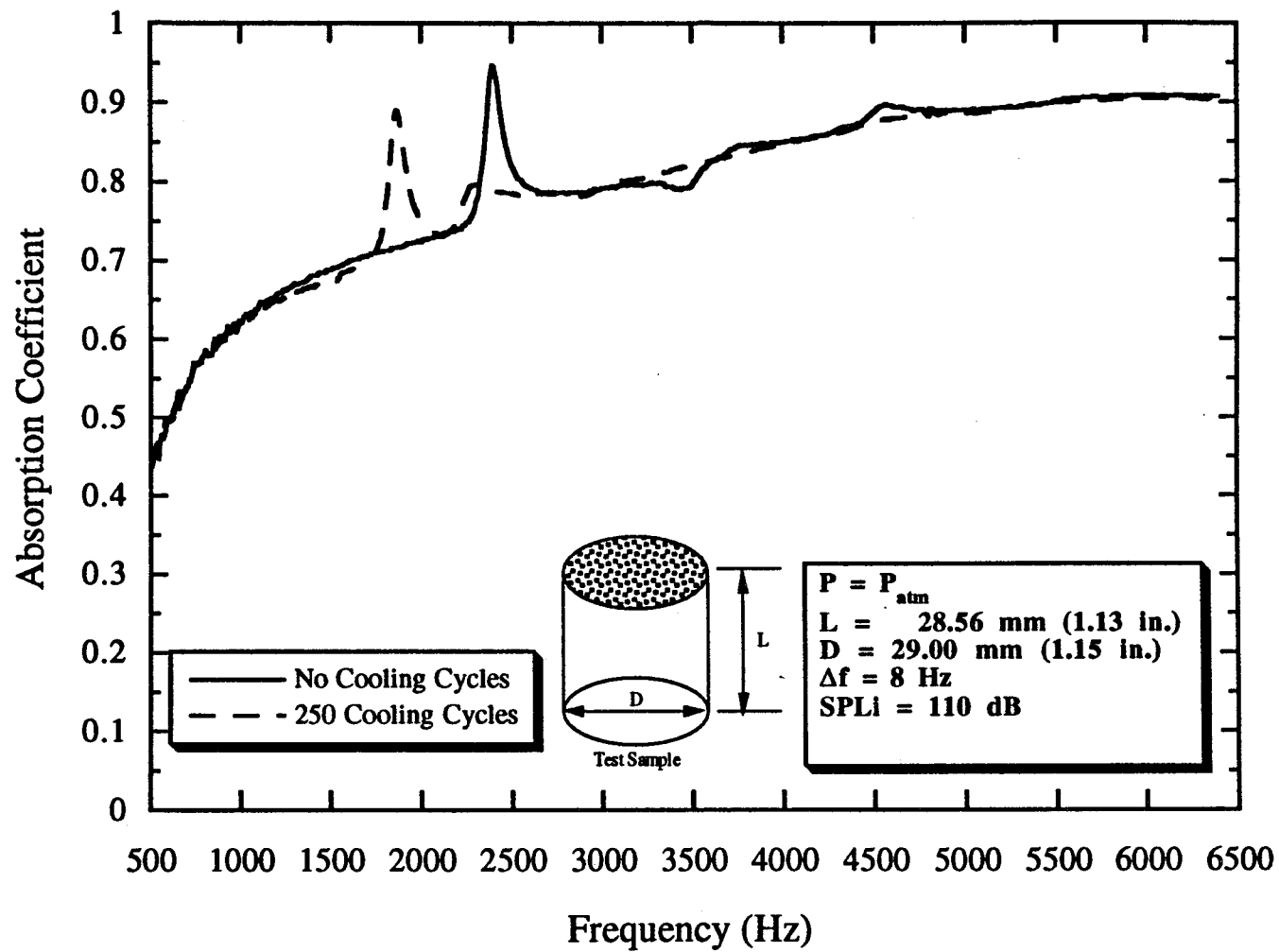


Figure B33. Absorption coefficient of Kevlar, $P = P_{atm}$, $L = 28.56 \text{ mm}$, $D = 29.0 \text{ mm}$.

B.34

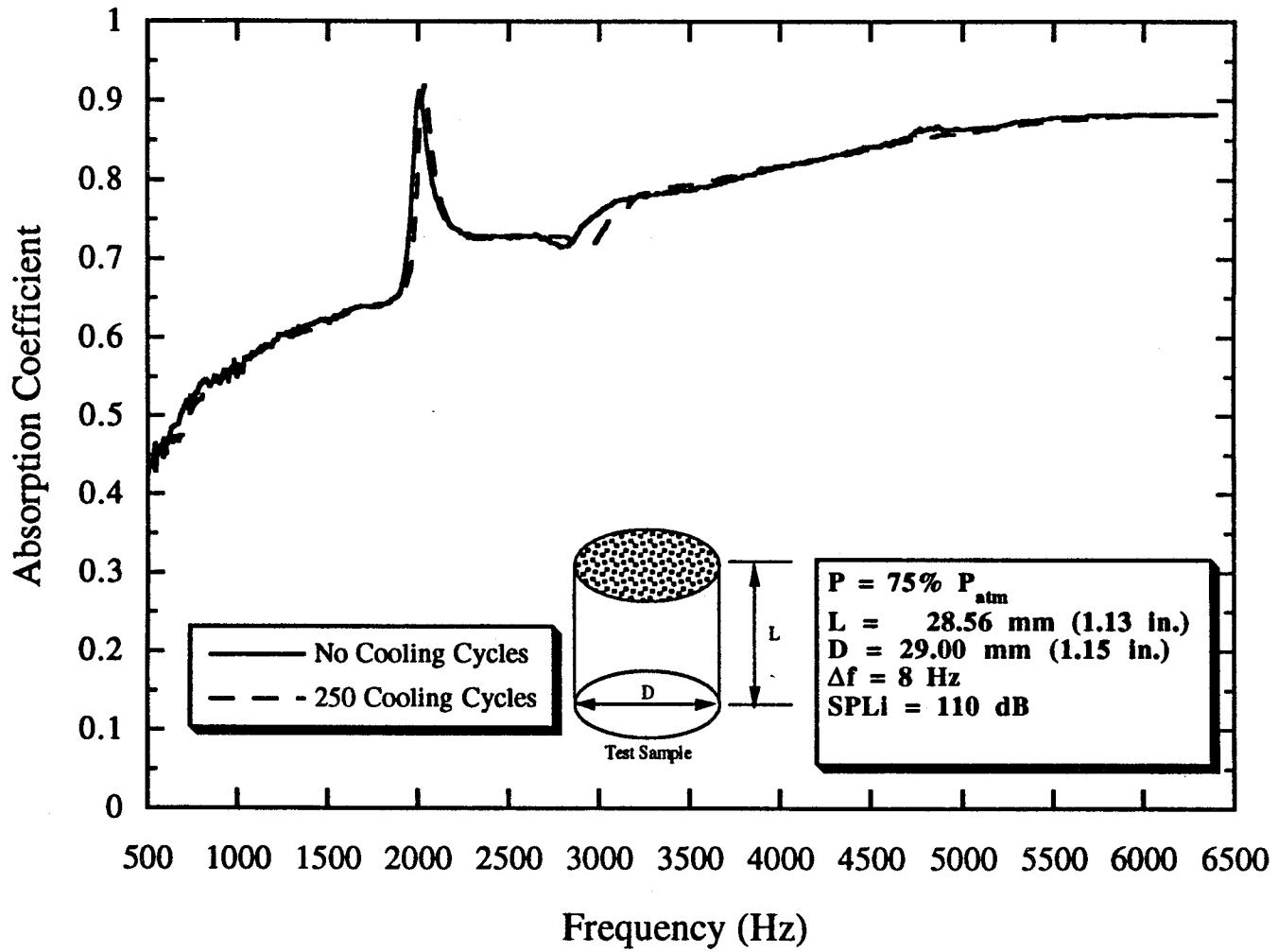


Figure B34. Absorption coefficient of Kevlar, $P = 75\% P_{atm}$, $L = 28.56 \text{ mm}$, $D = 29.0 \text{ mm}$.

B.35

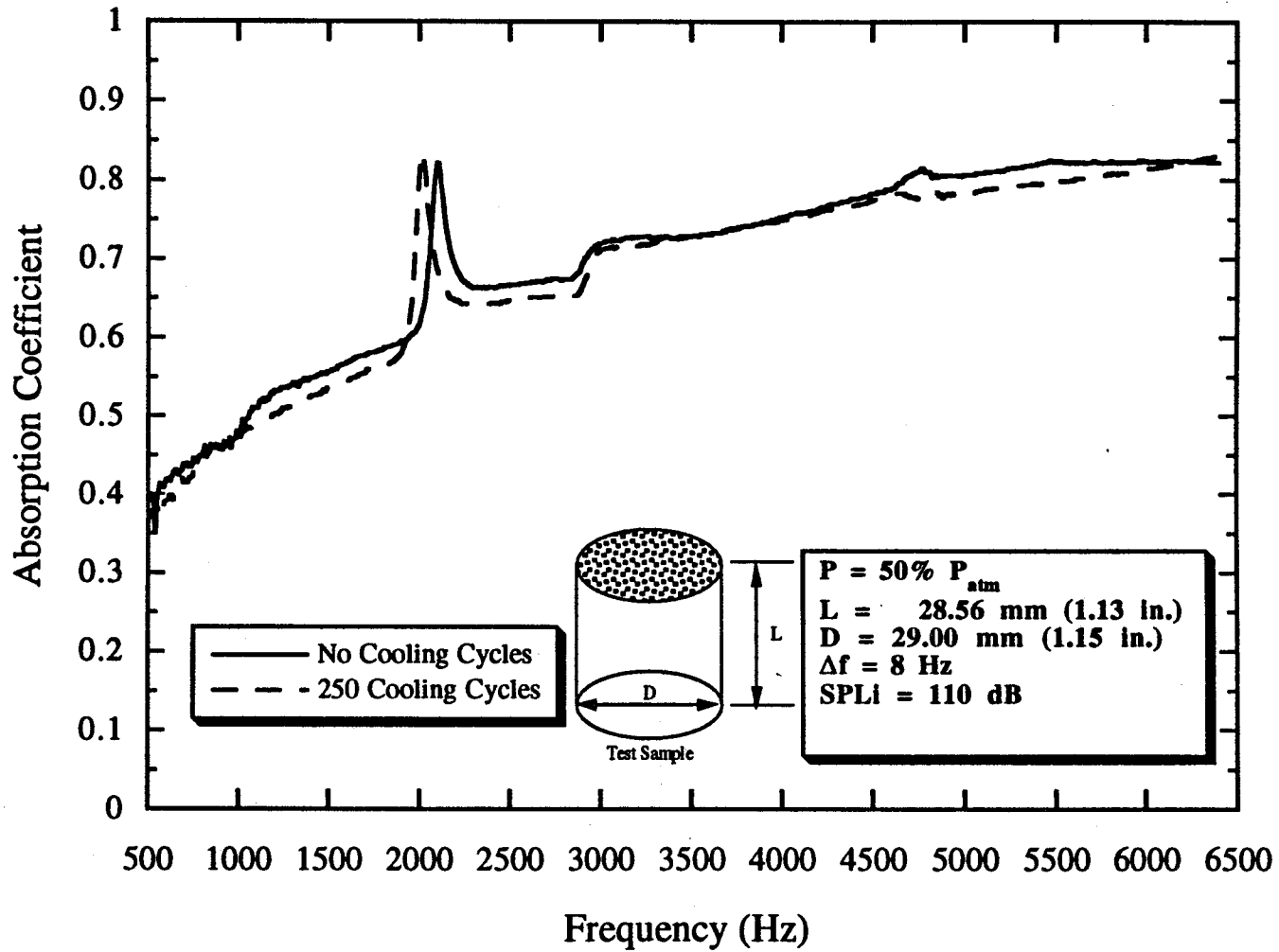


Figure B35. Absorption coefficient of Kevlar, $P = 50\% P_{atm}$, $L = 28.56 \text{ mm}$, $D = 29.0 \text{ mm}$.

B.36

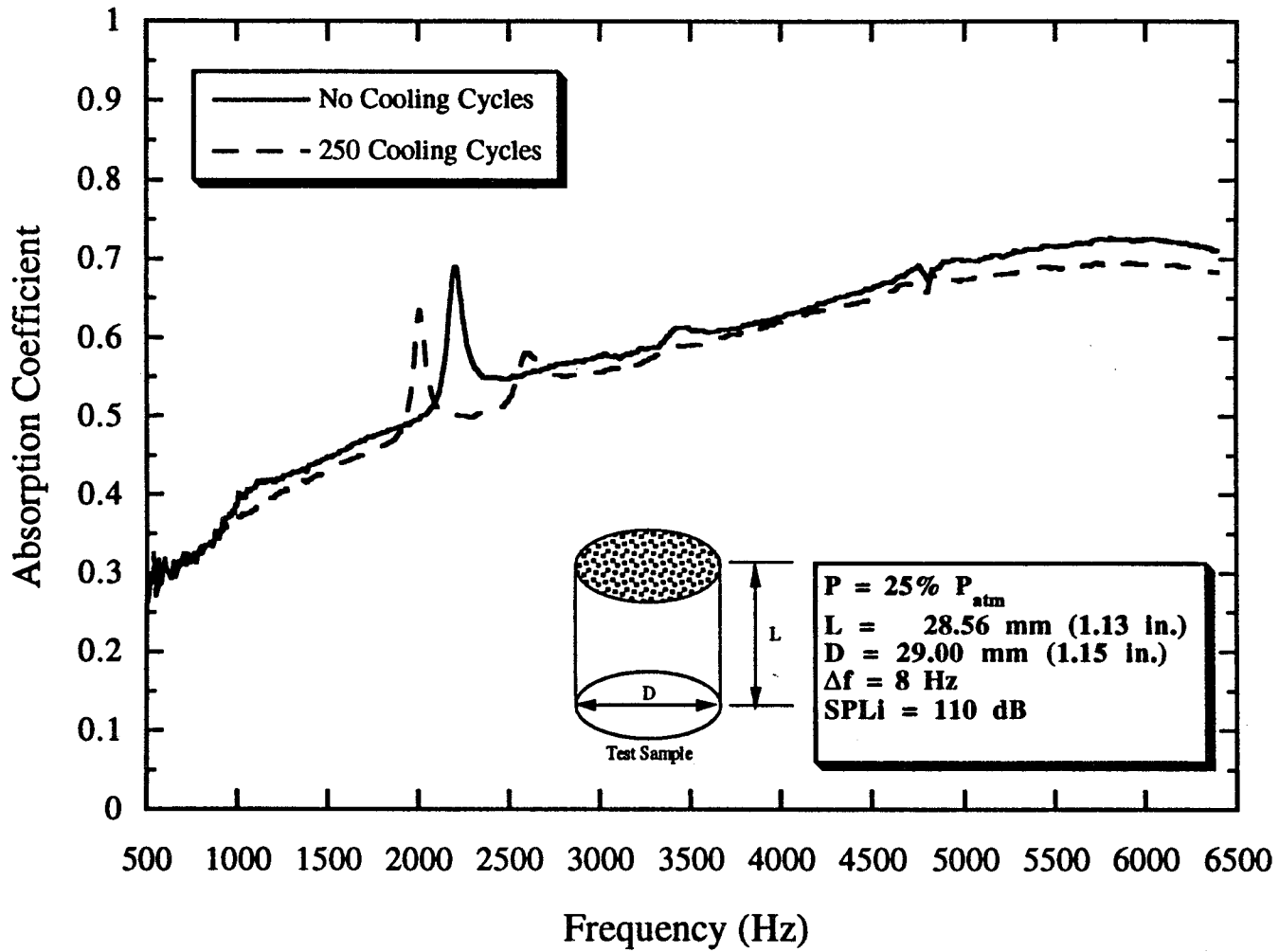


Figure B36. Absorption coefficient of Kevlar, $P = 25\% P_{atm}$, $L = 28.56$ mm, $D = 29.0$ mm.

B.37

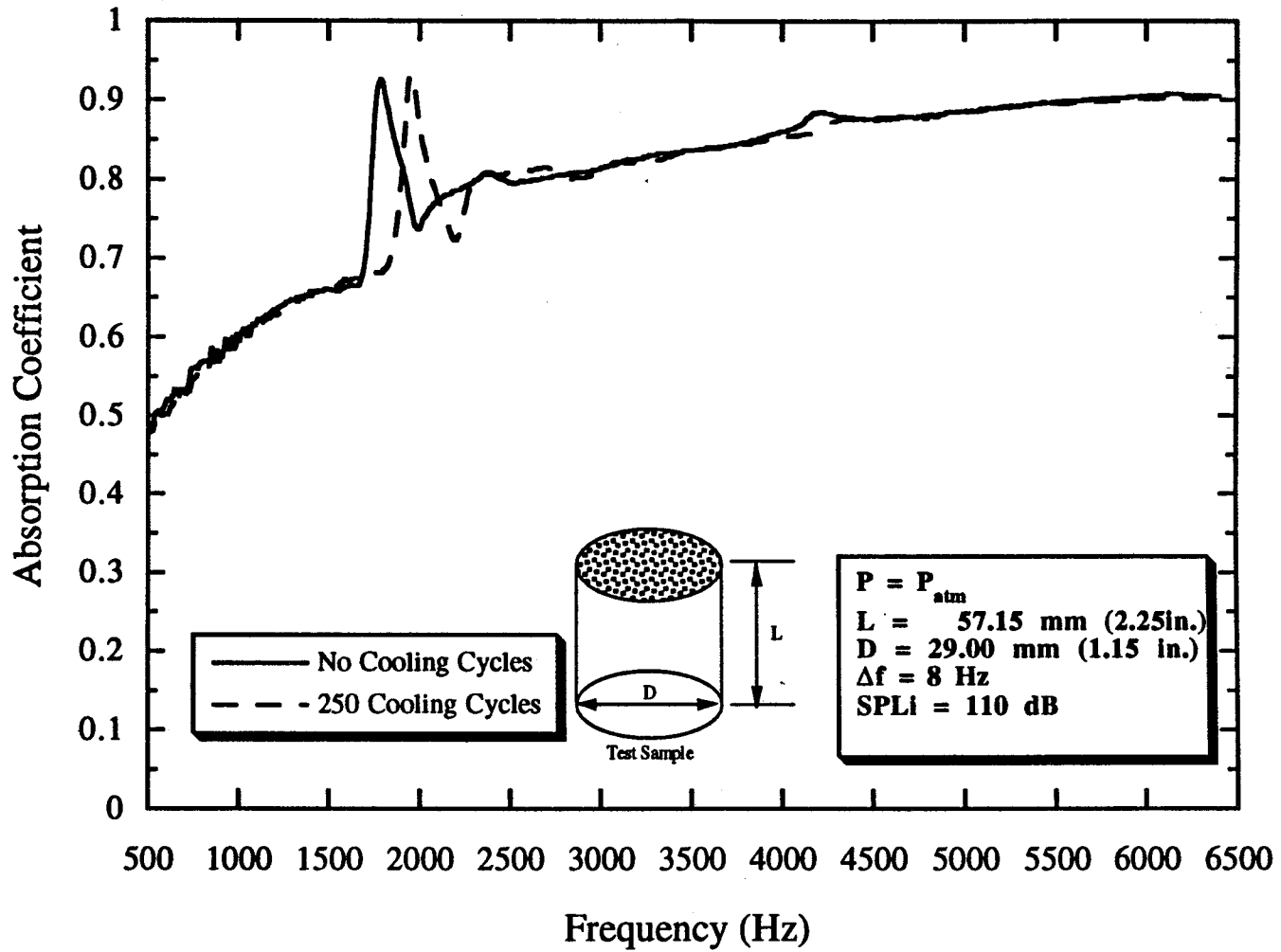


Figure B37. Absorption coefficient of Kevlar, $P = P_{atm}$, $L = 57.15 \text{ mm}$, $D = 29.0 \text{ mm}$.

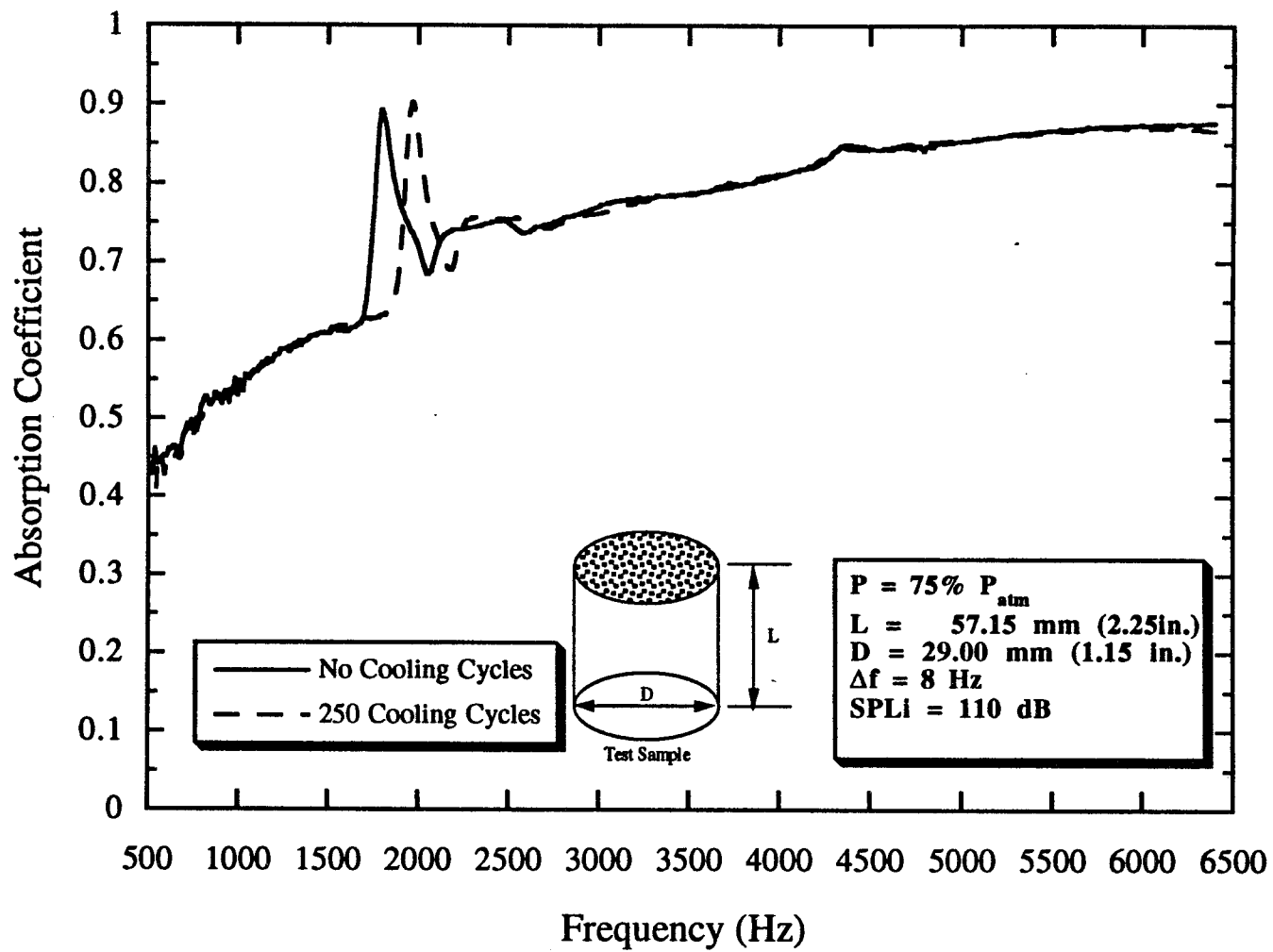


Figure B38. Absorption coefficient of Kevlar, $P = 75\% P_{atm}$, $L = 57.15 \text{ mm}$, $D = 29.0 \text{ mm}$.

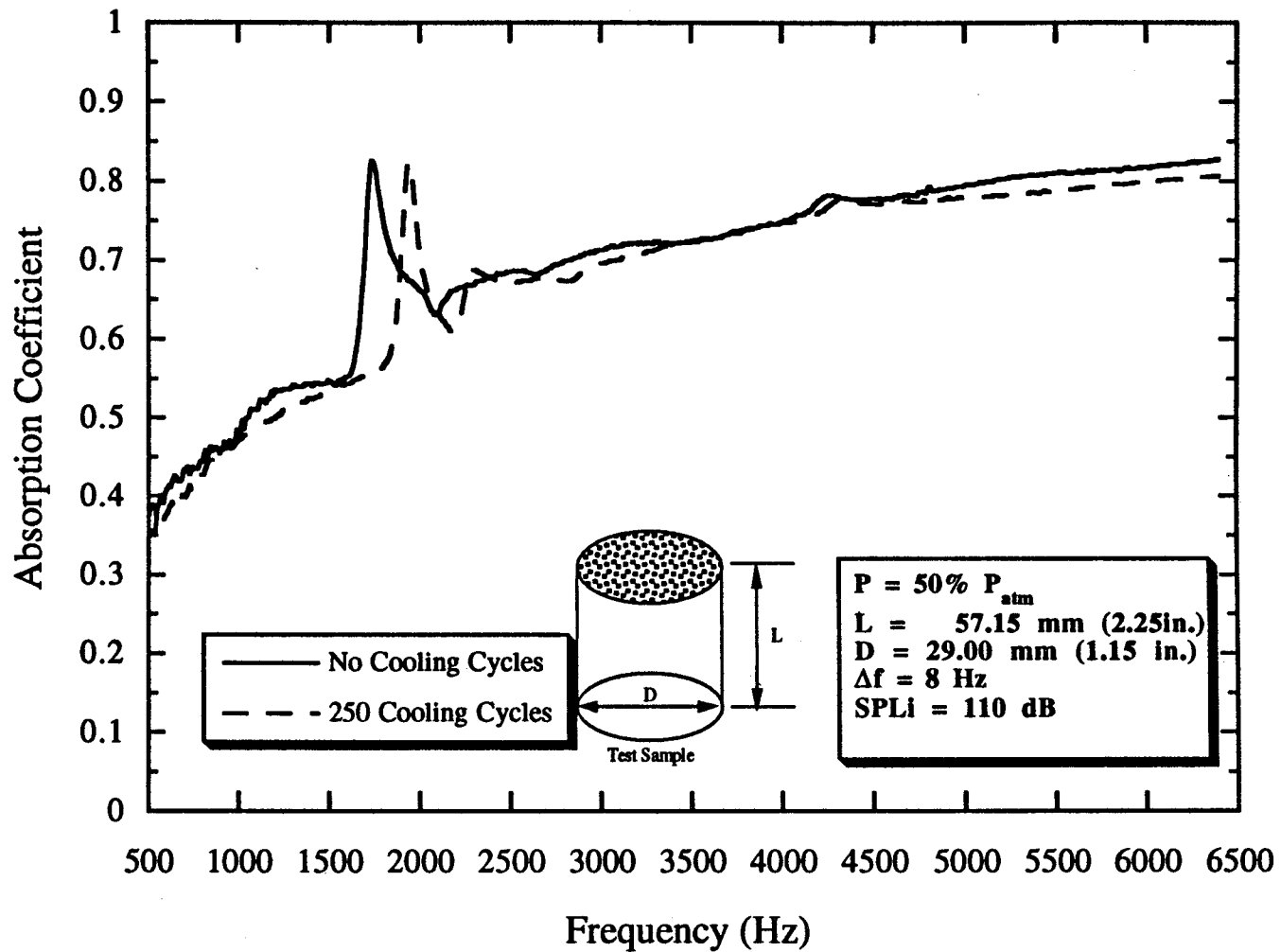


Figure B39. Absorption coefficient of Kevlar, $P = 50\% P_{atm}$, $L = 57.15 \text{ mm}$, $D = 29.0 \text{ mm}$.

B.40

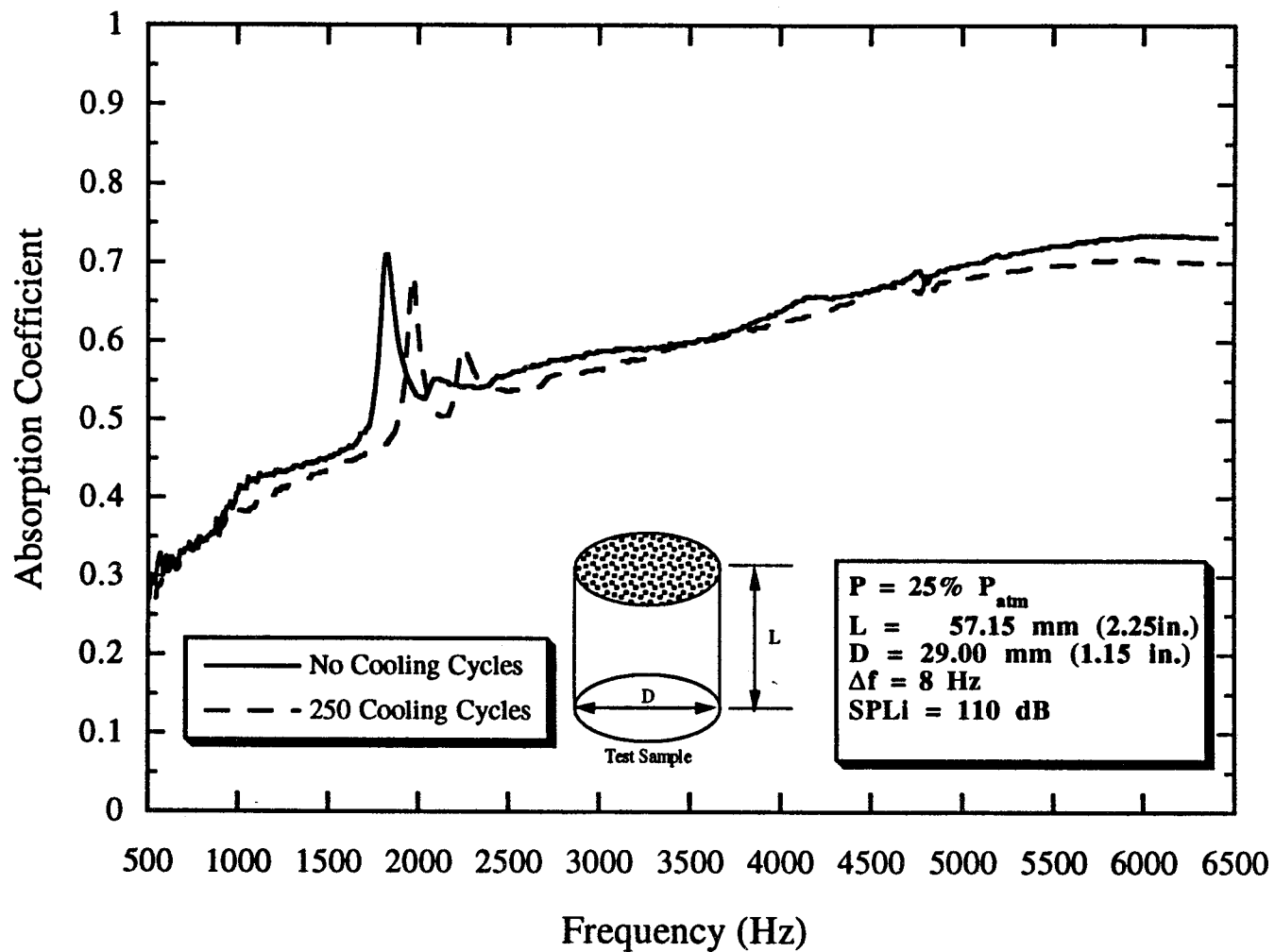


Figure B40. Absorption coefficient of Kevlar, $P = 25\% P_{atm}$, $L = 57.15 \text{ mm}$, $D = 29.0 \text{ mm}$.

B.41

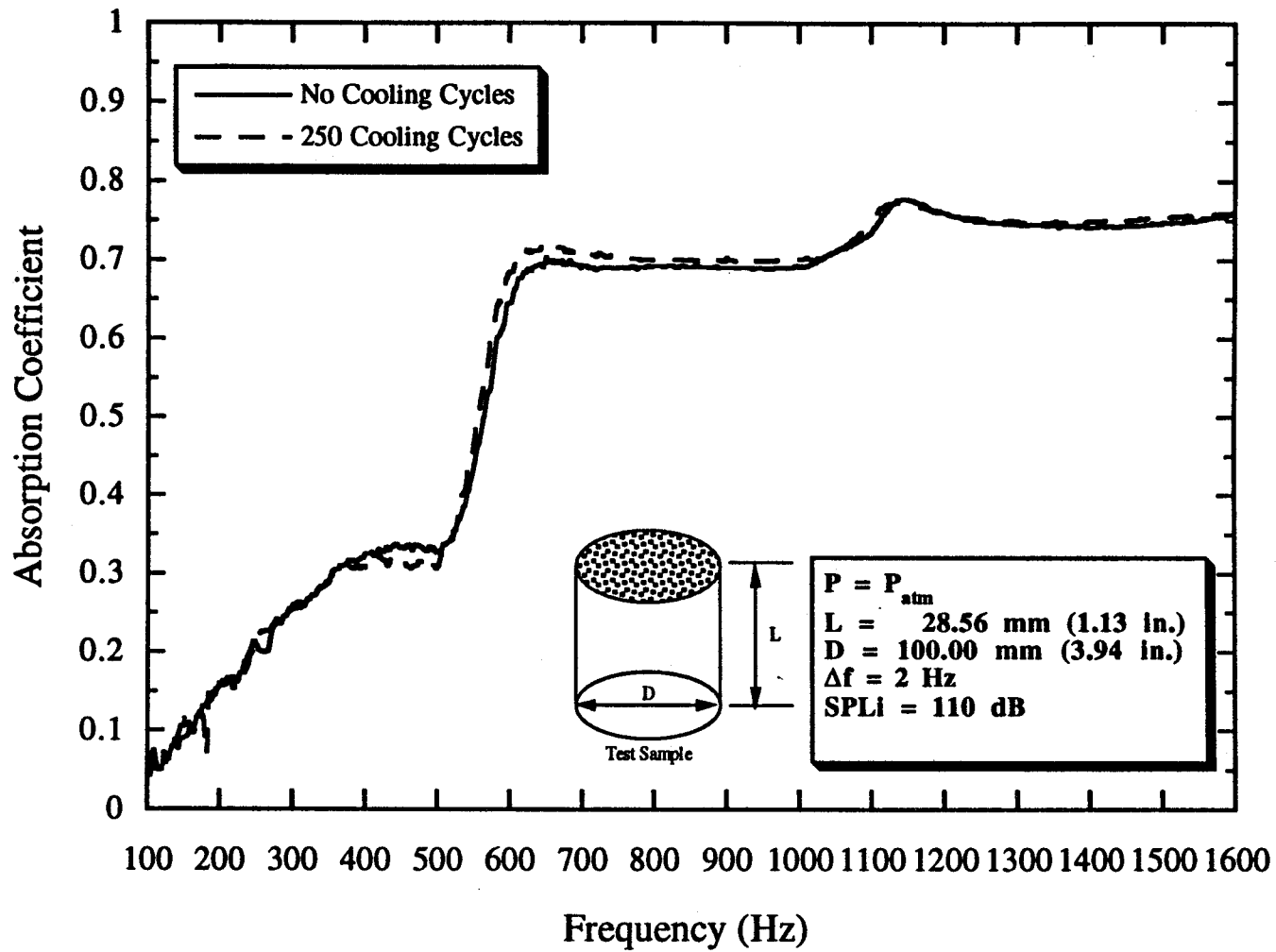


Figure B41. Absorption coefficient of Kevlar, $P = P_{atm}$, $L = 28.56 \text{ mm}$, $D = 100.0 \text{ mm}$.

B.42

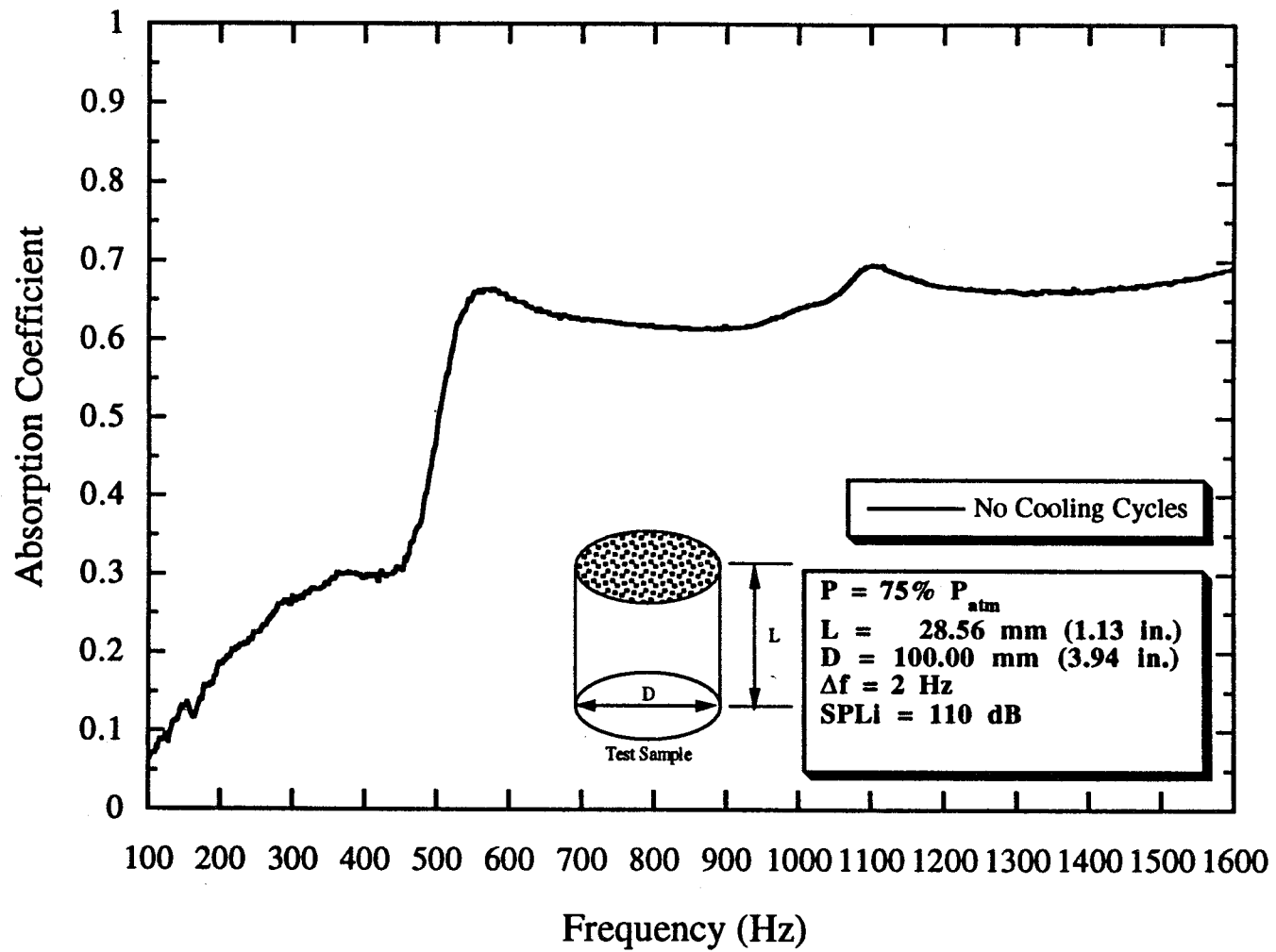


Figure B42. Absorption coefficient of Kevlar, $P = 75\% P_{atm}$, $L = 28.56 \text{ mm}$, $D = 100.0 \text{ mm}$.

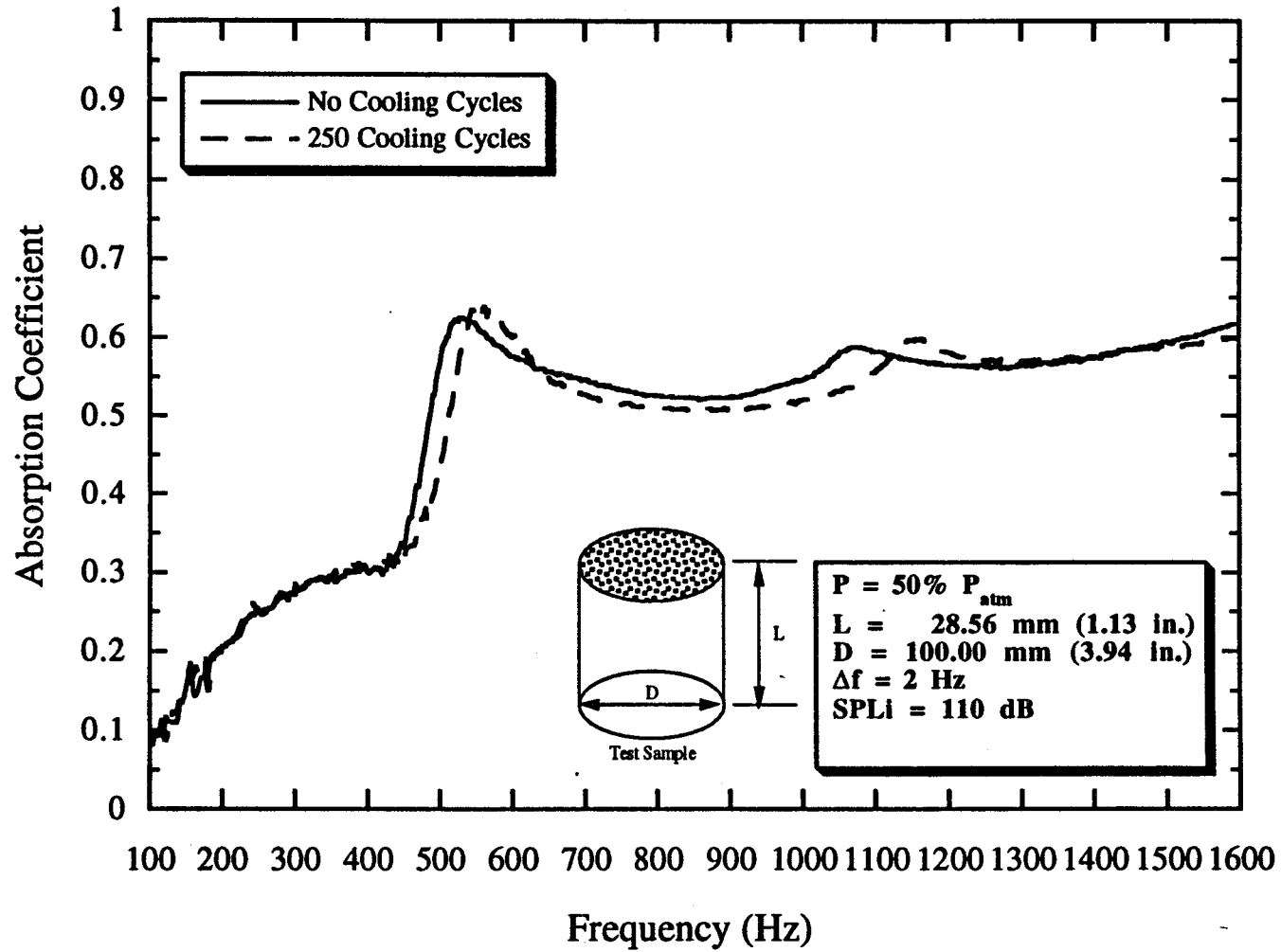


Figure B43. Absorption coefficient of Kevlar, $P = 50\% P_{atm}$, $L = 28.56 \text{ mm}$, $D = 100.0 \text{ mm}$.

B.44

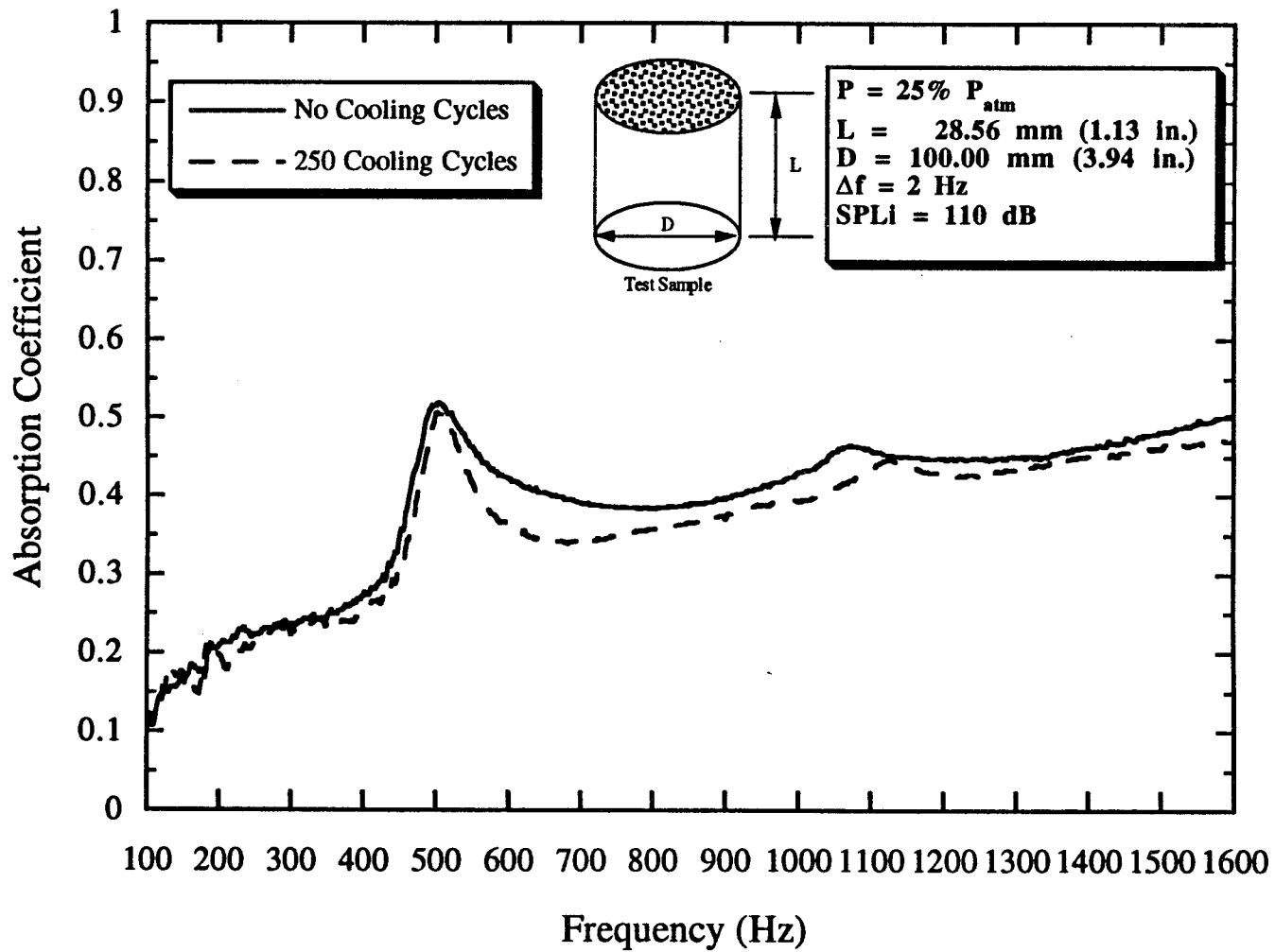


Figure B44. Absorption coefficient of Kevlar, $P = 25\% P_{atm}$, $L = 28.56 \text{ mm}$, $D = 100.0 \text{ mm}$.

B.45

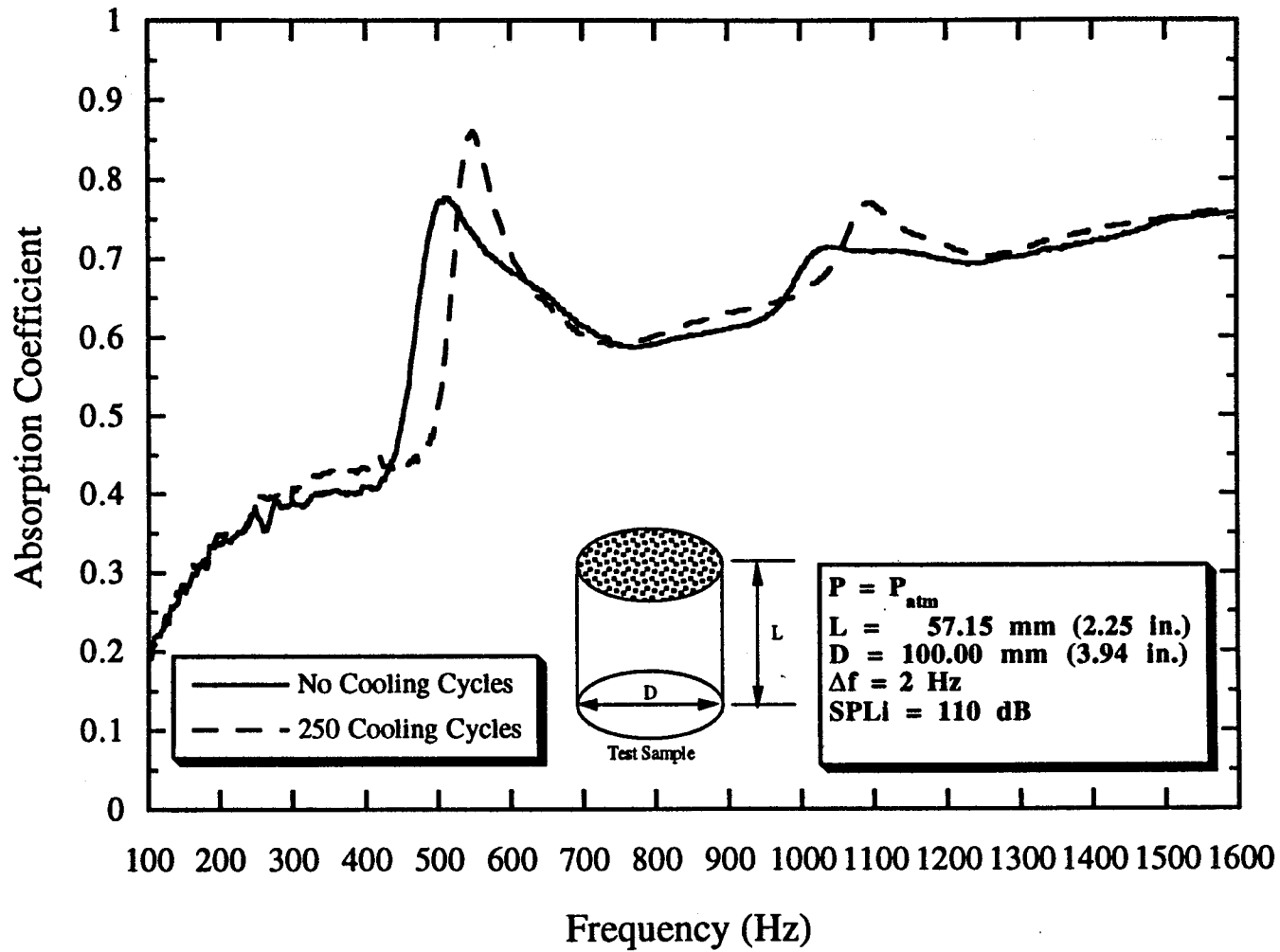


Figure B45. Absorption coefficient of Kevlar, $P = P_{atm}$, $L = 57.15 \text{ mm}$, $D = 100.0 \text{ mm}$.

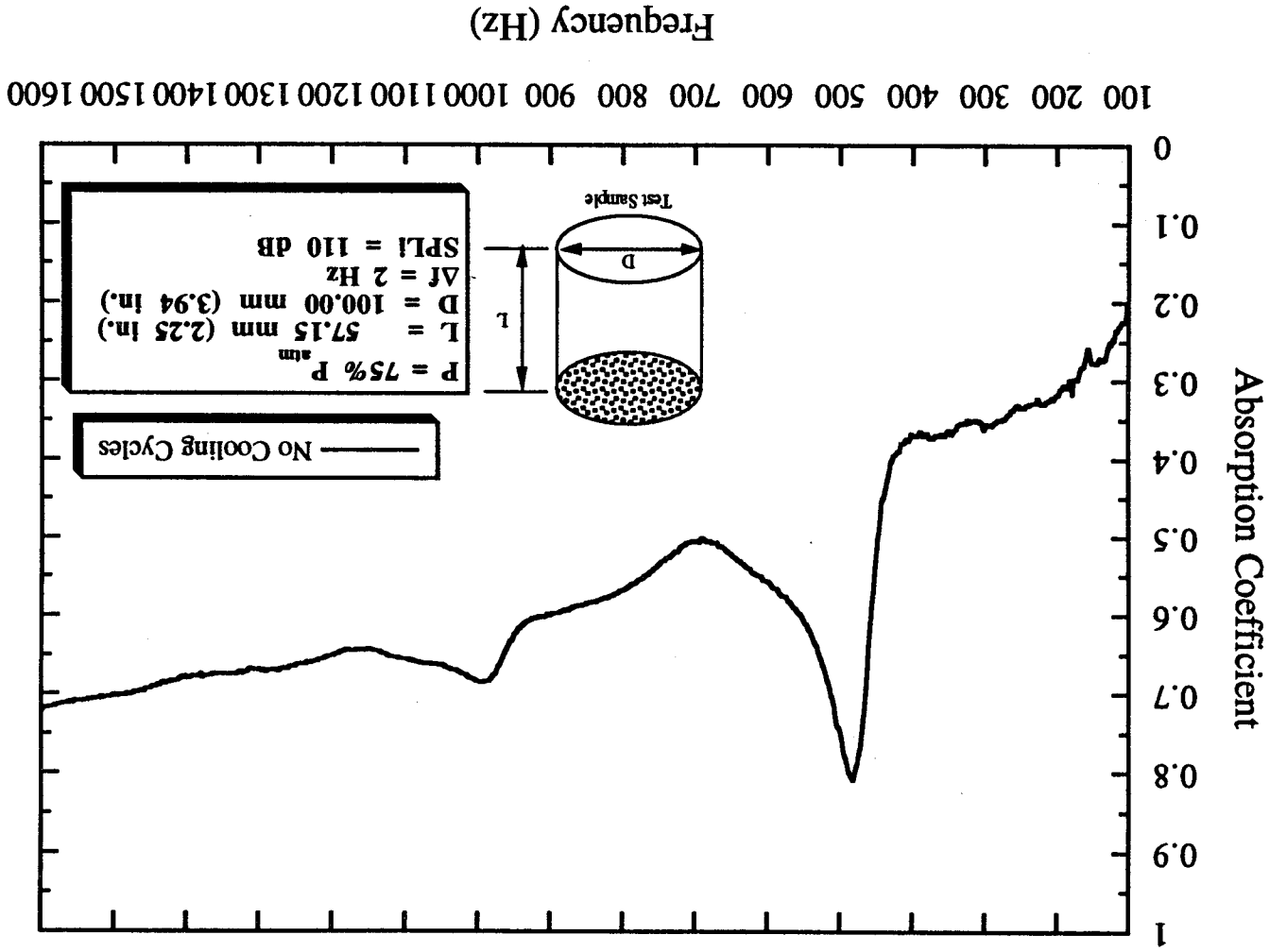


Figure B46. Absorption coefficient of Kevlar, $P = 75\% P_{atm}$, $L = 57.15$ mm, $D = 100.0$ mm.

B.47

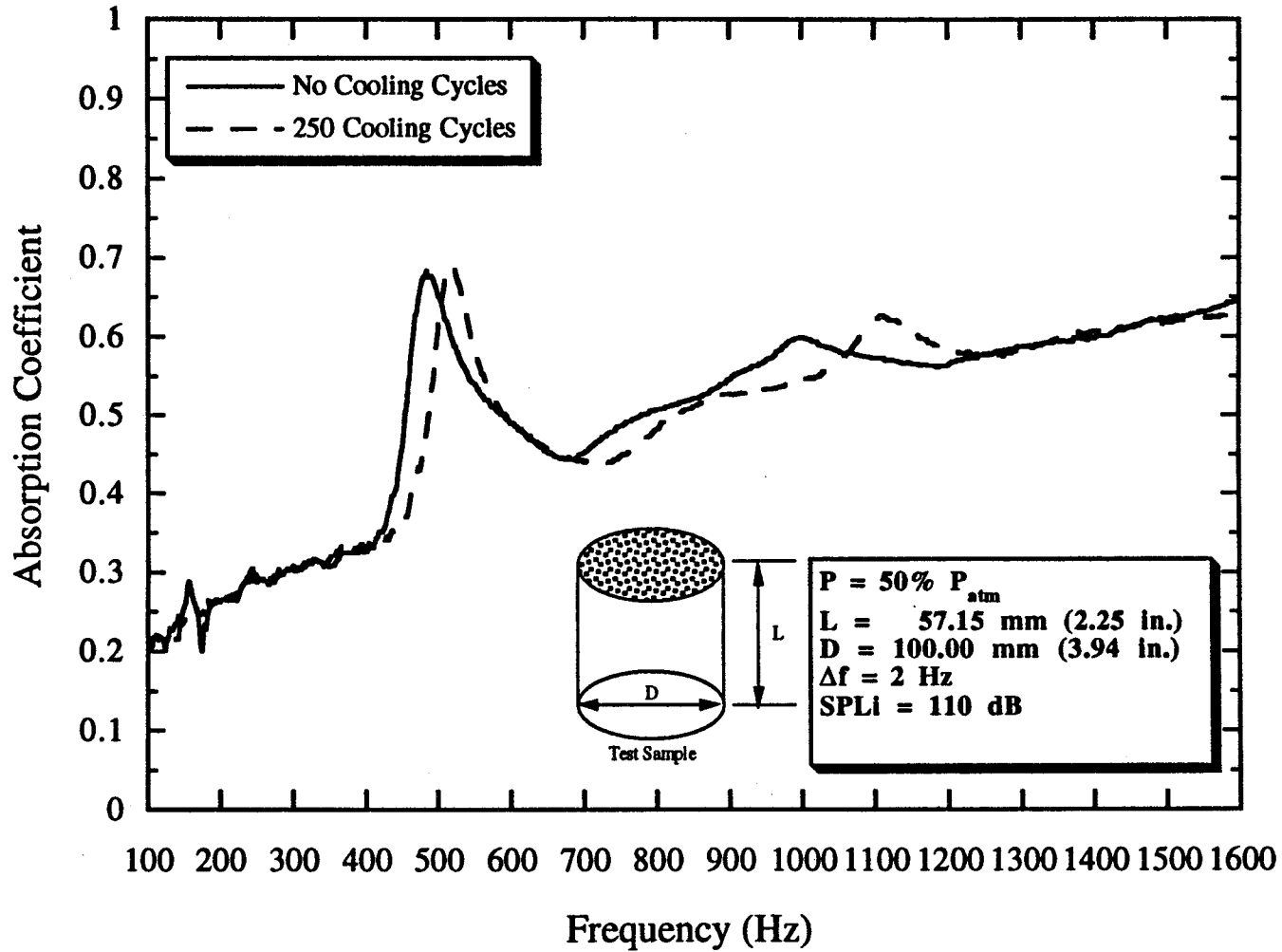


Figure B47. Absorption coefficient of Kevlar, $P = 50\% P_{atm}$, $L = 57.15 \text{ mm}$, $D = 100.0 \text{ mm}$.

B.48

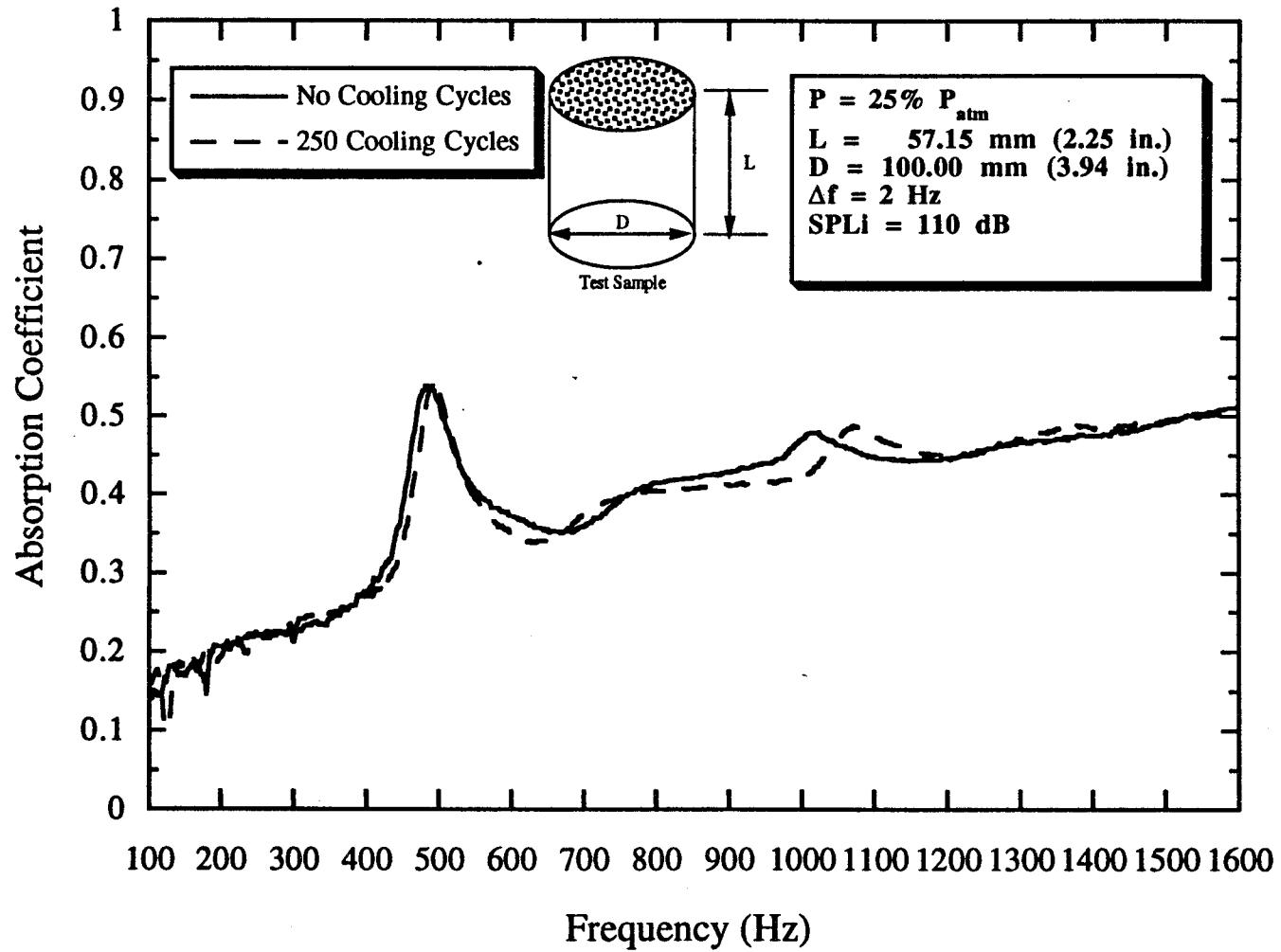


Figure B48. Absorption coefficient of Kevlar, $P = 25\% P_{atm}$, $L = 57.15 \text{ mm}$, $D = 100.0 \text{ mm}$.

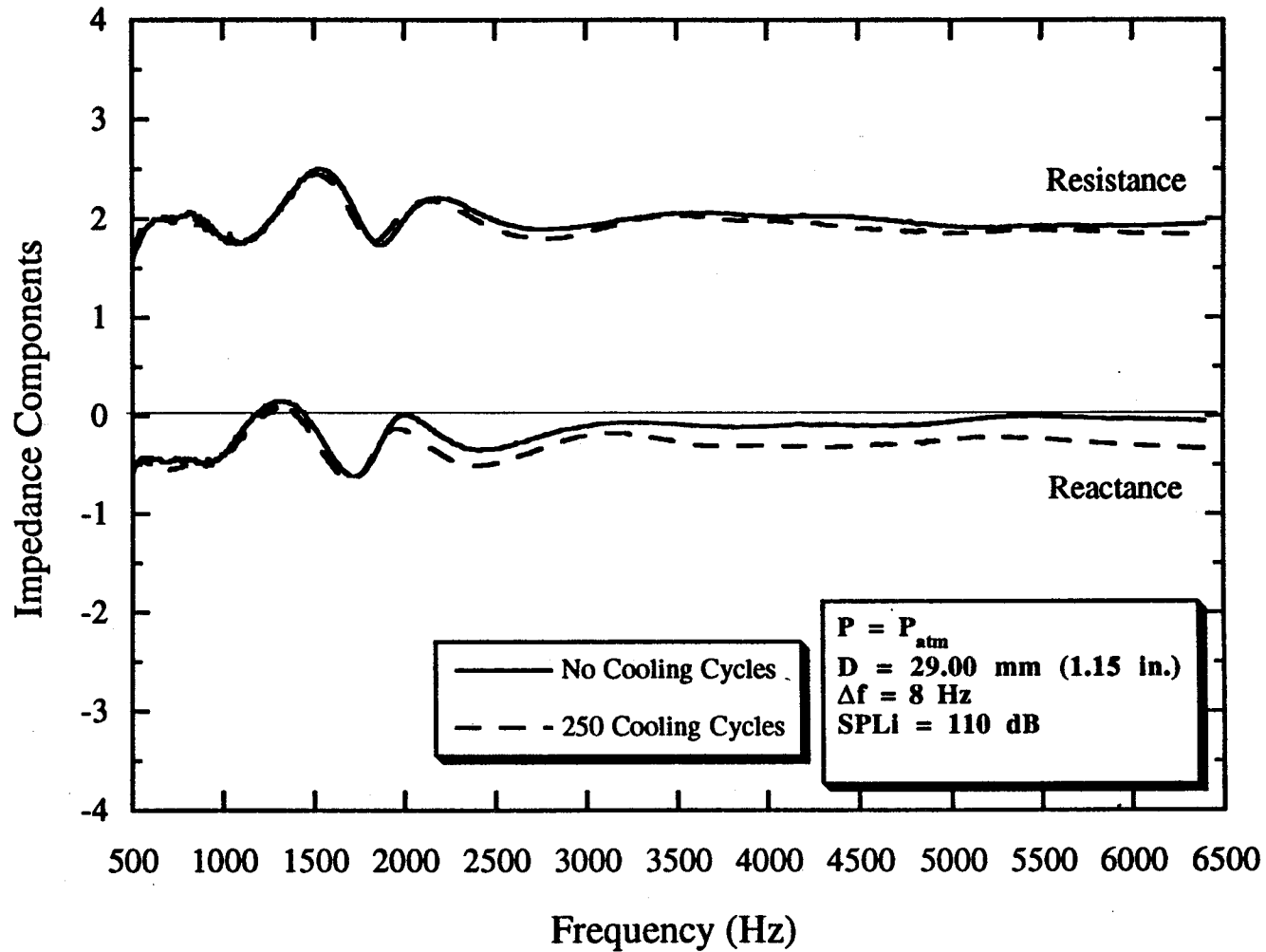


Figure B49. Characteristic Impedance of Pyrell foam, $P = P_{atm}$, $D = 29.0 \text{ mm}$.

B.50

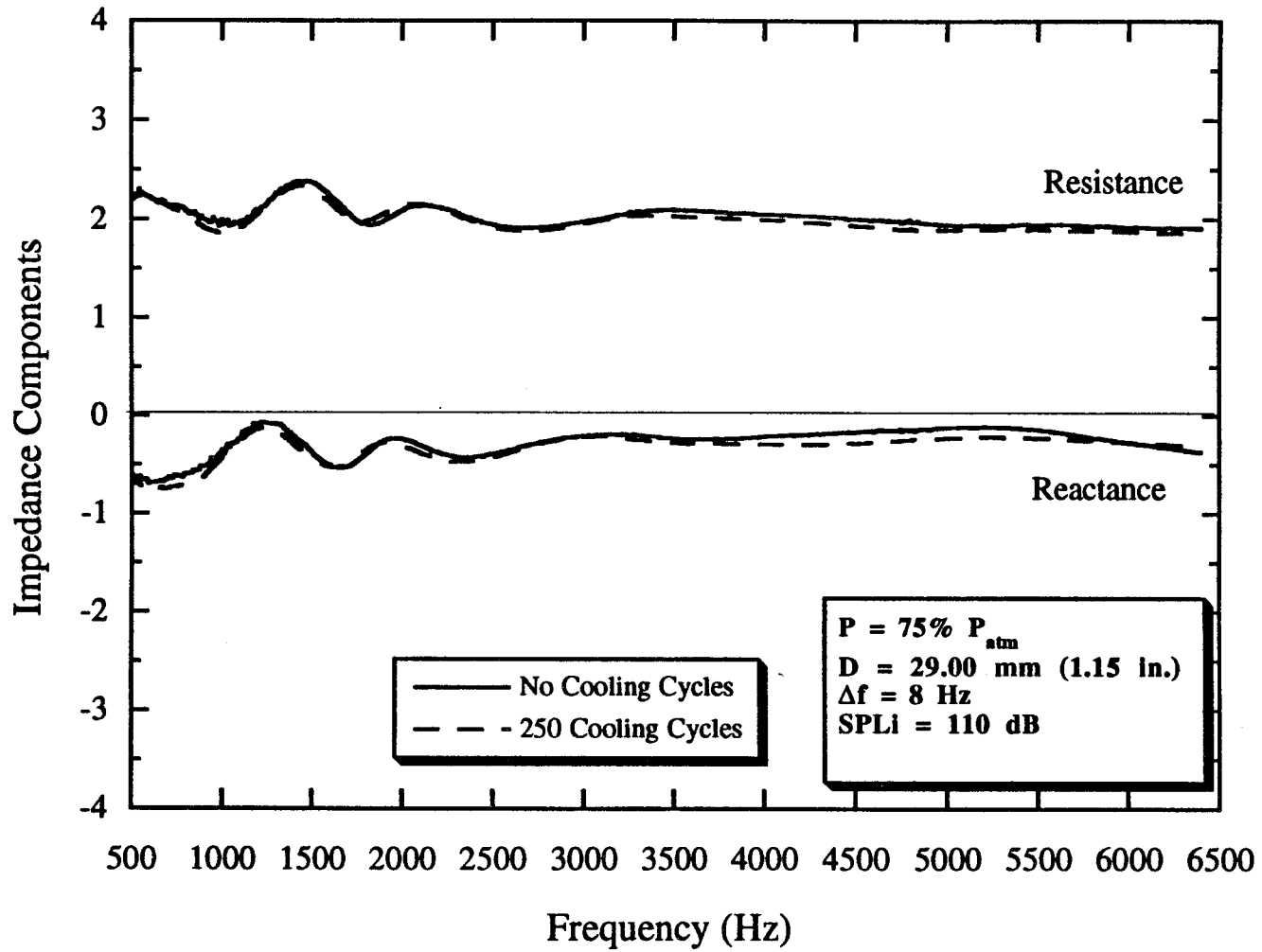


Figure B50. Characteristic Impedance of Pyrell foam, $P = 75\% P_{atm}$, $D = 29.0 \text{ mm}$.

B.51

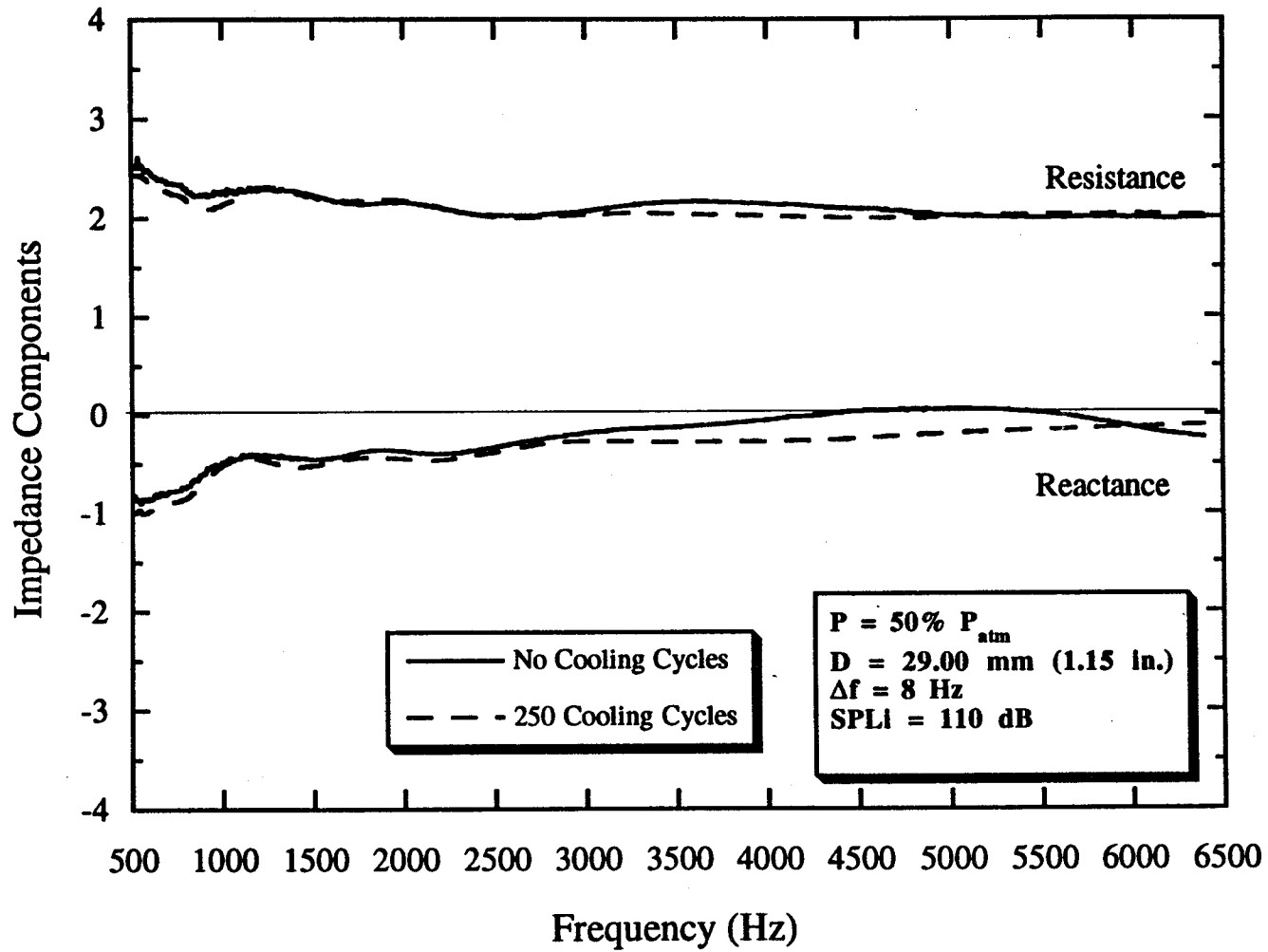


Figure B51. Characteristic Impedance of Pyrell foam, $P = 50\% P_{atm}$, $D = 29.0 \text{ mm}$.

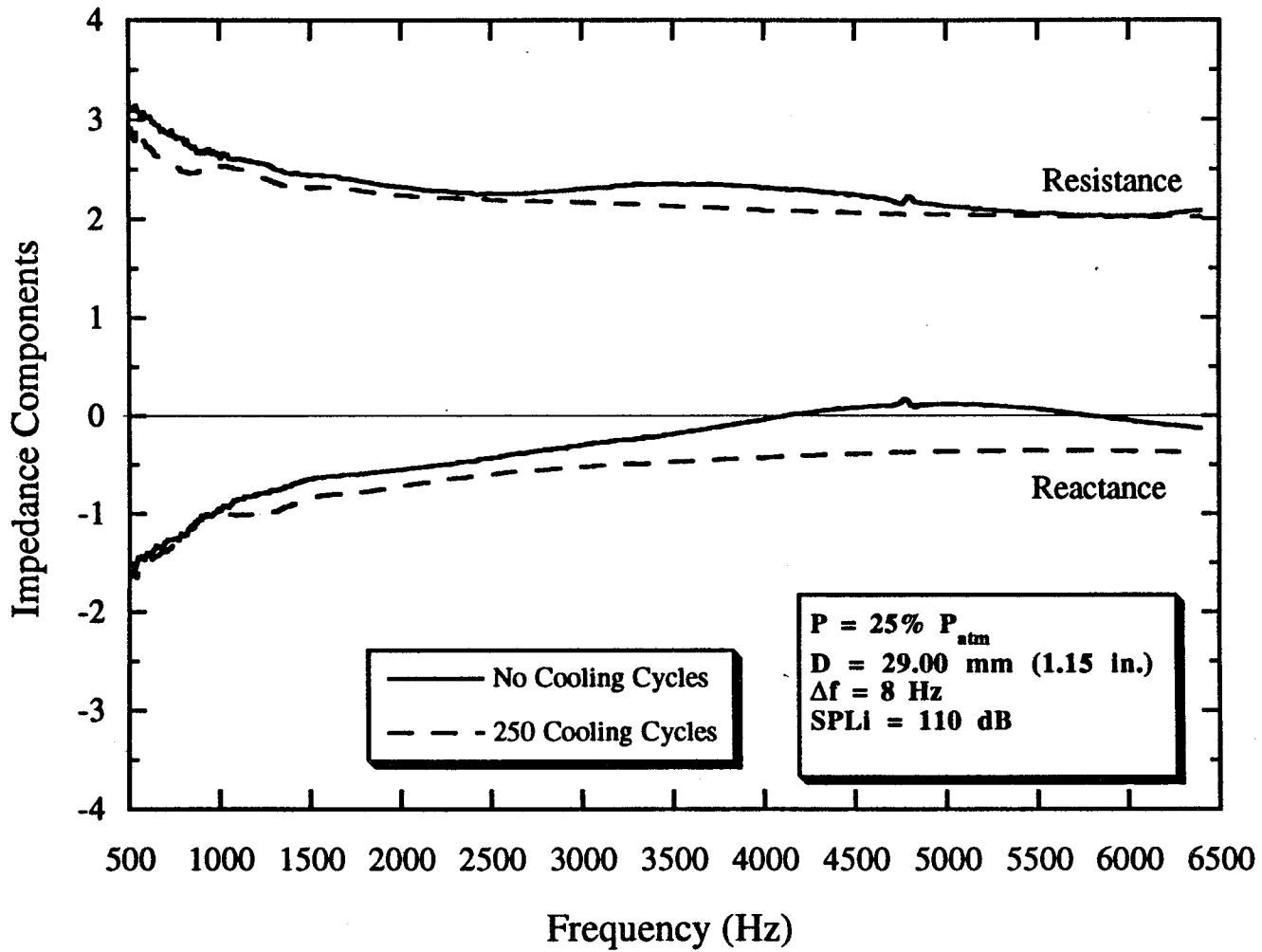


Figure B52. Characteristic Impedance of Pyrell foam, $P = 25\% P_{atm}$, $D = 29.0 \text{ mm}$.

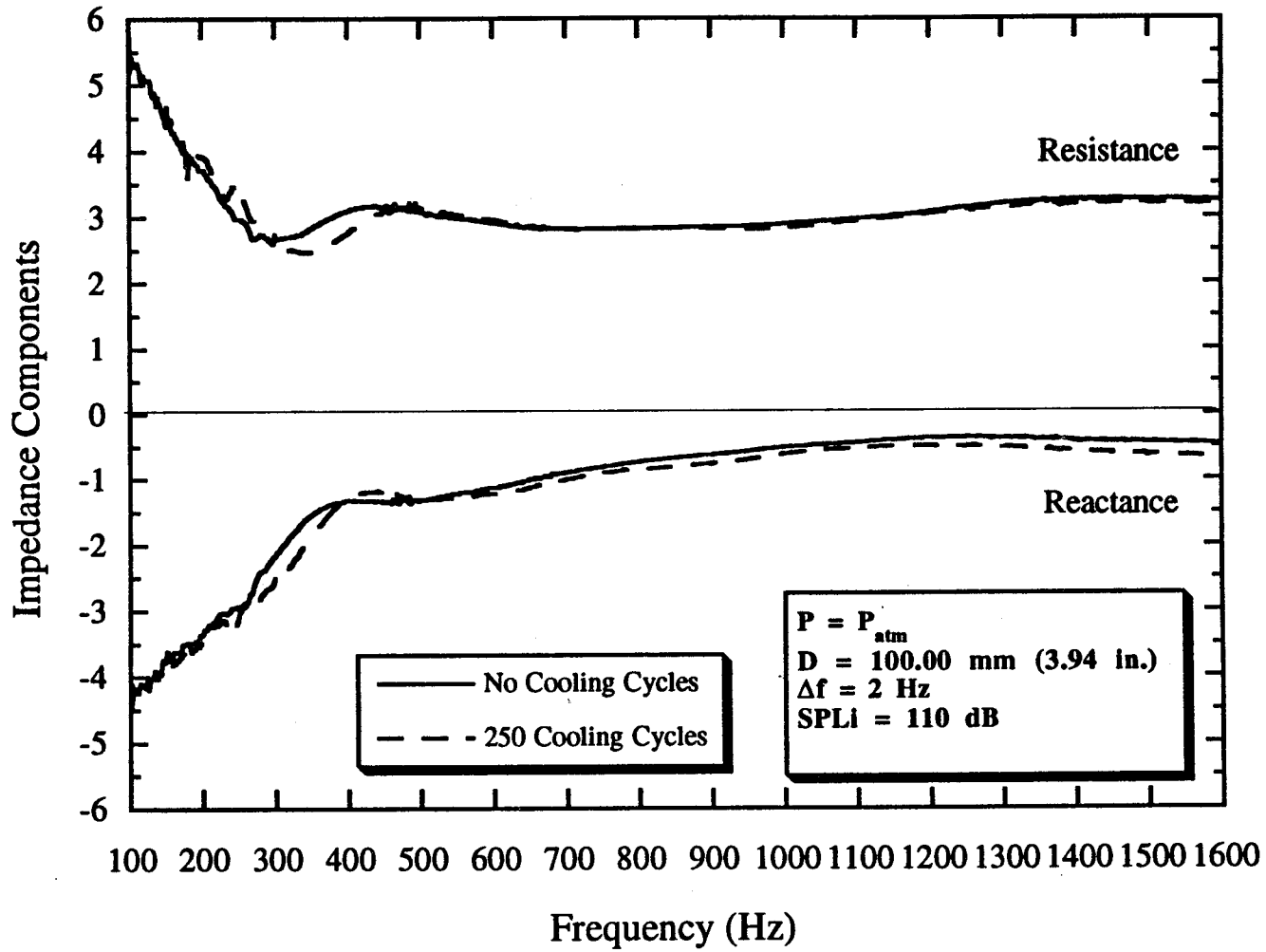


Figure B53. Characteristic Impedance of Pyrell foam, $P = P_{atm}$, $D = 100.0$ mm.

B.54

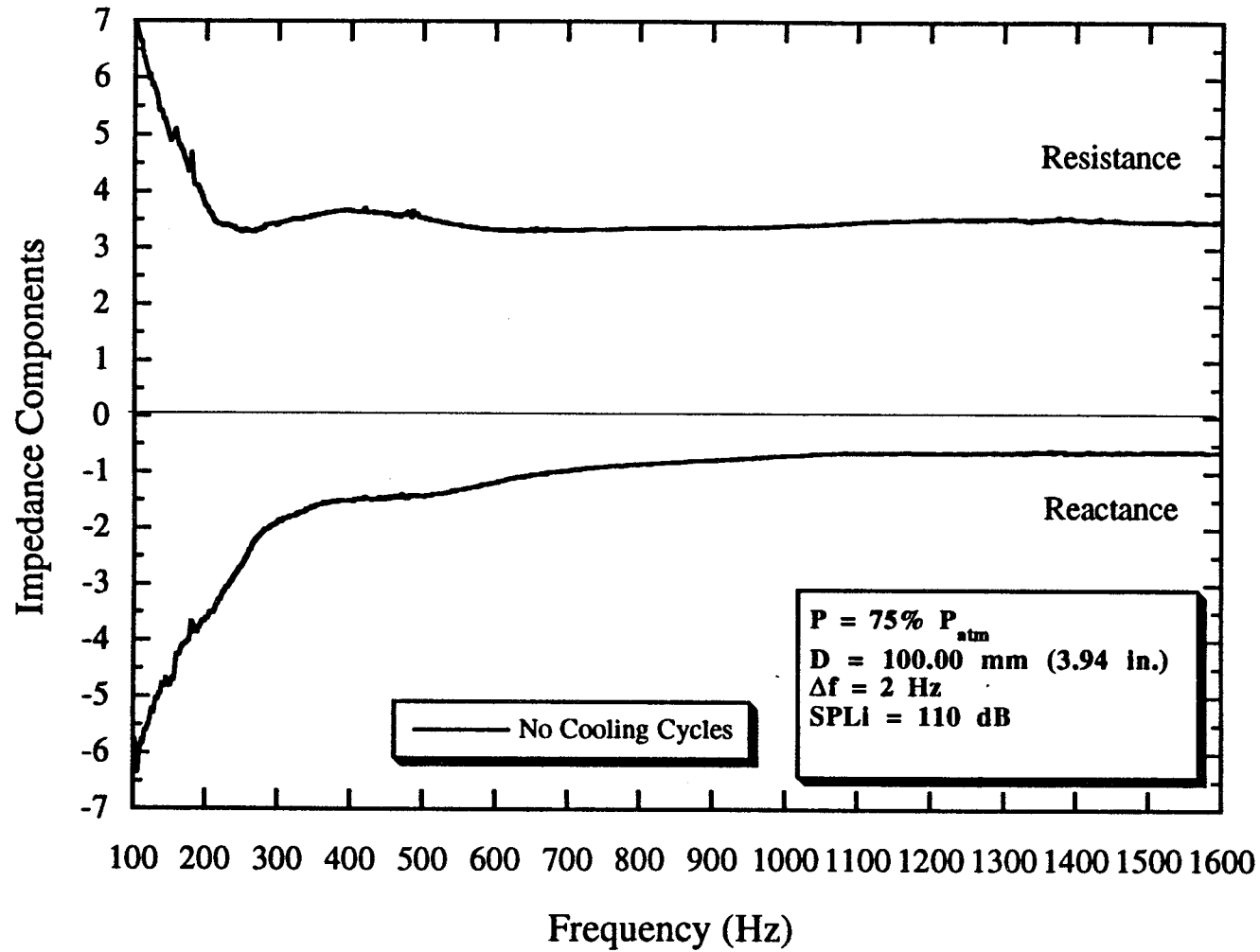


Figure B54. Characteristic Impedance of Pyrell foam, $P = 75\% P_{atm}$, $D = 100.0 \text{ mm}$.

B.55

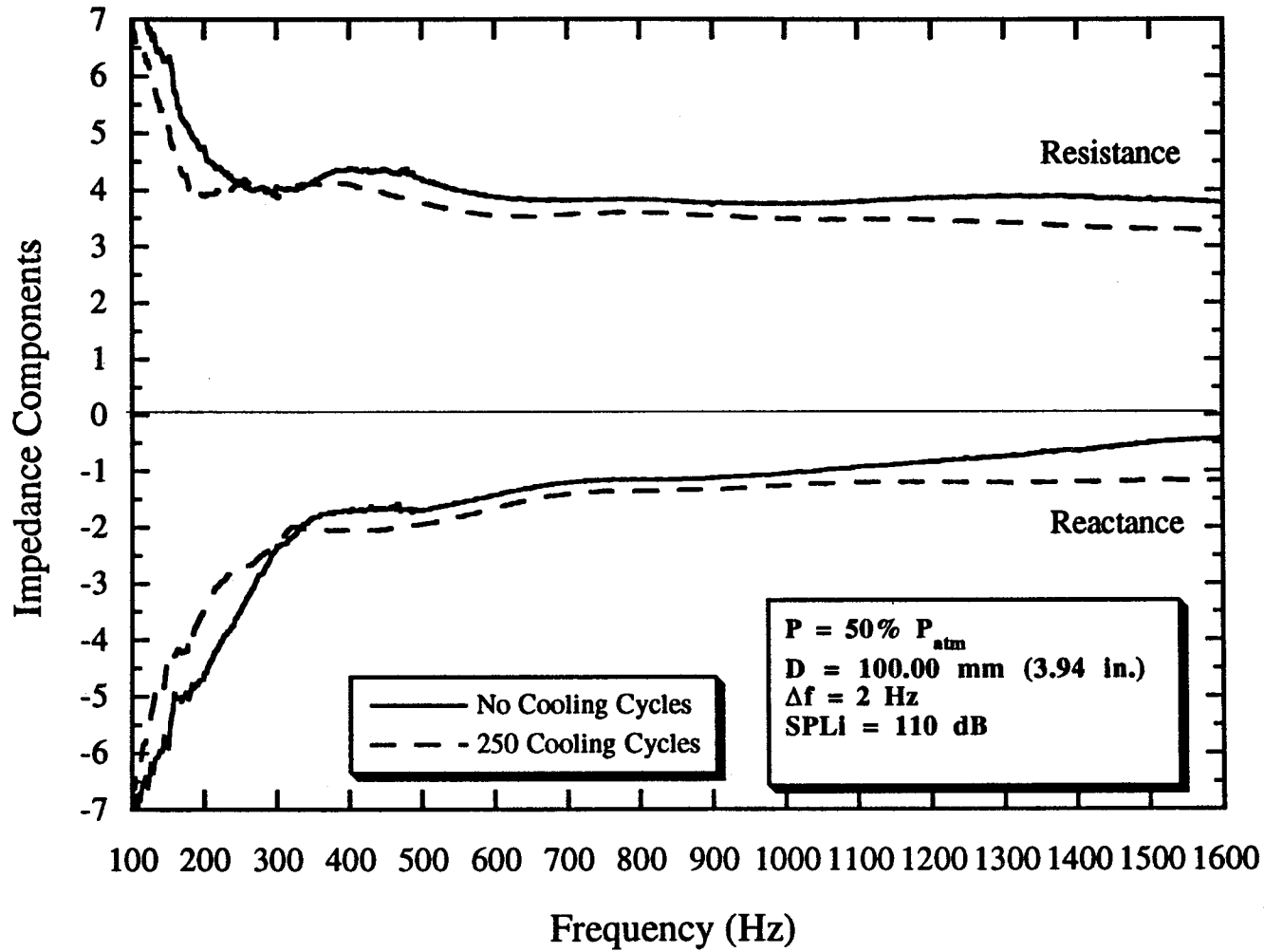


Figure B55. Characteristic Impedance of Pyrell foam, $P = 50\% P_{atm}$, $D = 100.0 \text{ mm}$.

B.56

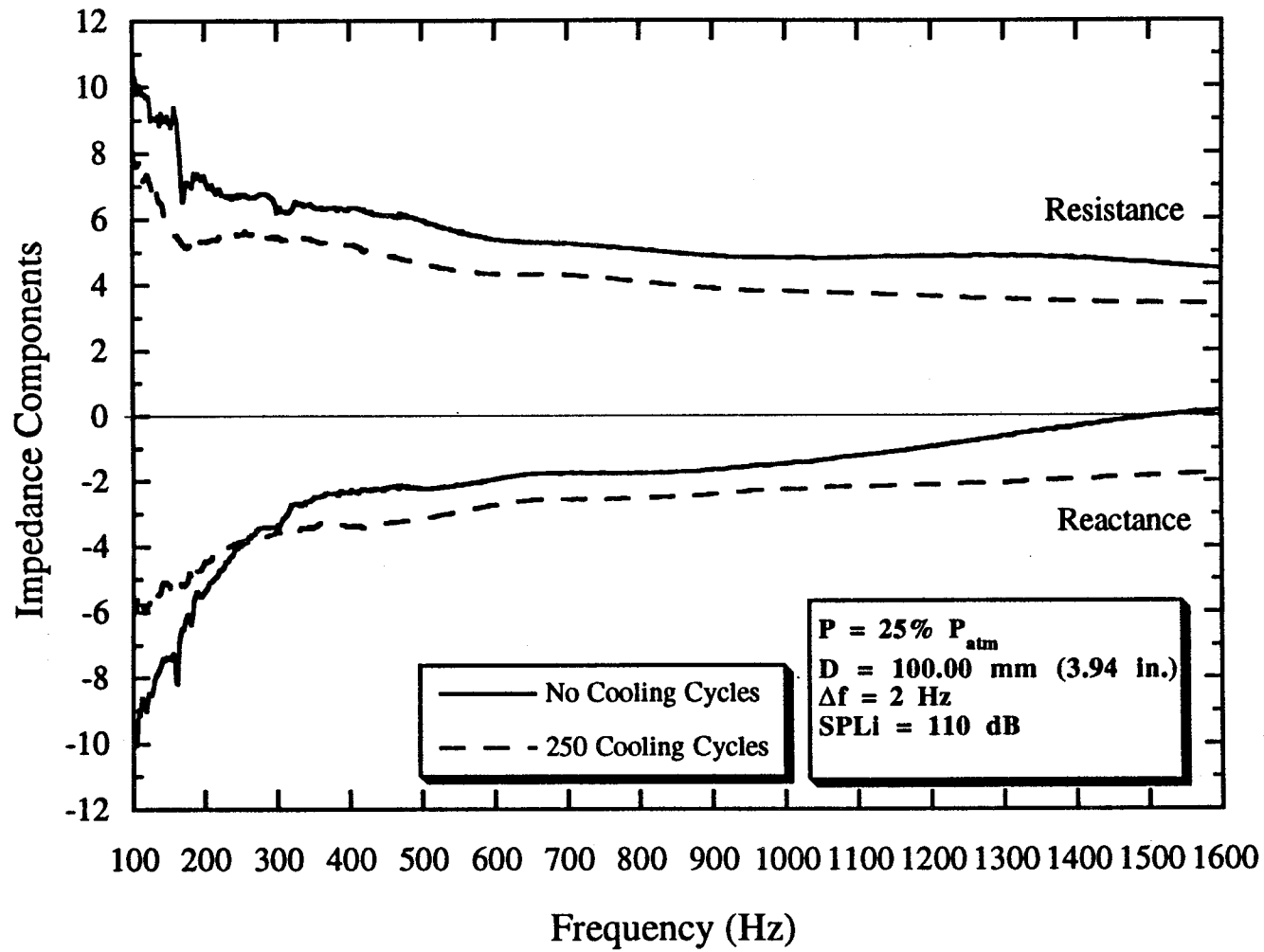


Figure B56. Characteristic Impedance of Pyrell foam, $P = 25\% P_{atm}$, $D = 100.0$ mm.

B.57

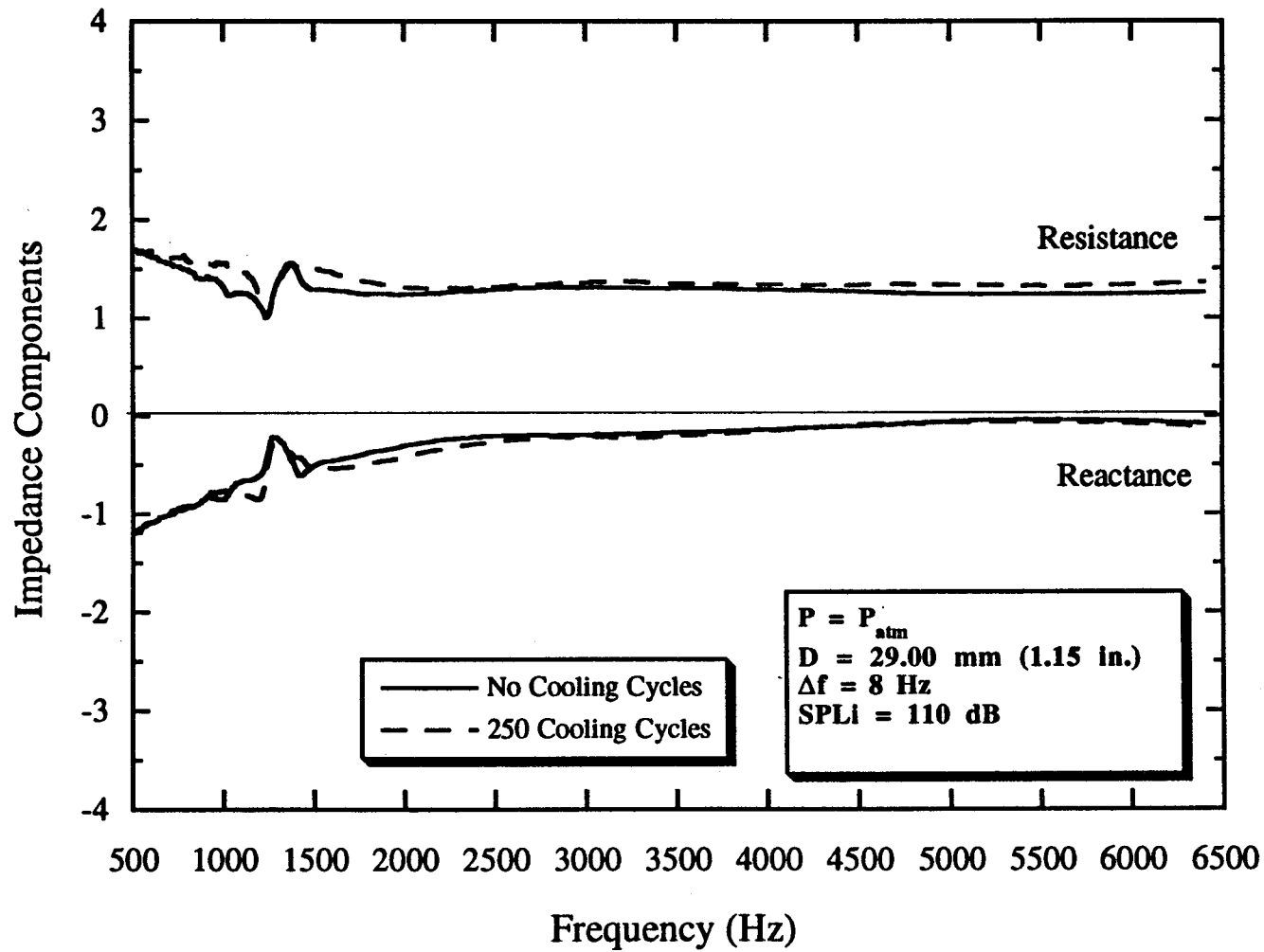


Figure B57. Characteristic Impedance of Fiberglass, $P = P_{atm}$, $D = 29.0 \text{ mm}$.

B.58

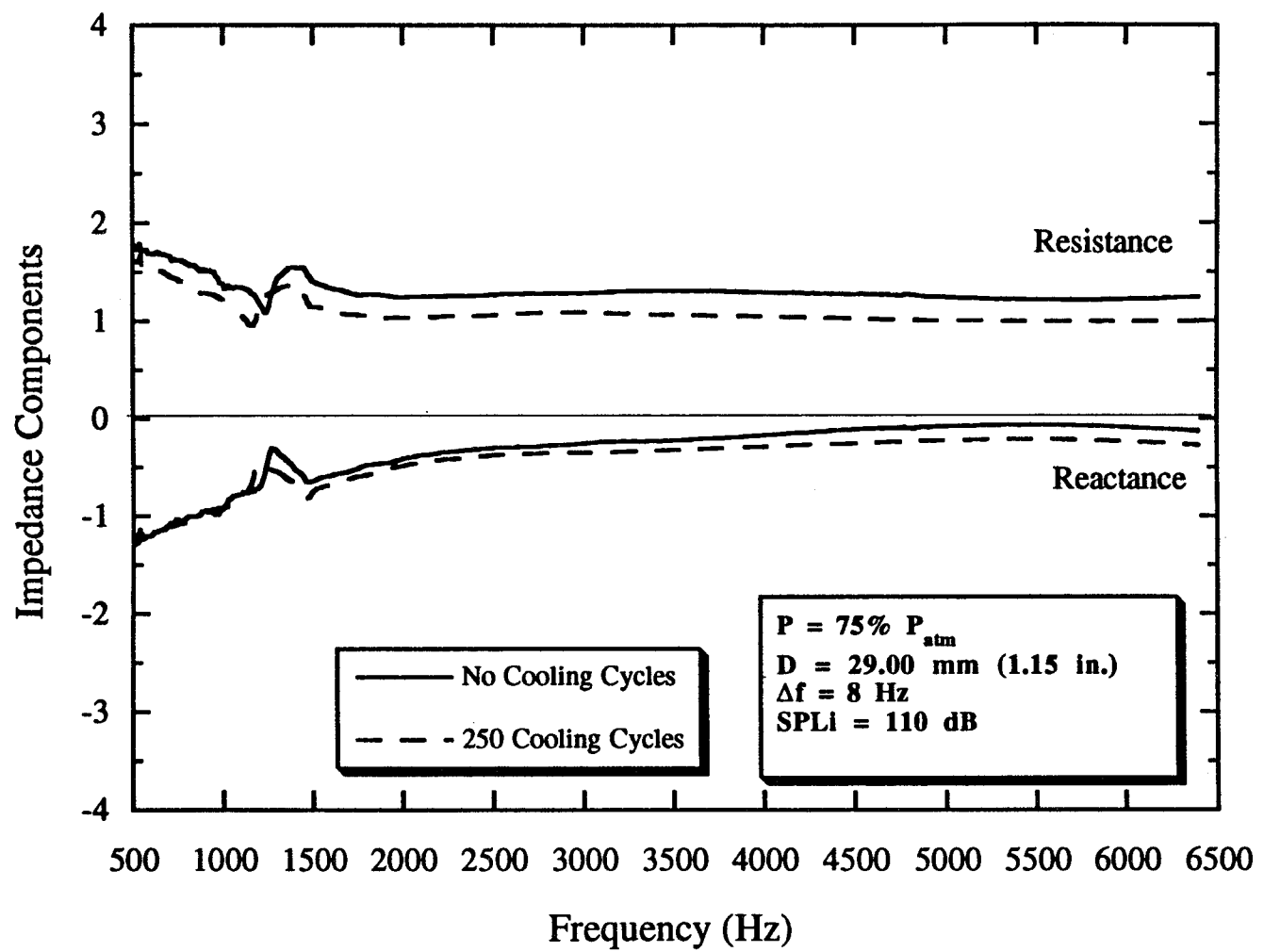


Figure B58. Characteristic Impedance of Fiberglass, $75\% P = P_{atm}$, $D = 29.0 \text{ mm}$.

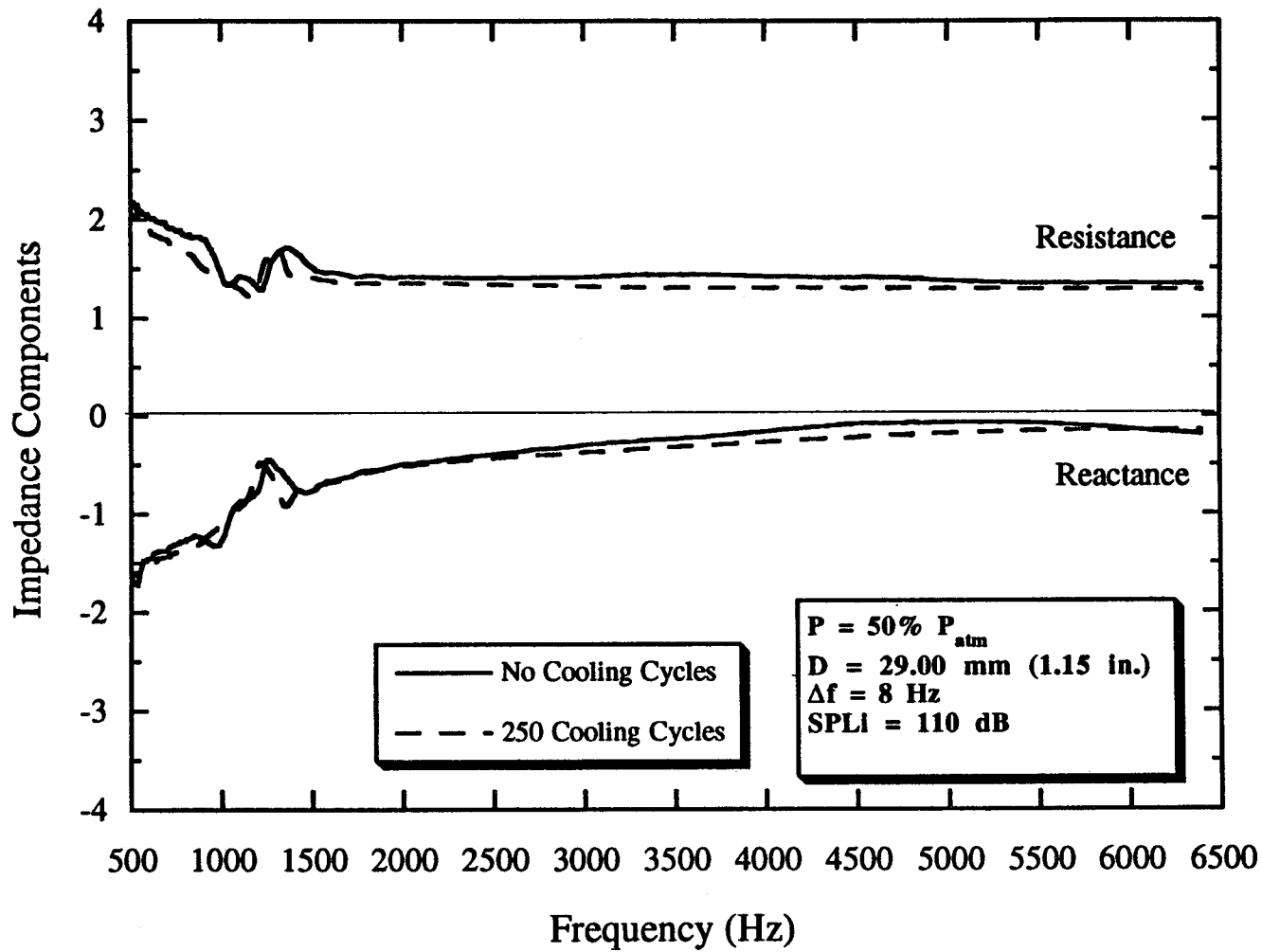


Figure B59. Characteristic Impedance of Fiberglass, 50% P = P_{atm}, D = 29.0 mm.

B.60

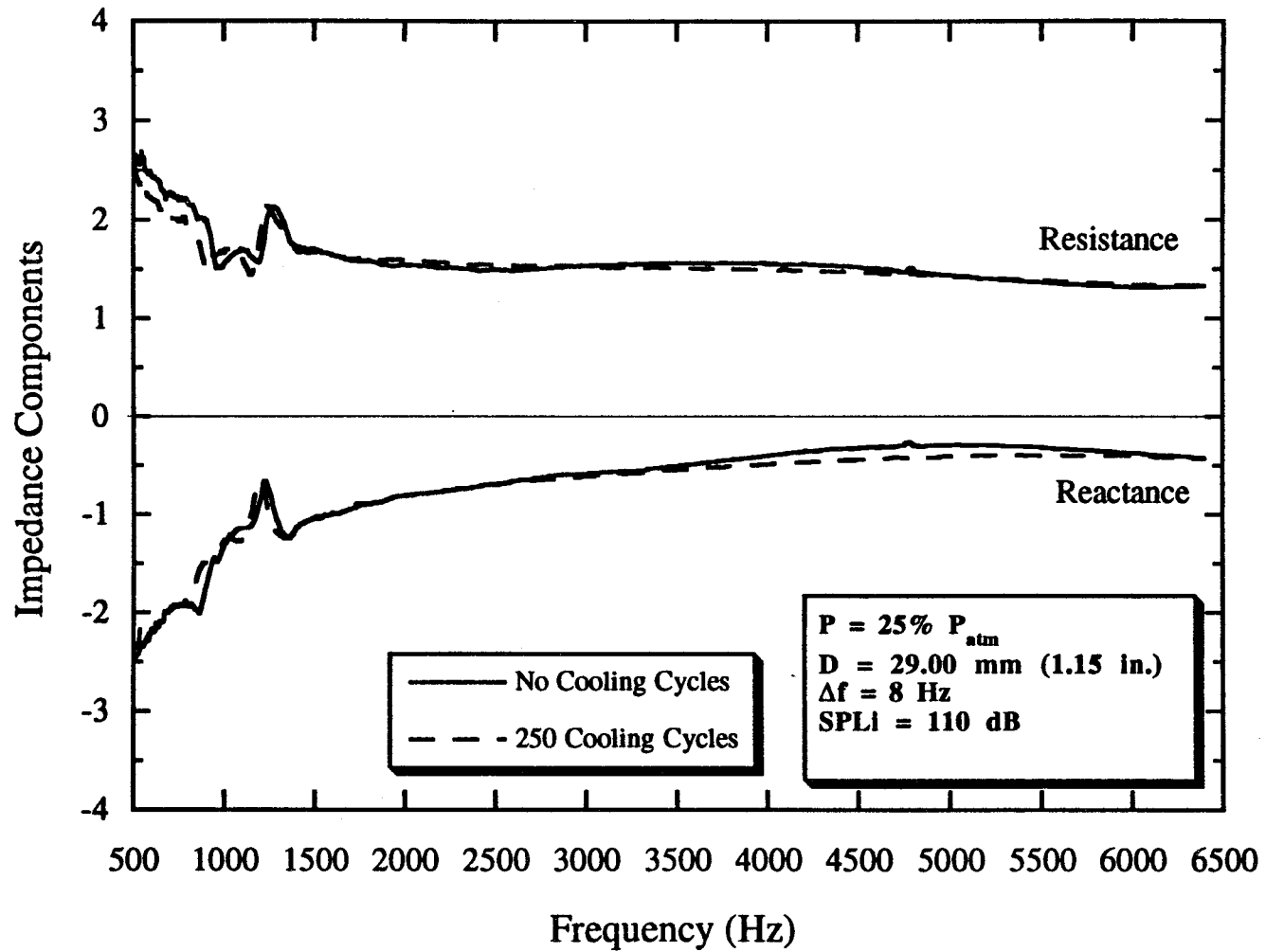


Figure B60. Characteristic Impedance of Fiberglass, 25% $P = P_{atm}$, $D = 29.0 \text{ mm}$.

B.61

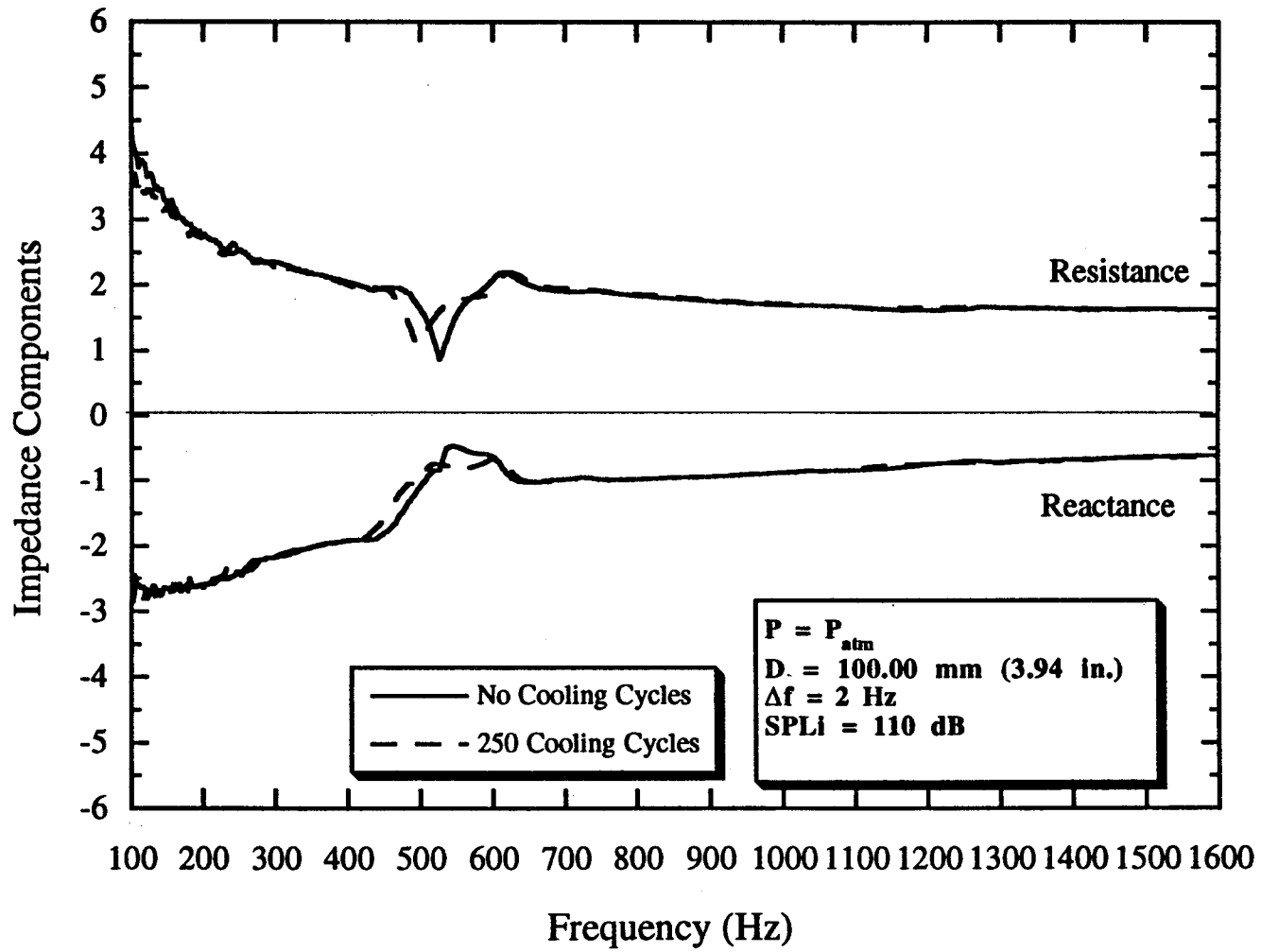


Figure B61. Characteristic Impedance of Fiberglass, $P = P_{atm}$, $D = 100.0 \text{ mm}$.

B.62

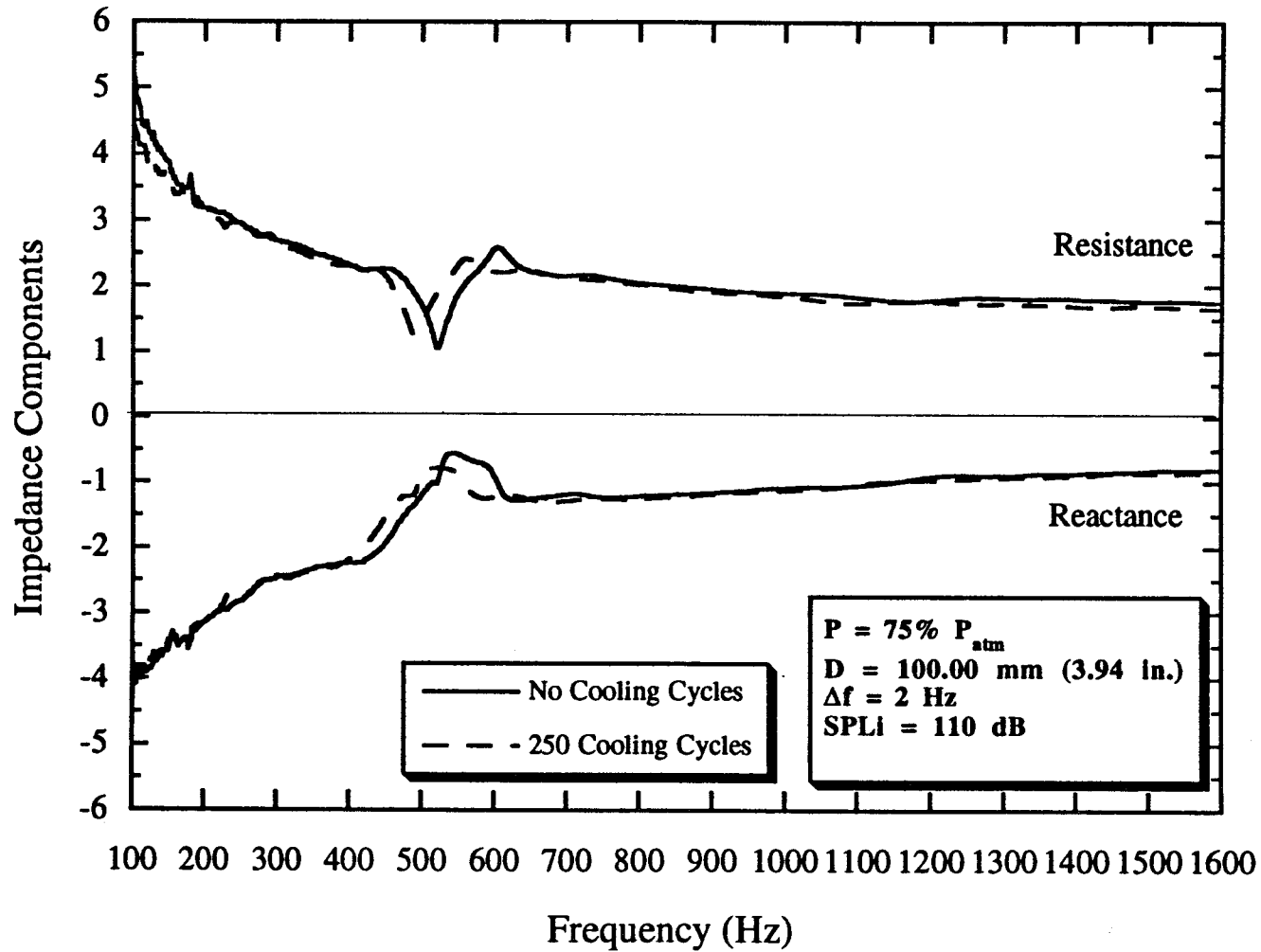


Figure B62. Characteristic Impedance of Fiberglass, $P = 75\% P_{atm}$, $D = 100.0 \text{ mm}$.

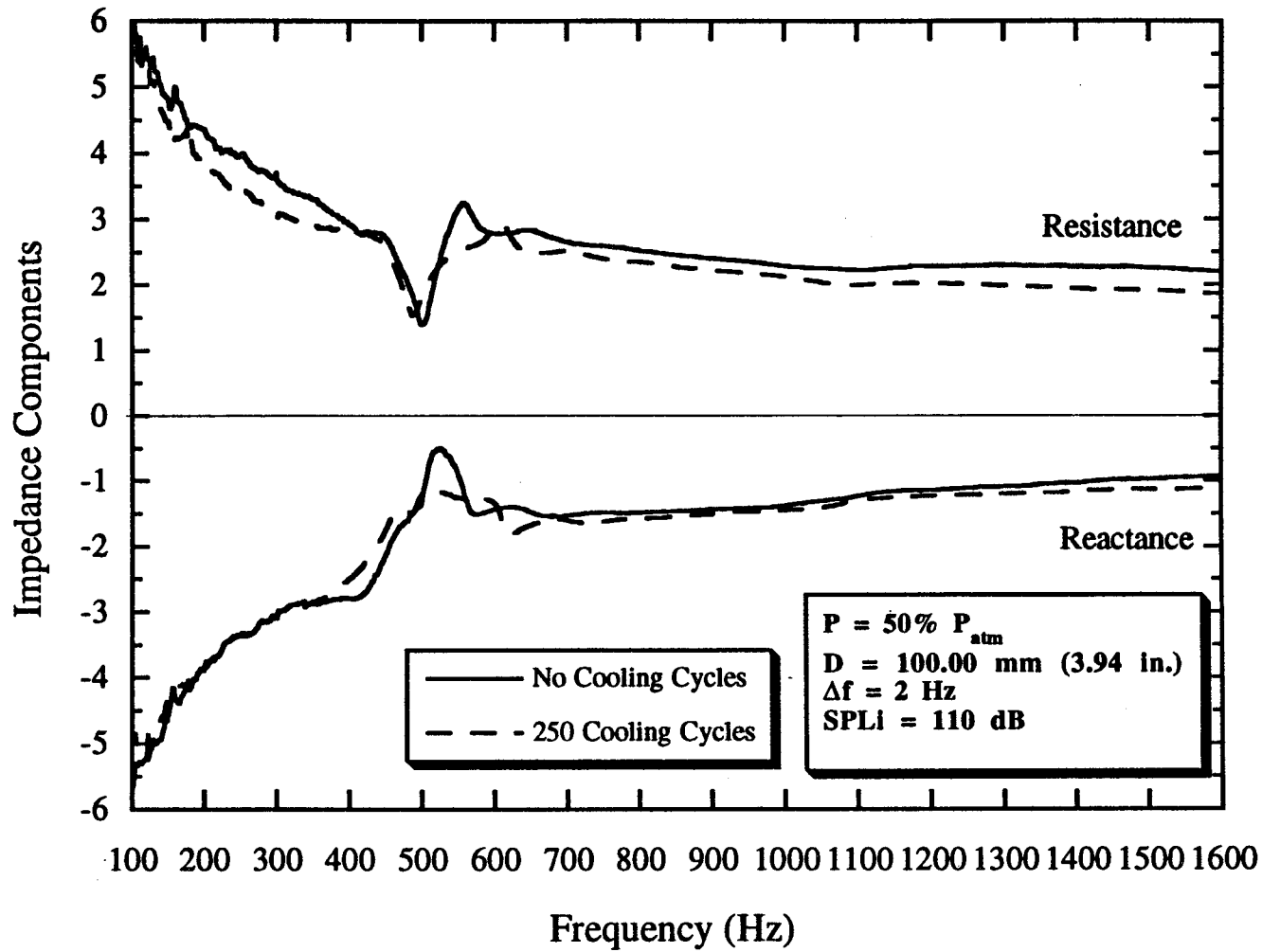


Figure B63. Characteristic Impedance of Fiberglass, $P = 50\% P_{atm}$, $D = 100.0 \text{ mm}$.

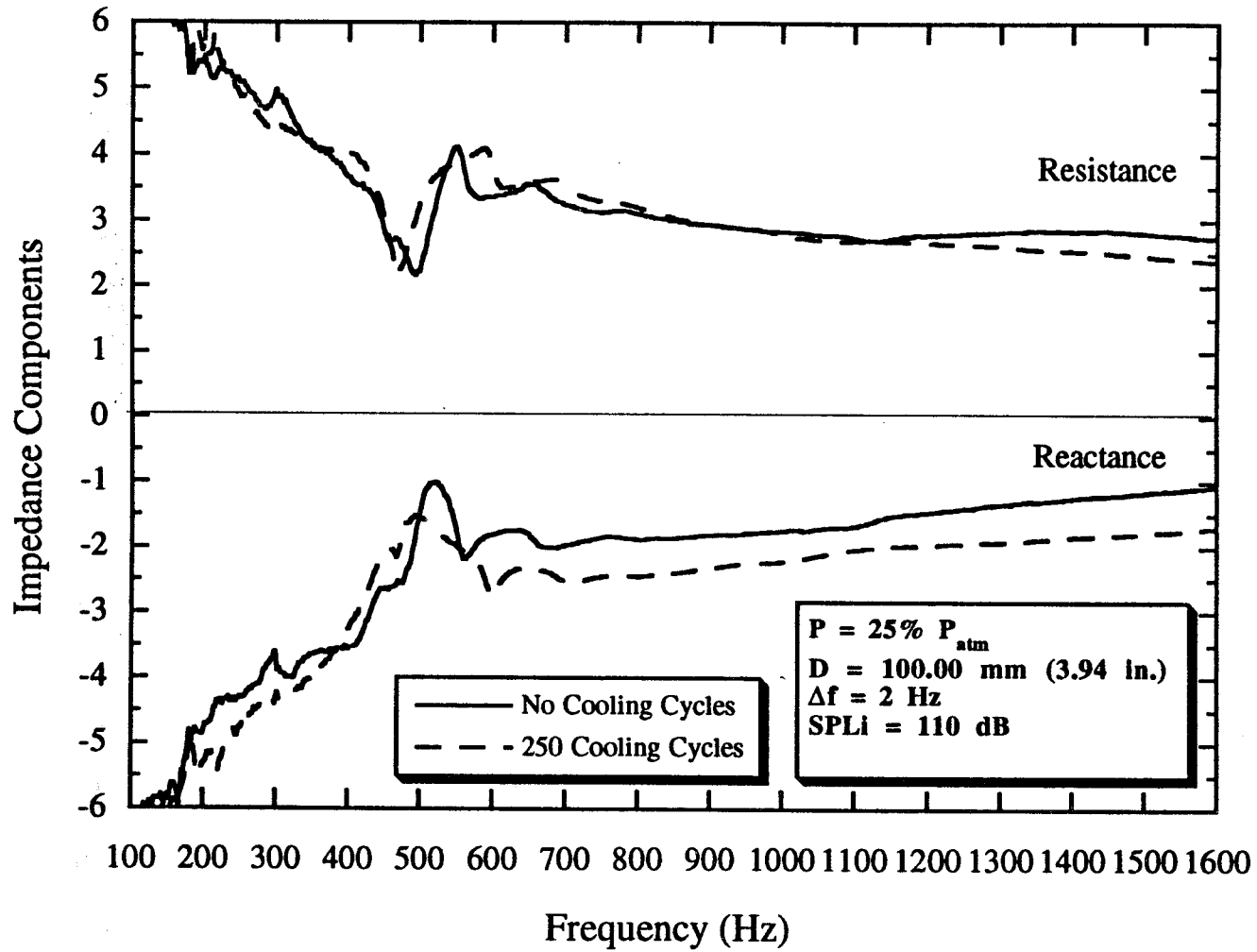


Figure B64. Characteristic Impedance of Fiberglass, $P = 25\% P_{atm}$, $D = 100.0$ mm.

B.65

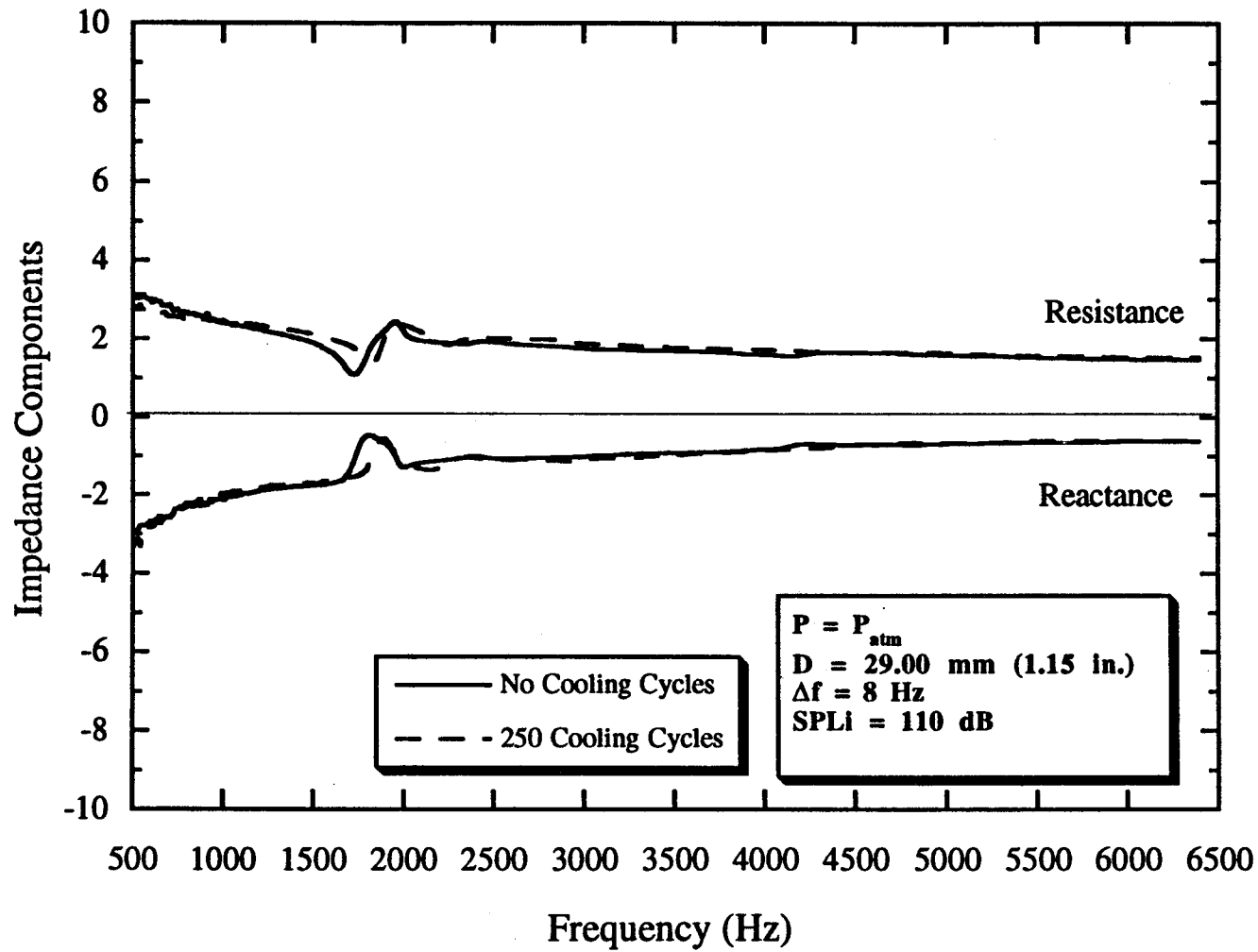


Figure B65. Characteristic Impedance of Kevlar, $P = P_{atm}$, $D = 29.0 \text{ mm}$.

B.66

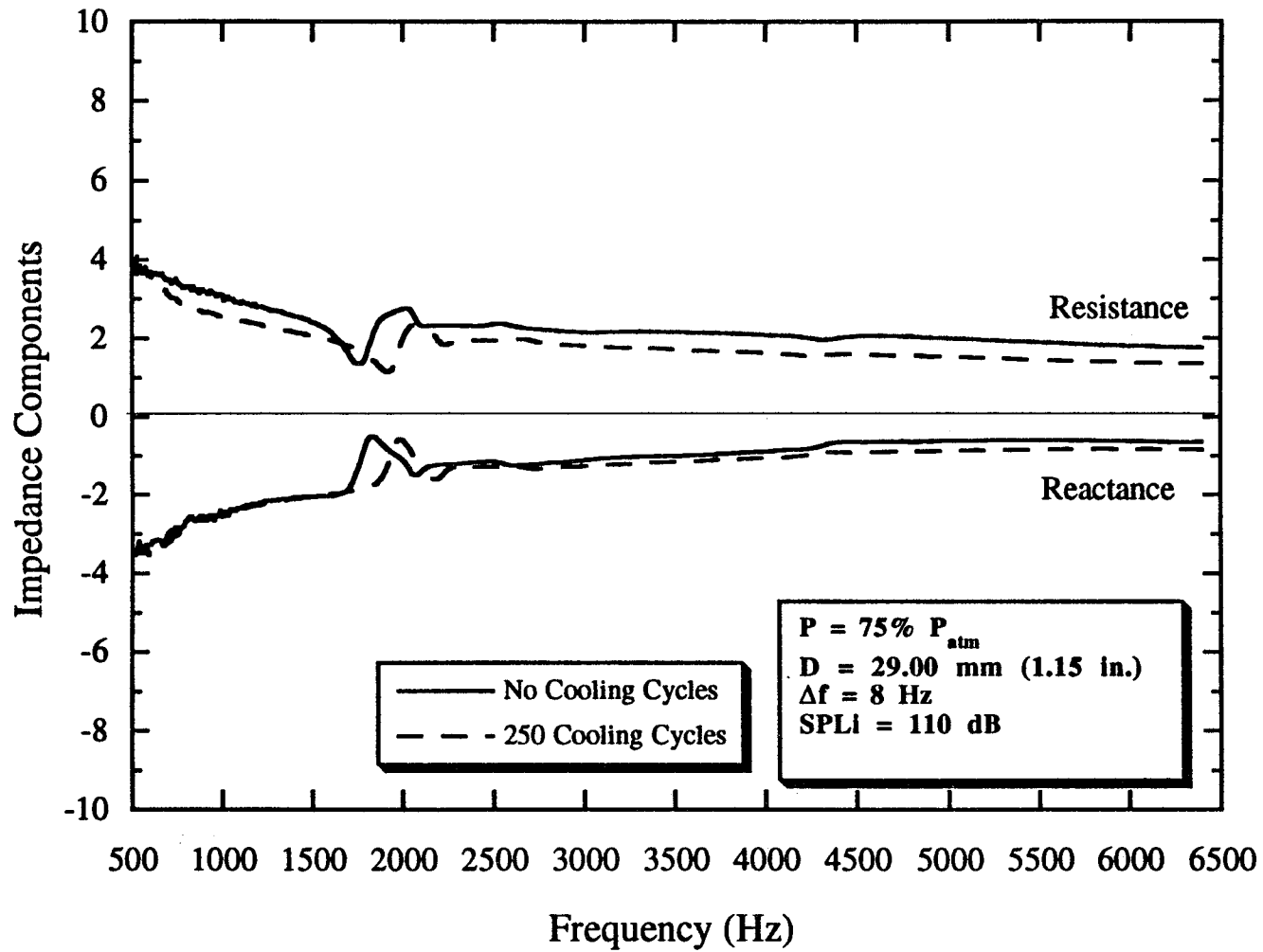


Figure B66. Characteristic Impedance of Kevlar, $P = 75\% P_{atm}$, $D = 29.0 \text{ mm}$.

B.67

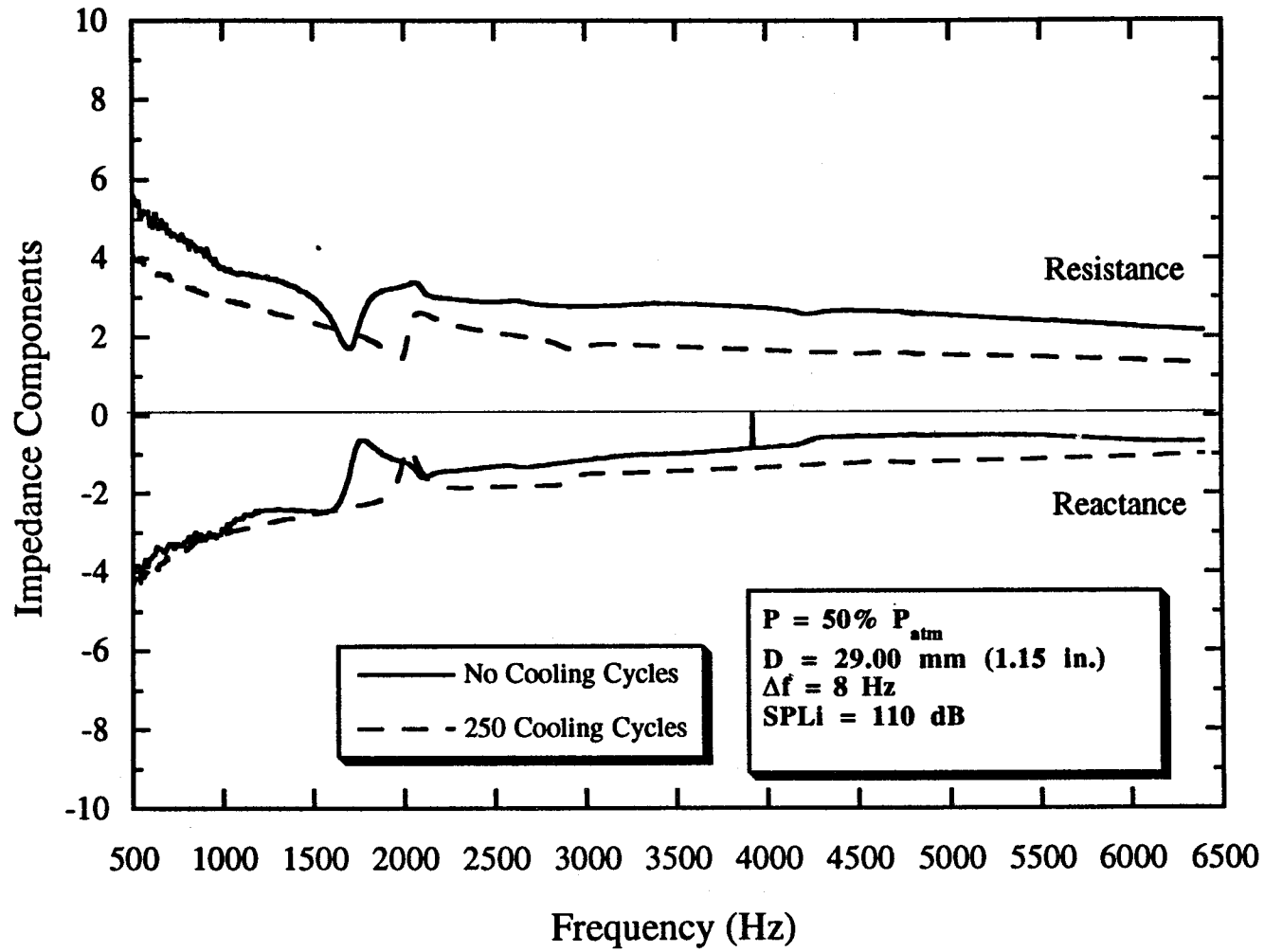


Figure B67. Characteristic Impedance of Kevlar, $P = 50\% P_{atm}$, $D = 29.0 \text{ mm}$.

B.68

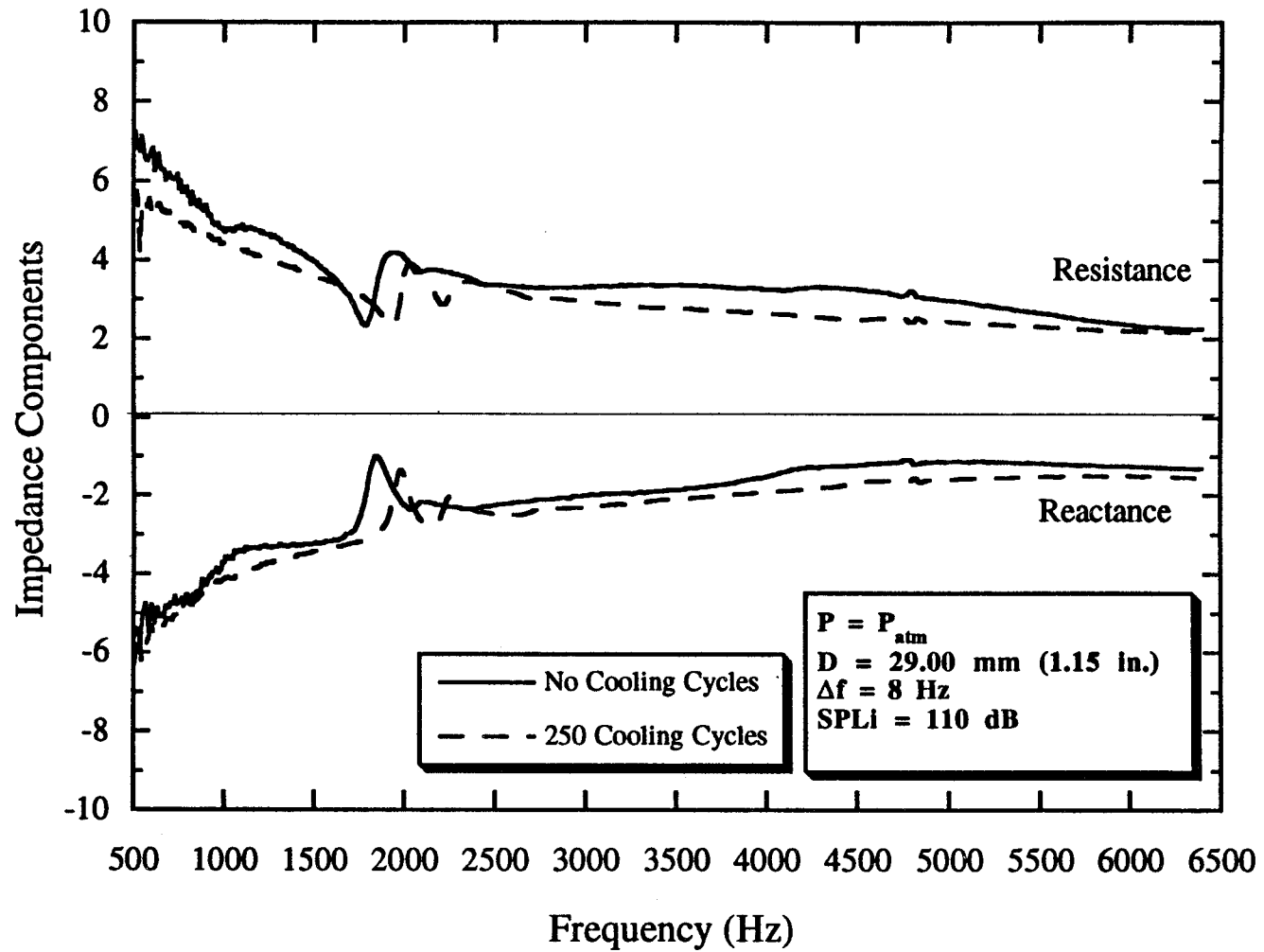


Figure B68. Characteristic Impedance of Kevlar, $P = 25\% P_{atm}$, $D = 29.0$ mm.

B.69

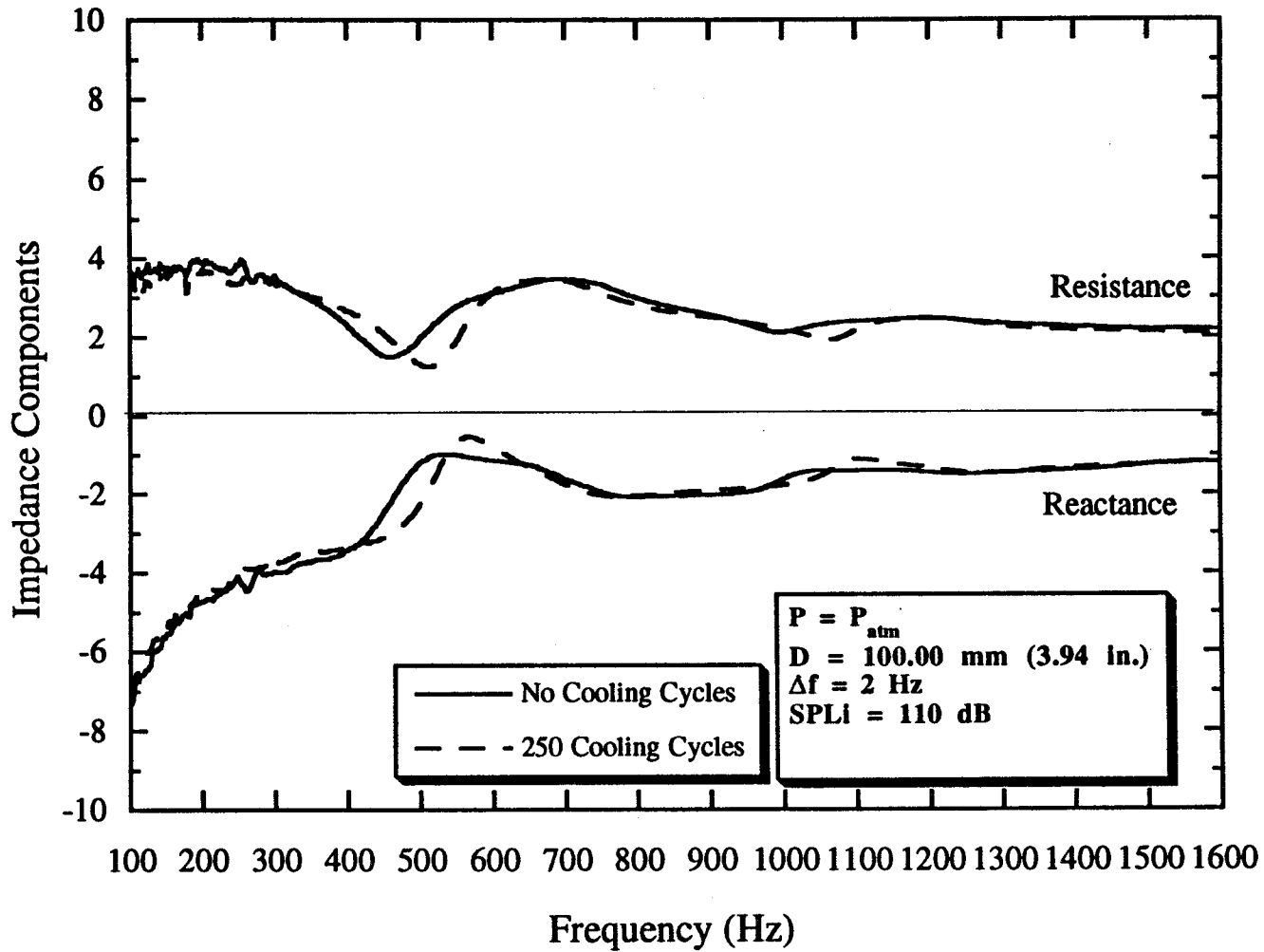


Figure B69. Characteristic Impedance of Kevlar, $P = P_{atm}$, $D = 100.0 \text{ mm}$.

B.70

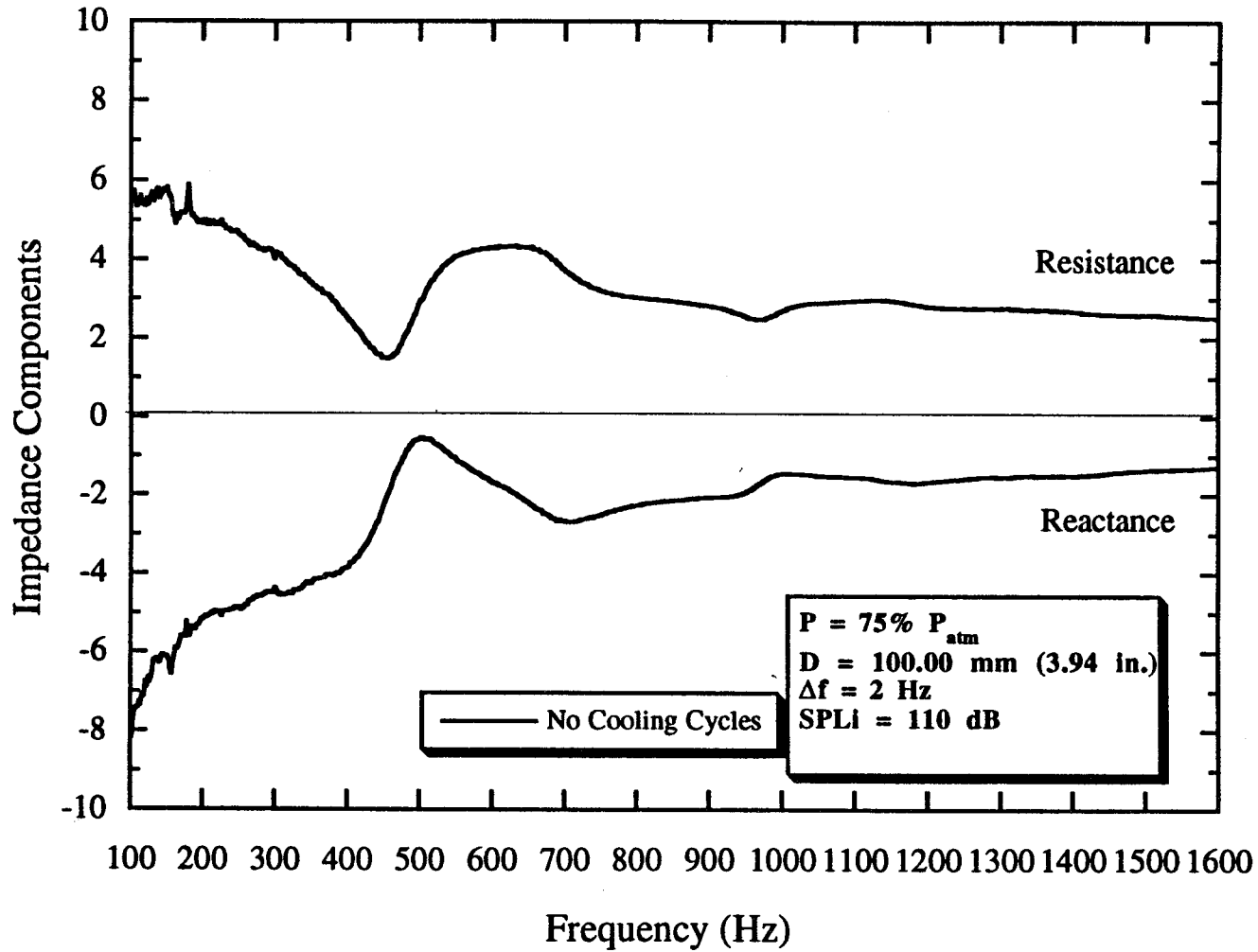


Figure B70. Characteristic Impedance of Kevlar, $P = 75\% P_{atm}$, $D = 100.0$ mm.

B.71

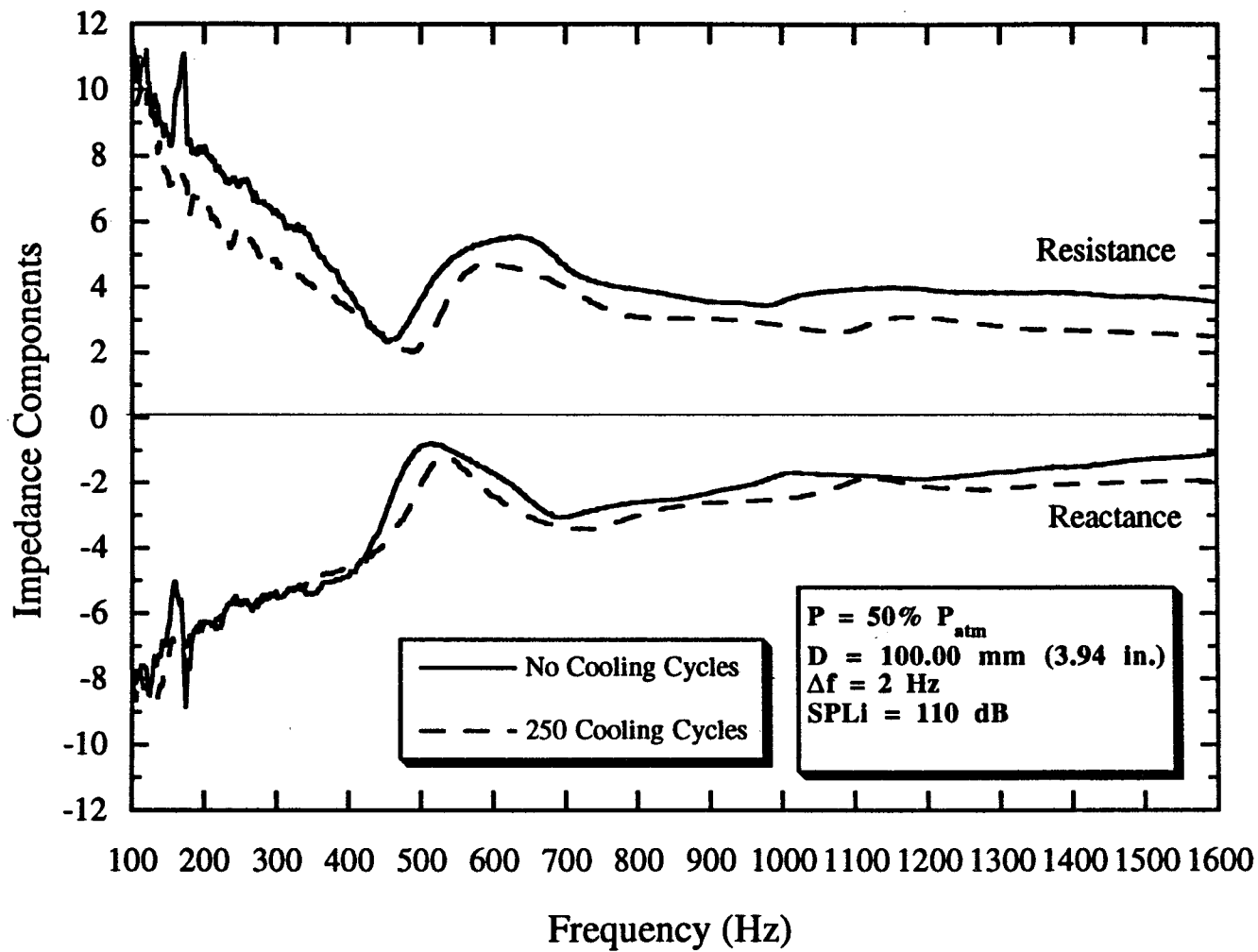


Figure B71. Characteristic Impedance of Kevlar, $P = 50\% P_{atm}$, $D = 100.0 \text{ mm}$.

B.72

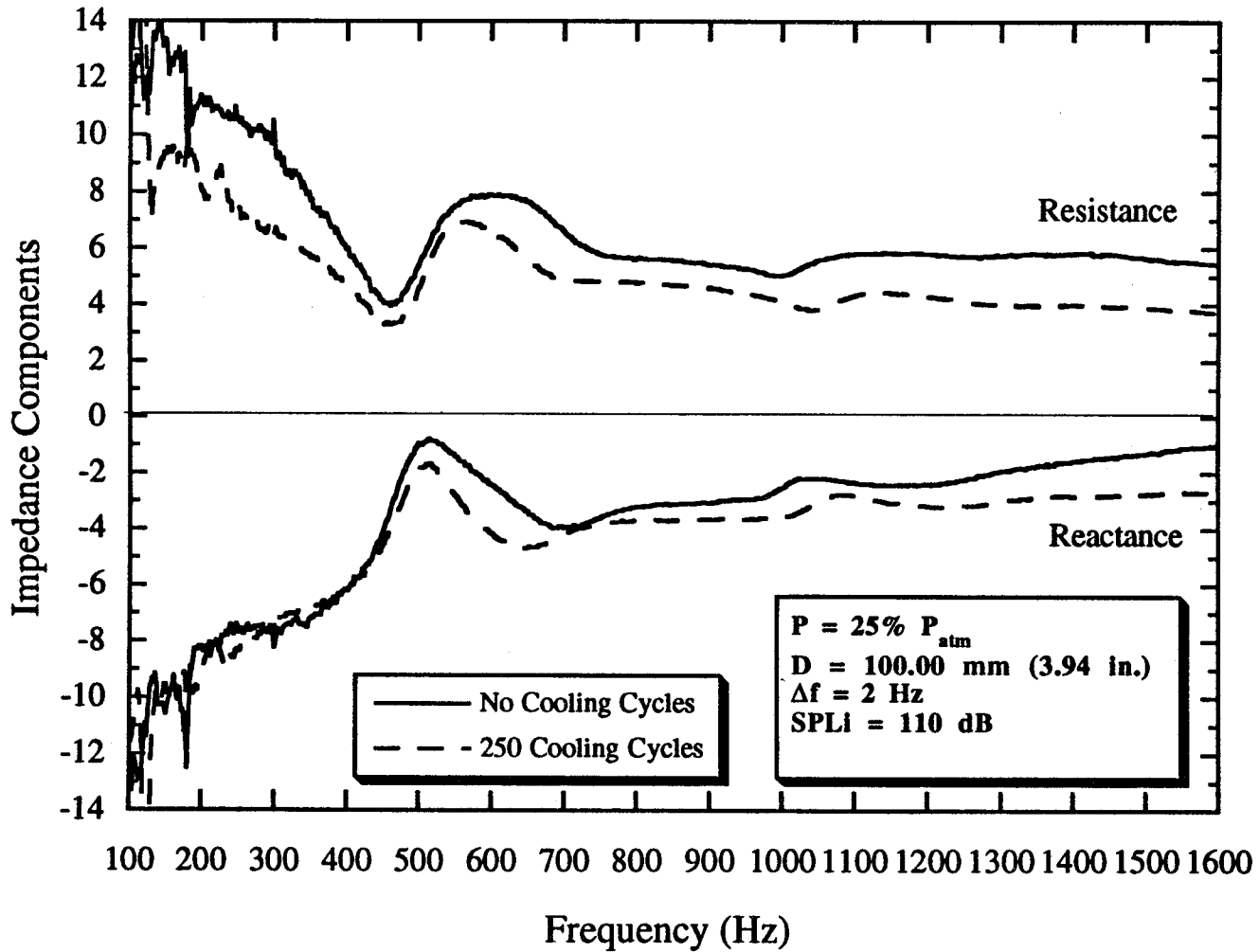


Figure B72. Characteristic Impedance of Kevlar, $P = 25\% P_{atm}$, $D = 100.0 \text{ mm}$.

B.73

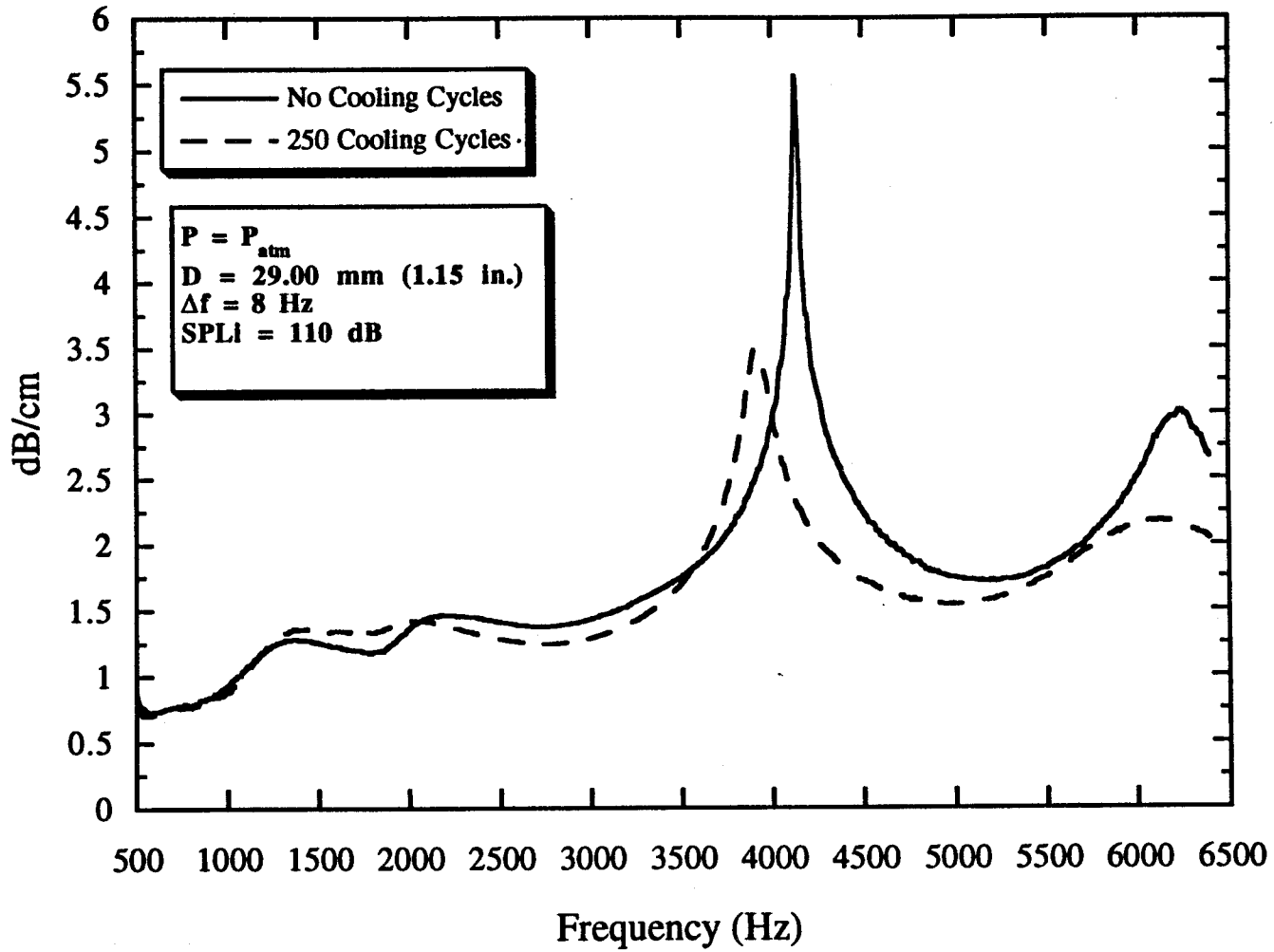


Figure B73. Attenuation rate of Pyrell foam, $P = P_{atm}$, $D = 29.0 \text{ mm}$.

B.74

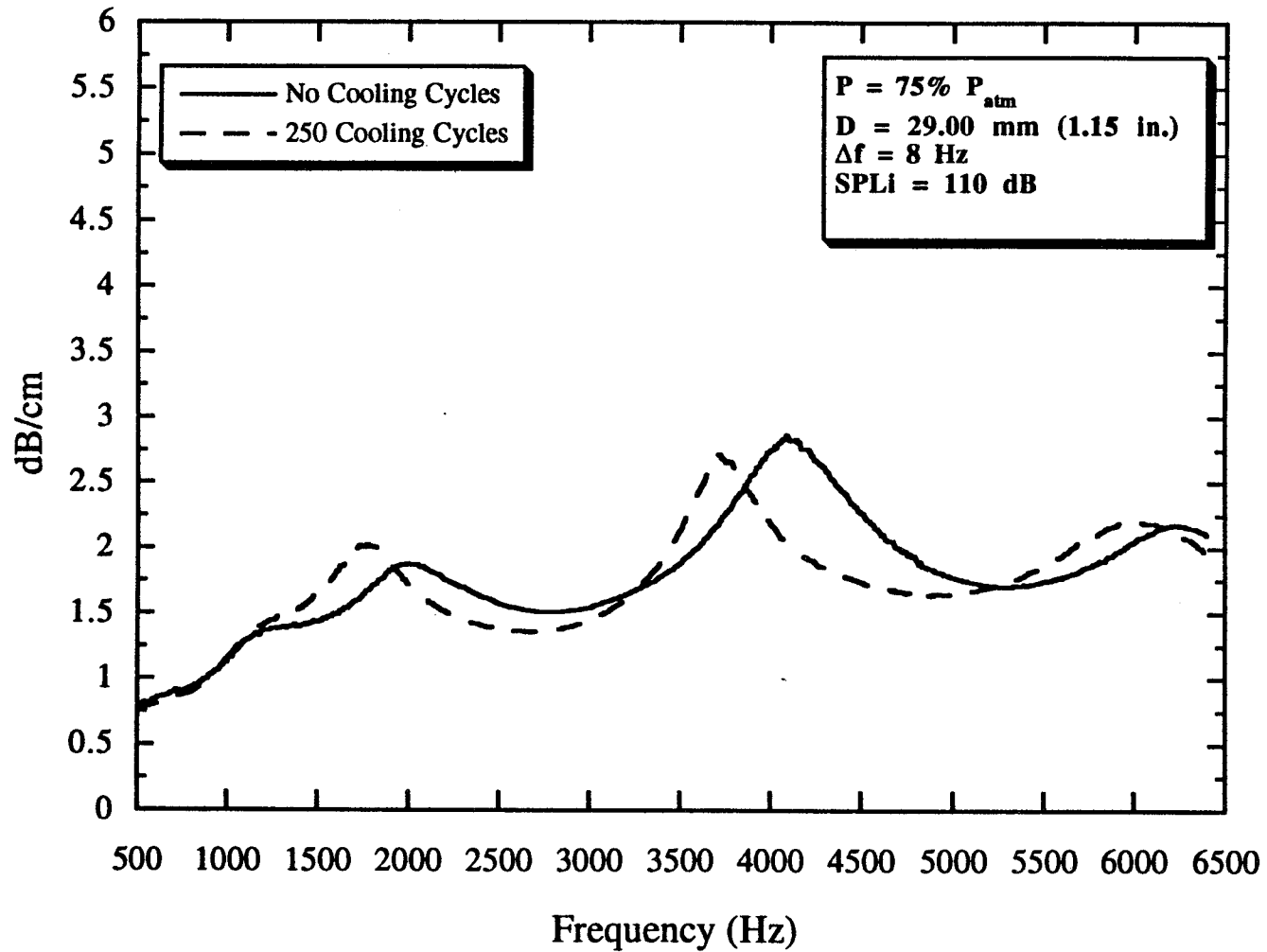


Figure B74. Attenuation rate of Pyrell foam, $P = 75\% P_{atm}$, $D = 29.0 \text{ mm}$.

B.75

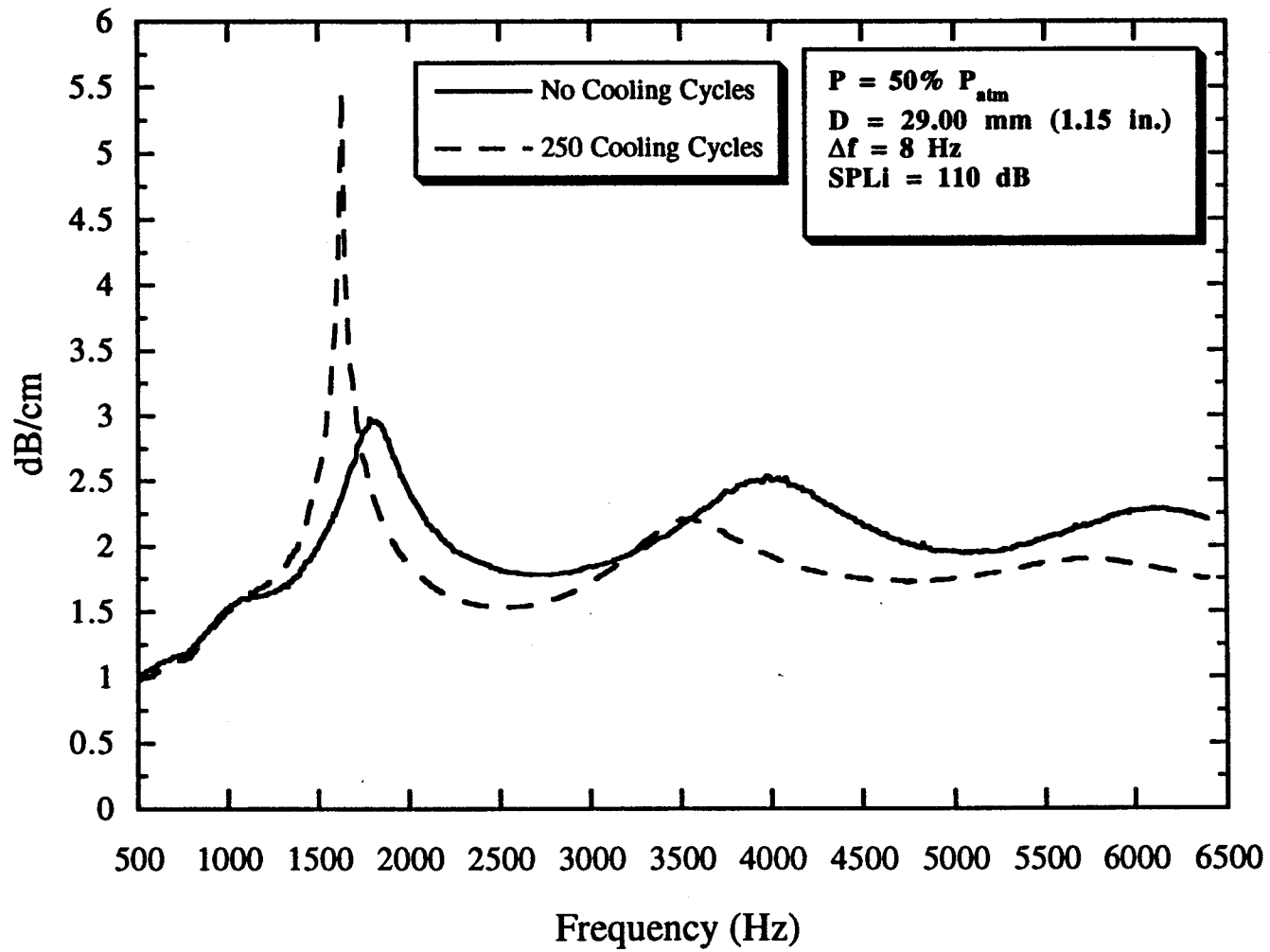


Figure B75. Attenuation rate of Pyrell foam, $P = 50\% P_{atm}$, $D = 29.0 \text{ mm}$.

B.76

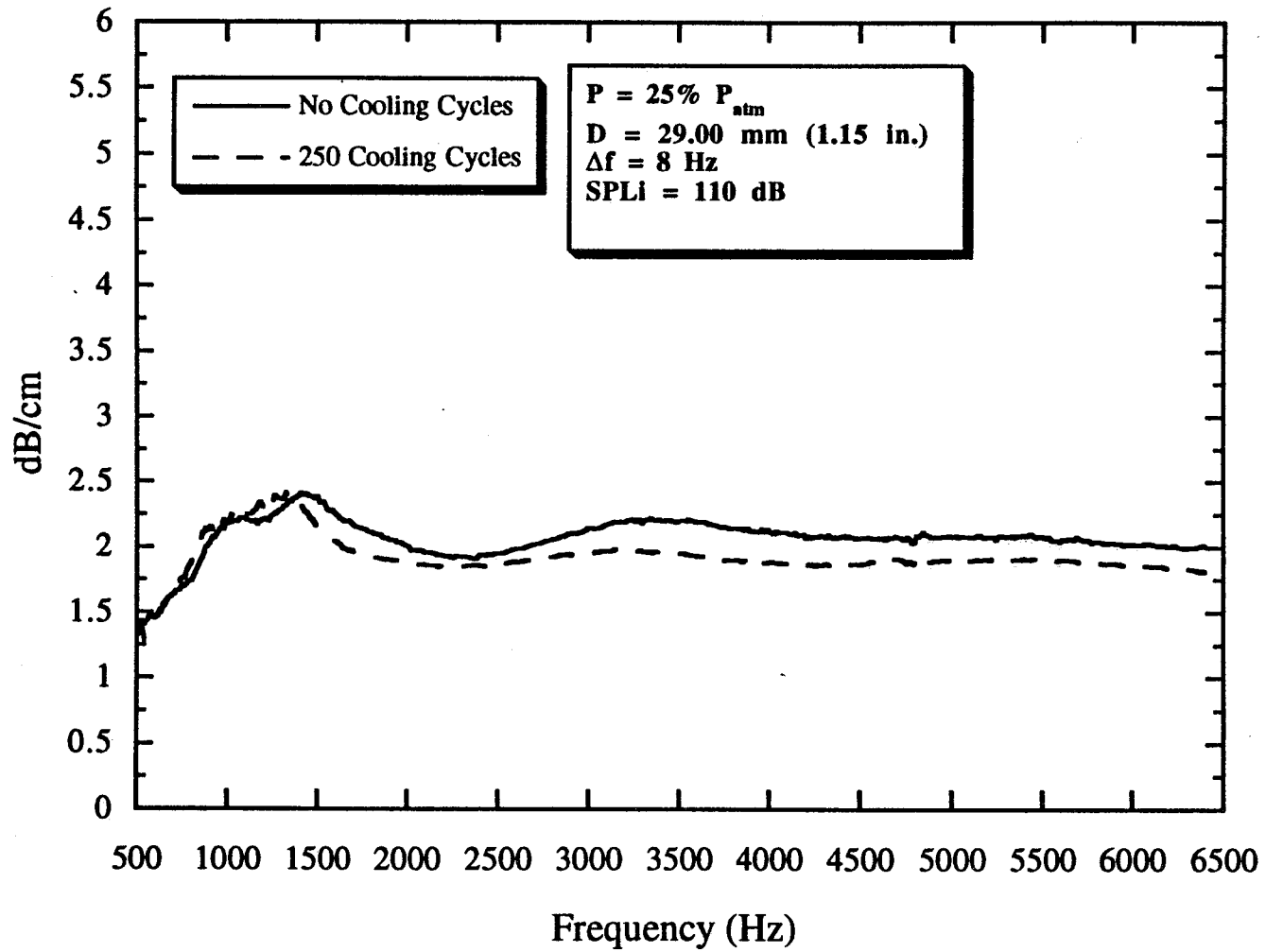


Figure B76. Attenuation rate of Pyrell foam, $P = 25\% P_{atm}$, $D = 29.0$ mm.

B.77

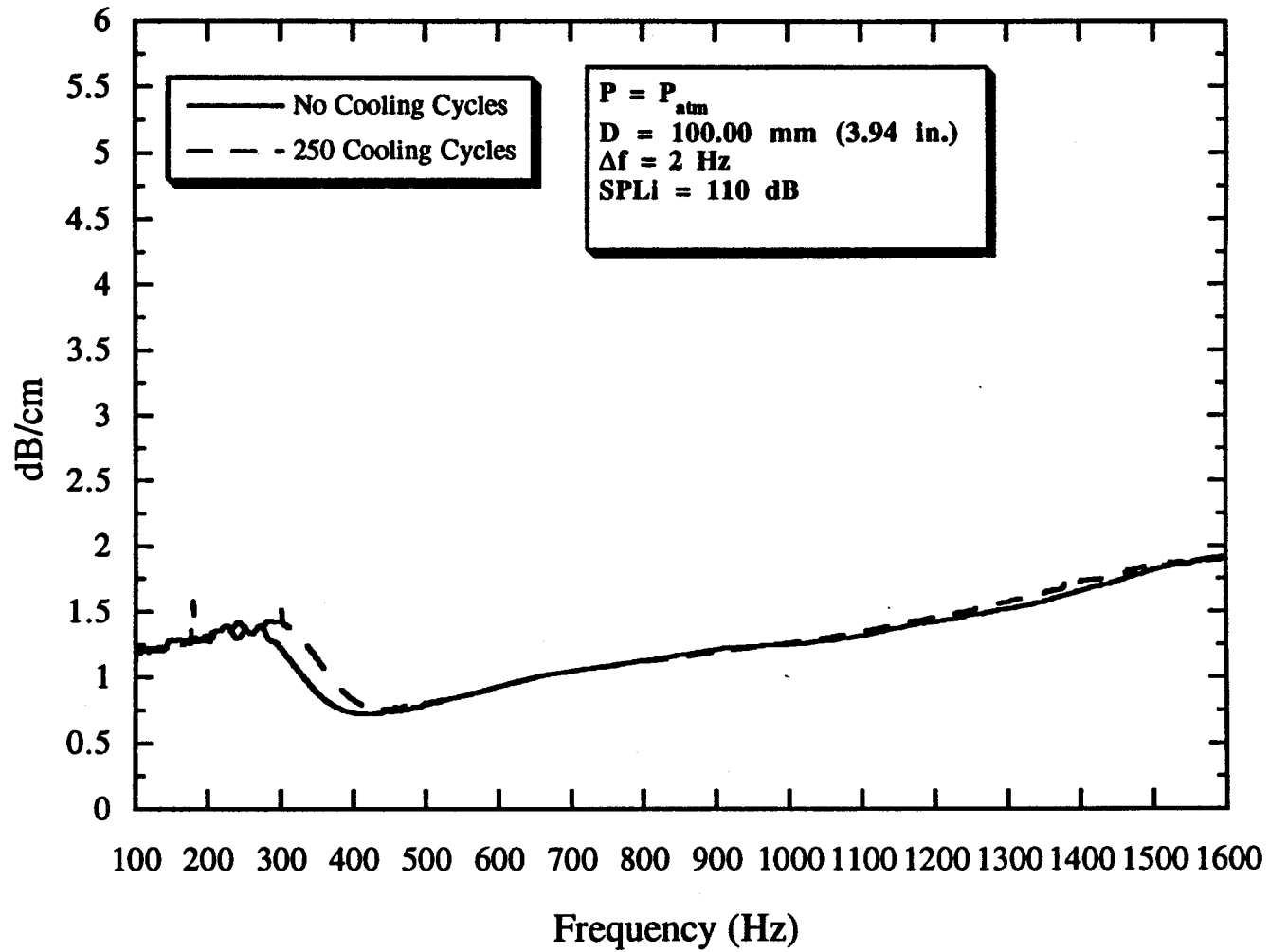


Figure B77. Attenuation rate of Pyrell foam, $P = P_{atm}$, $D = 100.0$ mm.

B.78

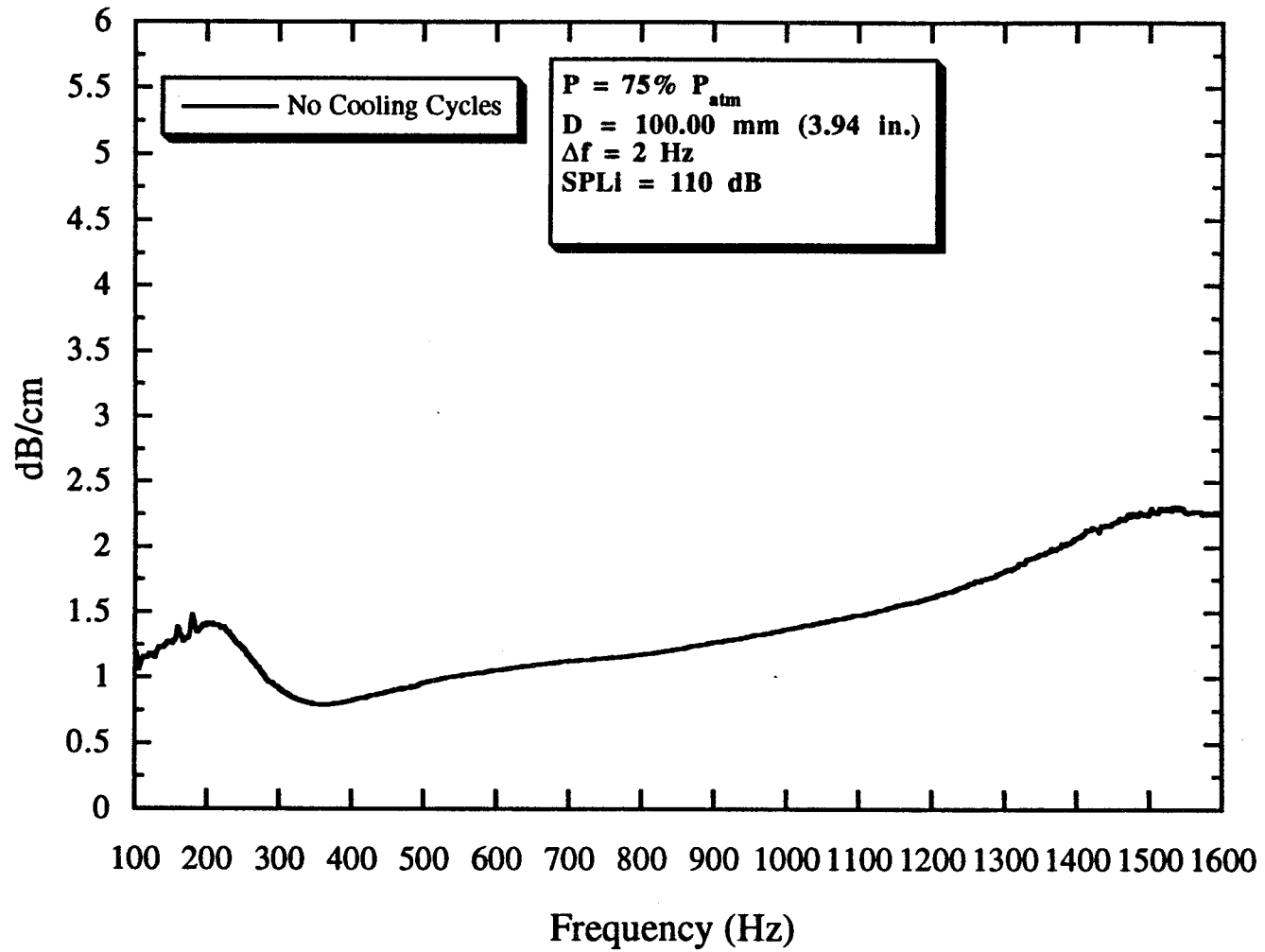


Figure B78. Attenuation rate of Pyrell foam, $P = 75\% P_{atm}$, $D = 100.0$ mm.

B.79

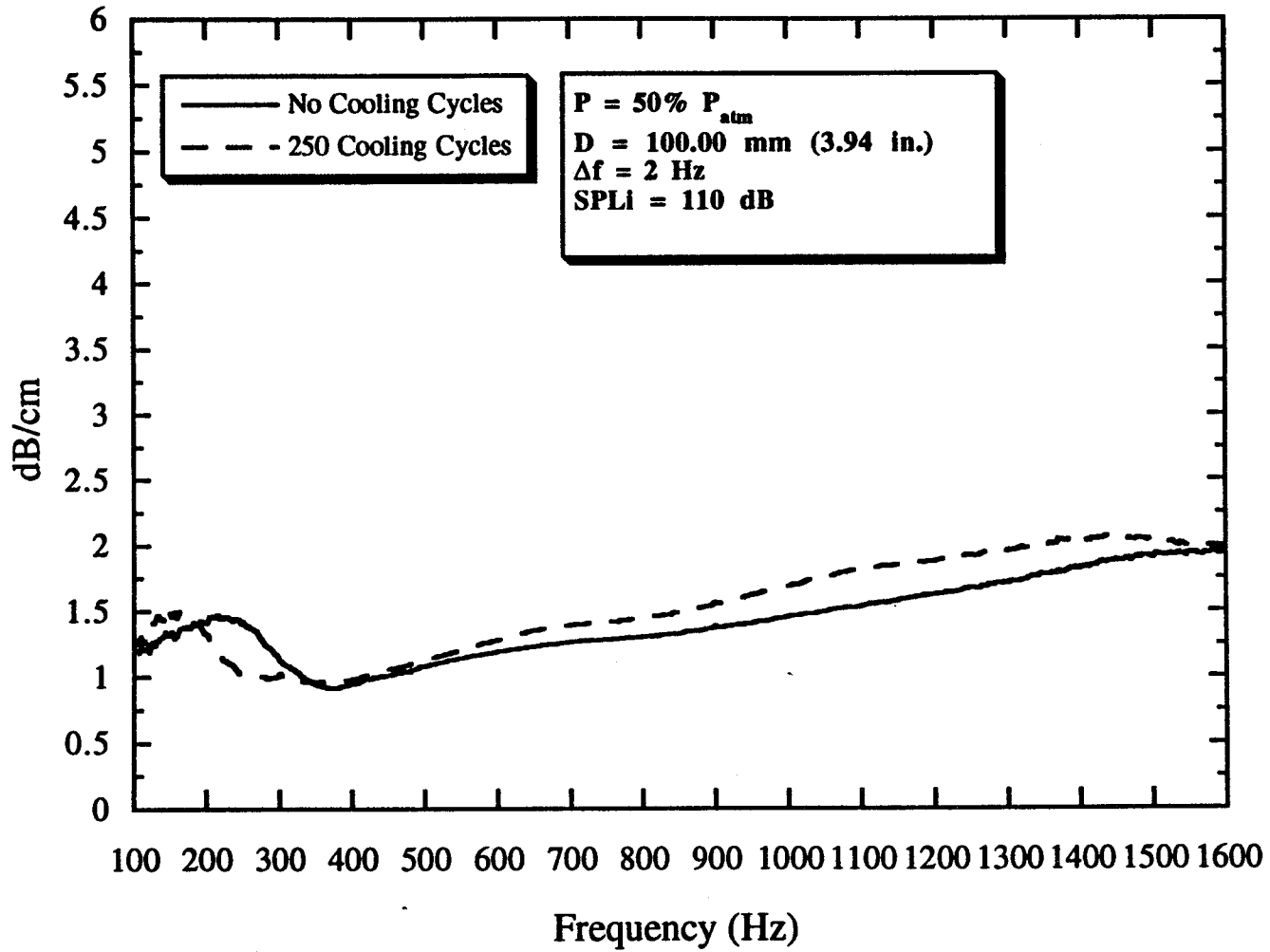


Figure B79. Attenuation rate of Pyrell foam, $P = 50\% P_{atm}$, $D = 100.0 \text{ mm}$.

B.80

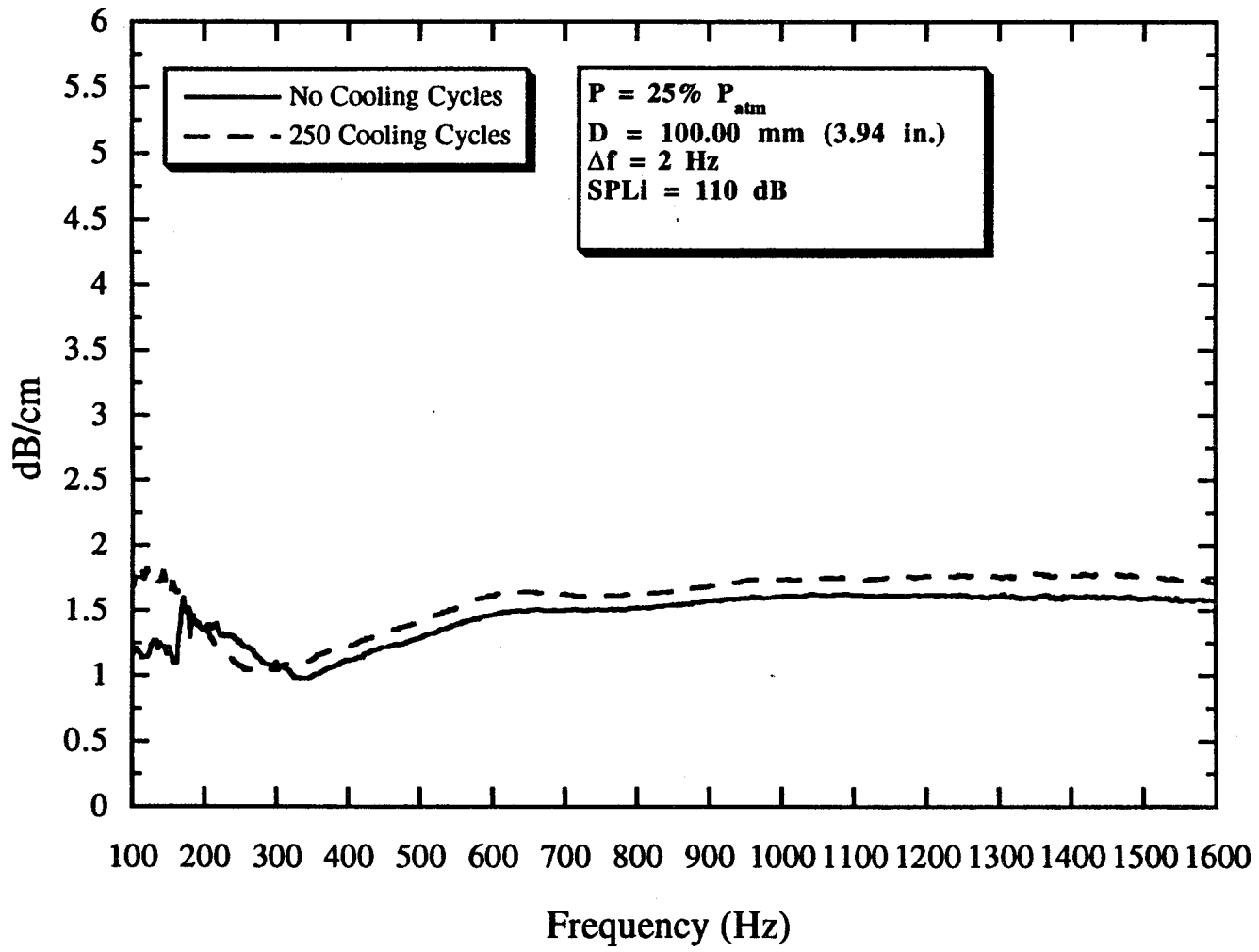


Figure B80. Attenuation rate of Pyrell foam, $P = 25\% P_{atm}$, $D = 100.0 \text{ mm}$.

B.81

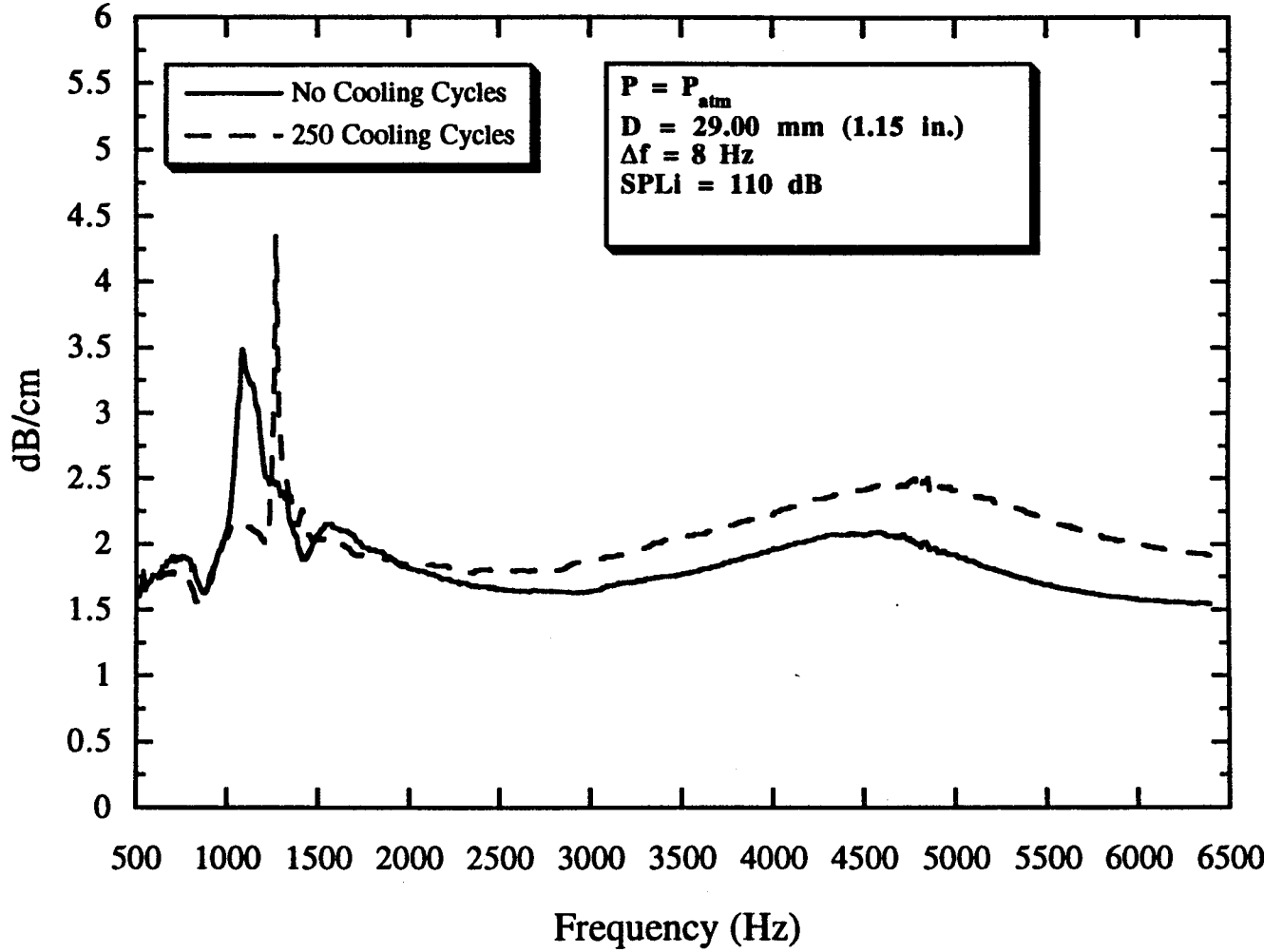


Figure B81. Attenuation rate of Fiberglass, $P = P_{atm}$, $D = 29.0$ mm.

B.82

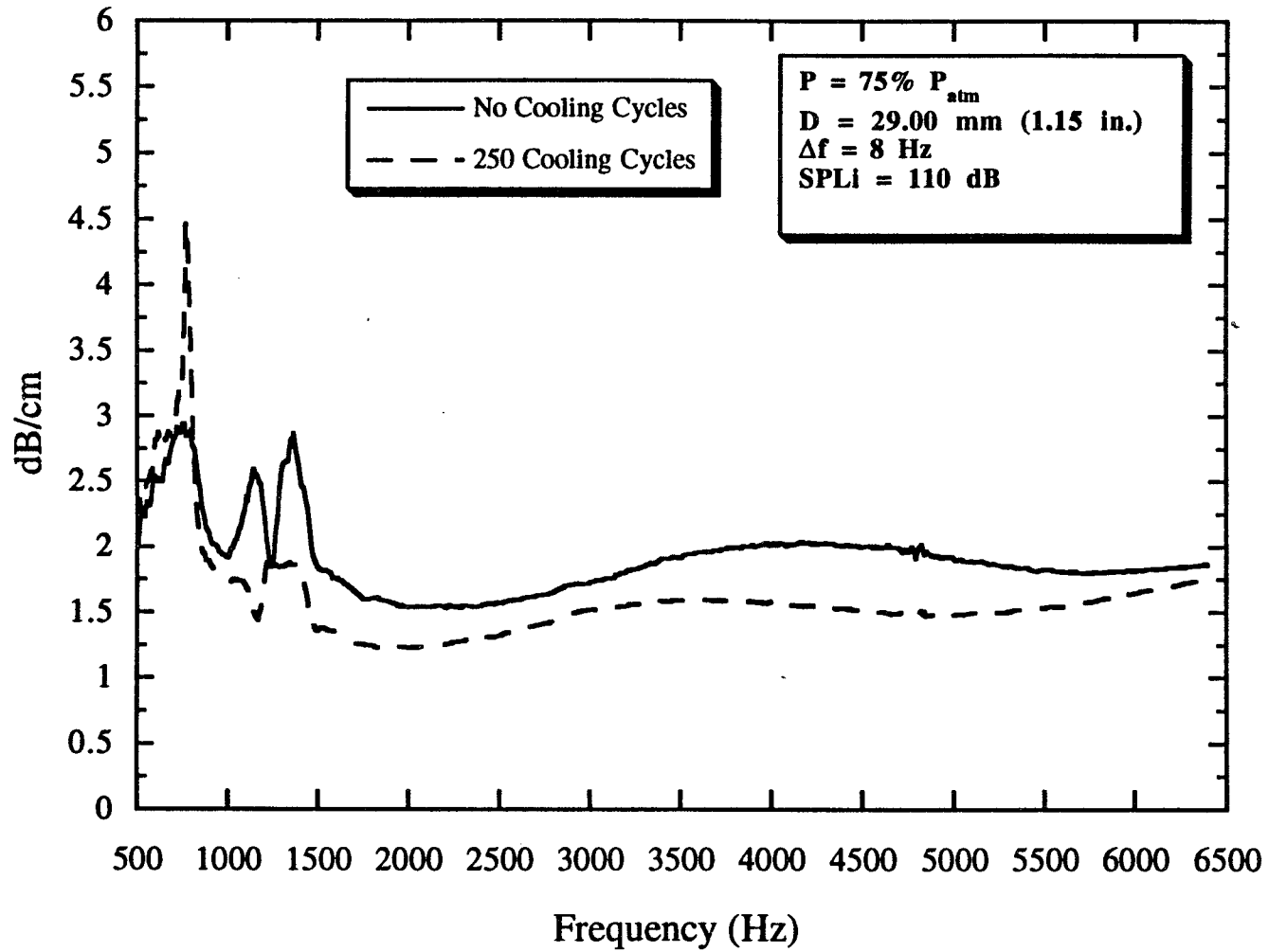


Figure B82. Attenuation rate of Fiberglass, $P = 75\% P_{atm}$, $D = 29.0 \text{ mm}$.

B.83

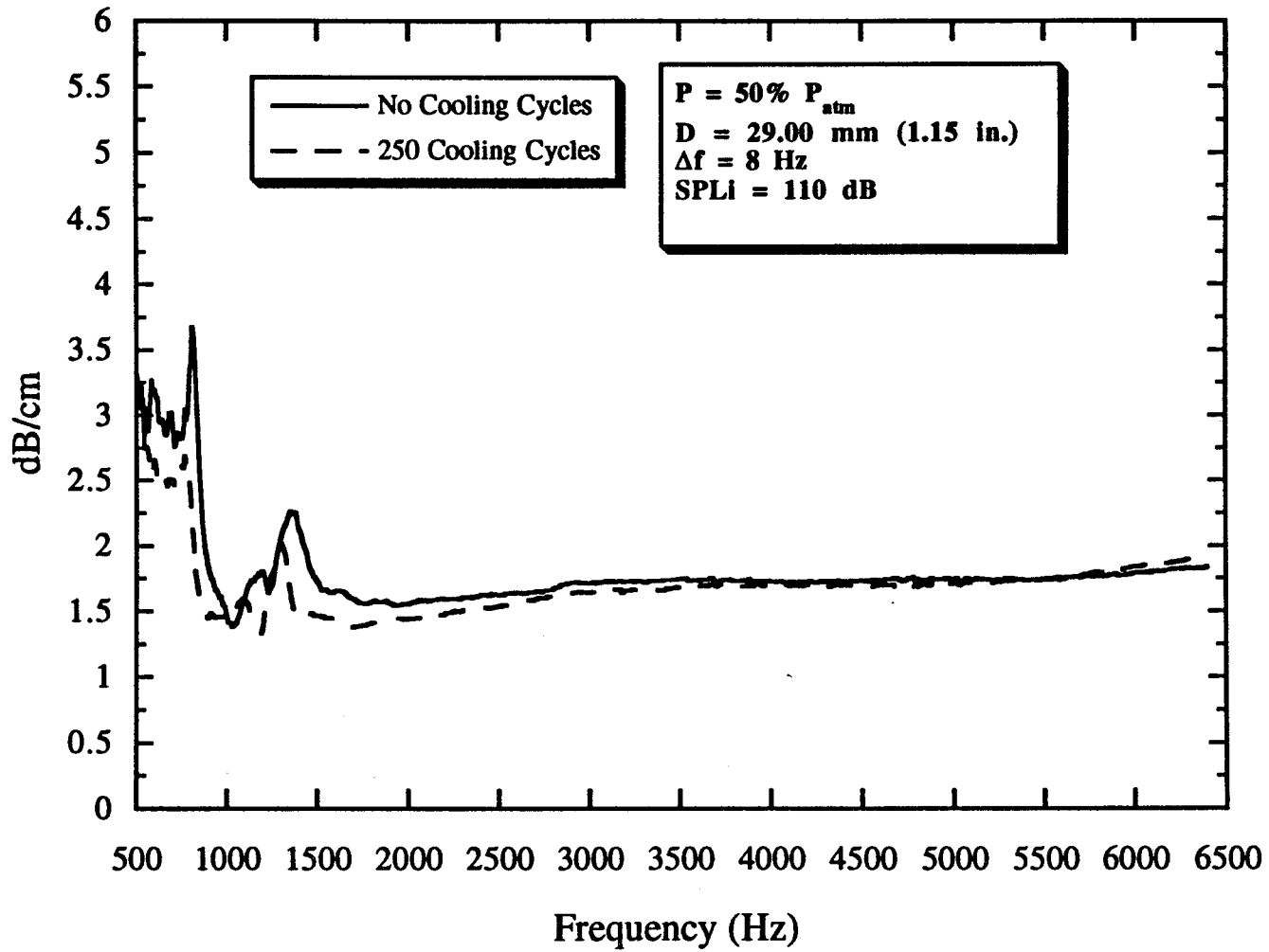


Figure B83. Attenuation rate of Fiberglass, $P = 50\% P_{atm}$, $D = 29.0$ mm.

B.84

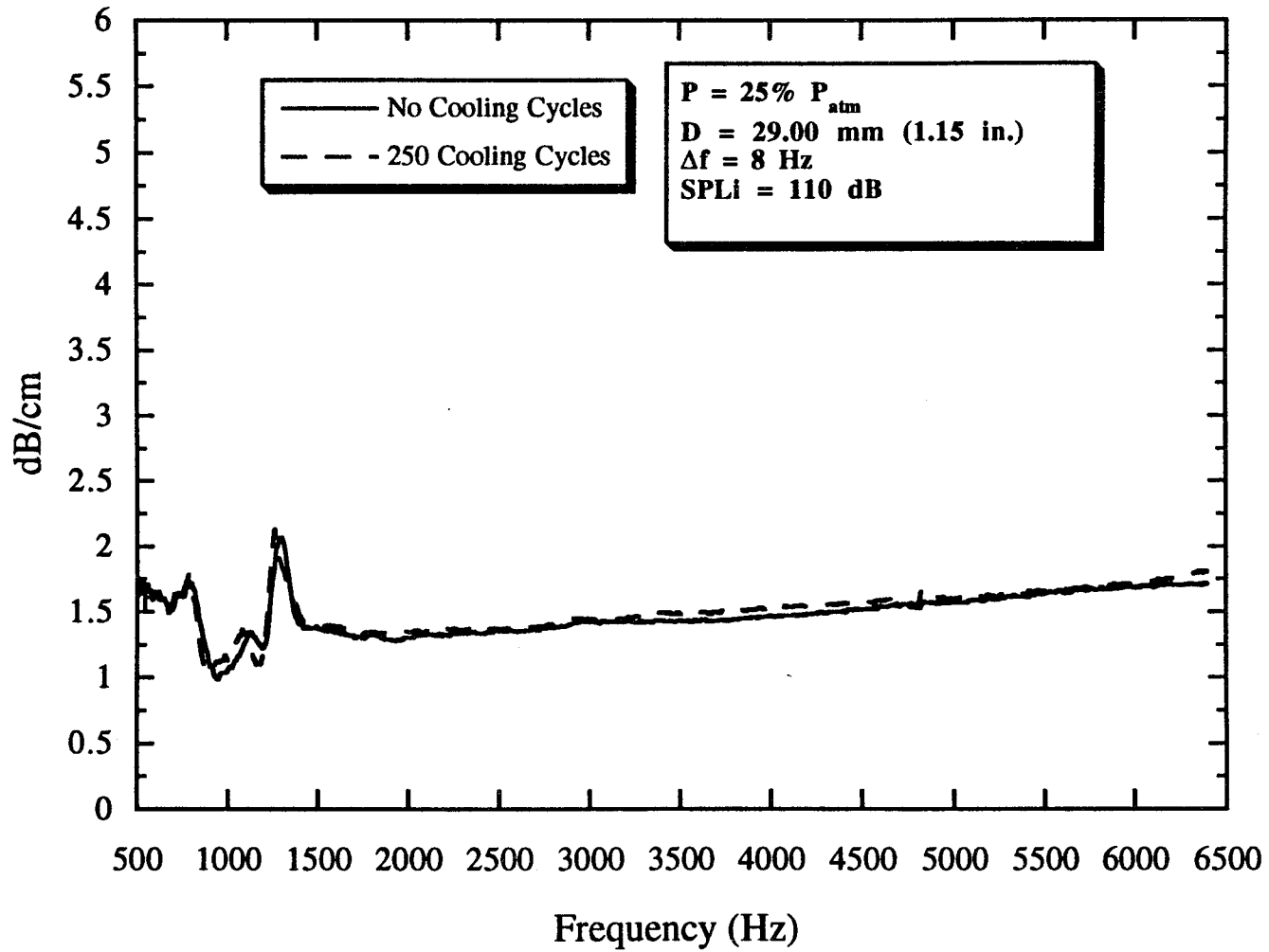


Figure B84. Attenuation rate of Fiberglass, $P = 25\% P_{atm}$, $D = 29.0 \text{ mm}$.

B.85

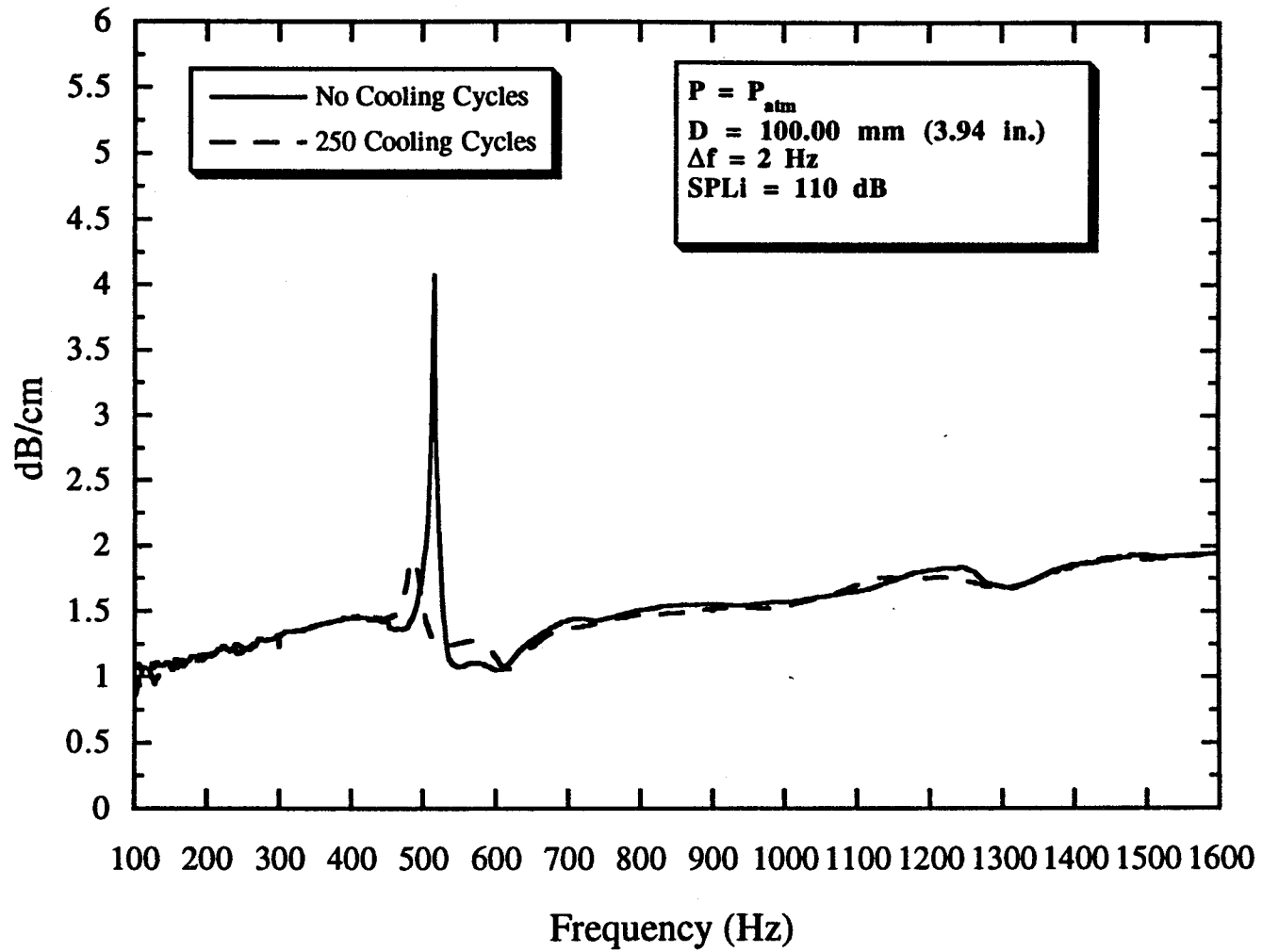


Figure B85. Attenuation Rate of Fiberglass, $P = P_{atm}$, $D = 100.0 \text{ mm}$.

B.86

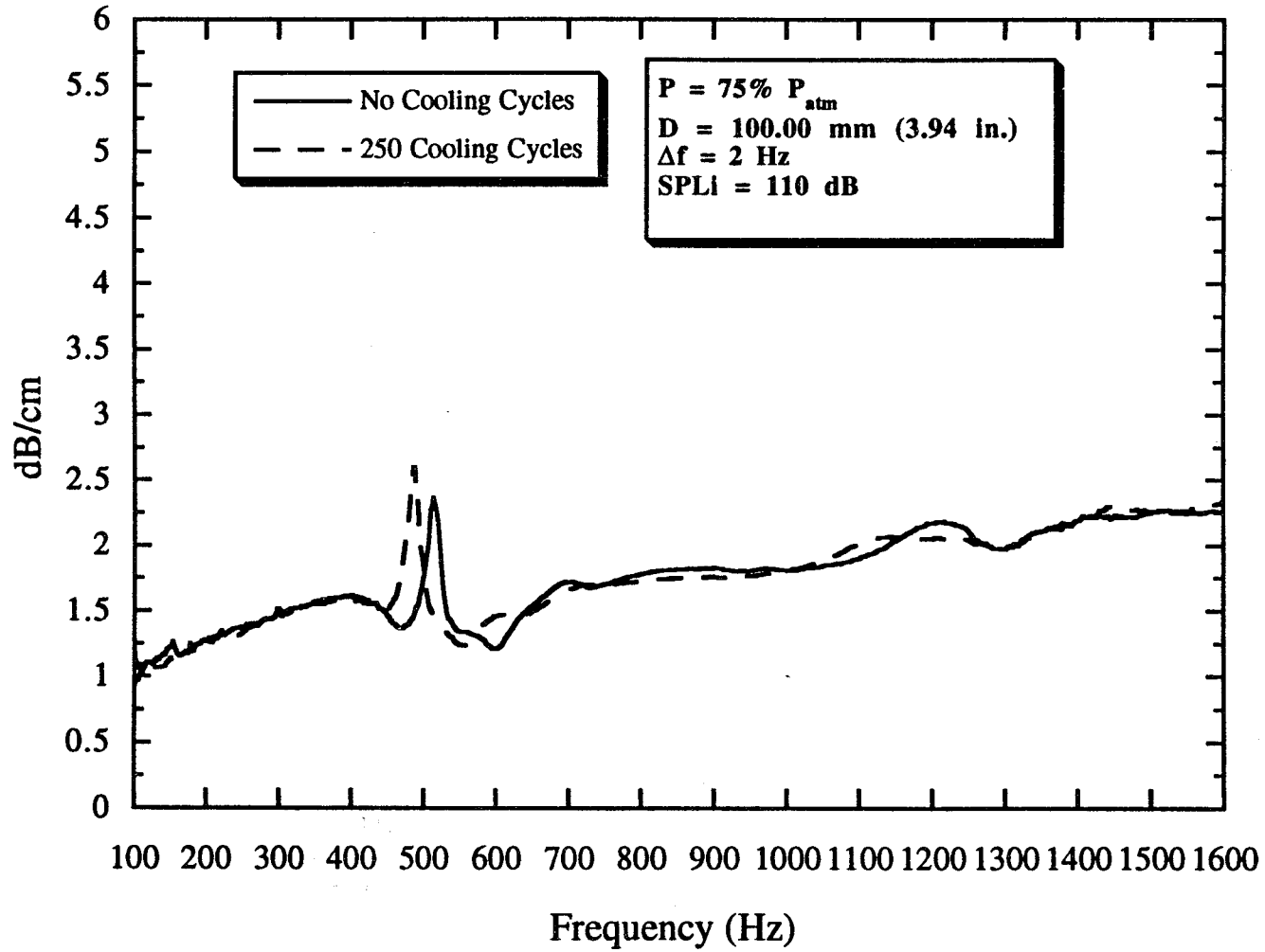


Figure B86. Attenuation Rate of Fiberglass, $P = 75\% P_{atm}$, $D = 100.0 \text{ mm}$.

B.87

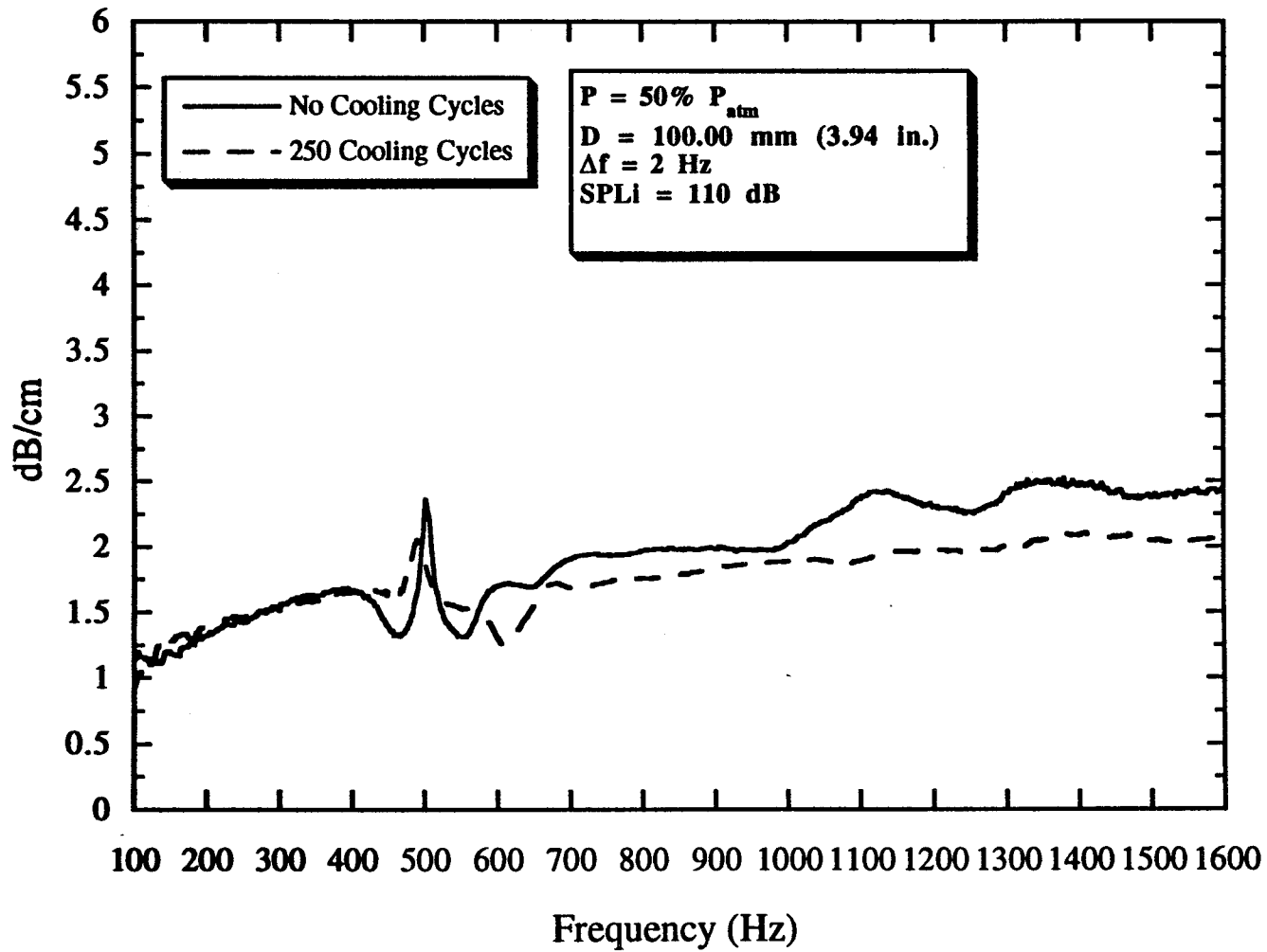


Figure B87. Attenuation Rate of Fiberglass, $P = 50\% P_{atm}$, $D = 100.0 \text{ mm}$.

B.88

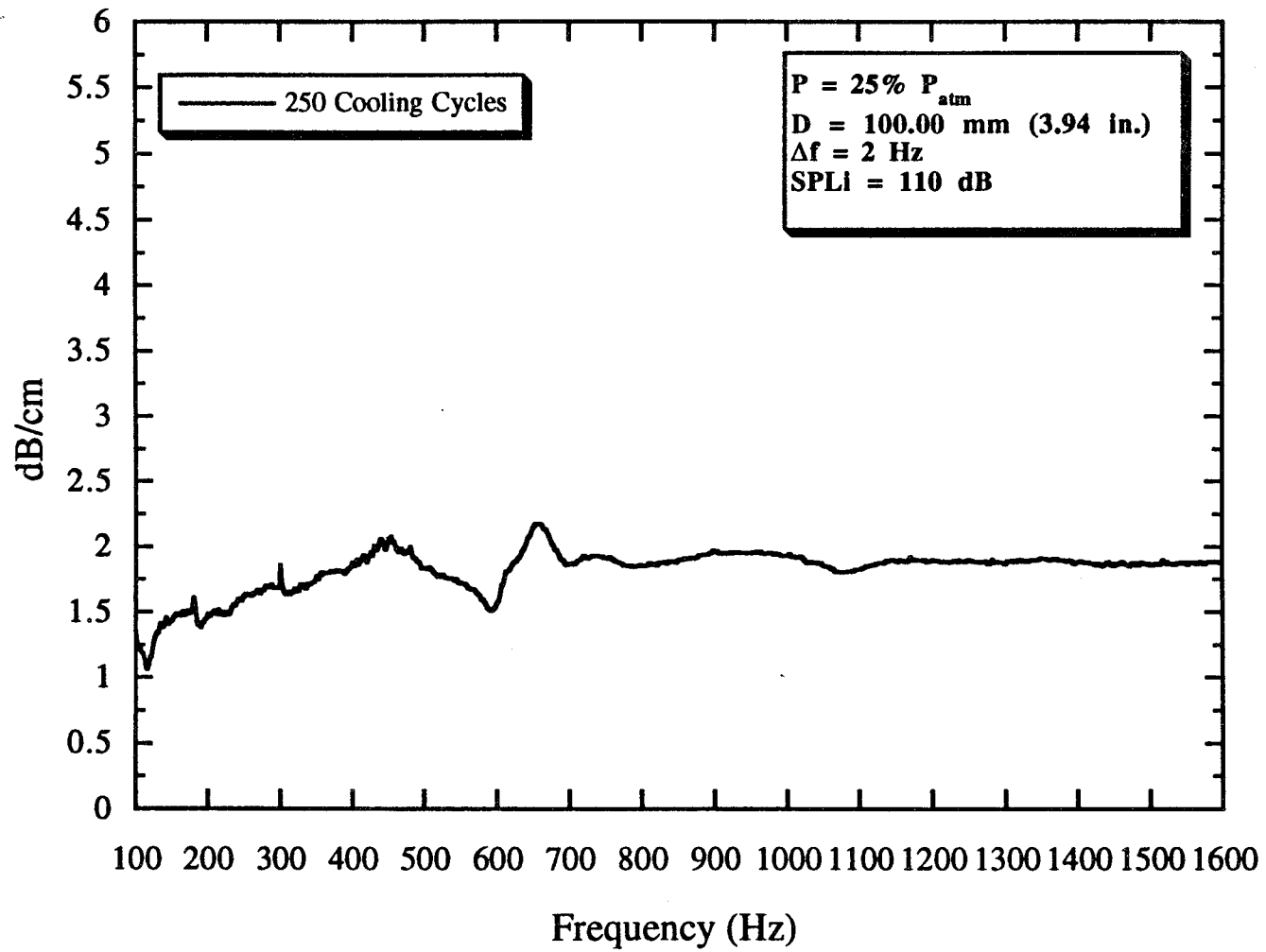


Figure B88. Attenuation Rate of Fiberglass, $P = 25\% P_{atm}$, $D = 100.0 \text{ mm}$.

B.89

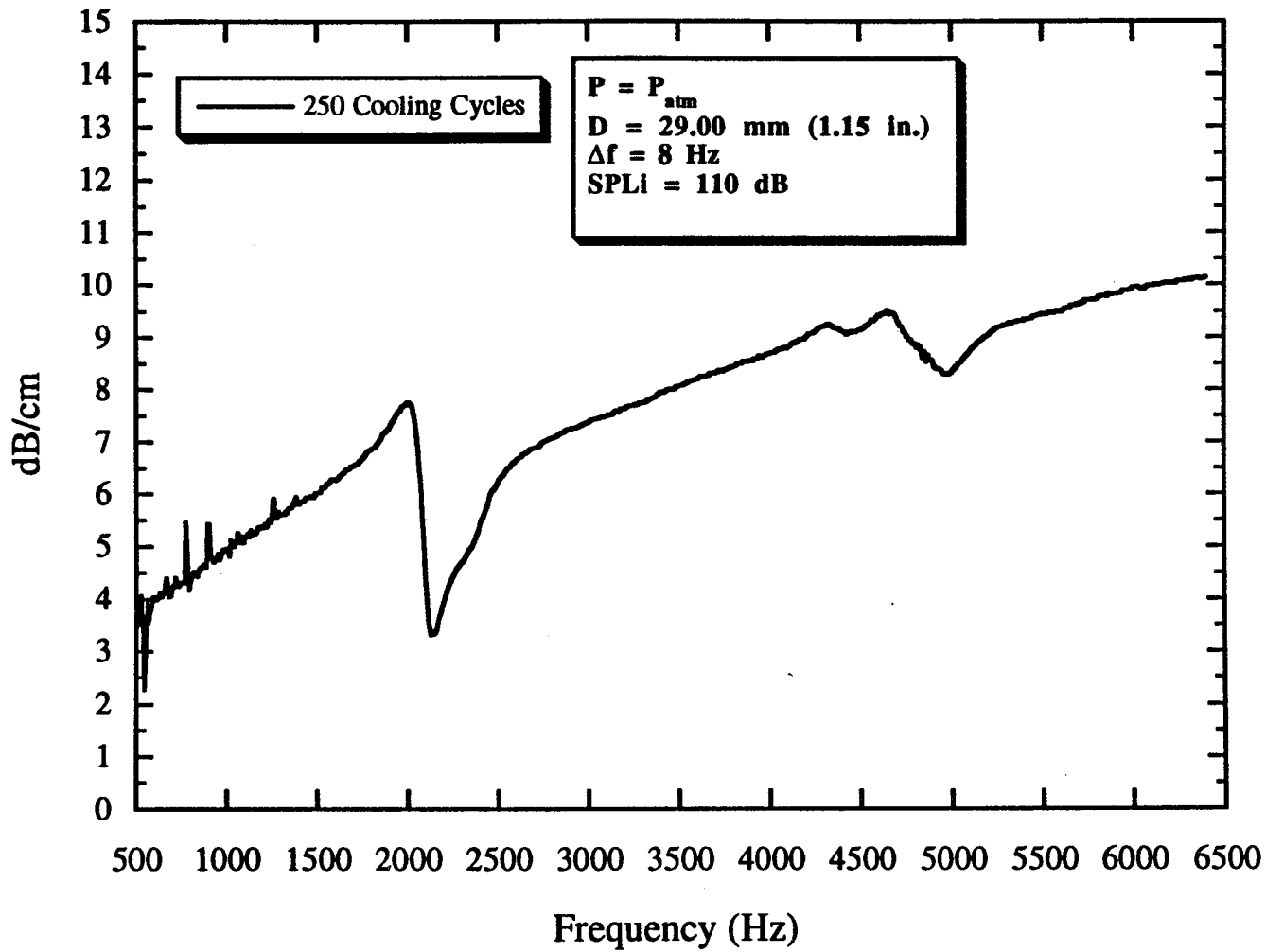


Figure B89. Attenuation rate of Kevlar, $P = P_{atm}$, $D = 29.0$ mm.

B.90

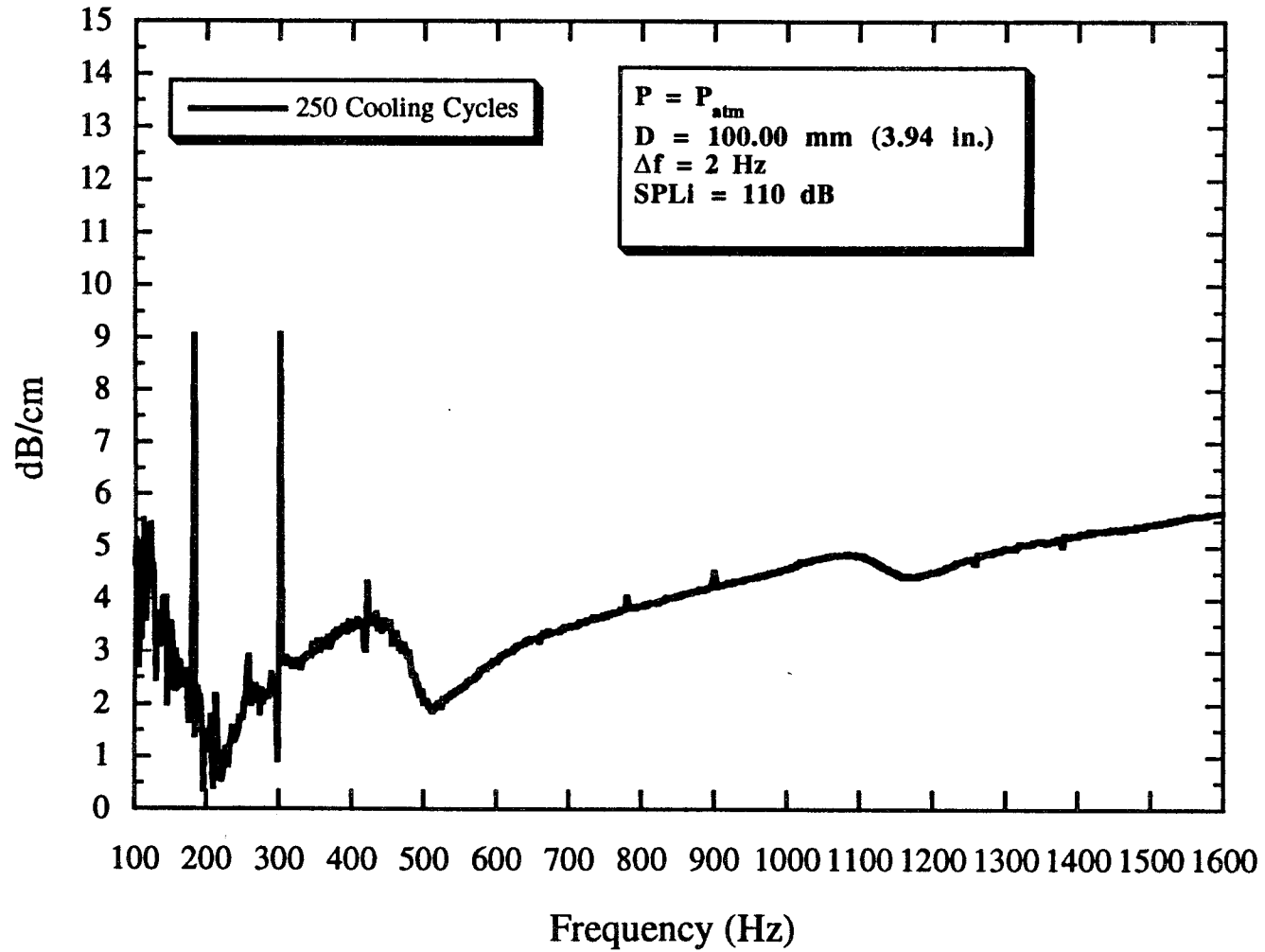


Figure B90. Attenuation rate of Kevlar, $P = P_{atm}$, $D = 100.0$ mm.

B.91

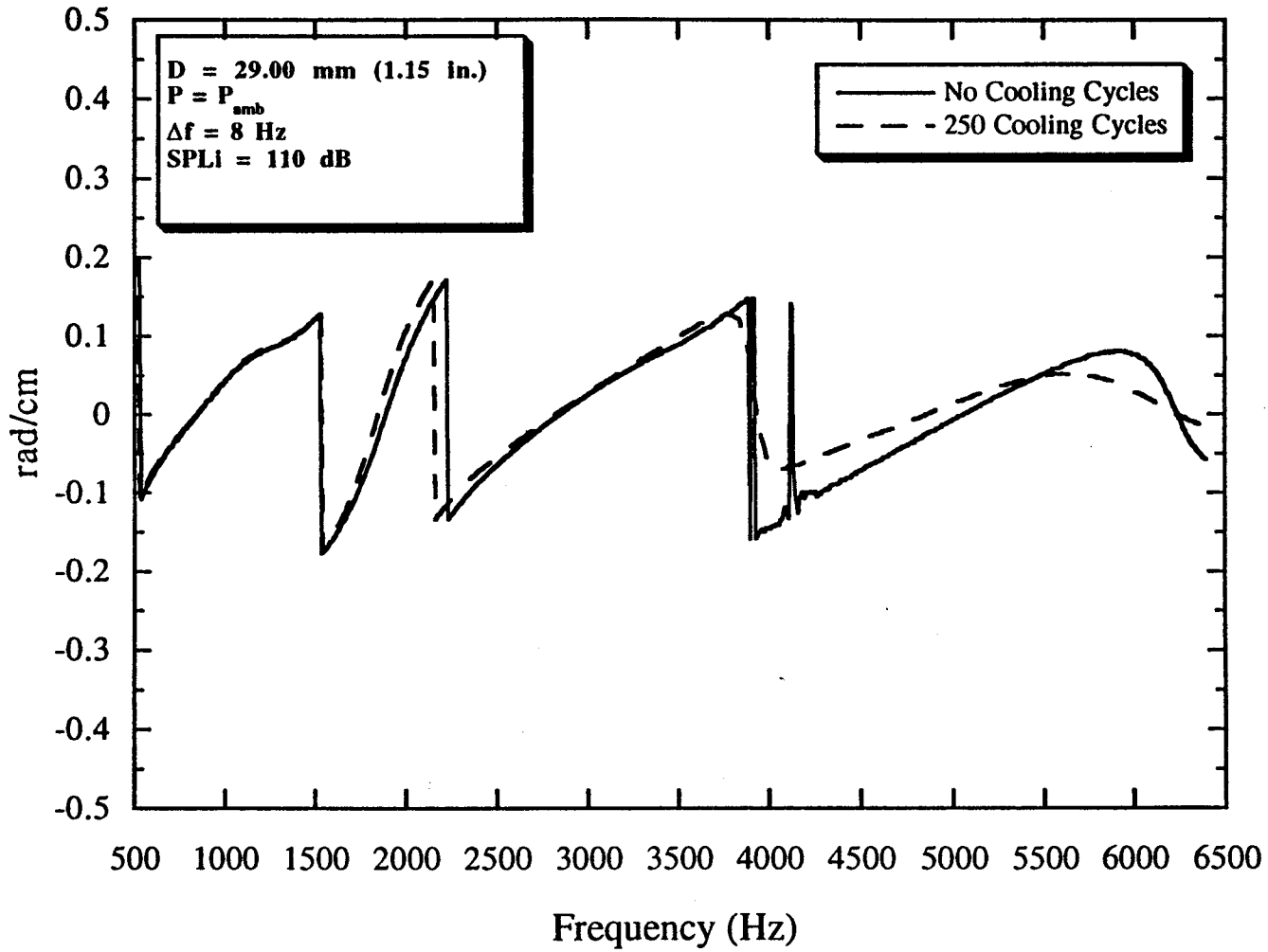


Figure B91. Phase Constant of Pyrell foam, $P = P_{amb}$, $D = 29.0$ mm.

B.92

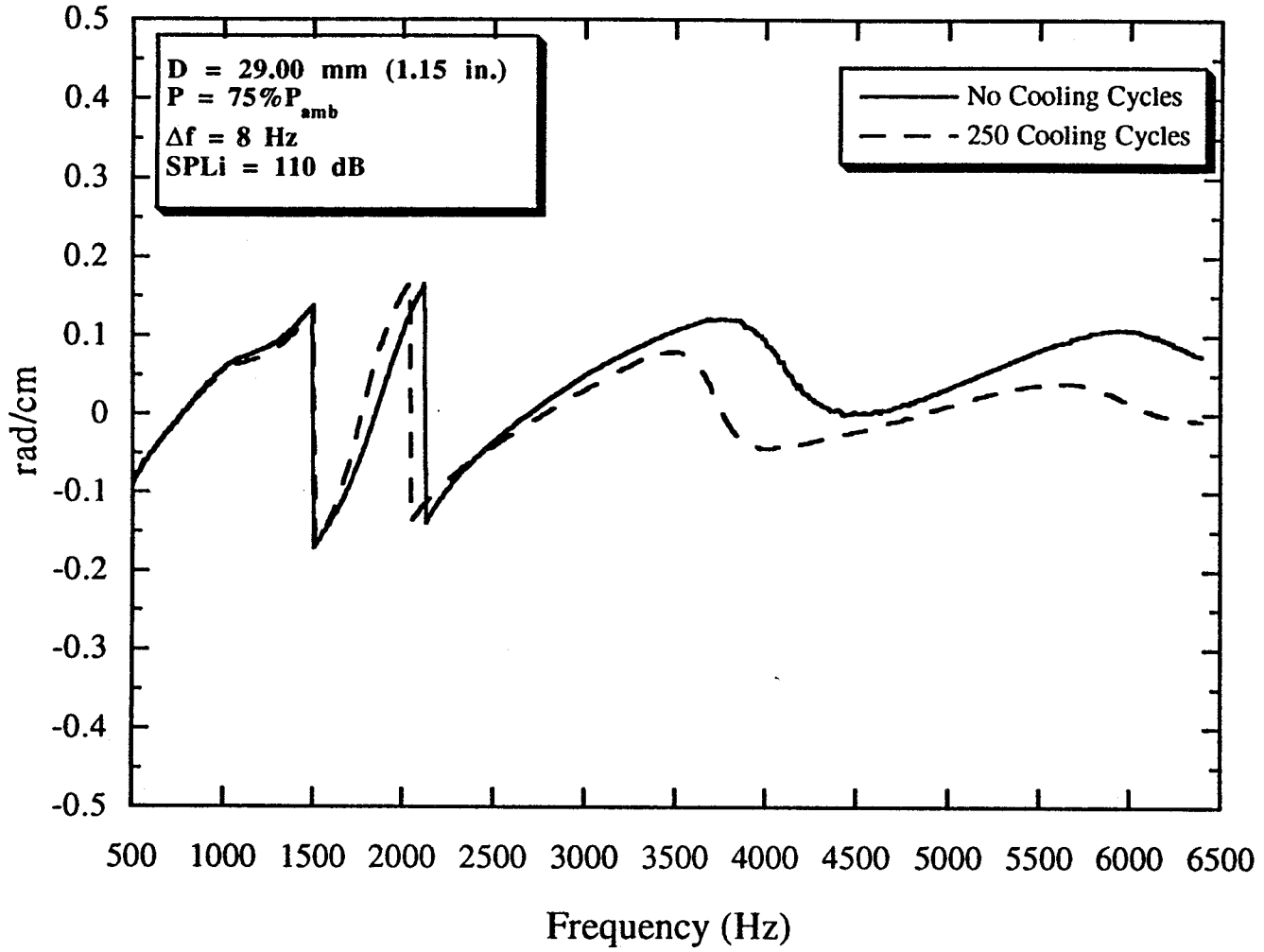


Figure B92. Phase Constant of Pyrell foam, $P = 75\%P_{amb}$, $D = 29.0$ mm.

B.93

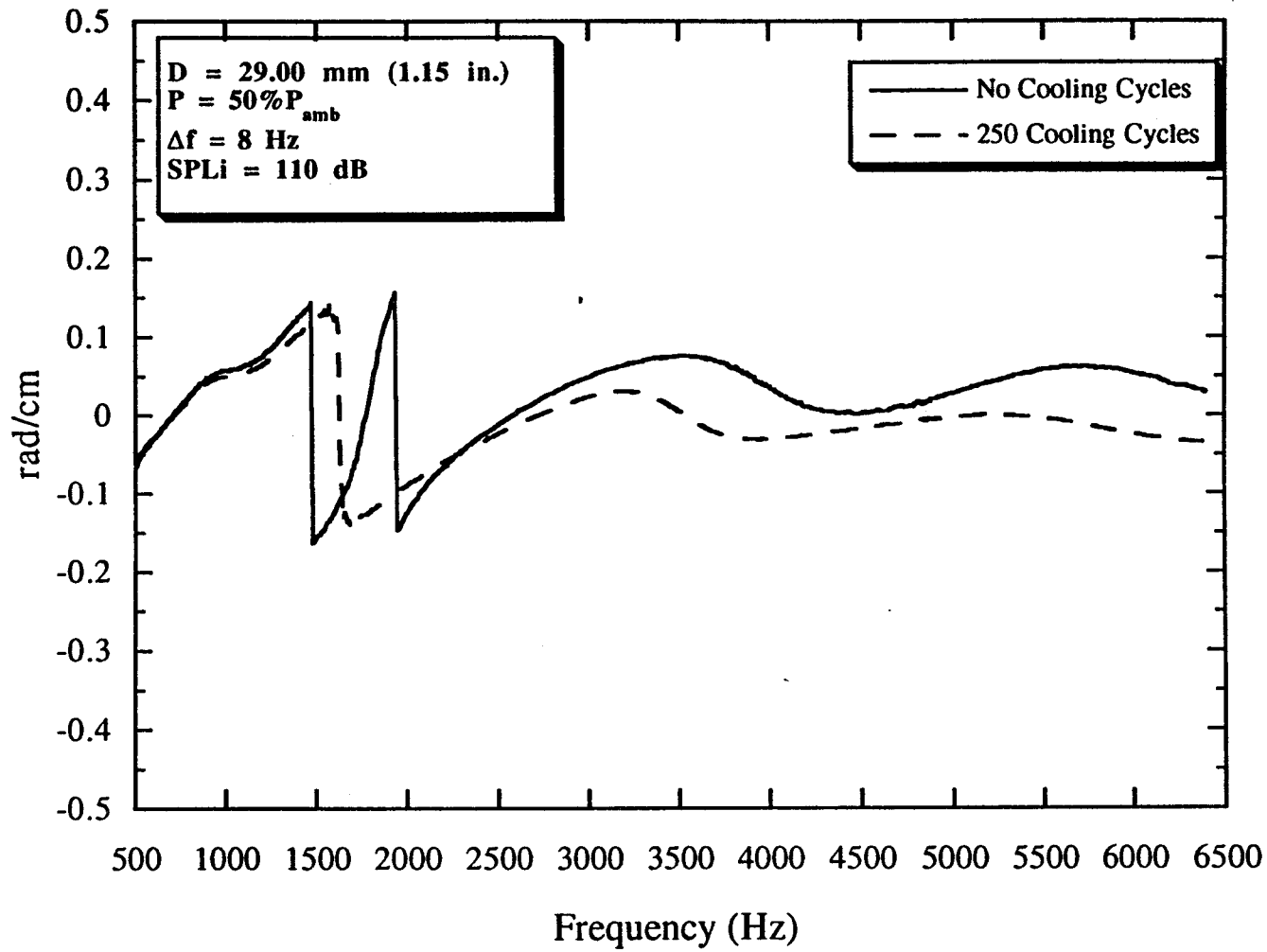


Figure B93. Phase Constant of Pyrell foam, $P = 50\%P_{amb}$, $D = 29.0$ mm.

B.94

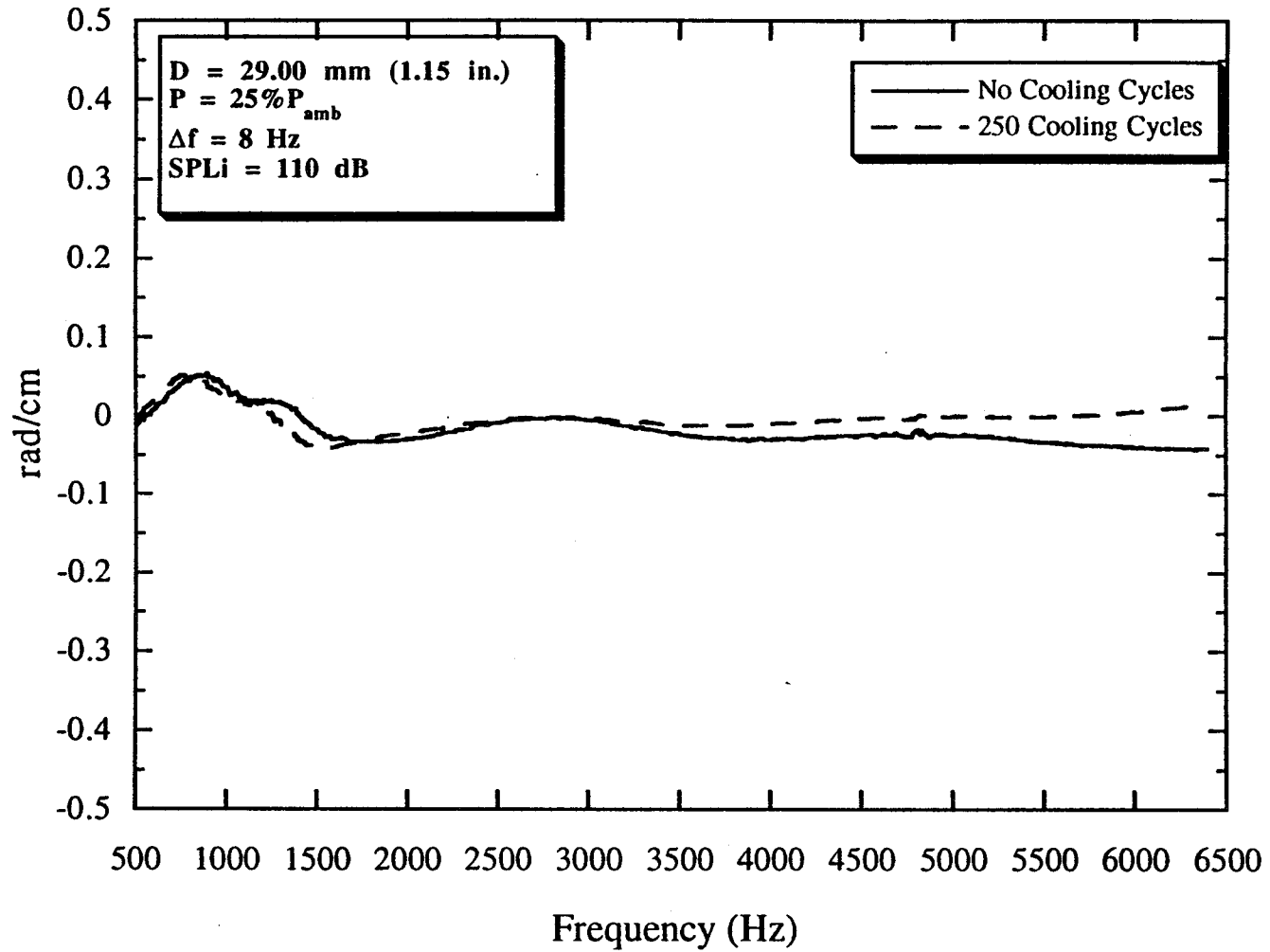


Figure B94. Phase Constant of Pyrell foam, $P = 25\%P_{amb}$, $D = 29.0$ mm.

B.95

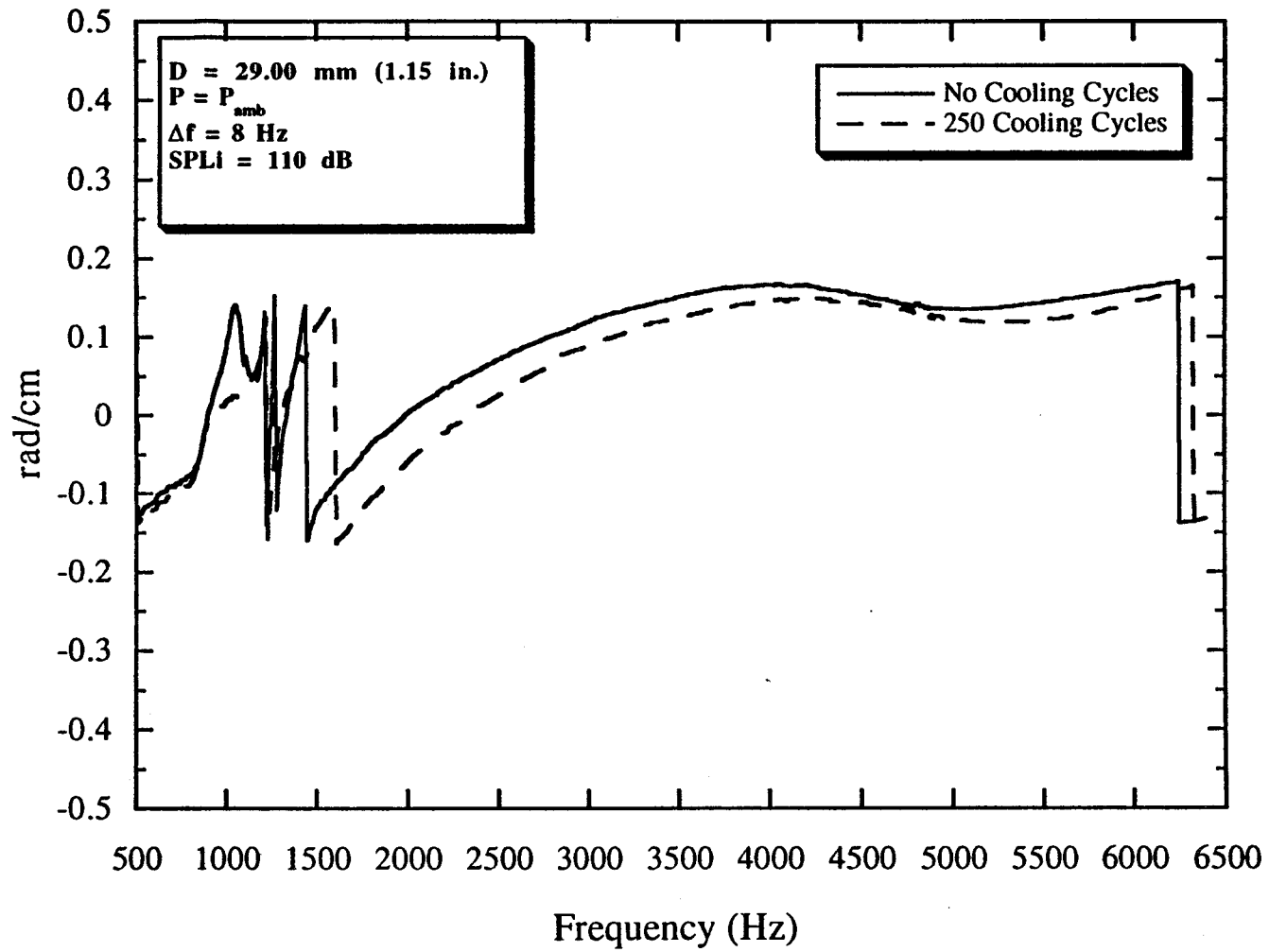


Figure B95. Phase Constant of Fiberglass, $P = P_{amb}$, $D = 29.0$ mm.

B.96

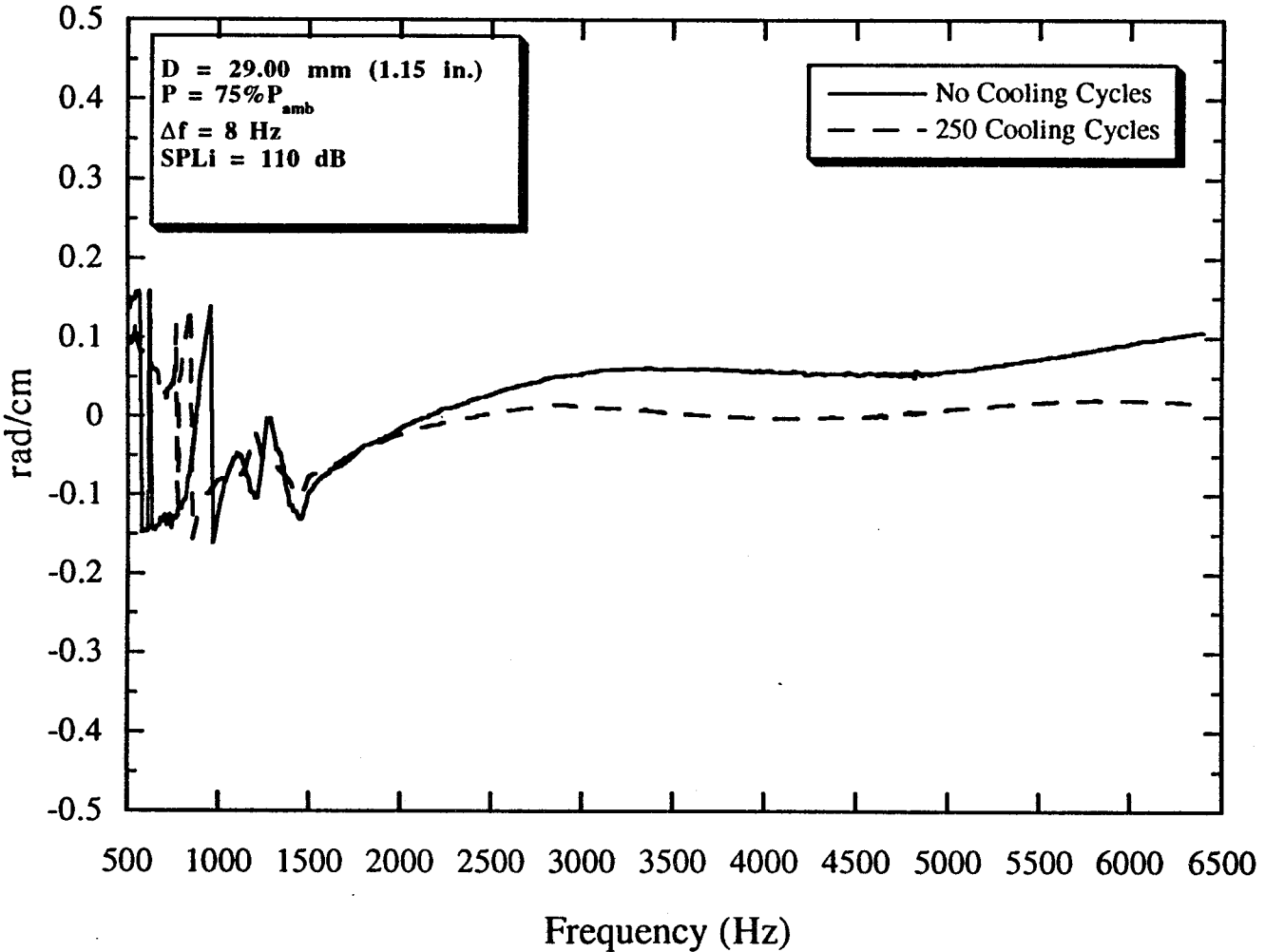


Figure B96. Phase Constant of Fiberglass, $P = 75\%P_{amb}$, $D = 29.0$ mm.

B.97

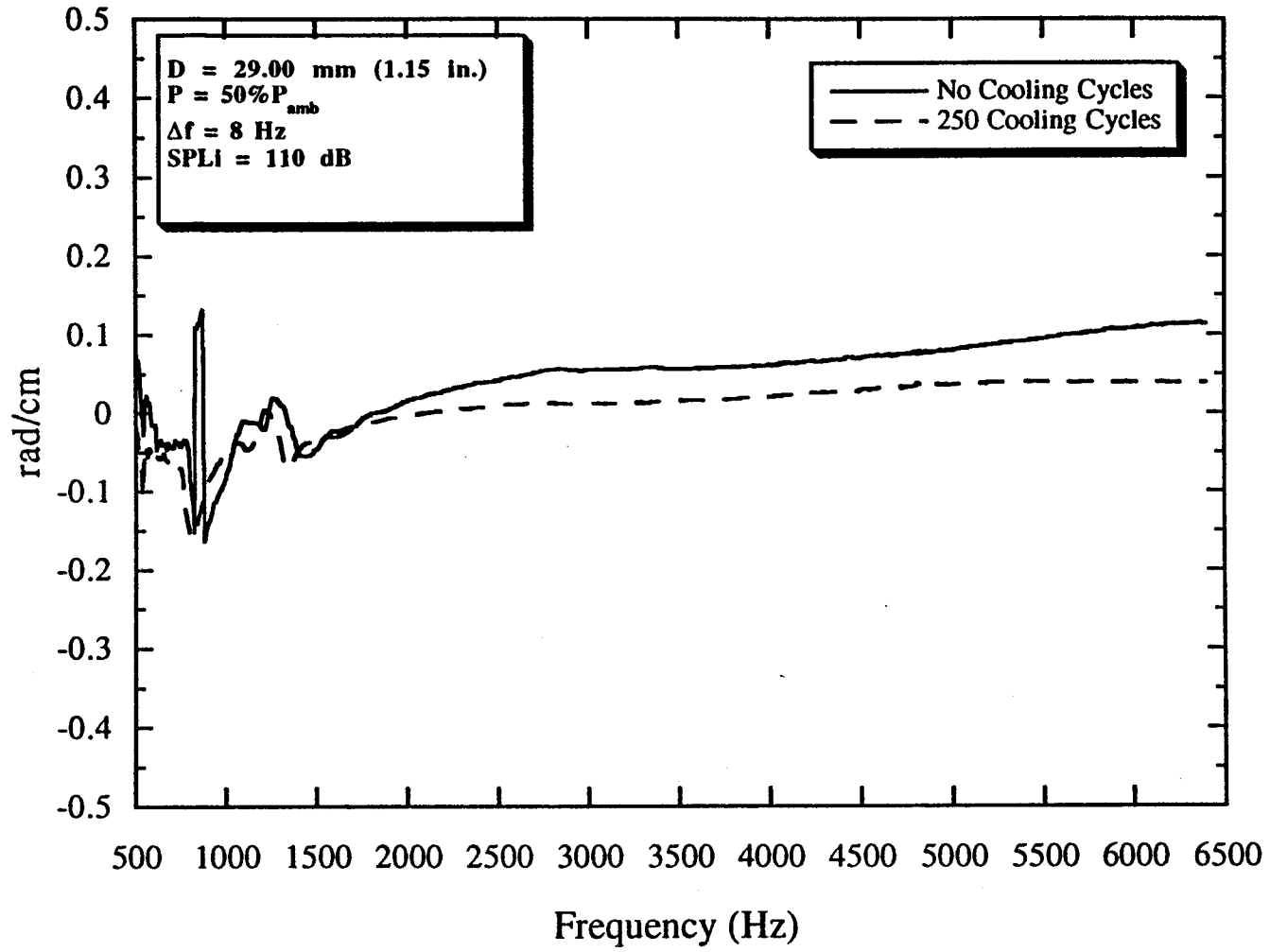


Figure B97. Phase Constant of Fiberglass, $P = 50\%P_{amb}$, $D = 29.0$ mm.

B.98

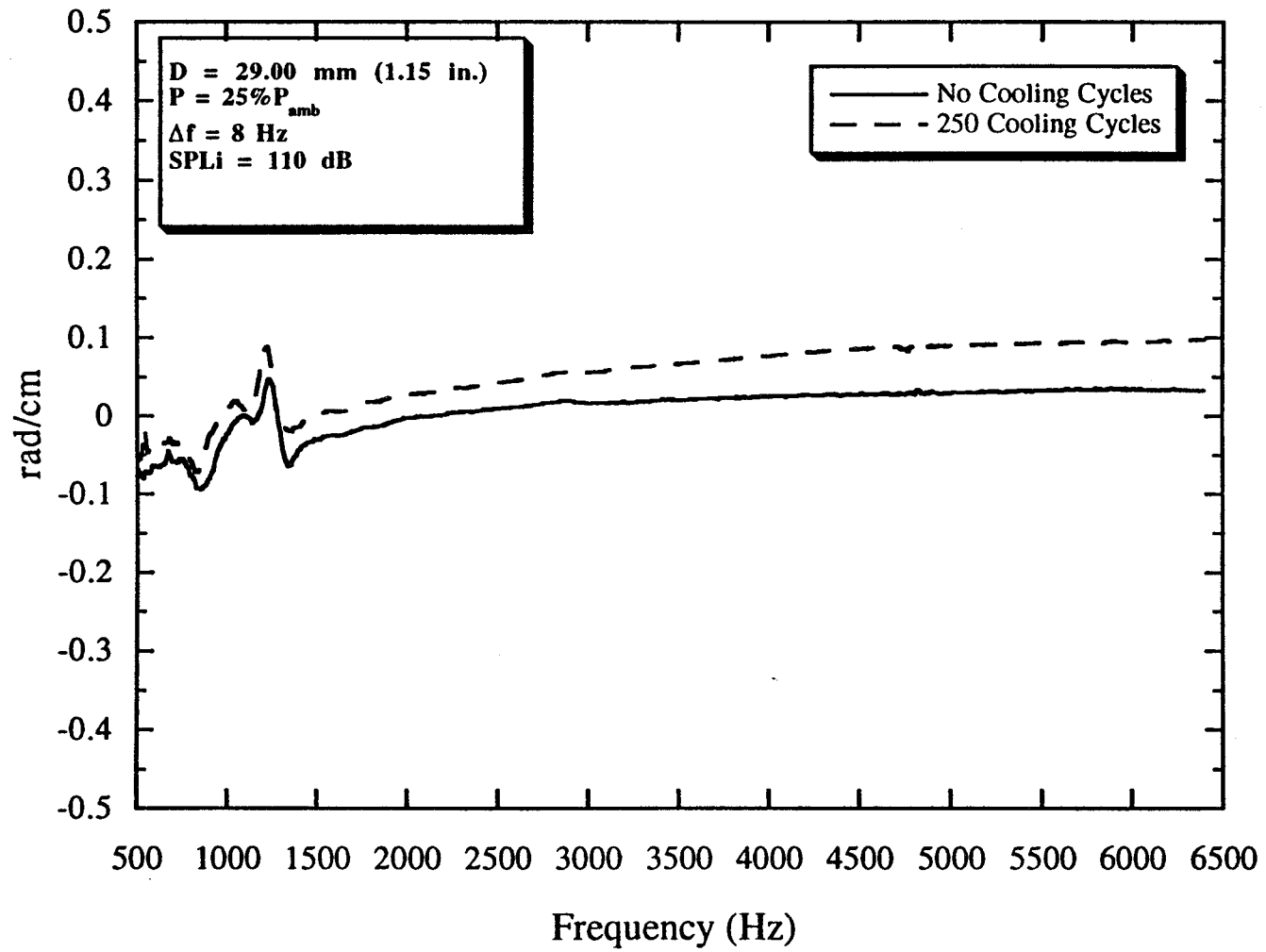


Figure B98. Phase Constant of Fiberglass, $P = 25\%P_{amb}$, $D = 29.0$ mm.

REPORT DOCUMENTATION PAGE			Form Approved OMB No. 0704-0188	
Public reporting burden for this collection of information is estimated to average 1 hour per response, including the time for reviewing instructions, searching existing data sources, gathering and maintaining the data needed, and completing and reviewing the collection of information. Send comments regarding this burden estimate or any other aspect of this collection of information, including suggestions for reducing this burden, to Washington Headquarters Services, Directorate for Information Operations and Reports, 1215 Jefferson Davis Highway, Suite 1204, Arlington, VA 22202-4302, and to the Office of Management and Budget, Paperwork Reduction Project (0704-0188), Washington, DC 20503.				
1. AGENCY USE ONLY (Leave blank)	2. REPORT DATE November 1994	3. REPORT TYPE AND DATES COVERED Contractor Report		
4. TITLE AND SUBTITLE Acoustic Properties and Durability of Liner Materials at Non-Standard Atmospheric Conditions			5. FUNDING NUMBERS NAS1-19061 (Task Assignment 15) 505-59-52-01	
6. AUTHOR(S) K.K. Ahuja, R.J. Gaeta, Jr. and J. S. Hsu				
7. PERFORMING ORGANIZATION NAME(S) AND ADDRESS(ES) Georgia Institute of Technology GTRI/AERO Acoustic, Aerodynamics, and Advanced Vehicles Div. Atlanta, Georgia 30332-0800			8. PERFORMING ORGANIZATION REPORT NUMBER A8612-015	
9. SPONSORING / MONITORING AGENCY NAME(S) AND ADDRESS(ES) National Aeronautics and Space Administration Langley Research Center Hampton, VA 23681-0001			10. SPONSORING / MONITORING AGENCY REPORT NUMBER NASA CR-195010	
11. SUPPLEMENTARY NOTES NASA Langley Technical Monitor: Earl Booth, Jr. GTRI Program Manager: Krish K. Ahuja				
12a. DISTRIBUTION / AVAILABILITY STATEMENT Unclassified - Unlimited Subject Category 71			12b. DISTRIBUTION CODE	
13. ABSTRACT (Maximum 200 words) This report documents the results of an experimental study on how acoustic properties of certain absorbing liner materials are affected by non-standard atmospheric conditions. This study was motivated by the need to assess risks associated with incorporating acoustic testing capability in wind tunnels with semi-cryogenic high Reynolds number aerodynamic and/or low pressure capabilities. The study consisted of three phases: 1) Measurement of acoustic properties of selected liner materials at sub-atmospheric pressure conditions, 2) Periodic cold soak and high pressure exposure of liner materials for 250 cycles, and 3) Determination of the effect of periodic cold soak on the acoustic properties of the liner materials at sub-atmospheric conditions and the effect on mechanical resiliency. The selected liner materials were Pyrell foam, Fiberglass, and Kevlar. A vacuum facility was used to create the sub-atmospheric environment in which an impedance tube was placed to measure acoustic properties of the test materials. An automated cryogenic cooling system was used to simulate periodic cold soak and high pressure exposure. It was found that lower ambient pressure reduced the absorption effectiveness of the liner materials to varying degrees. Also no significant change in the acoustic properties occurred after the periodic cold soak. Furthermore, mechanical resiliency tests indicated no noticeable change.				
14. SUBJECT TERMS Acoustic Liners, Duct Acoustics, Impedance Tube Wind Tunnel Acoustic Treatment, Two-microphone Method, Liner Materials			15. NUMBER OF PAGES 201	
			16. PRICE CODE A10	
17. SECURITY CLASSIFICATION OF REPORT Unclassified	18. SECURITY CLASSIFICATION OF THIS PAGE Unclassified	19. SECURITY CLASSIFICATION OF ABSTRACT	20. LIMITATION OF ABSTRACT	